Bioengineering hepatic organoids

Development of an alternative model for liver toxicity

Manon Bouwmeester

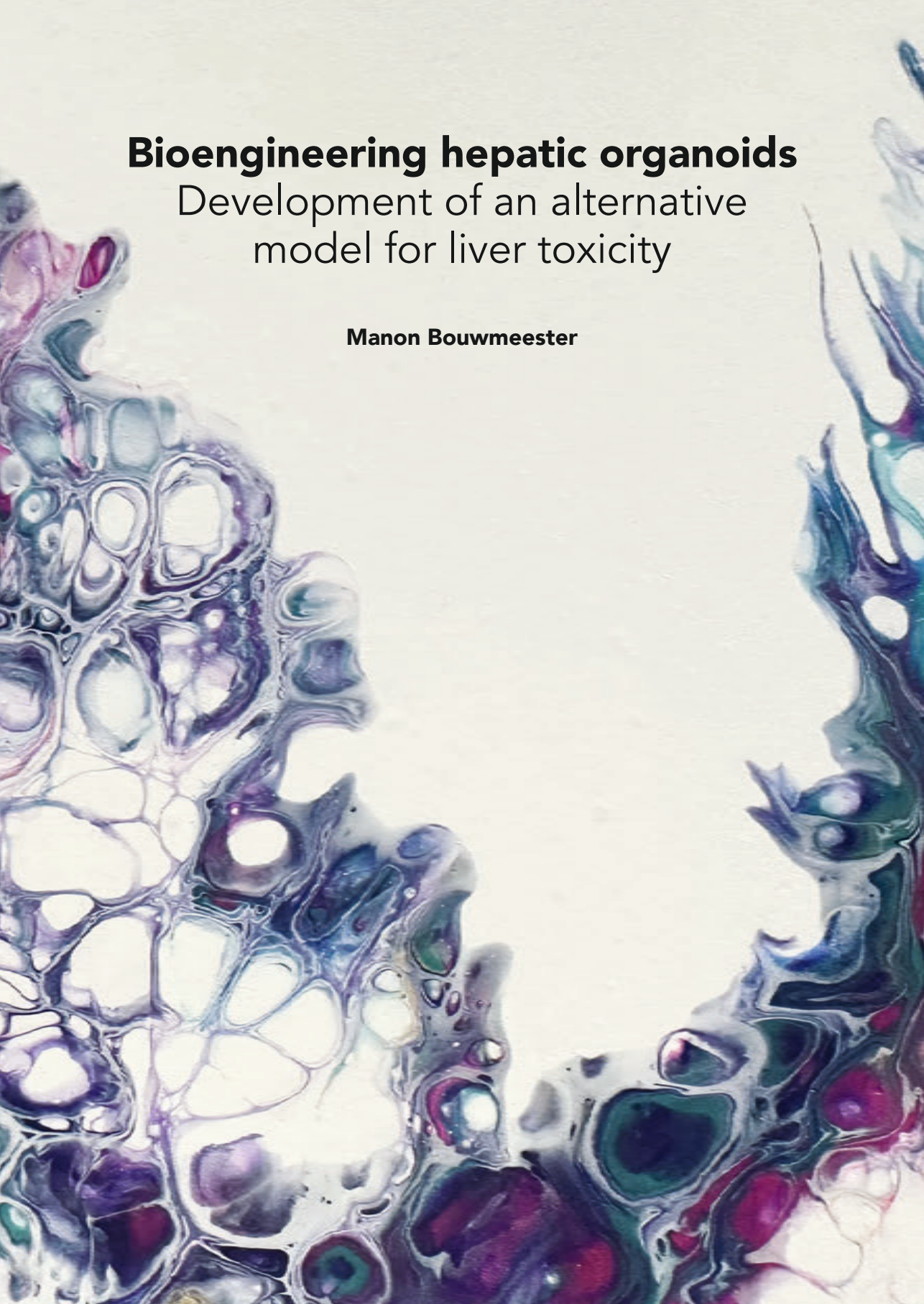

Bioengineering hepatic organoids

Development of an alternative model for liver toxicity

Manon Bouwmeester

Bioengineering hepatic organoids
Development of an alternative model for toxicity testing
Copyright © 2023 Manon Bouwmeester

The Netherlands. All rights reserved. No parts of this thesis may be reproduced, stored or transmitted in any way or by any means without the prior permission of the author. The copyright of the articles that have been published has been transferred to the respective journals.

ISBN | 978-94-6483-510-6

Cover design | Manon Bouwmeester
Printing: | Ridderprint, www.ridderprint.nl
Layout and design: | Michèle Duquesnoy, persoonlijkproefschrift.nl

The research described in this thesis was performed at the department of Clinical Sciences and at the Toxicology Division of Institute for Risk Assessment Sciences (IRAS) at the Faculty of Veterinary Medicine, Utrecht University, the Netherlands.

Printing of this thesis was financially supported by the Netherlands Association for the Study of the Liver (NASL).

Bioengineering hepatic organoids

Development of an alternative model for liver toxicity

Leverorganoïden en biofabricage

Het ontwikkelen van een alternatief model voor levertoxiciteit

(met een samenvatting in het Nederlands)

Proefschrift

ter verkrijging van de graad van doctor aan de
Universiteit Utrecht
op gezag van de
rector magnificus, prof.dr. H.R.B.M. Kummeling,
ingevolge het besluit van het college voor promoties
in het openbaar te verdedigen op

donderdag 14 december 2023 des middags te 2.15 uur

door

Manon Christel Bouwmeester

geboren op 17 juni 1991
te Voorst

Promotor:

Prof.dr.ir. J. Legler

Copromotoren:

Dr. B. Spee
Dr. N.I. Kramer

Beoordelingscommissie:

Prof.dr. P. Baptista
Prof.dr. M. van den Berg
Prof.dr. J.B. Helms
Dr. A. Kienhuis
Prof.dr. R. Masereeuw

Dit proefschrift werd (mede) mogelijk gemaakt met financiële steun van de Nederlandse Organisatie voor Wetenschappelijk Onderzoek (NWO; onderzoeksprogramma Toegepaste en Technische wetenschappen (TTW) met projectnummer 15498).

CONTENTS

Chapter 1	General introduction and thesis outline	7
Chapter 2	Drug Metabolism of Hepatocyte-Like Organoids and Their Applicability in In Vitro Toxicity Testing	27
Chapter 3	Bioprinting of Human Liver-derived Epithelial Organoids for Toxicity Studies	55
Chapter 4	Volumetric Bioprinting of Organoids and Optically Tuned Hydrogels to Build Liver-Like Metabolic Biofactories	85
Chapter 5	Establishment of a tailor-made bioreactor for dynamic culture of bioprinted hepatic constructs	139
Chapter 6	Summary and general discussion	159
Addendum	Nederlandse samenvatting	188
	PhD portfolio	191
	List of publications	193
	Dankwoord	194
	Curriculum Vitae	198

General introduction and thesis outline

1

The liver is the major organ involved in the metabolism of drugs and other chemicals. It is susceptible to toxicity, as drug metabolism is a key determinant in hepatotoxicity. Currently drug safety evaluations are mainly based on animal testing, however interspecies differences hamper accurate prediction for the human situation [1-3]. A shift towards human-based cell models to screen for drug-induced hepatotoxicity is ongoing. The focus of these models is on elucidating the molecular underpinnings of toxicity. Different hepatic cell models exist to study human liver function and disease. New in the field are intrahepatic cholangiocyte organoids, which are donor-derived adult stem cells that can be differentiated towards hepatocyte-like cells with applications in disease modelling and regenerative medicine [4,5]. Their potential in toxicity testing is unknown so far. The addition of microphysiological relevant features, e.g., co-culture and/or flow, in *in vitro* systems is known to improve hepatic functionality of (stem cell-derived) hepatic cells, which can be accomplished using 3D culturing methods and bioengineering techniques, including bioprinting [6]. The aim of this thesis is to assess the hepatic function of hepatocyte-like organoids and their applicability as an alternative (non-animal) model in toxicology. Moreover, the combination of organoid technology with bioprinting approaches is explored, by testing two bioprinting methods including flow perfusion. To this end, the effect of bioprinting on the hepatic maturation state of hepatocyte-like organoids is examined to ascertain how predictive this cell type can be for toxicity testing. In this chapter, the state of the art of *in vitro* liver models is explained to provide context to the aims, objective and structure of this thesis.

MORPHOLOGY OF THE LIVER

In vitro hepatocyte models vary in their mimicry of liver architecture. The liver has a unique architecture, as it is organized into functional units called lobules. These hexagonal units contain intrahepatic vessels, sinusoids, ranging from portal tracts at its periphery to a central vein around which liver cells radiate (Figure 1) [7]. The portal vein and hepatic artery provide oxygen- and nutrient-rich blood which is filtered and modified by hepatocytes before reaching the central vein. The liver consists of parenchymal cells, hepatocytes, and non-parenchymal cells, such as sinusoidal endothelial cells, stellate cells, liver-resident macrophages Kupffer cells and biliary endothelial cells – cholangiocytes. Hepatocytes are polarized cells which contain specific proteins and receptors localized to the basolateral (sinusoidal) or apical (canalicular) membrane. The latter forms the bile canaliculi enclosed by adjacent hepatocytes for biliary excretion (Figure 1) [8]. Hepatocytes make up about sixty percent of the hepatic cells and carry out most of the liver's metabolic functions, such as synthesis and excretion of plasma proteins (e.g., albumin), gluconeogenesis, urea synthesis, and triglyceride storage. Moreover, the liver is involved in metabolism of

xenobiotics and drugs and biliary excretion and is the main detoxifying organ of the body. Hepatic functionality is heterogenous among hepatocytes, since the location of the hepatocytes in the hepatic lobule defines their role. This zonation is modulated by gradual presence of oxygen, nutrients, hormones together with the structure and composition of extracellular matrix (ECM) containing different types of collagen and laminin [9]. For example, xenobiotic metabolism occurs predominantly in the pericentral area. Taken together, the morphology of the hepatic lobule and the liver-specific venous and arterial system play an important role in the metabolic function.

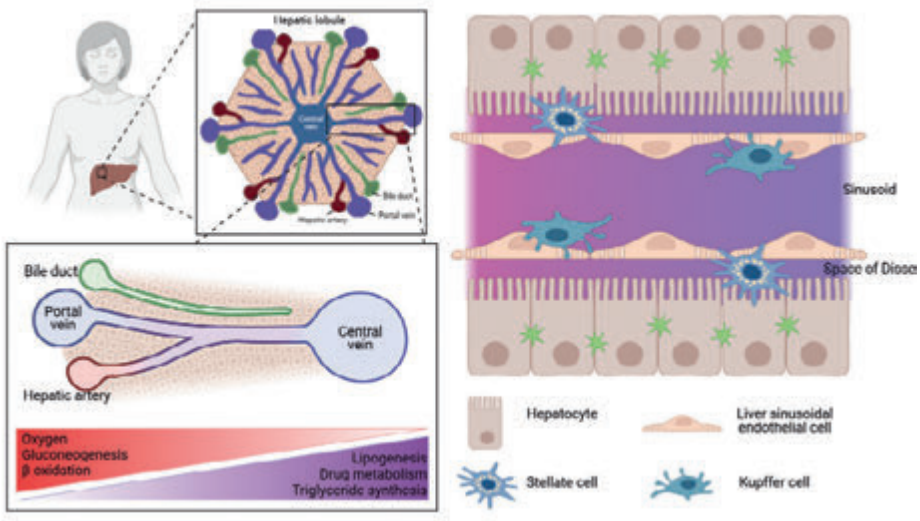

Figure 1. Liver morphology. The liver consists of hepatic lobules with portal veins and hepatic arteries at its periphery guiding blood towards the central vein in the center of the lobule. Hepatocytes align the sinusoids, where stellate cells are located between the hepatocytes and sinusoidal endothelial cells in the Space of Disse. Kupffer cells are residential in the sinusoids. Hepatocytes are polarized with an apical domain enclosing bile canaliculi.

DRUG METABOLISM

Xenobiotics including drugs are metabolized by hepatocytes, which generally occurs through a two-phase metabolic process. In phase I, drugs can undergo various reactions, including oxidation, reduction and hydrolysis. The most common reaction is oxidation and the most common enzyme family involved in these reactions is cytochrome P450 (CYP) super family. CYP family members are thoroughly studied to examine their role in drug induced liver injury, especially the isomers most abundantly present in human livers, namely

CYP3A4, CYP2E1, CYP2C9, CYP2C8 and CYP1A2 [10]. Phase II metabolism involves the conjugation of substrates, generally formed in phase I metabolism, to hydrophilic groups by UDP-glucuronyl transferases (UGTs), glutathione-S-transferases (GSTs) or sulfotransferases (SULTs). These reactions generally detoxify reactive metabolites formed by phase I metabolism, however in some cases phase II metabolism results in reactive metabolites. These reactive metabolites can interact with hepatocellular macromolecules (such as proteins, lipids, and nucleic acids) leading to protein dysfunction, lipid peroxidation, DNA damage, and oxidative stress [11]. Hepatic transporters, including superfamilies ATP-binding cassette (ABC) transporters and solute carrier (SLC) transporters, are involved in excretion of drugs and endogenous compounds like bile acids and bilirubin into bile canaliculi. These two phases of drug metabolism and the functionality of hepatic transporters are crucial in hepatotoxicity, as they are responsible for the (de)activation and excretion of xenobiotics, and thus influence their potential accumulation in the body at toxic levels [12,13]. Some xenobiotics can induce and/or inhibit these biotransformation enzymes and transporters and thus potentiate drug-induced hepatotoxicity. Similarly, genetic polymorphisms are known to alter the function of isozymes and transporter and thus alter a person's sensitivity to drugs [10,14-16].

DRUG INDUCED LIVER INJURY

Due to its crucial role in drug metabolism, the liver is susceptible to drug induced injury. Drug induced liver injury (DILI) is a major cause for discontinuation of drug candidates in the drug development pipeline and the withdrawal of drugs from the market, which has major public health and economic impact [17-19]. DILI is generally classified as intrinsic or idiosyncratic. Intrinsic DILI involves dose-dependent and predictable adverse effects after exposure. A typical example of intrinsic DILI is acetaminophen (paracetamol, N-acetyl-p-aminophenol (APAP)). APAP overdose accounts for about half of all acute liver failure (ALF) cases in the U.S. and in some European countries [20-22]. Idiosyncratic DILI (iDILI) includes unpredictable adverse effects as they derive from individual susceptibility without obvious dose-dependency. iDILI accounts for 11% of the ALF cases in the U.S. [21,22]. An example of iDILI is the anti-diabetic drug troglitazone, which was withdrawn from the market in the U.S. in 2000 due to hepatotoxicity [23]. DILI can be caused by multiple cellular mechanisms and can therefore lead to different types of pathologies, such as (1) hepatocyte necrosis, as in the case of acetaminophen, (2) cholestasis, e.g., drug-induced inhibition of transporters responsible for bile salt excretion by hepatocytes, or (3) steatosis, which occurs due to an imbalance between hepatic lipid uptake, *de novo* lipogenesis and lipid clearance, in which perturbation of mitochondrial function can play a role [24]. The onset of iDILI is considered a multifactorial process involving other risk

factors than drug metabolism alone, such as environmental, physiological and (immune-related) genetic factors, leading to interindividual differences [25,26].

ANIMAL MODELS FOR HUMAN SAFETY ASSESSMENT

Preclinical safety testing is traditionally performed in animals, predominantly rodents, which allows for drug evaluation in the presence of a complete immune system and cross-talk with other organs [27]. However, significant interspecies and interindividual differences in, amongst others, drug metabolism, hamper accurate prediction for hepatotoxic potential of new drugs in humans [1,28,29]. For acetaminophen, species differences for toxicity is mainly due the rate of formation of the toxic metabolite N-acetyl-p-benzoquinone imine (NAPQI) [30]. Troglitazone is an example of failed human safety prediction due to interspecies differences, including rodent models and monkeys. Interestingly, a recent study illustrated that troglitazone-induced hepatotoxicity could be predicted using human-based *in vitro* assays instead of pre-clinical animal testing [31] indicating the potential of such *in vitro* models in predicting toxicity.

Preclinical evaluation of DILI demands that models reflect the human biology and reproduce features of DILI described in humans in order to have a higher predictive value than current animal testing, resulting in a shift to testing in human-based models [32,33]. This human-based approach potentially not only overcomes drug development hurdles due to interspecies differences in liver function, additionally it gives more insight in the molecular mechanisms of toxicity, which are summarized into conceptual adverse outcome pathways (AOPs) [34]. Emerging developments in the last decades resulted in a variety of alternative (non-animal) models to explore human biology, including omics-based technologies, stem cells, organ-on-chips and computational (*in silico*) approaches. The application and integration of these new approach methodologies – also referred to as non-animal methods - (NAMs) to assess the toxicological hazard and risk of xenobiotic exposure is referred to as next generation risk assessment [35,36]. Moreover, these NAMs will aid in an approach to replace, reduce and refine (3R) animal use in safety evaluations [11,37,38].

HEPATIC CELL MODELS

Hepatic *in vitro* models ideally reflect both the liver's function and the mechanism of liver injury to be able to evaluate the effectiveness and toxic potential of a drug, respectively. The functional characteristics of the different hepatic cell sources (Figure 2) need to be considered for a fit-for-purpose approach to drug testing. Primary human hepatocytes (PHHs) are considered the gold standard

in toxicity testing as they exhibit hepatic function similar to human hepatocytes *in vivo* [39,40]. Their major drawback is the dedifferentiation of hepatic marker expression and functions within hours as soon as they are cultured as monolayer [41,42]. Moreover, their proliferation capacity and availability are limited, which adds a difficulty to their use in long-term or robust experiments. PHHs represent genetic heterogeneity between individuals, which can be essential in screening for DILI. Hepatic tumorigenic cell lines, including the commonly used HepG2 and HepaRG cell lines, are single-donor derived and cannot provide these interindividual insights. However, they do enable near limitless availability and long-term culture. Unlike HepG2, HepaRG cell reflect PHHs in a number of key hepatic functions [43], including activity of drug metabolizing enzymes [40]. Immortalized PHHs combine favorable characteristics of PHHs and hepatic cell lines. They can proliferate as well as maintain the expression of hepatic markers over longer periods of time than fresh and cryopreserved PHH [44-46]. Long-term culture and interindividual heterogeneity *in vitro* can also be provided by human stem cell models. Induced pluripotent stem cells (iPSCs) are donor-derived without the need of a liver biopsy (e.g., skin fibroblasts) and therefore enable *in vitro* cultures of multiple donors and thereby individuals with particular phenotypes or genotypes [47,48]. The collection of human adult stem cells (ASCs) is more invasive, as they are isolated from a liver biopsy. Both stem cell-based models can be differentiated towards hepatocyte-like cells (HLCs) expressing hepatic markers like albumin and CYP3A4, however current state of hepatic maturation needs improvement when compared to PHHs.

Improvement of hepatic functionality and/or delay of dedifferentiation, and thereby increased applicability for *in vitro* toxicity prediction can be addressed by advanced culture methodologies. Although 2D monolayer cultures are technically simple, convenient and affordable, there has been a shift towards the development and use of more complex 3D culture models [39,49,50]. These more complex models can consist of cell spheroids or organoids, stimulating cell-cell interaction, or by the use of a liver-like ECM environment, such as collagen or Matrigel™ (Matrigel), which can stimulate cell-matrix interaction in the form of a hydrogel droplet or sandwich culture (overlay of ECM on cellular monolayer; Figure 2) [39,51,52]. Other advances to stimulate hepatic function *in vitro* by mimicking the hepatic *in vivo* environment focus on achieving a structural resemblance to the liver's architecture, by using (decellularized) scaffolds, bioprinting techniques, via incorporation of other cell types (co-culture), such as non-parenchymal cells (NPCs), and/or a dynamic culture environment, e.g., by applying flow perfusion (Figure 2) [52-54]. Features of the liver's microenvironment that are addressed using these methodologies are, among others, the shear stress that cells *in vivo* experience [55-57], zonal orientation of the cells in the hepatic lobules [58-61] and/or co-cultures with non-

parenchymal cells [62-64] or even multi-organ [65-67]. Both organ-on-a-chips and bioreactors provide a system to combine these different physiologically relevant features *in vitro,* although at different levels of throughput and complexity, under standardized conditions into a tissue microenvironment [36,68-71].

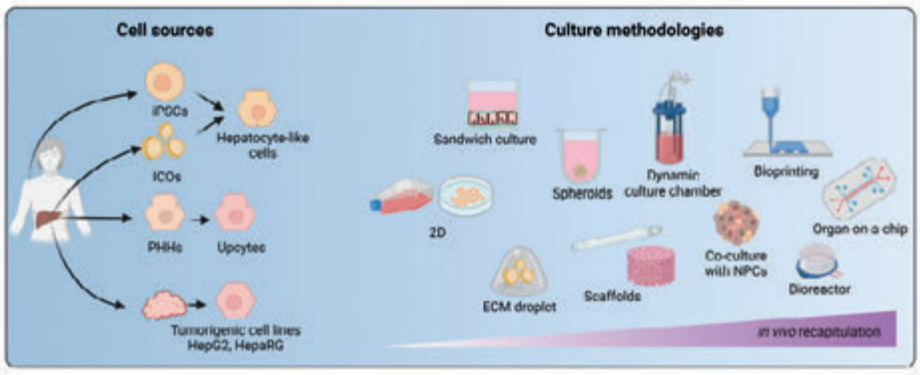

Figure 2. Hepatic cell models and advancements in culture technologies. Hepatic cell models can be derived from different sources, as depicted on the left. Different culture methodologies can be applied to these cell models, as depicted on the right. The more advanced the culture method is (depicted further to the right), the more it mimics the *in vivo* liver environment. iPSCs: induced pluripotent stem cells. ICOs: Intrahepatic cholangiocyte organoids. PHHs: Primary human hepatocytes. 2D: 2 dimensional cultures. ECM: Extracellular matrix. NPCs: Non-parenchymal cells.

ORGANOID TERMINOLOGY

At first, the term 'organoids' was used to describe any three-dimensional (3D) organotypic cultures derived from primary hepatocytes, embryonic stem cells, induced pluripotent stem cells, well-established cell lines or even whole or segmented tissue [72]. Over the years, terminology for cell models evolved together with the development of novel cell models and culture techniques. Spheroids are considered 3D cell aggregates that are formed in hanging-drop or ultra-low attachment cultures in the absence of a matrix. On the other hand, organoids are defined as self-organizing 3D structures derived from stem cells, progenitor cells and/or differentiated cells in a matrix [73].

Terminology is changing fast. When the organoids used in this thesis were established in 2015, they were described as Lgr5+ liver stem cells [5]. Later, they became known as, among others, LGR5 positive bipotential human liver stem cells [74], human liver organoids [75], human liver-derived epithelial organoids [76], human liver epithelial organoids [77], and 3D human liver organoids [78]. A

recent consensus paper aimed to harmonize organoid terminology to improve communication between researchers and in return help in the application of these models [73]. The organoid model used in this thesis is referred to as liver-derived intrahepatic cholangiocyte organoids (ICOs), which can be differentiated towards a hepatic and cholangiocyte phenotype [73]. In this thesis several names for the organoid model are used: ICOs and after hepatic differentiation as hepatocyte-like ICOs (HL-ICOs; Chapter 2), liver-derived epithelial organoids (Chapter 3), and liver epithelial organoids in Chapter 4. In this chapter, Chapter 5, and 6, the organoid model is referred to as liver organoids.

INTRAHEPATIC CHOLANGIOCYTE ORGANOIDS

Under culture conditions where the developmental Wnt/β-catenin pathways are induced, liver-derived adult stem cells form hollow 3D structures embedded in a matrix-rich environment, such as Matrigel, and upregulate stem cell marker LGR5 [5]. The formed liver organoids are highly proliferative. They expand and reform as cystic structures, which are genetically stable [5]. The formed liver organoids can be differentiated into the cholangiocyte- or hepatocyte-lineage indicating the bipotential nature of the adult stem cells [5,79]. Once differentiated towards the hepatic phenotype, they acquire hepatic functions such as albumin secretion, glycogen storage, phase I and II drug activity, and ammonia detoxification and show polarized expression of hepatic apical transporters facing the organoid lumen [5]. Considering their donor-derived origin, the application of liver organoids in disease modelling and regenerative medicine is well-described [4,78,80-82]. Although, the current hepatic maturation state is still limited compared to primary human hepatocytes as indicated by lower hepatic function (e.g., albumin expression and cytochrome activity).

BIOENGINEERED HEPATIC MODELS

Three-dimensional cell cultures range from 3D cellular structures, such as spheroids and organoids, to far more advanced systems involving 3D bioprinting and physiological fluid flow (Figure 2). Biofabrication techniques offer the opportunity to create structures like the complex liver architecture and the sinusoidal organization, which are essential for proper liver function *in vivo*, and also *in vitro* the spatial microenvironment is important for the functionality [83]. With the introduction of biofabrication technologies, cells are combined with biomaterials and bioactive components and patterned into 3D constructs through fabrication methods such as bioprinting [84]. The printable hydrogel that contains cells is termed bioink, which is used to create 3D cell-laden

constructs with a controlled geometry, which can allow for vascularization and enhanced exchange of nutrients. As the bioprinting field is an emerging field, the development of hydrogels of decellularized liver, animal-free, or degradable hydrogels for transplantation purposes is ongoing [85-87].

Bioprinting techniques have been significantly developed since the start of the research project in which the work described in this thesis was performed. Although inkjet-based bioprinting, also known as droplet-based bioprinting, and extrusion-based bioprinting, a layer-by-layer method, were already described for hepatic models [88,89], the combination with liver organoids was undiscovered. The potential to converge bioprinting and self-organizing structures like liver organoids, has sparked attention in the biofabrication field due to the possibility to create models at the tissue-like level of detail [90-92]. Volumetric bioprinting is a novel bioprinting technique [93], which was not described yet at the time this research project started. This light-based layerless printing approach is capable of printing high resolution and relatively large constructs within seconds.

Another point to consider in the biofabrication of liver modes is the biomaterials. Biomaterials play an important role in the function of the hepatic models [85,94]. The biomaterials can be tailored to mimic the extracellular matrix found *in vivo*. In case of the liver, important extracellular matrix proteins include collagens, glycosaminoglycans and laminins, which constitute the microenvironment of hepatic cells [95]. This can be used in creating biomaterials which are aimed to mimic the microenvironment of the liver and will help in establishing liver function in hepatic models. Interestingly, organoids differentiated towards the hepatic lineage in different biological or synthetic hydrogels all express higher hepatic markers compared to the standard animal-derived hydrogels [75,96,97].

Through the years the focus of the biofabrication field shifted from technological advances towards biology-focused bioengineered models, and thereby creating a valuable approach for microphysiological relevant human *in vitro* models [98]. The ongoing developments in the biofabrication field result in novel strategies enabling implementation of these advanced methods in *in vitro* testing, e.g., high-throughput approaches. Cell models in combination with such bioengineering techniques have potential to bridge the gap between animal models and humans [49,99,100].

THESIS OUTLINE – AIMS AND OBJECTIVES

Safety evaluation of new drugs is traditionally based on animal studies. However interspecies and interindividual differences in drug metabolism – a

key component in hepatotoxicity etiologies – hamper accurate prediction of human drug efficacy and toxicity. In order to reliably assess drug efficacy and toxic potency, a predictive model representing human biology and human DILI outcomes is necessary. The development of non-animal alternatives evolved to meet the 3R principle (to replace, reduce and refine animal use) to generate human-relevant efficacy and toxicity data and thus better understand interspecies difference in drug sensitivity. Several human hepatic cell models are described which can be applied in *in vitro* toxicity testing. This said, some of the major drawbacks of these models is the lack of proliferation or function [39,99,100]. Hepatocyte-like intrahepatic cholangiocyte organoids (hereafter called liver organoids) are liver-derived adult stem cells cultured as 3D structures with shown applicability in regenerative medicine and disease modelling. Their potential for *in vitro* toxicity testing however remained undetermined so far. Although a variety of hepatic models is available, these donor-derived liver organoids may possess characteristics involved in toxicity that others models cannot provide. Moreover, by creating vast biobanks of liver organoids, individual susceptibility to liver disease can be studied in detail, including metabolic liver diseases [101]. An *in vitro* model needs to represent the liver's function to be able to evaluate the toxicity potential of a drug accurately. Therefore it is desirable to improve the hepatic state of hepatic cells by increasing the physiological relevance of *in vitro* systems using advanced culture methods, e.g., the use of ECM components, or biofabrication techniques, such as bioprinting. The aim of this thesis is to assess the hepatic function of liver organoids and their application as alternative (non-animal) model in *in vitro* toxicity studies. Additionally, organoid technology was combined with bioprinting approaches in order to examine the effect of bioprinting on the hepatic maturation of hepatocyte-like organoids to ascertain how predictive this cell type can be for toxicity testing.

The research questions and corresponding approach of this thesis are:

1. What is the potential of liver organoids as *in vitro* model for toxicity testing?

In **Chapter 2**, liver-derived organoids differentiated towards hepatocyte-like cells are introduced as an hepatic *in vitro* model and their hepatotoxicity testing potential was evaluated. This chapter focused on the biotransformation capacity as expression levels of involved genes and the activity of CYP enzymes was examined in liver organoids compared to well-known hepatic models primary human hepatocytes and the hepatic cell line HepaRG. Additionally, the sensitivity of the liver organoids to a set of known hepatotoxic drugs was examined.

2. Can the hepatic functionality of liver organoids be stimulated by creating an *in vivo*-like culture environment using bioprinting techniques and flow perfusion?

In **Chapter 3** and **Chapter 4**, two bioprinting techniques demonstrate how to create a more advanced *in vitro* culture environment for the liver organoids. Chapter 3 described extrusion-based bioprinting of liver organoids, which is a layer-by-layer technique in which constructs are created by positioning a cell-laden bioink in a desired design. In chapter 4, a light-based bioprinting technique is used, which tackles challenges posed by conventional approaches through the layerless biofabrication of highly complex cell-laden structures within seconds. Both techniques pave the way towards the robust construction of advanced *in vitro* culture environment for liver organoids. **Chapter 5** presented a tailor-made bioreactor system to provide a standardized environment to test the effect of flow perfusion on hepatic maturation of bioprinted hydrogel-embedded liver organoids.

Finally, in **Chapter 6**, all data in this thesis is summarized and discussed. In this general discussion, future perspectives for the utility of liver organoids and specifically their application in risk assessment are deliberated.

REFERENCES

[1] Turpeinen, M.; Ghiciuc, C.; Opritoui, M.; Tursas, L.; Pelkonen, O.; Pasanen, M. Predictive Value of Animal Models for Human Cytochrome P450 (CYP)-Mediated Metabolism: A Comparative Study in Vitro. Xenobiotica **2007**, *37*, 1367-1377.

[2] Hammer, H.; Schmidt, F.; Marx-Stoelting, P.; Pötz, O.; Braeuning, A. Cross-Species Analysis of Hepatic Cytochrome P450 and Transport Protein Expression. Arch. Toxicol. **2021**, *95*, 117-133.

[3] Mumtaz, M.M.; Pohl, H.R. Interspecies Uncertainty in Molecular Responses and Toxicity of Mixtures. Exp. Suppl. **2012**, *101*, 361-379.

[4] Prior, N.; Inacio, P.; Huch, M. Liver Organoids: From Basic Research to Therapeutic Applications. Gut **2019**, *68*, 2228-2237.

[5] Huch, M.; Gehart, H.; van Boxtel, R.; Hamer, K.; Blokzijl, F.; Verstegen, M.M.; Ellis, E.; van Wenum, M.; Fuchs, S.A.; de Ligt, J. *et al.* Long-Term Culture of Genome-Stable Bipotent Stem Cells from Adult Human Liver. Cell **2015**, *160*, 299-312.

[6] Chen, C.; Soto-Gutierrez, A.; Baptista, P.M.; Spee, B. Biotechnology Challenges to in Vitro Maturation of Hepatic Stem Cells. Gastroenterology **2018**, *154*, 1258-1272.

[7] Malarkey, D.E.; Johnson, K.; Ryan, L.; Boorman, G.; Maronpot, R.R. New Insights into Functional Aspects of Liver Morphology. Toxicol. Pathol. **2005**, *33*, 27-34.

[8] Schulze, R.J.; Schott, M.B.; Casey, C.A.; Tuma, P.L.; McNiven, M.A. The Cell Biology of the Hepatocyte: A Membrane Trafficking Machine. J. Cell Biol. **2019**, *218*, 2096-2112.

[9] Kietzmann, T. Metabolic Zonation of the Liver: The Oxygen Gradient Revisited. Redox Biol. **2017**, *11*, 622-630.

[10] Zanger, U.M.; Schwab, M. Cytochrome P450 Enzymes in Drug Metabolism: Regulation of Gene Expression, Enzyme Activities, and Impact of Genetic Variation. Pharmacol. Ther. **2013**, *138*, 103-141.

[11] Weaver, R.J.; Blomme, E.A.; Chadwick, A.E.; Copple, I.M.; Gerets, H.H.J.; Goldring, C.E.; Guillouzo, A.; Hewitt, P.G.; Ingelman-Sundberg, M.; Jensen, K.G. *et al.* Managing the Challenge of Drug-Induced Liver Injury: A Roadmap for the Development and Deployment of Preclinical Predictive Models. Nat. Rev. Drug Discov. **2020**, *19*, 131-148.

[12] Gu, R.; Liang, A.; Liao, G.; To, I.; Shehu, A.; Ma, X. Roles of Cofactors in Drug-Induced Liver Injury: Drug Metabolism and Beyond. Drug Metab. Dispos. **2022**, *50*, 646-654.

[13] Jetter, A.; Kullak-Ublick, G.A. Drugs and Hepatic Transporters: A Review. Pharmacol. Res. **2020**, *154*, 104234.

[14] Zhou, S.F.; Liu, J.P.; Chowbay, B. Polymorphism of Human Cytochrome P450 Enzymes and its Clinical Impact. Drug Metab. Rev. **2009**, *41*, 89-295.

[15] Kurogi, K.; Rasool, M.I.; Alherz, F.A.; El Daibani, A.A.; Bairam, A.F.; Abunnaja, M.S.; Yasuda, S.; Wilson, L.J.; Hui, Y.; Liu, M. SULT Genetic Polymorphisms: Physiological, Pharmacological and Clinical Implications. Expert Opin. Drug Metab. Toxicol. **2021**, *17*, 767-784.

[16] Nie, Y.; Yang, J.; Liu, S.; Sun, R.; Chen, H.; Long, N.; Jiang, R.; Gui, C. Genetic Polymorphisms of Human Hepatic OATPs: Functional Consequences and Effect on Drug Pharmacokinetics. Xenobiotica **2020**, *50*, 297-317.

[17] Temple, R.J.; Himmel, M.H. Safety of Newly Approved Drugs: Implications for Prescribing. JAMA **2002**, *287*, 2273-2275.

[18] Schuster, D.; Laggner, C.; Langer, T. Why Drugs Fail--a Study on Side Effects in New Chemical Entities. Curr. Pharm. Des. **2005**, *11*, 3545-3559.
[19] Alempijevic, T.; Zec, S.; Milosavljevic, T. Drug-Induced Liver Injury: Do we Know Everything? World J. Hepatol. **2017**, *9*, 491-502.
[20] Ramachandran, A.; Jaeschke, H. Acetaminophen Hepatotoxicity: A Mitochondrial Perspective. Adv. Pharmacol. **2019**, *85*, 195-219.
[21] Reuben, A.; Tillman, H.; Fontana, R.J.; Davern, T.; McGuire, B.; Stravitz, R.T.; Durkalski, V.; Larson, A.M.; Liou, I.; Fix, O. *et al.* Outcomes in Adults with Acute Liver Failure between 1998 and 2013: An Observational Cohort Study. Ann. Intern. Med. **2016**, *164*, 724-732.
[22] Reuben, A.; Koch, D.G.; Lee, W.M.; Acute Liver Failure Study Group. Drug-Induced Acute Liver Failure: Results of a U.S. Multicenter, Prospective Study. Hepatology **2010**, *52*, 2065-2076.
[23] Jaeschke, H. Troglitazone Hepatotoxicity: Are we Getting Closer to Understanding Idiosyncratic Liver Injury? Toxicol. Sci. **2007**, *97*, 1-3.
[24] Andrade, R.J.; Chalasani, N.; Björnsson, E.S.; Suzuki, A.; Kullak-Ublick, G.A.; Watkins, P.B.; Devarbhavi, H.; Merz, M.; Lucena, M.I.; Kaplowitz, N. *et al.* Drug-Induced Liver Injury. Nat. Rev. Dis. Primers **2019**, *5*, 58-0.
[25] Daly, A.K. Genetics of Drug-Induced Liver Injury: Current Knowledge and Future Prospects. Clin. Transl. Sci. **2022**.
[26] Chalasani, N.; Björnsson, E. Risk Factors for Idiosyncratic Drug-Induced Liver Injury. Gastroenterology **2010**, *138*, 2246-2259.
[27] McGill, M.R.; Jaeschke, H. Animal Models of Drug-Induced Liver Injury. Biochimica et Biophysica Acta - Molecular Basis of Disease **2019**, *1865*, 1031-1039.
[28] Ballet, F.c. Preventing Drug-Induced Liver Injury: How Useful are Animal Models? Digestive Diseases **2015**, *33*, 477-485.
[29] Olson, H.; Betton, G.; Robinson, D.; Thomas, K.; Monro, A.; Kolaja, G.; Lilly, P.; Sanders, J.; Sipes, G.; Bracken, W. *et al.* Concordance of the Toxicity of Pharmaceuticals in Humans and in Animals. Regulatory Toxicology and Pharmacology **2000**, *32*, 56-67.
[30] Tee, L.B.; Davies, D.S.; Seddon, C.E.; Boobis, A.R. Species Differences in the Hepatotoxicity of Paracetamol are due to Differences in the Rate of Conversion to its Cytotoxic Metabolite. Biochem. Pharmacol. **1987**, *36*, 1041-1052.
[31] Dirven, H.; Vist, G.E.; Bandhakavi, S.; Mehta, J.; Fitch, S.E.; Pound, P.; Ram, R.; Kincaid, B.; Leenaars, C.H.C.; Chen, M. *et al.* Performance of Preclinical Models in Predicting Drug-Induced Liver Injury in Humans: A Systematic Review. Sci. Rep. **2021**, *11*, 6403-2.
[32] Krewski, D.; Acosta, D.,Jr; Andersen, M.; Anderson, H.; Bailar, J.C.,3rd; Boekelheide, K.; Brent, R.; Charnley, G.; Cheung, V.G.; Green, S.,Jr *et al.* Toxicity Testing in the 21st Century: A Vision and a Strategy. J. Toxicol. Environ. Health B Crit. Rev. **2010**, *13*, 51-138.
[33] Zink, D.; Chuah, J.K.C.; Ying, J.Y. Assessing Toxicity with Human Cell-Based in Vitro Methods. Trends Mol. Med. **2020**, *26*, 570-582.
[34] Arnesdotter, E.; Gijbels, E.; Dos Santos Rodrigues, B.; Vilas-Boas, V.; Vinken, M. Adverse Outcome Pathways as Versatile Tools in Liver Toxicity Testing. Methods Mol. Biol. **2022**, *2425*, 521-535.
[35] Brescia, S.; Alexander-White, C.; Li, H.; Cayley, A. Risk Assessment in the 21st Century: Where are we Heading? Toxicol. Res. **2023**, *12*, 1-11.

[36] Nitsche, K.S.; Müller, I.; Malcomber, S.; Carmichael, P.L.; Bouwmeester, H. Implementing Organ-on-Chip in a Next-Generation Risk Assessment of Chemicals: A Review. Arch. Toxicol. **2022**, *96*, 711-741.

[37] Vinken, M.; Benfenati, E.; Busquet, F.; Castell, J.; Clevert, D.A.; de Kok, T.M.; Dirven, H.; Fritsche, E.; Geris, L.; Gozalbes, R. *et al.* Safer Chemicals using Less Animals: Kick-Off of the European ONTOX Project. Toxicology **2021**, *458*, 152846.

[38] Punt, A.; Bouwmeester, H.; Blaauboer, B.J.; Coecke, S.; Hakkert, B.; Hendriks, D.F.G.; Jennings, P.; Kramer, N.I.; Neuhoff, S.; Masereeuw, R. *et al.* New Approach Methodologies (NAMs) for Human-Relevant Biokinetics Predictions. Meeting the Paradigm Shift in Toxicology Towards an Animal-Free Chemical Risk Assessment. ALTEX **2020**, *37*, 607-622.

[39] Godoy, P.; Hewitt, N.J.; Albrecht, U.; Andersen, M.E.; Ansari, N.; Bhattacharya, S.; Bode, J.G.; Bolleyn, J.; Borner, C.; Böttger, J. *et al.* Recent Advances in 2D and 3D in Vitro Systems using Primary Hepatocytes, Alternative Hepatocyte Sources and Non-Parenchymal Liver Cells and their use in Investigating Mechanisms of Hepatotoxicity, Cell Signaling and ADME. Arch. Toxicol. **2013**, *87*, 1315-1530.

[40] Gómez-Lechón, M.J.; Tolosa, L.; Conde, I.; Donato, M.T. Competency of Different Cell Models to Predict Human Hepatotoxic Drugs. Expert Opin. Drug Metab. Toxicol. **2014**, *10*, 1553-1568.

[41] Elaut, G.; Henkens, T.; Papeleu, P.; Snykers, S.; Vinken, M.; Vanhaecke, T.; Rogiers, V. Molecular Mechanisms Underlying the Dedifferentiation Process of Isolated Hepatocytes and their Cultures. Curr. Drug Metab. **2006**, *7*, 629-660.

[42] Kim, Y.; Lasher, C.D.; Milford, L.M.; Murali, T.M.; Rajagopalan, P. A Comparative Study of Genome-Wide Transcriptional Profiles of Primary Hepatocytes in Collagen Sandwich and Monolayer Cultures. Tissue Eng. Part C. Methods **2010**, *16*, 1449-1460.

[43] Anthérieu, S.; Chesné, C.; Li, R.; Guguen-Guillouzo, C.; Guillouzo, A. Optimization of the HepaRG Cell Model for Drug Metabolism and Toxicity Studies. Toxicol. In. Vitro. **2012**, *26*, 1278-1285.

[44] Ramachandran, S.D.; Vivarès, A.; Klieber, S.; Hewitt, N.J.; Muenst, B.; Heinz, S.; Walles, H.; Braspenning, J. Applicability of Second-Generation Upcyte® Human Hepatocytes for use in CYP Inhibition and Induction Studies. Pharmacol. Res. Perspect. **2015**, *3*, e00161.

[45] Levy, G.; Bomze, D.; Heinz, S.; Ramachandran, S.D.; Noerenberg, A.; Cohen, M.; Shibolet, O.; Sklan, E.; Braspenning, J.; Nahmias, Y. Long-Term Culture and Expansion of Primary Human Hepatocytes. Nat. Biotechnol. **2015**, *33*, 1264-1271.

[46] Tolosa, L.; Jiménez, N.; Pelechá, M.; Castell, J.V.; Gómez-Lechón, M.J.; Donato, M.T. Long-Term and Mechanistic Evaluation of Drug-Induced Liver Injury in Upcyte Human Hepatocytes. Arch. Toxicol. **2019**, *93*, 519-532.

[47] Gao, X.; Liu, Y. A Transcriptomic Study Suggesting Human iPSC-Derived Hepatocytes Potentially Offer a Better in Vitro Model of Hepatotoxicity than most Hepatoma Cell Lines. Cell Biol. Toxicol. **2017**, *33*, 407-421.

[48] Ulvestad, M.; Nordell, P.; Asplund, A.; Rehnström, M.; Jacobsson, S.; Holmgren, G.; Davidson, L.; Brolén, G.; Edsbagge, J.; Björquist, P. *et al.* Drug Metabolizing Enzyme and Transporter Protein Profiles of Hepatocytes Derived from Human Embryonic and Induced Pluripotent Stem Cells. Biochem. Pharmacol. **2013**, *86*, 691-702.

[49] Cacciamali, A.; Villa, R.; Dotti, S. 3D Cell Cultures: Evolution of an Ancient Tool for New Applications. Front. Physiol. **2022**, *13*, 836480.

[50] Jensen, C.; Teng, Y. Is it Time to Start Transitioning from 2D to 3D Cell Culture? Front. Mol. Biosci. **2020**, *7*, 33.
[51] Fraczek, J.; Bolleyn, J.; Vanhaecke, T.; Rogiers, V.; Vinken, M. Primary Hepatocyte Cultures for Pharmaco-Toxicological Studies: At the Busy Crossroad of various Anti-Dedifferentiation Strategies. Arch. Toxicol. **2013**, *87*, 577-610.
[52] Ruoß, M.; Vosough, M.; Konigsrainer, A.; Nadalin, S.; Wagner, S.; Sajadian, S.; Huber, D.; Heydari, Z.; Ehnert, S.; Hengstler, J.G. *et al.* Towards Improved Hepatocyte Cultures: Progress and Limitations. Food and Chemical Toxicology **2020**, *138*, 111188.
[53] Yun, C.; Kim, S.H.; Jung, Y. Current Research Trends in the Application of in Vitro Three-Dimensional Models of Liver Cells. Pharmaceutics **2022**, *15*, 54.
[54] Paradiso, A.; Volpi, M.; Rinoldi, C.; Celikkin, N.; Contessi Negrini, N.; Bilgen, M.; Dallera, G.; Pierini, F.; Costantini, M.; Święszkowski, W. *et al.* In Vitro Functional Models for Human Liver Diseases and Drug Screening: Beyond Animal Testing. Biomater. Sci. **2022**.
[55] Nishii, K.; Brodin, E.; Renshaw, T.; Weesner, R.; Moran, E.; Soker, S.; Sparks, J.L. Shear Stress Upregulates Regeneration-Related Immediate Early Genes in Liver Progenitors in 3D ECM-Like Microenvironments. J. Cell. Physiol. **2018**, *233*, 4272-4281.
[56] Rashidi, H.; Alhaque, S.; Szkolnicka, D.; Flint, O.; Hay, D.C. Fluid Shear Stress Modulation of Hepatocyte-Like Cell Function. Arch. Toxicol. **2016**, *90*, 1757-1761.
[57] Du, Y.; Li, N.; Yang, H.; Luo, C.; Gong, Y.; Tong, C.; Gao, Y.; Lü, S.; Long, M. Mimicking Liver Sinusoidal Structures and Functions using a 3D-Configured Microfluidic Chip. Lab. Chip **2017**, *17*, 782-794.
[58] Lee-Montiel, F.T.; George, S.M.; Gough, A.H.; Sharma, A.D.; Wu, J.; DeBiasio, R.; Vernetti, L.A.; Taylor, D.L. Control of Oxygen Tension Recapitulates Zone-Specific Functions in Human Liver Microphysiology Systems. Exp. Biol. Med. (Maywood) **2017**, *242*, 1617-1632.
[59] Ahn, J.; Ahn, J.; Yoon, S.; Nam, Y.S.; Son, M.; Oh, J. Human Three-Dimensional in Vitro Model of Hepatic Zonation to Predict Zonal Hepatotoxicity. **2019**, *5*, 1-15.
[60] Kwon, D.; Choi, G.; Park, S.; Cho, S.; Cho, S.; Ko, S. Liver Acinus Dynamic Chip for Assessment of Drug-Induced Zonal Hepatotoxicity. Biosensors (Basel) **2022**, *12*, 445. doi: 10.3390/bios12070445.
[61] Wesseler, M.F.; Taebnia, N.; Harrison, S.; Youhanna, S.; Preiss, L.C.; Kemas, A.M.; Vegvari, A.; Mokry, J.; Sullivan, G.J.; Lauschke, V.M. *et al.* 3D Microperfusion of Mesoscale Human Microphysiological Liver Models Improves Functionality and Recapitulates Hepatic Zonation. Acta Biomater. **2023**.
[62] Janani, G.; Priya, S.; Dey, S.; Mandal, B.B. Mimicking Native Liver Lobule Microarchitecture in Vitro with Parenchymal and Non-Parenchymal Cells using 3D Bioprinting for Drug Toxicity and Drug Screening Applications. ACS Appl. Mater. Interfaces **2022**, *14*, 10167-10186.
[63] Baze, A.; Parmentier, C.; Hendriks, D.F.G.; Hurrell, T.; Heyd, B.; Bachellier, P.; Schuster, C.; Ingelman-Sundberg, M.; Richert, L. Three-Dimensional Spheroid Primary Human Hepatocytes in Monoculture and Coculture with Nonparenchymal Cells. Tissue Eng. Part C. Methods **2018**, *24*, 534-545.
[64] Esch, M.B.; Prot, J.; Wang, Y.I.; Miller, P.; Llamas-Vidales, J.R.; Naughton, B.A.; Applegate, D.R.; Shuler, M.L. Multi-Cellular 3D Human Primary Liver Cell Culture Elevates Metabolic Activity Under Fluidic Flow. Lab. Chip **2015**, *15*, 2269-2277.

[65] Nguyen, V.V.T.; Ye, S.; Gkouzioti, V.; van Wolferen, M.E.; Yengej, F.Y.; Melkert, D.; Siti, S.; de Jong, B.; Besseling, P.J.; Spee, B. *et al.* A Human Kidney and Liver Organoid-Based Multi-Organ-on-a-Chip Model to Study the Therapeutic Effects and Biodistribution of Mesenchymal Stromal Cell-Derived Extracellular Vesicles. J. Extracell Vesicles **2022**, *11*, e12280.

[66] Skardal, A.; Aleman, J.; Forsythe, S.; Rajan, S.; Murphy, S.; Devarasetty, M.; Pourhabibi Zarandi, N.; Nzou, G.; Wicks, R.; Sadri-Ardekani, H. *et al.* Drug Compound Screening in Single and Integrated Multi-Organoid Body-on-a-Chip Systems. Biofabrication **2020**, *12*, 025017-5090/ab6d36.

[67] Ferrari, E.; Rasponi, M. Liver-Heart on Chip Models for Drug Safety. APL. Bioeng. **2021**, *5*, 031505.

[68] Telles-Silva, K.A.; Pacheco, L.; Komatsu, S.; Chianca, F.; Caires-Júnior, L.C.; Araujo, B.H.S.; Goulart, E.; Zatz, M. Applied Hepatic Bioengineering: Modeling the Human Liver using Organoid and Liver-on-a-Chip Technologies. Front. Bioeng. Biotechnol. **2022**, *10*, 845360.

[69] Dalsbecker, P.; Beck Adiels, C.; Goksör, M. Liver-on-a-Chip Devices: The Pros and Cons of Complexity. Am. J. Physiol. Gastrointest. Liver Physiol. **2022**, *323*, G188-G204.

[70] Ribeiro, A.J.S.; Yang, X.; Patel, V.; Madabushi, R.; Strauss, D.G. Liver Microphysiological Systems for Predicting and Evaluating Drug Effects. Clin. Pharmacol. Ther. **2019**, *106*, 139-147.

[71] Hughes, D.J.; Kostrzewski, T.; Sceats, E.L. Opportunities and Challenges in the Wider Adoption of Liver and Interconnected Microphysiological Systems. Exp. Biol. Med. (Maywood) **2017**, *242*, 1593-1604.

[72] Simian, M.; Bissell, M.J. Organoids: A Historical Perspective of Thinking in Three Dimensions. J. Cell Biol. **2017**, *216*, 31-40.

[73] Marsee, A.; Roos, F.J.M.; Verstegen, M.M.A.; HPB Organoid Consortium; Gehart, H.; de Koning, E.; Lemaigre, F.; Forbes, S.J.; Peng, W.C.; Huch, M. *et al.* Building Consensus on Definition and Nomenclature of Hepatic, Pancreatic, and Biliary Organoids. Cell. Stem Cell. **2021**, *28*, 816-832.

[74] Schneeberger, K.; Sánchez-Romero, N.; Ye, S.; van Steenbeek, F.G.; Oosterhoff, L.A.; Pla Palacin, I.; Chen, C.; van Wolferen, M.E.; van Tienderen, G.; Lieshout, R. *et al.* Large-Scale Production of LGR5-Positive Bipotential Human Liver Stem Cells. Hepatology **2020**, *72*, 257-270.

[75] Ye, S.; Boeter, J.W.B.; Mihajlovic, M.; van Steenbeek, F.G.; van Wolferen, M.E.; Oosterhoff, L.A.; Marsee, A.; Caiazzo, M.; van der Laan, L.J.W.; Penning, L.C. *et al.* A Chemically Defined Hydrogel for Human Liver Organoid Culture. Adv. Funct. Mater. **2020**, *30*, 2000893.

[76] Bouwmeester, M.C.; Bernal, P.N.; Oosterhoff, L.A.; van Wolferen, M.E.; Lehmann, V.; Vermaas, M.; Buchholz, M.; Peiffer, Q.C.; Malda, J.; van der Laan, L.J.W. *et al.* Bioprinting of Human Liver-Derived Epithelial Organoids for Toxicity Studies. Macromol. Biosci. **2021**, *21*, e2100327.

[77] Bernal, P.N.; Bouwmeester, M.; Madrid-Wolff, J.; Falandt, M.; Florczak, S.; Rodriguez, N.G.; Li, Y.; Größbacher, G.; Samsom, R.; van Wolferen, M. *et al.* Volumetric Bioprinting of Organoids and Optically Tuned Hydrogels to Build Liver-Like Metabolic Biofactories. Adv Mater **2022**, *34*, e2110054.

[78] Lee, J.Y.; Han, H.J.; Lee, S.J.; Cho, E.H.; Lee, H.B.; Seok, J.H.; Lim, H.S.; Son, W.C. Use of 3D Human Liver Organoids to Predict Drug-Induced Phospholipidosis. Int. J. Mol. Sci. **2020**, *21*, 2982.

[79] Wang, Z.; Faria, J.; van der Laan, L.J.W.; Penning, L.C.; Masereeuw, R.; Spee, B. Human Cholangiocytes Form a Polarized and Functional Bile Duct on Hollow Fiber Membranes. Front. Bioeng. Biotechnol. **2022**, *10*, 868857.
[80] Nuciforo, S.; Heim, M.H. Organoids to Model Liver Disease. JHEP Rep. **2020**, *3*, 100198.
[81] He, C.; Lu, D.; Lin, Z.; Chen, H.; Li, H.; Yang, X.; Yang, M.; Wang, K.; Wei, X.; Zheng, S. *et al.* Liver Organoids, Novel and Promising Modalities for Exploring and Repairing Liver Injury. Stem Cell. Rev. Rep. **2022**, 1-13.
[82] Wang, L.; Li, M.; Yu, B.; Shi, S.; Liu, J.; Zhang, R.; Ayada, I.; Verstegen, M.M.A.; van der Laan, L.J.W.; Peppelenbosch, M.P. *et al.* Recapitulating Lipid Accumulation and Related Metabolic Dysregulation in Human Liver-Derived Organoids. J. Mol. Med. (Berl) **2022**, *100*, 471-484.
[83] Guagliano, G.; Volpini, C.; Briatico-Vangosa, F.; Cornaglia, A.I.; Visai, L.; Petrini, P. Toward 3D-Bioprinted Models of the Liver to Boost Drug Development. Macromol. Biosci. **2022**, *22*, e2200264.
[84] Zhang, X.; Jiang, T.; Chen, D.; Wang, Q.; Zhang, L.W. Three-Dimensional Liver Models: State of the Art and their Application for Hepatotoxicity Evaluation. Crit. Rev. Toxicol. **2020**, *50*, 279-309.
[85] Ye, S.; Boeter, J.W.B.; Penning, L.C.; Spee, B.; Schneeberger, K. Hydrogels for Liver Tissue Engineering. Bioengineering (Basel) **2019**, *6*, 59.
[86] Moghaddam, A.S.; Khonakdar, H.A.; Arjmand, M.; Jafari, S.H.; Bagher, Z.; Moghaddam, Z.S.; Chimerad, M.; Sisakht, M.M.; Shojaei, S. Review of Bioprinting in Regenerative Medicine: Naturally Derived Bioinks and Stem Cells. ACS Appl. Bio Mater. **2021**, *4*, 4049-4070.
[87] Aisenbrey, E.A.; Murphy, W.L. Synthetic Alternatives to Matrigel. Nat. Rev. Mater. **2020**, *5*, 539-551.
[88] Kryou, C.; Leva, V.; Chatzipetrou, M.; Zergioti, I. Bioprinting for Liver Transplantation. Bioengineering (Basel) **2019**, *6*, 95.
[89] Ma, X.; Liu, J.; Zhu, W.; Tang, M.; Lawrence, N.; Yu, C.; Gou, M.; Chen, S. 3D Bioprinting of Functional Tissue Models for Personalized Drug Screening and in Vitro Disease Modeling. Adv. Drug Deliv. Rev. **2018**, *132*, 235-251.
[90] Levato, R.; Jungst, T.; Scheuring, R.G.; Blunk, T.; Groll, J.; Malda, J. From Shape to Function: The Next Step in Bioprinting. Adv Mater **2020**, *32*.
[91] Goulart, E. A Review of Stem Cell Technology Targeting Hepatocyte Growth as an Alternative to Organ Transplantation. Methods Mol. Biol. **2023**, *2575*, 181-193.
[92] Chawla, S.; Das, A. Preclinical-to-Clinical Innovations in Stem Cell Therapies for Liver Regeneration. Curr. Res. Transl. Med. **2022**, *71*, 103365.
[93] Bernal, P.N.; Delrot, P.; Loterie, D.; Li, Y.; Malda, J.; Moser, C.; Levato, R. Volumetric Bioprinting of Complex Living-Tissue Constructs within Seconds. Adv Mater **2019**, *31*, e1904209.
[94] Natarajan, V.; Berglund, E.J.; Chen, D.X.; Kidambi, S. Substrate Stiffness Regulates Primary Hepatocyte Functions. RSC Adv. **2015**, *5*, 80956-80966.
[95] Martinez-Hernandez, A.; Amenta, P.S. The Hepatic Extracellular Matrix. I. Components and Distribution in Normal Liver. Virchows Arch. A Pathol. Anat. Histopathol. **1993**, *423*, 1-11.
[96] Krüger, M.; Oosterhoff, L.A.; van Wolferen, M.E.; Schiele, S.A.; Walther, A.; Geijsen, N.; De Laporte Laura; van der Laan, L.J.W.; Kock, L.M.; Spee, B. Cellulose Nanofibril Hydrogel Promotes Hepatic Differentiation of Human Liver Organoids. Advanced healthcare materials **2020**, e1901658.

[97] Klotz, B.J.; Oosterhoff, L.A.; Utomo, L.; Lim, K.S.; Vallmajo-Martin, Q.; Clevers, H.; Woodfield, T.B.F.; Rosenberg, A.J.W.P.; Malda, J.; Ehrbar, M. *et al.* A Versatile Biosynthetic Hydrogel Platform for Engineering of Tissue Analogues. Advanced Healthcare Materials **2019***, 8*.

[98] Mironov, V.; Trusk, T.; Kasyanov, V.; Little, S.; Swaja, R.; Markwald, R. Biofabrication: A 21st Century Manufacturing Paradigm. Biofabrication *, 1*. **2009**.

[99] Collins, S.D.; Yuen, G.; Tu, T.; Budzinska, M.A.; Spring, K.; Bryant, K.; Shackel, N.A. In Vitro Models of the Liver: Disease Modeling, Drug Discovery and Clinical Applications. In *Hepatocellular Carcinoma*.; Tirnitz-Parker, J.E.E., Ed.: Brisbane (AU), 2019.

[100] Kammerer, S. Three-Dimensional Liver Culture Systems to Maintain Primary Hepatic Properties for Toxicological Analysis in Vitro. Int. J. Mol. Sci. **2021***, 22*, 10214.

[101] Lehmann, V.; Schene, I.F.; Ardisasmita, A.I.; Liv, N.; Veenendaal, T.; Klumperman, J.; van der Doef, H.P.J.; Verkade, H.J.; Verstegen, M.M.A.; van der Laan, L.J.W. *et al.* The Potential and Limitations of Intrahepatic Cholangiocyte Organoids to Study Inborn Errors of Metabolism. J. Inherit. Metab. Dis. **2022***, 45*, 353-365.

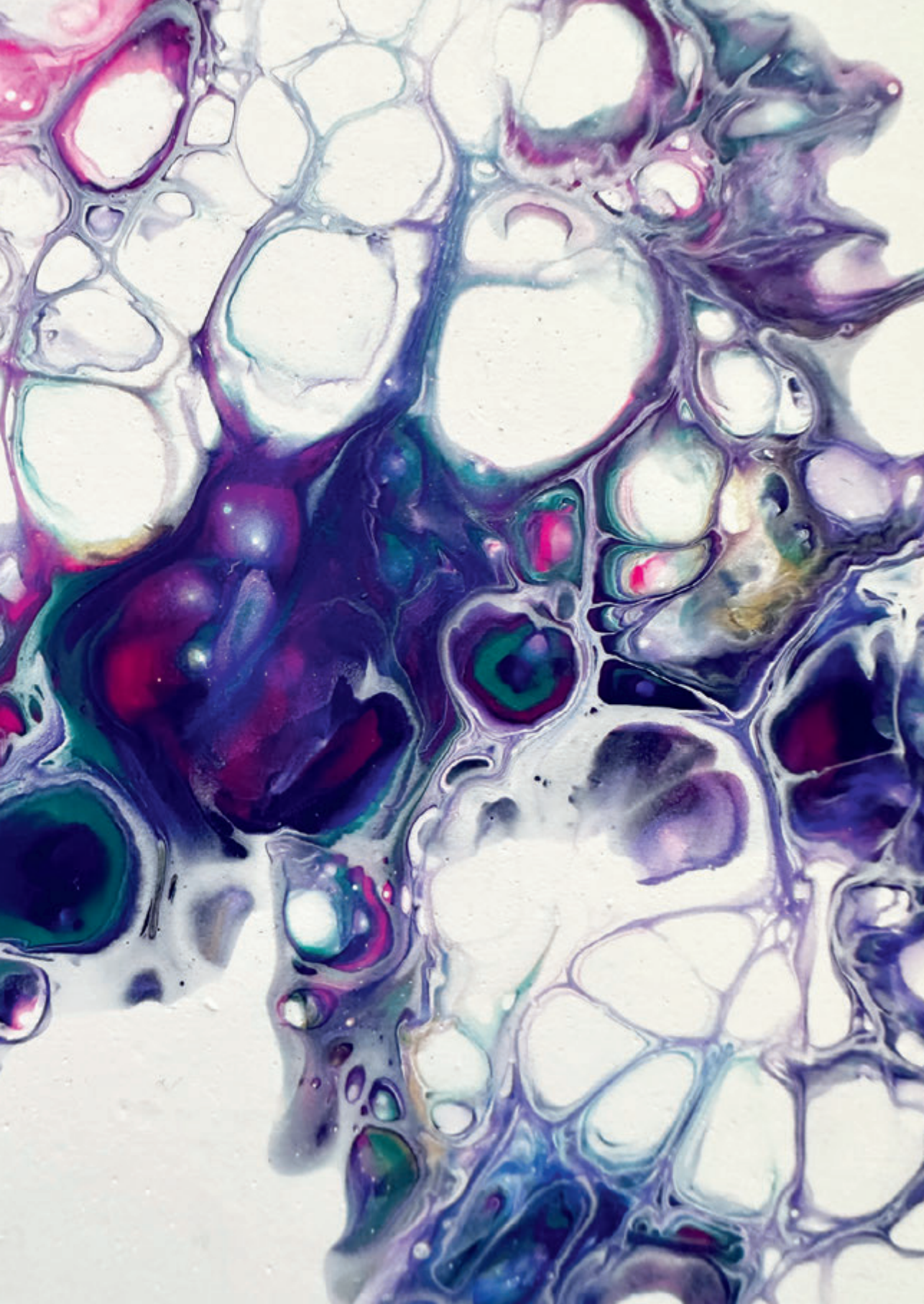

Drug Metabolism of Hepatocyte-Like Organoids and Their Applicability in In Vitro Toxicity Testing

Manon C. Bouwmeester[1], Yu Tao[1], Susana Proença[2,3], Frank G. van Steenbeek[1,4], Roos-Anne Samsom[1], Sandra M. Nijmeijer[3], Theo Sinnige[3], Luc J. W. van der Laan[5], Juliette Legler[3], Kerstin Schneeberger[1], Nynke I. Kramer[2,3,†] and Bart Spee[1,†]

1 Department of Clinical Sciences, Faculty of Veterinary Medicine, Regenerative Medicine Center Utrecht, Utrecht University, 3584 CT Utrecht, The Netherlands
2 Division of Toxicology, Wageningen University, 6700 EA Wageningen, The Netherlands;
3 Institute for Risk Assessment Sciences, Utrecht University, 3584 CM Utrecht, The Netherlands;
4 Department of Cardiology, Division Heart & Lungs, University Medical Center Utrecht, 3508 GA Utrecht, The Netherlands
5 Department of Surgery, Erasmus MC Transplant Institute, University Medical Center Rotterdam, 3015 CN Rotterdam, The Netherlands
† These authors contributed equally to this work.

Published in Molecules (2023); 28(2):621. doi: 10.3390/molecules28020621.

2

ABSTRACT

Emerging advances in the field of *in vitro* toxicity testing attempt to meet the need for reliable human-based safety assessment in drug development. Intrahepatic cholangiocyte organoids (ICOs) are described as a donor-derived *in vitro* model for disease modelling and regenerative medicine. Here, we explored the potential of hepatocyte-like ICOs (HL-ICOs) in *in vitro* toxicity testing by exploring the expression and activity of genes involved in drug metabolism, a key determinant in drug-induced toxicity, and the exposure of HL-ICOs to well-known hepatotoxi-cants. The current state of drug metabolism in HL-ICOs showed levels comparable to those of PHHs and HepaRGs for CYP3A4; however, other enzymes, such as CYP2B6 and CYP2D6, were expressed at lower levels. Additionally, EC50 values were determined in HL-ICOs for acetaminophen (24.0 - 26.8 mM), diclofenac (475.5 - >500 μM), perhexiline (9.7 - >31.5 μM), troglitazone (23.1 - 90.8 μM), and valproic acid (>10 mM). Exposure to the hepatotoxicants showed EC50s in HL-ICOs comparable to those in PHHs and HepaRGs; however, for acetaminophen exposure, HL-ICOs were less sensitive. Further elucidation of enzyme and transporter activity in drug metabolism in HL-ICOs and exposure to a more extensive compound set are needed to accurately define the potential of HL-ICOs in *in vitro* toxicity testing.

Keywords
Drug-induced liver injury; Hepatic *in vitro* model; Hepatotoxicity; Intrahepatic cholangiocyte organoids; Hepatocyte-like cells

INTRODUCTION

Drug metabolism is a key determinant in drug-induced toxicity [1]. The liver plays a crucial role in drug metabolism and is, therefore, susceptible to drug-induced injury. Despite the implementation of novel human-based strategies in drug development such as *in vitro* and *in silico* pre-clinical testing [2,3], drug-induced liver injury (DILI) remains a major cause for discontinuation of drug development and the withdrawal of drugs from the market [4]. Gaining human-relevant mechanistic insights into DILI is essential to improve toxicity prediction and further minimize adverse drug reactions.

The metabolism of drugs in the liver is generally a two-step process. In phase I, polar functional groups are added or opened up so that phase II enzymes can conjugate the drug to facilitate the drug's excretion. The cytochrome P450 (CYP) superfamily forms the most prominent and most studied family of phase I biotransformation enzymes [5]. CYP oxidation often leads to bioactivation and is associated with DILI [6]. Genetic polymorphisms in common human CYP isoforms, including CYP2B6, CYP2C9, and CYP2D6, are a common mechanism of adverse drug reactions requiring hospitalization [7,8]. Generally, phase II metabolism by uridine 5′ -diphospho-glucuronosyltransferases (UDP-glucuronosyltransferases, UGTs), sulfotransferases (SULTs), and glutathione transferases (GSTs) is a detoxification process, counteracting the reactivity of intermediate metabolites [9]. Hepatic transporters, including superfamilies ATP-binding cassette (ABC) transporters and solute carrier (SLC) transporters, are involved in the excretion of drugs and their conjugated metabolites. Inhibition of efflux transporters leading to intracellular accumulation is another risk factor for drug–drug interaction and DILI [10]. The activities of these two phases of drug metabolism and functionality of hepatic transporters are crucial in hepatotoxicity, as they are responsible for the (de)activation and excretion of chemicals [11,12].

Significant interspecies and interindividual differences in the expression and function of drug metabolism enzymes and transporters hamper accurate prediction of pharmacokinetics in patients and hepatotoxic potency of new drugs, as this is traditionally performed in animal models [13-15]. Over the years, the development of non-animal alternatives evolved to generate human-based toxicity data as well as to replace, reduce and refine animal use (3Rs) in safety evaluations [16,17]. To perform reliable human-based toxicity screens or mechanistic studies into DILI pathways, hepatic human *in vitro* models need to express morphological and functional features, such as drug metabolism, similar to an *in vivo* situation [18].

Human-based hepatic *in vitro* models have been developed using a range of cell sources, where primary human hepatocytes (PHHs), human hepatic cancer cell lines, and human stem cell-derived hepatocyte-like cells are three main hepatic cell sources used in current models [19,20]. In an effort to increase the *in vitro* toxicity prediction by these models, different approaches to enhance the physiological relevance and thereby maintain or improve hepatic function are being developed [21,22]. PHHs are considered the gold standard in *in vitro* toxicity testing, as their phenotype is most comparable to hepatocytes *in vivo*, which can be maintained longer due to advances in the culture method [23]. Besides interspecies differences in drug metabolism that are covered by the use of human-based *in vitro* models, interindividual differences in drug metabolism and thus drug sensitivity are of particular interest [6]. PHHs can represent real human population variability; however, their availability is limited and expansion is very difficult [24-26]. Donor-derived hepatic cell models, such as induced pluripotent stem cells (iPSCs) or adult stem cells (ASCs), can reflect the heterogenous phenotype of the human population and have the potential to be expanded for high-throughput purposes [27].

Human intrahepatic cholangiocyte organoids (ICOs) are liver-derived ASCs that form hollow polarized 3D structures *in vitro* and, once differentiated towards the hepatic lineage, show an increased expression of hepatic markers such as albumin, CYP enzymes, and transporters [28]. The applicability of these hepatocyte-like ICOs (HL-ICOs) for disease modelling and regenerative medicine has been described [29-32]; however, the potential of HL-ICOs as a novel cell model for DILI still needs to be explored [33]. Here, we sought to explore the potential of HL-ICOs for *in vitro* toxicity testing compared to PHHs and the tumor-derived hepatic cell line HepaRG. We focused on the expression of genes involved in phase I and II drug metabolism and hepatic transporters and phase I enzyme and UGT activity. Additionally, we tested a set of known hepatotoxic compounds, namely acetaminophen, diclofenac, perhexiline, troglitazone, and valproic acid, to study cytotoxicity after exposure.

RESULTS

Intrahepatic cholangiocyte organoids (ICOs) were cultured in conventional Matrigel™ (Matrigel) droplets and differentiated towards the hepatic lineage. After differentiation, hepatocyte-like ICOs (HL-ICOs) formed polarized 3D structures with a hollow lumen with a submembranous positivity for F-actin (Figure 1). The hepatic differentiation status of HL-ICOs indicated an increase in hepatic markers including albumin and CYP3A4 (Supplemental Figure S1), comparable to previous studies [28,31,34]. The hepatic cell line HepaRG was cultured in standard 2D monolayer, and PHHs were cultured as monolayer in

a collagen I sandwich (Figure 1), both with an F-actin located on intercellular filaments.

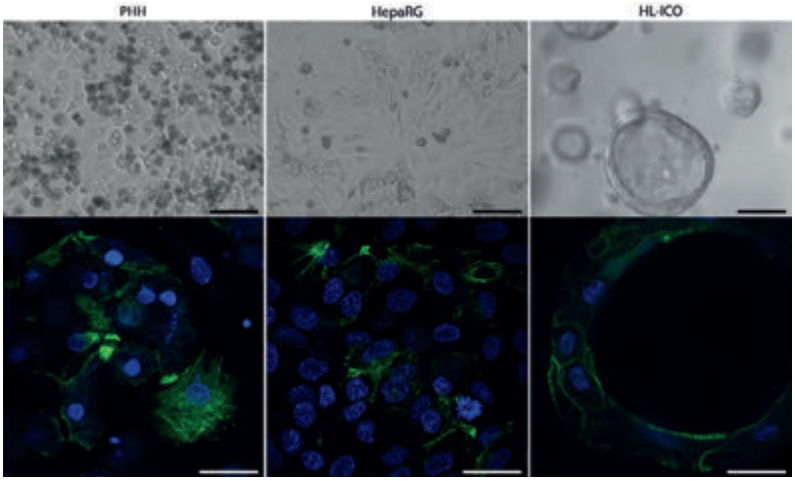

Figure 1. Morphology of primary human hepatocytes (PHHs), hepatic cell line HepaRG and hepatocyte-like intrahepatic cholangiocyte organoids (HL-ICOs) on differentiation day 12. Top: Brightfield pictures of morphology. Scale bar = 100 µm. Bottom: Phalloidin staining (green) of filamentous actin. Scale bar = 25 µm.

Expression of Phase I, and II Enzymes and Hepatic Transporters

Gene expression levels of selected key genes involved in phase I and II drug metabolism and hepatic transporters were examined in liver tissue from two donors, primary human hepatocytes, differentiated HepaRG and ICOs (3 donors) in expansion condition (EM), and hepatic differentiation condition (DM day 5 and 12).

Expression levels in ICOs of most phase I enzymes including major cytochrome P450 enzymes, such as CYP1A2, CYP2B6, and CYP2D6, improved upon hepatocyte differentiation but showed low expression compared to PHHs and HepaRGs (Figure 2). Expression of major CYP enzymes CYP3A4 and CYP2C9 increased upon ICO differentiation, where expression levels at day 12 of differentiation were higher compared to HepaRGs. CYP1A1 expression levels also increased upon differentiation of ICOs, where expression levels at day 12 of differentiation were higher compared to PHHs and HepaRGs. Other upregulated genes upon hepatic differentiation compared to expansion condition were (among others) CYP2C19, CES1, FMO4, and FMO5 in phase I, UGT2B7, UGT2B11, SULT1C2 in phase II, and transporters ABCG2, ABCB1, and ABCB11 (Figure 2). Hepatic transporters ABCB1, ABCB11, and ABCB8 were more highly expressed in HL-ICOs compared to HepaRGs.

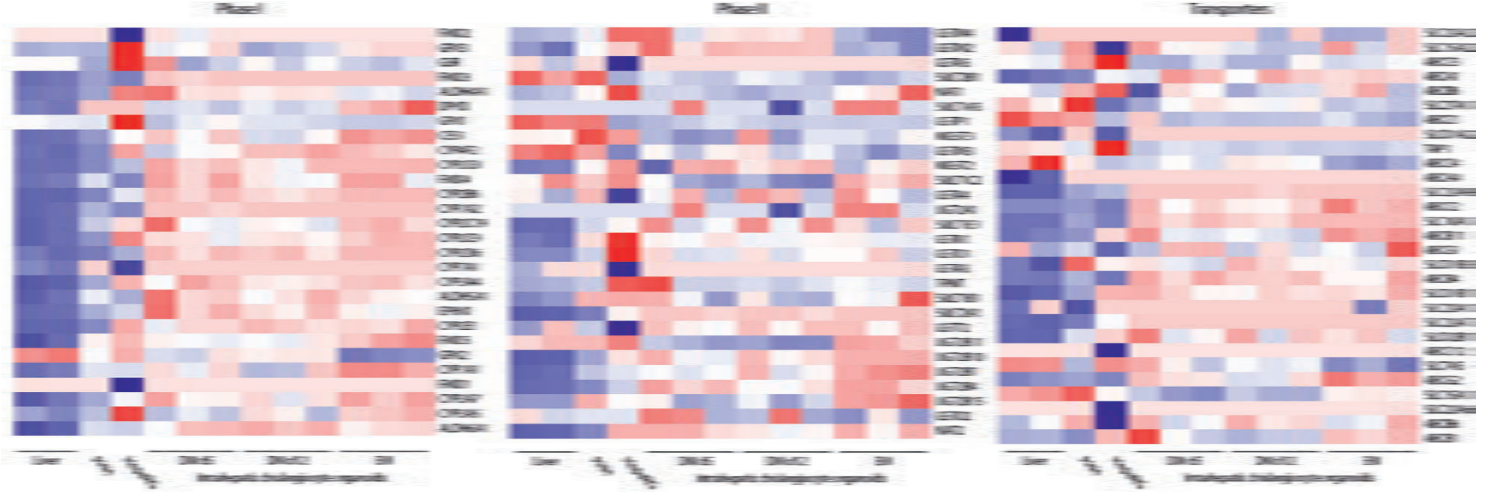

Figure 2. Heatmap showing the mRNA expression of intrahepatic cholangiocyte organoids from three independent donors in expansion (EM) and after hepatocyte differentiation (DM day 5 and day 12) compared with that of liver tissue, primary human hepatocytes (PHHs) and HepaRGs involved in drug metabolism (phase I (n = 28), phase II (n = 28), and transport (n = 29)). Red indicates low expression. Blue indicates high expression.

Interindividual differences between the three ICO donors could be observed in (among others) phase I enzymes CYP2C8, CYP2C19, CYP3A5, and CES1, phase II enzymes SULT1B1, UGT2B15, UGT2A1, SULT1A3, and transporters ABCB6, ABCG1, ABCB8, and SLCO2B1.

CYP family members were thoroughly studied to examine their role in DILI, especially the members most abundantly present in humans: CYP3A4, CYP2E1, CYP2C9, CYP2C8, and CYP1A2. Based on the increased expression of these CYP enzymes, differentiation day 12 was selected for further experiments. Due to practical considerations, four different ICO donors were used in further experiments.

Phase I and II Enzyme Activity

The activities of cytochrome P450 enzymes 1A2, 2B6, 2C9, 2D6, 2E1, and 3A4 and UGT were examined in the three hepatic cell models. Cells were exposed to two cocktails of, in total, seven specific enzyme substrates. Metabolite formation was used as a measure for activity of the specific CYP enzyme and UGT (Figure 3). For each cell model, metabolite formation was measured at three timepoints, which differed per hepatic cell model (HL-ICOs: 4, 8, 24 h; PHH: 1, 2, 4 h; HepaRG: 2, 4, 8 h). Metabolite formation rates were calculated using the linear correlation of formed metabolite (pmol/106 cells) in time (Table 1).

Activity could not be determined in HL-ICOs for CYP2B6, CYP2C9, CYP2D6, and CYP2E1, as there was no metabolite formation. The chlorzoxazone metabolite (6-hydroxy-chlorzoxazone formed by CYP2E1) was also not formed by PHHs, and in HepaRG cells only in one (out of three) experiments at the last timepoint (8 h) of incubation, indicating low activity for CYP2E1 (data not shown). Metabolite formation by CYP2B6 (hydroxybupropion), CYP2C9 (4-hydroxytolbutamide), and CYP2D6 (dextrorphan) in both HepaRGs and PHHs showed a linear trend (Supplemental Figure S2). In all three systems, depletion of bupropion was observed in control (no cells; data not shown), indicating degradation due to other components in the system, such as binding to the polystyrene culture plate.

CYP1A2 activity in HL-ICOs only showed metabolite (acetaminophen) formation in two of the four donors at the last timepoint (24 h) of incubation (Figure 3). CYP1A2 activity in HepaRGs was not consistent over the three independent experiments, as in one of the three experiments no metabolite was formed. CYP1A2 activity in PHHs was highest compared to the other two hepatic cell models. CYP3A4 activity in HL-ICOs showed interindividual variation, as one of the four tested donors showed CYP3A4 activity comparable to PHHs (Figure

3; Table 1). CYP3A4 activity in the other three donors was comparable to HepaRGs. Glucuronidation of 7-hydroxycoumarin by UGT showed complete depletion of parent compound 7-hydroxycoumarin in all three hepatic models. In PHHs and HepaRGs, metabolite formation was to the same extent as the parent compound; however, in HL-ICOs, metabolite formation was only 24–72% of the parent compound (data not shown). UGT activity in HL-ICOs was lower compared to PHHs and HepaRGs and was variable between the different ICO donors (Figure 3; Table 1).

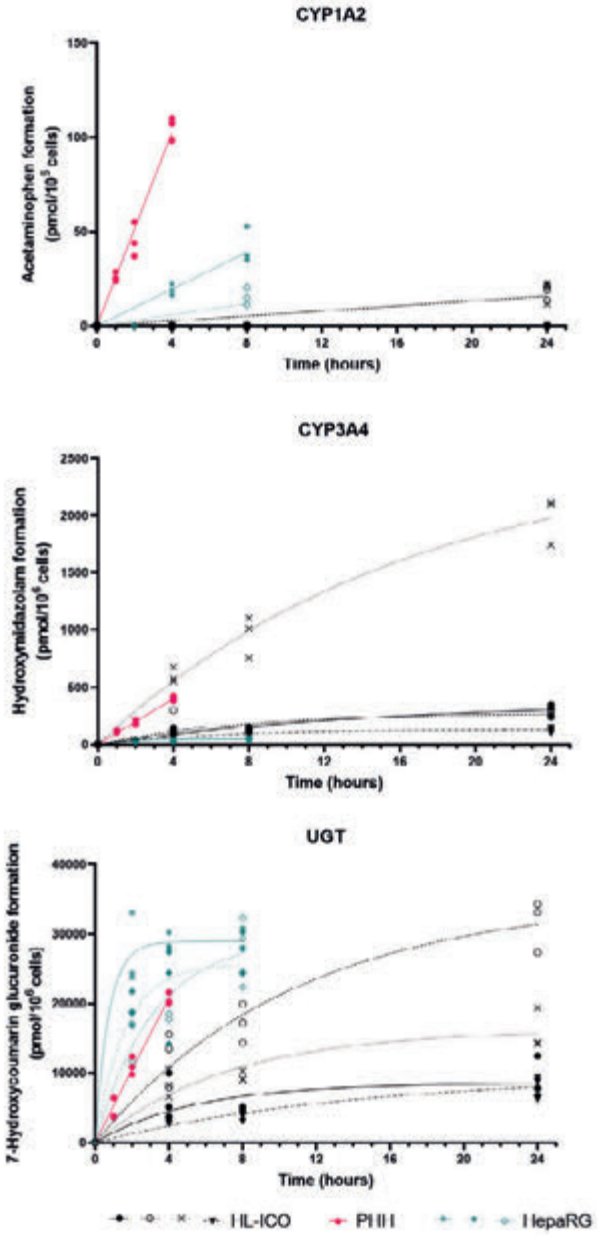

Figure 3. Metabolite formation as a measure of enzyme activity in hepatocyte-like intrahepatic cholangiocyte organoids (HL-ICOs) on differentiation day 12, primary human hepatocytes (PHHs), and HepaRG cells. HL-ICO: each black symbol indicates a different donor (n = 4). HepaRG: Each green symbol represents an independent experiment. PHH: Technical triplicates are shown in pink.

Table 1. Comparison of enzyme-specific metabolite formation rates in HL-ICOs, PHHs and HepaRG.

	HL-ICOs				PHH	HepaRG
CYP1A2	nd	0.01249	0.01293	nd	0.4269	0.03237 (nd - 0.08552)
CYP2B6	nd	nd	nd	nd	50.13	1.228 (0.9913 - 1.358)
CYP2C9	nd	nd	nd	nd	15.33	2.161 (1.365 - 2.521)
CYP2D6	nd	nd	nd	nd	9.601	0.1656 (0.1567 - 0.2866)
CYP2E1	nd	nd	nd	nd	nd	nd
CYP3A4	0.3294	0.3603	2.098	0.2278	1.680	0.3136 (0.2645 - 0.3296)
UGT	13.18	38.93	22.89	8.778	86.79	158.9 (132.6 - 225.4)

Values presented are the metabolite formation rates (pmol/min/10^6 cells). Hepatocyte-like ICOs (HL-ICOs; differentiation day 12): values are calculated per donor. PHH: Value represents the mean of a technical triplicate. HepaRG: Value represents median of three independent experiments, minimum and maximum formation rate within brackets. nd: not determinable (i.e., no metabolite formation).

Table 2. Determined EC50 values in HL-ICOs, PHH, and HepaRGs.

	HL-ICOs				PHH	HepaRG
Acetaminophen	24,870	24,630	26,840	24,010	4,186	4,036 (3,465 - 6,045)
Diclofenac	>500	>500	>500	475.5	421.2	351.7 (272.4 - 434.9)
Perhexiline	>31.5	9.675	>31.5	>31.5	8.072	25.97 (10.45 - 26.37)
Troglitazone	42.80	90.83	23.13	24.40	57.09	45.15 (14.89 - 45.17)
Valproic Acid	>10,000	>10,000	>10,000	>10,000	9,885	4,582 (4,168 - 6,066)

Values in µM. HepaRG cells: the median value of three independent experiments is shown with the minimum and maximum EC50 within brackets. HL-ICOs (differentiation day 12): determined EC50 values are shown for each donor separately.

Cytotoxicity

HL-ICOs (four independent donors), PHHs, and the hepatic cell line HepaRG (three independent experiments) were exposed to five known hepatotoxic compounds for 48 h (Table 2; Figure 4). Concentration ranges differed per compound but were the same for the different hepatic cell models.

The determined EC50 of acetaminophen for the four ICO donors (24.01 - 24.87 mM) was higher compared to that for PHHs (4.19 mM) and the hepatic cell line HepaRG (ranging from 3.46 to 6.04 mM). For diclofenac, the EC50 was determined for only one of the tested ICO donors (475.5 μM), while for the other three ICO donors, the EC50 was higher than the highest tested concentration (500 μM). The EC50 of diclofenac for PHHs (421.2 μM) and HepaRGs (ranging from 272.4 to 434.9 μM) was fairly similar. Perhexiline exposure showed no cytotoxicity in three ICO donors; in one donor, cytotoxicity was observed in the highest concentration (32 μM; EC50 of 9.675 μM). PHHs and HepaRGs had a similar cytotoxicity curve (PHH: 8.072 μM; HepaRG: ranging from 10.45 to 26.37 μM). The determined EC50 of troglitazone in HL-ICOs and HepaRGs was in the same range and followed a similar trend (HL-ICOs: ranging from 23.13 - 90.83 μM; HepaRG: ranging from 14.89 to 45.17 μM). The EC50 of valproic acid could not be determined in HL-ICOs (PHH: 9.88 mM; HepaRG: ranging from 4.17 to 6.07 mM).

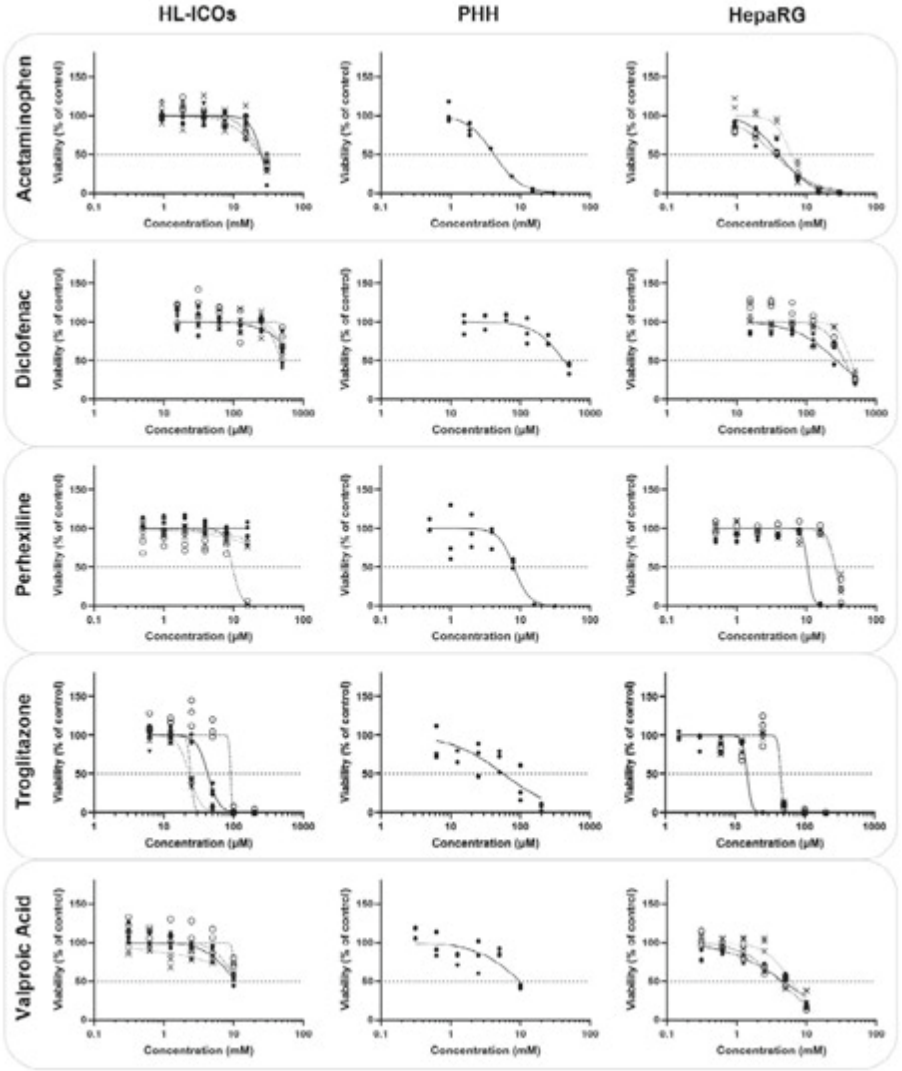

Figure 4. Sensitivity to known hepatotoxic compounds of HL-ICOs, PHHs, and HepaRGs. PHHs, HepaRG cells, and HL-ICOs (differentiation day 12) were exposed to acetaminophen, diclofenac, perhexiline, troglitazone, and valproic acid for 48 h (single dose). Data are presented as the percentage relative to the viability of (vehicle-treated) controls. For PHHs, one replicate experiment is shown. For HepaRG cells, three replicate experiments (different symbols) are shown (replicate experiments can be different between tested compounds). For HL-ICOs, four replicate experiments using different donors are shown, represented by different symbols. For all cell models, three replicate measurements per concentration are shown. Dashed line indicates 50% viability.

DISCUSSION

Emerging advances in the field of *in vitro* and *in silico* toxicity testing attempt to meet the need for reliable human-based safety assessment in drug development [35,36]. Well-established *in vitro* models, such as PHHs or human hepatic cancer cell lines, are used for high-throughput toxicity screens [37-39] and/or in studies of the mechanisms driving DILI [40]. Intrahepatic cholangiocyte organoids (ICOs) have been recently described as a donor-derived hepatic *in vitro* model with potential in disease modelling and regenerative medicine [29]. Here, we explored the potential of liver-derived hepatocyte-like ICOs (HL-ICOs) in *in vitro* toxicity testing by quantifying the expression and activity of genes involved in drug metabolism and exposure to well-known hepatotoxicants.

Drug metabolism is of particular interest due to (de)toxification of compounds in the liver by phase I or phase II enzymes and excretion of compounds by hepatic transporters [6,12]. Two timepoints of hepatic differentiation of ICOs were included in the RNAseq analysis, as hepatic markers are known to rise and fall asynchronously, resulting in no optimal differentiation day for all markers [34]. Based on increased expression levels of CYP enzymes and hepatic transporters on the late differentiation day (d12), further experiments were executed in this differentiation window. In ICOs, the gene expression of abundant CYP enzymes in human CYP2B6, CYP2C9, and CYP2D6 improved upon hepatic differentiation; however, expression was lower than in PHHs. This was reflected in the CYP activity results, even though different ICO donors were used. CYP3A4 expression, which is responsible for metabolism of most therapeutic categories [5], was increased upon differentiation to levels higher than in HepaRG, which was reflected in the CYP activity data. One donor reached a formation rate comparable to PHHs, indicating the interindividual differences in CYP expression [5]. Even though CYP2D6 and CYP2C9 are highly variable in the human population [8], the used ICO donors did not show activity of these enzymes, as metabolite formation was not measurable. Expression of phase II enzymes in ICOs was generally higher than that of phase I enzymes. Notably, we observed relatively high expression of phase II enzymes in HL-ICOs compared to PHHs and HepaRGs, such as UGT2B11, UGT2B15, SULT1C2, and SULT1B1, suggesting differential activity in phase II metabolism pathways, as was observed by 7-hydroxycoumarin metabolite formation [41].

In order to further elucidate the potential of HL-ICOs in *in vitro* toxicity testing, the sensitivity of HL-ICOs to five well-known hepatotoxicants with different mechanisms of action was examined [42]. The three cell models were exposed to acetaminophen, a classic example of intrinsic DILI due to its predictable and dose-dependent toxicity [43]. The formation of its toxic metabolite NAPQI,

catalyzed by CYP2E1, CYP3A4, and CYP1A2, is known to cause subsequent glutathione depletion [43,44]. However, we did not see a donor difference regarding the ICO donor with high CYP3A4 activity. The established EC50 in HL-ICOs was five-fold higher than those in PHHs and HepaRGs (which were comparable to the literature [19]). This difference could possibly be due to different media compositions (high levels of glutathione increase NAPQI conjugation) or increased activity in the alternative glucuronidation and sulfation pathways, as previously mentioned [44-46]. Exposure to the non-steroidal anti-inflammatory drug (NSAID) diclofenac showed that the sensitivity of one ICO donor was comparable to that of HepaRGs and PHHs [19]. Although no metabolite formation was measurable for CYP2C9 activity in HL-ICOs, the diclofenac data suggested that this specific donor did have CYP2C9 activity, as this CYP enzyme is involved in the bioactivation of diclofenac [47]. Perhexiline is a coronary vasodilator that was withdrawn from the market due to hepatotoxicity and neurotoxicity. The exact mechanism of perhexiline toxicity has not yet been clarified; however, it is suggested that perhexiline hepatotoxicity is mostly caused by the parent drug and that CYP2D6 is involved in the detoxification [48,49]. The observed cytotoxicity for PHHs and HepaRGs and one ICO donor was comparable to the literature [48]. Notably, no cytotoxicity was observed in three ICO donors, while higher toxicity was expected in a system with low metabolism [49,50]. Troglitazone, a thiazolidinedione derivative, is known to cause parent compound toxicity, but its metabolites also cause toxicity, such as inhibition of hepatic transporter BSEP, resulting in intrahepatic cholestasis [51]. Established EC50s by troglitazone exposure were comparable to those reported in the literature [19], even though a different trend was observed for PHHs compared to HepaRGs and HL-ICOs. Slight interindividual differences in cytotoxicity were observed between the ICO donors; however, this could not be linked to CYP and UGT activity data in this study. In the literature, troglitazone cytotoxicity cannot be correlated to CYP activity either; however, sulfotransferases possibly play a role in its cytotoxicity [52,53]. Anticonvulsant valproic acid hepatotoxicity is mainly caused by its metabolites, resulting in drug-induced steatosis [54]. Toxic metabolite formation is catalyzed by CYP2C9 and CYP2B6, the activity of which could not be measured in HL-ICOs. For HL-ICOs, an EC50 could not be established; however, the trend seems comparable to that of PHHs.

To improve the comparison between different cell systems, it is essential to determine the concentration that is actually available to be taken up by the cells in the *in vitro* system. In the case of lipophilic compounds such as perhexiline, *in vitro* system components such as Matrigel or medium components can decrease this available concentration [55,56]. In the case of bupropion (CYP2B6 activity), abiotic degradation of the compound was observed, especially in the

HL-ICOs. Determining the real *in vitro* dose facilitates reliable extrapolation of *in vitro* data towards *in silico* models [18,57].

The current state of drug metabolism in HL-ICOs showed comparable levels for, among others, CYP3A4. However, the expression and activity of other enzymes, such as CYP2B6 and CYP2D6, need improvement in HL-ICOs compared to PHHs and HepaRGs. The donor-derived origin of the HL-ICOs was clearly represented in the CYP3A4, CYP1A2, and UGT activity data and in gene expression levels, such as for CYP2C8, CES1, and SLCO2B1, which are known to have polymorphisms [8,58,59]. Genotyping ICOs of different donors would give more insight into the donor differences and enable the selection of a panel of donors with slow/fast metabolizers or specific polymorphisms associated with DILI [47]. Moreover, extending the set of donors could also provide insight into sex-specific drug responses [60]. A more mechanistic approach would help in further characterization of HL-ICOs as an *in vitro* toxicity model [40,61]. Recent papers explored the potential of HL-ICOs with a more mechanistic approach to study the applicability of HL-ICOs as an *in vitro* model for cholestasis [62] and phospholipidosis [31]. While bile production in ICOs was shown to be low compared to HepaRGs and PHHs, ICOs were more sensitive in drug-induced phospholipidosis screening compared to HepG2 cells. A unique feature of HL-ICOs is their polarization and relative expression of hepatic transporters compared to PHHs, suggesting possibilities for HL-ICOs in toxicity screens involving transporters that are important in toxicity prediction [63]. Further characterization of the functionality of HL-ICOs, for example, using a comprehensive phase II enzyme activity assay [64,65], and their predictive potential to compound toxicity using a more extensive set of test compounds and readouts in a high-throughput fashion [66,67], will illustrate their potential in *in vitro* toxicity testing.

CONCLUSIONS

Here, we explored the levels of drug metabolism in hepatocyte-like intrahepatic cholangiocyte organoids and their potential in *in vitro* toxicity testing. We found that although the hepatic differentiation and the expression and activity of most drug metabolizing enzymes in ICOs were still below that of PHHs and HepaRGs, HL-ICOs could be a valuable platform for individualized toxicity screenings in the future. Further elucidation of enzyme and transporter activity in drug metabolism in HL-ICOs is needed to better define their potential. Additionally, exposure to a more extensive compound set including subtoxic concentrations and mechanistic studies would give more insight into the specific application of HL-ICOs in *in vitro* toxicity testing.

EXPERIMENTAL SECTION

Cell Culture

LiverPool cryoplateable hepatocytes (pool of 10 donors, mixed gender; BioIVT, Hicksville, NY, USA) were cultured in a collagen I (Sigma-Aldrich, St Louis, MO, USA) sandwich in INVITROGRO CP medium (BioIVT) complemented with the TORPEDO Antibiotic mix (BioIVT). Seeding density was 49,000 cells/well in a 96-well plate (cytotoxicity assay) or 350,000 cells/well in a 24-well plate (CYP activity assay), according to the manufacturer's instructions. Exposure of the hepatocytes was started 48 h after seeding. For exposure assays, INVITROGRO HI medium (BioIVT) was used, as rec-ommended.

Undifferentiated HepaRG cells were purchased from Biopredic International (Saint Grégoire, France). Cells were cultured (passage number between p18 and p28) in T75 flasks in culture medium consisting of William's E medium (without phenol red; Thermo Fisher Scientific, Waltham, MA, USA) supplemented with 1% (v/v) penicillin-streptomycin (Thermo Fisher Scientific), 10% (v/v) fetal bovine serum (FBS; Thermo Fisher Scientific), 50 µM hydrocortisone 21-hemisuccinate (Sigma-Aldrich, St Louis, MO, USA), 2 mM GlutaMax (Thermo Fisher Scientific) and 5 µg/mL insulin (Sigma-Aldrich). For differentiation, cells were cultured for 7–10 days and upon confluence, the monolayer was switched to differentiation medium (culture medium supplemented with 1% (v/v) DMSO). After differentiation, cells were trypsinized using TrypLE (Thermo Fisher Scientific) and seeded at a density of 65,000 cells/well in a 96-well plate (cytotoxicity assay) or 130,000 cells/well in a 24-well plate (CYP activity assay). Cells were allowed to attach for 24 to 48 h. Before exposure, cells were washed with assay medium (culture medium without FBS), after which exposure was started.

Intrahepatic cholangiocyte organoids (ICOs) were isolated from healthy liver biopsies that were obtained during liver transplantation at the Erasmus Medical Center Rotterdam in accordance with the ethical standards of the institutional committee to use the tissue for research purposes (ethical approval number MEC 2014-060). The procedure was in accordance with the Helsinki Declaration of 1975, and informed consent in writing was obtained from each patient. Obtained human liver material was frozen down in Recovery Cell Freezing Medium for future experiments or used for organoid isolation directly. Organoid isolation is previously described [34]. In short, small pieces of tissue were enzymatically digested at 37 °C. The supernatant was collected every hour, and fresh enzyme-supplemented medium was added to the remaining tissue until only ducts and single cells were visible. Cells were washed with DMEM Glutamax (supplemented with 1% (v/v) FBS and 1% (v/v) P/S) and spun down at 453 g for 5 min.

The cell suspension was cultured in Matrigel™ (Corning, New York, NY, USA) droplets in expansion medium (EM) until organoids were formed, as previously described [28]. EM consisted of Advanced DMEM/F12 (Life Technologies) supplemented with 1% (v/v) penicillin-streptomycin (Life Technologies), 1% (v/v) GlutaMax (Life Technologies), 10 mM HEPES (4-(2-hydroxyethyl)-1-piperazineethanesulfonic acid, Life Technologies), 2% (v/v) B27 supplement without vitamin A (Invitrogen, Carlsbad, CA, USA), 1% (v/v) N2 supplement (Invitrogen), 10 mM nicotinamide (Sigma-Aldrich, St Louis, MO, USA), 1.25 mM N-acetylcysteine (Sigma-Aldrich), 10% (v/v) R-spondin-1 conditioned medium (the Rspo1-Fc-expressing cell line was a kind gift from Calvin J. Kuo), 10 µM forskolin (Sigma-Aldrich), 5 µM A83-01 (transforming growth factor beta inhibitor; Tocris Bioscience, Bristol, UK), 50 ng/mL EGF (Invitrogen), 25 ng/mL HGF (Peprotech, Rocky Hill, NJ, USA), 0.1 µg/mL FGF10 (Peprotech) and 10 nM recombinant human (Leu15)-gastrin I (Sigma-Aldrich). Medium was changed twice a week. Passaging occurred every 7–10 days at ratios ranging between 1:2 and 1:4. All cultures were kept in a humidified atmosphere of 95% air and 5% CO2 at 37 °C. Organoids were primed for differentiation with BMP7 (25 ng/mL, Peprotech) through spiking EM 3 days before shifting to hepatic differentiation medium (DM). DM consisted of EM without R-spondin-1, FGF10, and nicotinamide, supplemented with 100 ng/mL FGF19 (Peprotech), 500 nM A83-01 (Tocris Bioscience), 10 µM DAPT (Selleckchem, Munich, Germany), 25 ng/mL BMP-7 (Peprotech), and 30 µM dexamethasone (Sigma-Aldrich). Organoids were kept on DM for up to 12 days. For exposure experiments, differentiation assay medium was prepared to reduce antioxidants in the medium. This assay medium consisted of DMEM GlutaMAX instead of DMEM-F12 medium complemented with the same components as differentiation medium excluding GlutaMAX, B27, and NAC. In 96-well format (cytotoxicity assay), 12,000 cells in 9 µL Matrigel per well were plated at the start of differentiation, and exposure was started at day 10 of differentiation for 48 h. In 24-well format (CYP activity assay), cells were densely plated in a fresh Matrigel droplet (50 µL) upon the start of differentiation, and cells were exposed to the CYP substrate cocktail on day 12 of differentiation. The median cell count after CYP cocktail assay was 290,415 (46,968–812,410).

All cell cultures were performed in a humidified atmosphere with 5% CO2 at 37 °C. The cellular morphology of the three cell models was visualized by immunofluorescence staining with a filamentous actin (F-actin) probe conjugated to a photostable green-fluorescent Alexa Fluor 488 dye (ThermoFisher) using confocal laser scanning microscopy (SP8, Leica Microsystems, the Netherlands), as previously described [68].

Whole Genome RNA Sequencing

For mRNA sequencing, ICOs of three independent donors in expanding conditions and differentiated for 5 and 12 days were collected. Additionally, freshly isolated hepatocytes and liver tissue were used. RNA was isolated using the RNeasy Mini Kit (Qiagen, Hilden, Germany) according to the manufacturer's instructions. As previously described [34], Poly(A) Beads (NEXTflex, Bio Scientific, Austin, TX) were used to isolate the polyadenylated mRNA fraction. Sequencing libraries were prepared using the Rapid Directional RNA-Seq Kit (NEXTflex). Illumina NextSeq500 sequencing produced single-end 75-base-pair long reads. RNA-sequencing reads were mapped using STAR (v2.4.2a). Read groups were added to the BAM files with Picard's AddOrReplaceReadGroups (v1.98) and sorted with Sambamba (v0.4.5). Transcript abundances were quantified with HTSeq-count (v0.6.1p1) using the union mode. The raw files were uploaded to Gene Expression Omnibus (GEO) database (accession number GSE123498). RNA sequencing data of the HepaRG cell line were retrieved from the GEO database (accession number GSE14654). Genes important in drug metabolism were selected [69]. Heatmaps were generated using edgeR.

Cytochrome P450 Activity

CYP activity was assessed by the addition of a CYP substrate cocktail prepared in assay medium (see methods cell culture). Two CYP cocktail sets were prepared to expose the hepatic cell models (Table 3): set A included phenacetin (CYP1A2, 15 µM), midazolam (CYP3A4, 5 µM), dextromethorphan (CYP2D6, 15 µM), tolbutamide (CYP2C9, 20 µM); and set B included 7-hydroxycoumarin (UGT, 12 µM), chlorzoxazone (CYP2E1, 25 µM) and bupropion (CYP2B6, 20 µM) [70,71]. At three cell model-specific timepoints (PHHs: 1, 2, 4 h; HepaRGs: 2, 4, 8 h; ICOs: 4, 8, 24 h), 400 µL exposure medium was placed into glass vials containing 400 µL acidified MeOH (0.1% (v/v) formic acid). The samples were stored at −20 °C until analysis. Prior to LC-MS/MS analysis, samples were centrifuged for 10 min at 1250 g to precipitate any protein.

Standards for LC-MS/MS analysis of phenacetin, acetaminophen, midazolam, hydroxy-midazolam, dextromethorphan, dextrorphan, tolbutamide, 4-hydroxy-tolbutamide, 7-hydroxy-coumarin, 7-hydroxy-coumarin glucuronide, chlorzoxazone, 6-hydroxy-chlorzoxazone, bupropion, and hydroxy-bupropion were prepared in the same matrix as the medium extracts. All chemicals were obtained from Sigma-Aldrich. All previously listed substrates and metabolites were analyzed in a single run using a Shimadzu triple-quadrupole LCMS 8050 system with two Nexera XR LC-20AD pumps, a Nexera XR SIL-20AC autosampler, a CTO-20AC column oven, an FCV-20AH2 valve unit (Shimadzu, 's Hertogenbosch, the Netherlands). The substrates and metabolites were separated on a Synergi Polar-RP column (150 × 2.0 mm, 4 µm, 80 Å) with a 4

× 2 mm C18 guard column (4 × 2 mm; Phenomenex, Torrance, CA, USA). The mobile phase consisted of 0.1% (v/v) formic acid in Millipore (A) and 0.1% (v/v) formic acid in MeOH (pH 2.7; B), and was set as 100% A (0–1 min), 100% to 5% A (1–8 min), 5% A (8–9 min), 5% to 100% A (9–9.5 min), and 100% A (9.5–12.5 min). The total run time was 12.5 min, and the flow rate was 0.2 mL/min. Peaks were integrated using LabSolutions software.

Table 3. Information on enzyme activity cocktails.

	Enzyme	Parent Compound	CAS Number	Dosed Concentration (μM)
Cocktail A	CYP1A2	Phenacetin	62-44-2	15
		Acetaminophen	103-90-2	
	CYP3A4	Midazolam	59467-70-8	5
		Midazolam-OH	59468-90-5	
	CYP2D6	Dextromethorphan	125-71-3	15
		Dextrorphan	143-98-6	
	CYP2C9	Tolbutamide	64-77-7	20
		4OH-Tolbutamide	5719-85-7	
Cocktail B	UGT	7-OH Coumarin	93-35-6	12
		7-OH Coumarin Glucuronide	66695-14-5	
	CYP2E1	Chlorzoxazone	95-25-0	25
		6OH-Chlorzoxazone	1750-45-4	
	CYP2B6	Bupropion	31677-93-7	20
		OH-Bupropion	92264-81-8	

Cytotoxicity

Cells plated in 96-well plates were exposed to a concentration range (six concentrations in 2x dilution) of five known hepatotoxic compounds for 48 h (single dose). Acetaminophen (CAS 103-90-2; 30 mM) and valproic acid (CAS 1069-66-5; 10 mM) were directly dissolved in assay medium (previously described for each hepatic cell model). Diclofenac (CAS 15307-79-6; 100 mM), perhexiline (CAS 6724-53-4; 6.3 mM), and troglitazone (CAS 15307-79-6; TRC, Toronto, Canada; 40 mM) were dissolved in dimethyl sulfoxide (DMSO), which was 200x diluted in the highest exposure concentration. For the latter, vehicle

control (0.5% (v/v) DMSO) was used in the exposure experiments. All chemicals were obtained from Sigma-Aldrich, unless stated otherwise. Dose ranges of exposure: acetaminophen 0.94–30 mM; diclofenac 15.57–500 µM; perhexiline 0.5–31.5 µM; troglitazone 6.25–200 µM; valproic acid 0.31–10 mM.

Cell Viability

The viability of exposed cells was determined by cellular ATP levels using the CellTiter-Glo Luminescent Cell Viability Assay (Promega, Madison, WI, USA). The CellTiter Glo reagent was prepared according to the manufacturer's instructions. Briefly, the culture plate was equilibrated at room temperature for 30 min. Medium was removed from the plate, after which phosphate-buffered saline (PBS) and the CellTiter Glo reagent were added to each well in equal volumes. The plate was mixed for 2 min on an orbital shaker and incubated for an additional 10 min at room temperature. Luminescence was measured on the TriStar2 (Berthold Technologies, Bad Wildbad, Germany), and samples were normalized to (vehicle) control.

FUNDING STATEMENT

This work is part of the research program Applied and Engineering Sciences with project number 15498, which is financed by the Dutch Research Council (NWO).

AUTHOR CONTRIBUTIONS

Conceptualization, M.C.B., B.S., K.S. and N.I.K.; methodology, M.C.B., S.P., T.S., Y.T. and S.M.N.; formal analysis, F.G.v.S.; investigation, M.C.B., Y.T., R.-A.S., T.S. and S.M.N.; resources, L.J.W.v.d.L.; writing—original draft preparation, M.C.B.; writing—review and editing, B.S., N.I.K., Y.T., S.P., F.G.v.S., T.S., L.J.W.v.d.L., J.L. and K.S.; visualization, M.C.B., Y.T. and F.G.v.S.; supervision, B.S. and N.I.K.; funding acquisition, B.S. and N.I.K. All authors have read and agreed to the published version of the manuscript.

CONFLICTS OF INTEREST

The authors declare no conflict of interest.

SUPPLEMENTARY MATERIALS

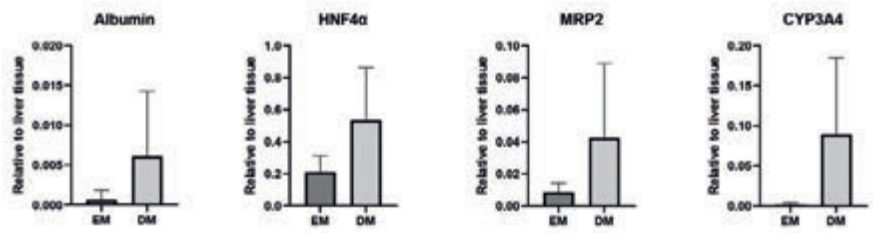

Figure S1. Gene expression of hepatic markers upon hepatic differentiation of ICOs. Gene expression levels are shown relative to levels in human liver tissue. EM: ICOs in expansion condition. DM: ICOs differentiated towards HL-ICOs. HNF4α, Hepatocyte Nucleus Factor 4 alpha; MRP2, Multi Resistance Protein 2; CYP3A4, Cytochrome P450 3A4. Expression is shown for multiple donors (n=6). Error bars represent the standard deviation.

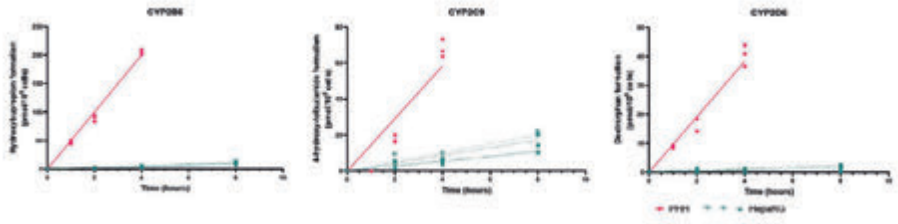

Figure S2. Metabolite formation of bupropion (CYP2B6), tolbutamide (CYP2C9), and dextrometrorphan (CYP2D6) in primary human hepatocytes and HepaRGs. HepaRG: Each green symbol represents an independent experiment. PHH: Technical triplicates are shown in pink.

REFERENCES

[1] Issa, N.T.; Wathieu, H.; Ojo, A.; Byers, S.W.; Dakshanamurthy, S. Drug Metabolism in Preclinical Drug Development: A Survey of the Discovery Process, Toxicology, and Computational Tools. Curr. Drug Metab. **2017**, *18*, 556-565.

[2] Sun, D.; Gao, W.; Hu, H.; Zhou, S. Why 90% of Clinical Drug Development Fails and how to Improve it? Acta Pharm. Sin. B. **2022**, *12*, 3049-3062.

[3] García-Cortés, M.; Ortega-Alonso, A.; Lucena, M.I.; Andrade, R.J.; Spanish Group for the Study of Drug-Induced Liver Disease (Grupo de Estudio para las Hepatopatías Asociadas a Medicamentos GEHAM).I. Drug-Induced Liver Injury: A Safety Review. Expert Opin. Drug Saf. **2018**, *17*, 795-804.

[4] Craveiro, N.S.; Lopes, B.S.; Tomás, L.; Almeida, S.F. Drug Withdrawal due to Safety: A Review of the Data Supporting Withdrawal Decision. Curr. Drug Saf. **2020**, *15*, 4-12.

[5] Zanger, U.M.; Schwab, M. Cytochrome P450 Enzymes in Drug Metabolism: Regulation of Gene Expression, Enzyme Activities, and Impact of Genetic Variation. Pharmacol. Ther. **2013**, *138*, 103-141.

[6] Utkarsh, D.; Loretz, C.; Li, A.P. In Vitro Evaluation of Hepatotoxic Drugs in Human Hepatocytes from Multiple Donors: Identification of P450 Activity as a Potential Risk Factor for Drug-Induced Liver Injuries. Chem. Biol. Interact. **2016**, *255*, 12-22.

[7] Wang, C.W.; Preclaro, I.A.C.; Lin, W.H.; Chung, W.H. An Updated Review of Genetic Associations with Severe Adverse Drug Reactions: Translation and Implementation of Pharmacogenomic Testing in Clinical Practice. Front. Pharmacol. **2022**, *13*, 886377.

[8] Zhou, S.F.; Liu, J.P.; Chowbay, B. Polymorphism of Human Cytochrome P450 Enzymes and its Clinical Impact. Drug Metab. Rev. **2009**, *41*, 89-295.

[9] Gan, J.; Ma, S.; Zhang, D. Non-Cytochrome P450-Mediated Bioactivation and its Toxicological Relevance. Drug Metab. Rev. **2016**, *48*, 473-501.

[10] Liu, H.; Sahi, J. Role of Hepatic Drug Transporters in Drug Development. J. Clin. Pharmacol. **2016**, *56 Suppl 7*, 11.

[11] Jetter, A.; Kullak-Ublick, G.A. Drugs and Hepatic Transporters: A Review. Pharmacol. Res. **2020**, *154*, 104234.

[12] Gu, R.; Liang, A.; Liao, G.; To, I.; Shehu, A.; Ma, X. Roles of Cofactors in Drug-Induced Liver Injury: Drug Metabolism and Beyond. Drug Metab. Dispos. **2022**, *50*, 646-654.

[13] Turpeinen, M.; Ghiciuc, C.; Opritoui, M.; Tursas, L.; Pelkonen, O.; Pasanen, M. Predictive Value of Animal Models for Human Cytochrome P450 (CYP)-Mediated Metabolism: A Comparative Study in Vitro. Xenobiotica **2007**, *37*, 1367-1377.

[14] Hammer, H.; Schmidt, F.; Marx-Stoelting, P.; Pötz, O.; Braeuning, A. Cross-Species Analysis of Hepatic Cytochrome P450 and Transport Protein Expression. Arch. Toxicol. **2021**, *95*, 117-133.

[15] Van Norman, G.A. Limitations of Animal Studies for Predicting Toxicity in Clinical Trials: Is it Time to Rethink our Current Approach? JACC Basic Transl. Sci. **2019**, *4*, 845-854.

[16] Krewski, D.; Acosta, D.,Jr; Andersen, M.; Anderson, H.; Bailar, J.C.,3rd; Boekelheide, K.; Brent, R.; Charnley, G.; Cheung, V.G.; Green, S.,Jr *et al.* Toxicity Testing in the 21st Century: A Vision and a Strategy. J. Toxicol. Environ. Health B Crit. Rev. **2010**, *13*, 51-138.

[17] Zink, D.; Chuah, J.K.C.; Ying, J.Y. Assessing Toxicity with Human Cell-Based in Vitro Methods. Trends Mol. Med. **2020**, *26*, 570-582.
[18] Yadav, J.; El Hassani, M.; Sodhi, J.; Lauschke, V.M.; Hartman, J.H.; Russell, L.E. Recent Developments in in Vitro and in Vivo Models for Improved Translation of Preclinical Pharmacokinetics and Pharmacodynamics Data. Drug Metab. Rev. **2021**, *53*, 207-233.
[19] Serras, A.S.; Rodrigues, J.S.; Cipriano, M.; Rodrigues, A.V.; Oliveira, N.G.; Miranda, J.P. A Critical Perspective on 3D Liver Models for Drug Metabolism and Toxicology Studies. Front. Cell. Dev. Biol. **2021**, *9*, 626805.
[20] Xu, Q. Human Three-Dimensional Hepatic Models: Cell Type Variety and Corresponding Applications. Front. Bioeng. Biotechnol. **2021**, *9*, 730008.
[21] Zhang, X.; Jiang, T.; Chen, D.; Wang, Q.; Zhang, L.W. Three-Dimensional Liver Models: State of the Art and their Application for Hepatotoxicity Evaluation. Crit. Rev. Toxicol. **2020**, *50*, 279-309.
[22] Kammerer, S. Three-Dimensional Liver Culture Systems to Maintain Primary Hepatic Properties for Toxicological Analysis in Vitro. Int. J. Mol. Sci. **2021**, *22*, 10214. doi: 10.3390/ijms221910214.
[23] Bell, C.C.; Hendriks, D.F.; Moro, S.M.; Ellis, E.; Walsh, J.; Renblom, A.; Fredriksson Puigvert, L.; Dankers, A.C.; Jacobs, F.; Snoeys, J. *et al.* Characterization of Primary Human Hepatocyte Spheroids as a Model System for Drug-Induced Liver Injury, Liver Function and Disease. Sci. Rep. **2016**, *6*, 25187.
[24] Zhang, K.; Zhang, L.; Liu, W.; Ma, X.; Cen, J.; Sun, Z.; Wang, C.; Feng, S.; Zhang, Z.; Yue, L. *et al.* In Vitro Expansion of Primary Human Hepatocytes with Efficient Liver Repopulation Capacity. Cell. Stem Cell. **2018**, *23*, 806-819.e4.
[25] Elaut, G.; Henkens, T.; Papeleu, P.; Snykers, S.; Vinken, M.; Vanhaecke, T.; Rogiers, V. Molecular Mechanisms Underlying the Dedifferentiation Process of Isolated Hepatocytes and their Cultures. Curr. Drug Metab. **2006**, *7*, 629-660.
[26] Kim, Y.; Lasher, C.D.; Milford, L.M.; Murali, T.M.; Rajagopalan, P. A Comparative Study of Genome-Wide Transcriptional Profiles of Primary Hepatocytes in Collagen Sandwich and Monolayer Cultures. Tissue Eng. Part C. Methods **2010**, *16*, 1449-1460.
[27] Akbari, S.; Arslan, N.; Senturk, S.; Erdal, E. Next-Generation Liver Medicine using Organoid Models. Front. Cell. Dev. Biol. **2019**, *7*, 345.
[28] Huch, M.; Gehart, H.; van Boxtel, R.; Hamer, K.; Blokzijl, F.; Verstegen, M.M.; Ellis, E.; van Wenum, M.; Fuchs, S.A.; de Ligt, J. *et al.* Long-Term Culture of Genome-Stable Bipotent Stem Cells from Adult Human Liver. Cell **2015**, *160*, 299-312.
[29] Prior, N.; Inacio, P.; Huch, M. Liver Organoids: From Basic Research to Therapeutic Applications. Gut **2019**, *68*, 2228-2237.
[30] Nuciforo, S.; Heim, M.H. Organoids to Model Liver Disease. JHEP Rep. **2020**, *3*, 100198.
[31] Lee, J.Y.; Han, H.J.; Lee, S.J.; Cho, E.H.; Lee, H.B.; Seok, J.H.; Lim, H.S.; Son, W.C. Use of 3D Human Liver Organoids to Predict Drug-Induced Phospholipidosis. Int. J. Mol. Sci. **2020**, *21*, 2982. doi: 10.3390/ijms21082982.
[32] He, C.; Lu, D.; Lin, Z.; Chen, H.; Li, H.; Yang, X.; Yang, M.; Wang, K.; Wei, X.; Zheng, S. *et al.* Liver Organoids, Novel and Promising Modalities for Exploring and Repairing Liver Injury. Stem Cell. Rev. Rep. **2022**, 1-13.
[33] Shiota, J.; Samuelson, L.C.; Razumilava, N. Hepatobiliary Organoids and their Applications for Studies of Liver Health and Disease: Are we there Yet? Hepatology **2021**, *74*, 2251-2263.

[34] Schneeberger, K.; Sánchez-Romero, N.; Ye, S.; van Steenbeek, F.G.; Oosterhoff, L.A.; Pla Palacin, I.; Chen, C.; van Wolferen, M.E.; van Tienderen, G.; Lieshout, R. *et al.* Large-Scale Production of LGR5-Positive Bipotential Human Liver Stem Cells. Hepatology **2020**, *72*, 257-270.

[35] Vinken, M.; Benfenati, E.; Busquet, F.; Castell, J.; Clevert, D.A.; de Kok, T.M.; Dirven, H.; Fritsche, E.; Geris, L.; Gozalbes, R. *et al.* Safer Chemicals using Less Animals: Kick-Off of the European ONTOX Project. Toxicology **2021**, *458*, 152846.

[36] Chang, X.; Tan, Y.M.; Allen, D.G.; Bell, S.; Brown, P.C.; Browning, L.; Ceger, P.; Gearhart, J.; Hakkinen, P.J.; Kabadi, S.V. *et al.* IVIVE: Facilitating the use of in Vitro Toxicity Data in Risk Assessment and Decision Making. Toxics **2022**, *10*, 232. doi: 10.3390/toxics10050232.

[37] Schadt, S.; Simon, S.; Kustermann, S.; Boess, F.; McGinnis, C.; Brink, A.; Lieven, R.; Fowler, S.; Youdim, K.; Ullah, M. *et al.* Minimizing DILI Risk in Drug Discovery - A Screening Tool for Drug Candidates. Toxicol. In. Vitro. **2015**, *30*, 429-437.

[38] Tolosa, L.; Gómez-Lechón, M.J.; Jiménez, N.; Hervás, D.; Jover, R.; Donato, M.T. Advantageous use of HepaRG Cells for the Screening and Mechanistic Study of Drug-Induced Steatosis. Toxicol. Appl. Pharmacol. **2016**, *302*, 1-9.

[39] Vorrink, S.U.; Zhou, Y.; Ingelman-Sundberg, M.; Lauschke, V.M. Prediction of Drug-Induced Hepatotoxicity using Long-Term Stable Primary Hepatic 3D Spheroid Cultures in Chemically Defined Conditions. Toxicol. Sci. **2018**, *163*, 655-665.

[40] Arnesdotter, E.; Gijbels, E.; Dos Santos Rodrigues, B.; Vilas-Boas, V.; Vinken, M. Adverse Outcome Pathways as Versatile Tools in Liver Toxicity Testing. Methods Mol. Biol. **2022**, *2425*, 521-535.

[41] Feng, W.Y.; Wen, J.; Stauber, K. In Vitro Drug Metabolism Investigation of 7-Ethoxycoumarin in Human, Monkey, Dog and Rat Hepatocytes by High Resolution LC-MS/MS. Drug Metab. Lett. **2018**, *12*, 33-53.

[42] Dragovic, S.; Vermeulen, N.P.E.; Gerets, H.H.; Hewitt, P.G.; Ingelman-Sundberg, M.; Park, B.K.; Juhila, S.; Snoeys, J.; Weaver, R.J. Evidence-Based Selection of Training Compounds for use in the Mechanism-Based Integrated Prediction of Drug-Induced Liver Injury in Man. Arch. Toxicol. **2016**, *90*, 2979-3003.

[43] James, L.P.; Mayeux, P.R.; Hinson, J.A. Acetaminophen-Induced Hepatotoxicity. Drug Metab. Dispos. **2003**, *31*, 1499-1506.

[44] Yoon, E.; Babar, A.; Choudhary, M.; Kutner, M.; Pyrsopoulos, N. Acetaminophen-Induced Hepatotoxicity: A Comprehensive Update. J. Clin. Transl. Hepatol. **2016**, *4*, 131-142.

[45] Court, M.H.; Zhu, Z.; Masse, G.; Duan, S.X.; James, L.P.; Harmatz, J.S.; Greenblatt, D.J. Race, Gender, and Genetic Polymorphism Contribute to Variability in Acetaminophen Pharmacokinetics, Metabolism, and Protein-Adduct Concentrations in Healthy African-American and European-American Volunteers. J. Pharmacol. Exp. Ther. **2017**, *362*, 431-440.

[46] Kurogi, K.; Rasool, M.I.; Alherz, F.A.; El Daibani, A.A.; Bairam, A.F.; Abunnaja, M.S.; Yasuda, S.; Wilson, L.J.; Hui, Y.; Liu, M. SULT Genetic Polymorphisms: Physiological, Pharmacological and Clinical Implications. Expert Opin. Drug Metab. Toxicol. **2021**, *17*, 767-784.

[47] Daly, A.K.; Aithal, G.P.; Leathart, J.B.; Swainsbury, R.A.; Dang, T.S.; Day, C.P. Genetic Susceptibility to Diclofenac-Induced Hepatotoxicity: Contribution of UGT2B7, CYP2C8, and ABCC2 Genotypes. Gastroenterology **2007**, *132*, 272-281.

[48] Ren, Z.; Chen, S.; Pak, S.; Guo, L. A Mechanism of Perhexiline's Cytotoxicity in Hepatic Cells Involves Endoplasmic Reticulum Stress and p38 Signaling Pathway. Chem. Biol. Interact. **2021**, *334*, 109353.
[49] Sørensen, L.B.; Sørensen, R.N.; Miners, J.O.; Somogyi, A.A.; Grgurinovich, N.; Birkett, D.J. Polymorphic Hydroxylation of Perhexiline in Vitro. Br. J. Clin. Pharmacol. **2003**, *55*, 635-638.
[50] Barclay, M.L.; Sawyers, S.M.; Begg, E.J.; Zhang, M.; Roberts, R.L.; Kennedy, M.A.; Elliott, J.M. Correlation of CYP2D6 Genotype with Perhexiline Phenotypic Metabolizer Status. Pharmacogenetics **2003**, *13*, 627-632.
[51] Jaeschke, H. Troglitazone Hepatotoxicity: Are we Getting Closer to Understanding Idiosyncratic Liver Injury? Toxicol. Sci. **2007**, *97*, 1-3.
[52] Hewitt, N.J.; Lloyd, S.; Hayden, M.; Butler, R.; Sakai, Y.; Springer, R.; Fackett, A.; Li, A.P. Correlation between Troglitazone Cytotoxicity and Drug Metabolic Enzyme Activities in Cryopreserved Human Hepatocytes. Chem. Biol. Interact. **2002**, *142*, 73-82.
[53] Saha, S.; New, L.S.; Ho, H.K.; Chui, W.K.; Chan, E.C.Y. Direct Toxicity Effects of Sulfo-Conjugated Troglitazone on Human Hepatocytes. Toxicol. Lett. **2010**, *195*, 135-141.
[54] Ezhilarasan, D.; Mani, U. Valproic Acid Induced Liver Injury: An Insight into Molecular Toxicological Mechanism. Environ. Toxicol. Pharmacol. **2022**, *95*, 103967.
[55] Dimitrijevic, D.; Fabian, E.; Nicol, B.; Funk-Weyer, D.; Landsiedel, R. Toward Realistic Dosimetry in Vitro: Determining Effective Concentrations of Test Substances in Cell Culture and their Prediction by an in Silico Mass Balance Model. Chem. Res. Toxicol. **2022**.
[56] Kang, H.K.; Sarsenova, M.; Kim, D.; Kim, M.S.; Lee, J.Y.; Sung, E.; Kook, M.G.; Kim, N.G.; Choi, S.W.; Ogay, V. *et al.* Establishing a 3D in Vitro Hepatic Model Mimicking Physiologically Relevant to in Vivo State. Cells **2021**, *10*, 1268. doi: 10.3390/cells10051268.
[57] Correia, C.; Ferreira, A.; Santos, J.; Lapa, R.; Yliperttula, M.; Urtti, A.; Vale, N. New in Vitro-in Silico Approach for the Prediction of in Vivo Performance of Drug Combinations. Molecules **2021**, *26*, 4257. doi: 10.3390/molecules26144257.
[58] Di, L. The Impact of Carboxylesterases in Drug Metabolism and Pharmacokinetics. Curr. Drug Metab. **2019**, *20*, 91-102.
[59] Nie, Y.; Yang, J.; Liu, S.; Sun, R.; Chen, H.; Long, N.; Jiang, R.; Gui, C. Genetic Polymorphisms of Human Hepatic OATPs: Functional Consequences and Effect on Drug Pharmacokinetics. Xenobiotica **2020**, *50*, 297-317.
[60] Mennecozzi, M.; Landesmann, B.; Palosaari, T.; Harris, G.; Whelan, M. Sex Differences in Liver Toxicity-do Female and Male Human Primary Hepatocytes React Differently to Toxicants in Vitro? PLoS One **2015**, *10*, e0122786.
[61] Vinken, M.; Hengstler, J.G. Characterization of Hepatocyte-Based in Vitro Systems for Reliable Toxicity Testing. Arch. Toxicol. **2018**, *92*, 2981-2986.
[62] de Bruijn, V.M.P.; Wang, Z.; Bakker, W.; Zheng, W.; Spee, B.; Bouwmeester, H. Hepatic Bile Acid Synthesis and Secretion: Comparison of in Vitro Methods. Toxicol. Lett. **2022**, *365*, 46-60.
[63] Brecklinghaus, T.; Albrecht, W.; Kappenberg, F.; Duda, J.; Vartak, N.; Edlund, K.; Marchan, R.; Ghallab, A.; Cadenas, C.; Günther, G. *et al.* The Hepatocyte Export Carrier Inhibition Assay Improves the Separation of Hepatotoxic from Non-Hepatotoxic Compounds. Chem. Biol. Interact. **2022**, *351*, 109728.

[64] Kasteel, E.E.J.; Darney, K.; Kramer, N.I.; Dorne, J.L.C.M.; Lautz, L.S. Human Variability in Isoform-Specific UDP-Glucuronosyltransferases: Markers of Acute and Chronic Exposure, Polymorphisms and Uncertainty Factors. Arch. Toxicol. **2020**, *94*, 2637-2661.

[65] den Braver-Sewradj, S.P.; den Braver, M.W.; Baze, A.; Decorde, J.; Fonsi, M.; Bachellier, P.; Vermeulen, N.P.E.; Commandeur, J.N.M.; Richert, L.; Vos, J.C. Direct Comparison of UDP-Glucuronosyltransferase and Cytochrome P450 Activities in Human Liver Microsomes, Plated and Suspended Primary Human Hepatocytes from Five Liver Donors. Eur. J. Pharm. Sci. **2017**, *109*, 96-110.

[66] Driehuis, E.; Kretzschmar, K.; Clevers, H. Establishment of Patient-Derived Cancer Organoids for Drug-Screening Applications. Nat. Protoc. **2020**, *15*, 3380-3409.

[67] Boehnke, K.; Iversen, P.W.; Schumacher, D.; Lallena, M.J.; Haro, R.; Amat, J.; Haybaeck, J.; Liebs, S.; Lange, M.; Schäfer, R. *et al.* Assay Establishment and Validation of a High-Throughput Screening Platform for Three-Dimensional Patient-Derived Colon Cancer Organoid Cultures. J. Biomol. Screen. **2016**, *21*, 931-941.

[68] Wang, Z.; Faria, J.; van der Laan, L.J.W.; Penning, L.C.; Masereeuw, R.; Spee, B. Human Cholangiocytes Form a Polarized and Functional Bile Duct on Hollow Fiber Membranes. Front. Bioeng. Biotechnol. **2022**, *10*, 868857.

[69] Bell, C.C.; Lauschke, V.M.; Vorrink, S.U.; Palmgren, H.; Duffin, R.; Andersson, T.B.; Ingelman-Sundberg, M. Transcriptional, Functional, and Mechanistic Comparisons of Stem Cell-Derived Hepatocytes, HepaRG Cells, and Three-Dimensional Human Hepatocyte Spheroids as Predictive in Vitro Systems for Drug-Induced Liver Injury. Drug Metab. Dispos. **2017**, *45*, 419-429.

[70] Leite, S.B.; Wilk-Zasadna, I.; Zaldivar, J.M.; Airola, E.; Reis-Fernandes, M.A.; Mennecozzi, M.; Guguen-Guillouzo, C.; Chesne, C.; Guillou, C.; Alves, P.M. *et al.* Three-Dimensional HepaRG Model as an Attractive Tool for Toxicity Testing. Toxicol. Sci. **2012**, *130*, 106-116.

[71] Gripon, P.; Rumin, S.; Urban, S.; Le Seyec, J.; Glaise, D.; Cannie, I.; Guyomard, C.; Lucas, J.; Trepo, C.; Guguen-Guillouzo, C. Infection of a Human Hepatoma Cell Line by Hepatitis B Virus. Proc. Natl. Acad. Sci. U. S. A. **2002**, *99*, 15655-15660.

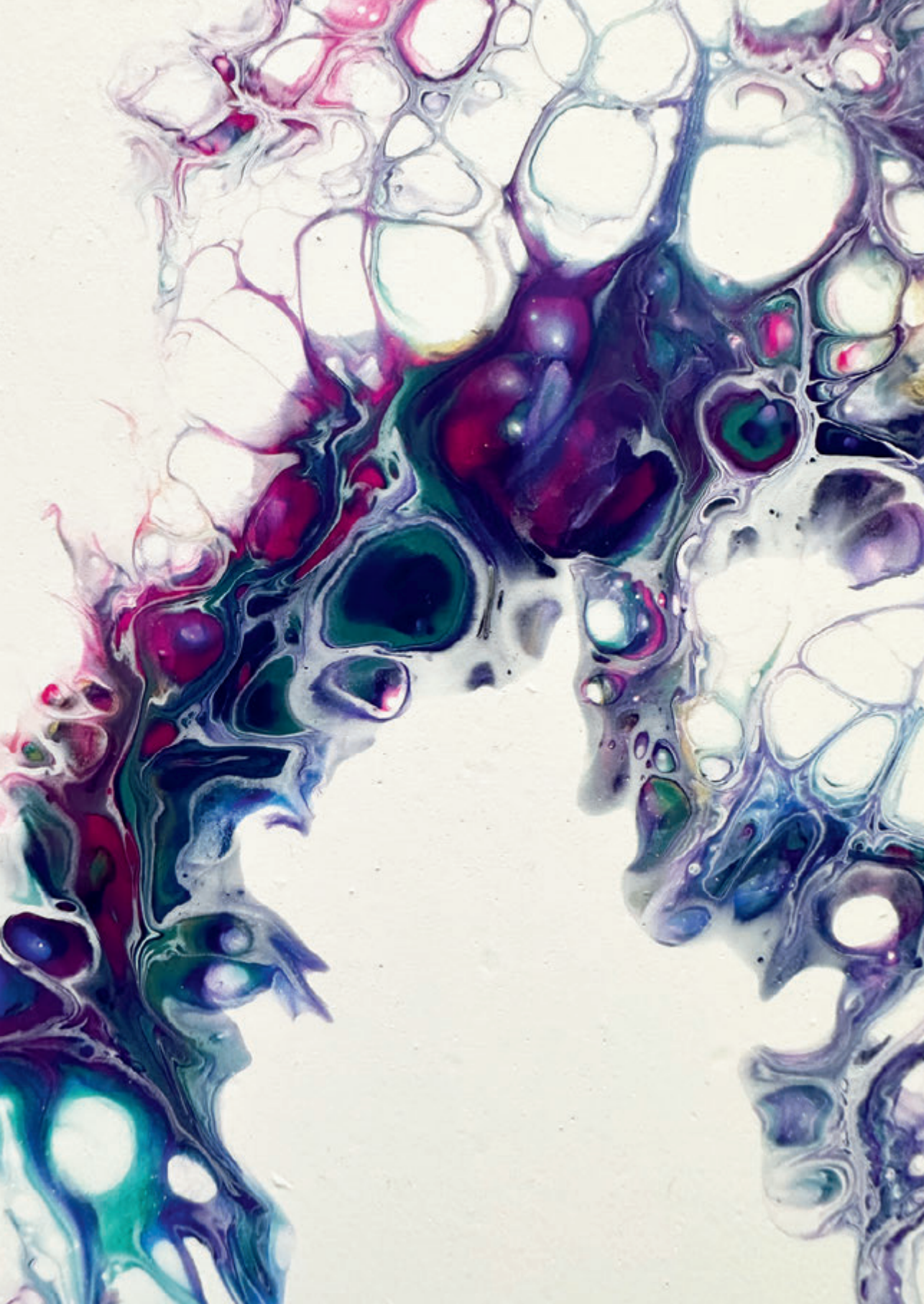

Bioprinting of Human Liver-derived Epithelial Organoids for Toxicity Studies

Manon C. Bouwmeester[1], Paulina Nuñez Bernal[2], Loes A. Oosterhoff[1], Monique van Wolferen[1], Vivian Lehmann[1,3], Monique Vermaas[1], Maj-Britt Buchholz[1], Quentin Peiffer[2], Jos Malda[1,2], Luc J. W. van der Laan[4], Nynke I. Kramer[5], Kerstin Schneeberger[1], Riccardo Levato[1,2], Bart Spee[1]

1 Department of Clinical Sciences, Faculty of Veterinary Medicine, Regenerative Medicine Center Utrecht, Utrecht University, 3584 CT Utrecht, The Netherlands
2 Department of Orthopaedics, University Medical Center Utrecht, Regenerative Medicine Center Utrecht, 3584 CT Utrecht, The Netherlands
3 Division of Pediatric Gastroenterology, Wilhelmina Children's Hospital, Regenerative Medicine Center Utrecht, 3584 CT Utrecht, The Netherlands
4 Department of Surgery, Erasmus MC Transplant Institute, University Medical Center Rotterdam, 3015 CN Rotterdam, The Netherlands
5 Institute for Risk Assessment Sciences, Utrecht University, 3584 CM Utrecht, The Netherlands

Published in Macromolecular Biosciences (2021); 21, 1–10. doi: 10.1002/mabi.202100327.

3

ABSTRACT

There is a need for long-lived hepatic *in vitro* models to better predict drug induced liver injury (DILI). Human liver-derived epithelial organoids are a promising cell source for advanced *in vitro* models. Here, organoid technology is combined with biofabrication techniques, which holds great potential for the design of *in vitro* models with complex and customizable architectures. In the present study, porous constructs with human hepatocyte-like cells derived from organoids were generated using extrusion-based printing technology. Cell viability of bioprinted organoids remained stable for up to ten days (88 - 107% cell viability compared to the day of printing). The expression of hepatic marker *G6PC*, transporters *BSEP* and *ABCG2* and phase I enzyme *CYP3A4* increased compared to undifferentiated controls (expansion condition), and was comparable to non-printed controls. Exposure to acetaminophen, a well-known hepatotoxic compound, decreased cell viability of bioprinted liver organoids to 21-51% ($p<0.05$) compared to the start of exposure and elevated levels of damage marker miR-122 were observed in the culture medium, indicating the potential use of the bioprinted constructs for toxicity testing. We showed that human liver-derived epithelial organoids can be combined with a biofabrication approach, thereby paving the way to create perfusable, complex constructs which can be used as toxicology- and disease-models.

GRAPHICAL ABSTRACT

Keywords
Extrusion-based bioprinting; Drug induced liver injury; In vitro modelling; Organoids

INTRODUCTION

Drug-induced liver injury (DILI) is the most frequent reason for drug failure in clinical trials and post-marketing drug withdrawal [1]. Thirty percent of drug candidates are discontinued due to hepatic dysfunction even post-marketing [2] Additionally, drug-induced liver injury accounts for more than fifty percent of the cases of acute liver failure in the United States [3]. Preclinical drug testing using rodent models allows for drug evaluation in the presence of a complete immune system and cross-talk with other organs [4]. However, significant interspecies differences in metabolic processes, disease mechanisms and modes of toxicity, hamper the extrapolation of obtained preclinical data to the human situation [5,6].

Compared to animal models, human hepatic *in vitro* models could give more insight in specific metabolic processes and mechanisms of toxicity, and allow for an ethically less controversial model [7]. Primary human hepatocytes (PHHs) are considered the golden standard due to the representative expression levels of metabolizing enzymes and expression of liver-specific markers. However, issues with PHHs are their rapid dedifferentiation leading to decreased hepatic function *in vitro* and the limited availability of these cells [8]. Nevertheless, PHHs are still widely used and recently introduced culture strategies are able to delay the dedifferentiation process in an attempt to set up a model that can be used for long-term toxicity testing [9-11]. To overcome previously mentioned limitations of PHHs, hepatic cell lines, such as HepG2 and HepaRG, are extensively used [12]. Although advantages of hepatic tumor-derived lines are their availability and nearly unlimited growth, they generally have reduced expression of key hepatic enzymes compared to PHHs [13]. Similar to PHHs, new culture strategies exist that are able to improve the hepatic function [14], however these cell lines are single-donor-derived and therefore do not exhibit interindividual differences. Especially in the case of the liver, a model needs to recapitulate the interindividual variation in metabolism, which is a major contributor to heterogeneity in drug clearance [15].

Organoids have a great potential to serve as liver models as they recapitulate aspects of the native tissue architecture and function *in vitro* [16]. Organoids are cultured as three-dimensional structures that are derived from primary cells (stem cells, progenitor, and/or differentiated cells) that self-organize through cell-cell and cell-matrix interactions [17]. Epithelial organoids are single germ layer-derived and under specific culture conditions expand and polarize to reproduce aspects of the native epithelium [18]. In the case of the liver, progenitor cells derived from the biliary tree can be cultured as organoids and differentiated into the cholangiocytic- and hepatocytic-lineage indicating a true

bipotential nature. In culture conditions where the Wnt/β-catenin pathway is induced, these progenitor cells form the intrahepatic biliary tree form organoids (intrahepatic cholangiocyte organoids, ICOs) and upregulate a stem cell marker LGR5 [19]. ICOs are highly proliferative, expanding as cystic structures for several months while remaining genetically stable and can be produced in large scale [20,21]. Under differentiating conditions ICOs upregulate hepatocyte markers and acquire mature hepatocyte functions, such as albumin and bile acid secretion, glycogen storage, phase I and II drug metabolism, and ammonia detoxification [20]. Unlike cellular aggregates or spheroids, the organoids are cystic-like structures which, in case of hepatic differentiation, are polarized with the apical side at the inside, facing the organoid lumen [21]. As ICOs are donor-derived, they can reflect interindividual variability in metabolic activity *in vitro*. Current hepatic maturity is limited compared to primary hepatocytes as indicated by lower hepatic function (e.g., albumin expression and cytochrome activity) [20]. In order to improve hepatic maturation the complexity of the *in vitro* constructs can be increased, thereby more closely mimicking the native liver environment [22]. Biofabrication techniques, and more specifically bioprinting, can provide such complexity through the precise placement of biomaterial inks or bioinks to promote cellular interactions, and through the production of constructs that allow for vascularization and enhanced exchange of nutrients [23,24].

The potential to converge bioprinting and self-assembled biological building units like organoids, has recently sparked attention in the biofabrication field, due to the possibility to create models at the tissue-like level scale [25,26]. Hence, novel models that benefit from both the 3D spatial control, as provided by bioprinting, and of the biological resemblance by using organoids as building blocks and bioink components, holds great potential to introduce a humanized testing platform for personalized medicine and drug screening. Here, we take the initial step towards increasing the culture complexity of human ICOs by showing that bioprinted organoids can be processed into functional liver constructs.

RESULTS

Hepatic constructs were created with extrusion-based bioprinting using organoid-derived hepatocyte-like cells and gelatin-based hydrogel (gelMA) as a bioink. After expanding the intrahepatic cholangiocyte organoids (ICOs) in Matrigel™ (Matrigel), in order to achieve the cell amount required for the bioprinting of the liver constructs, ICOs were resuspended in gelMA at a 2-5 million cells per mL density. Cell-laden gelMA was co-printed with the sacrificial hydrogel Pluronic-127 allowing to create porous constructs (Figure 1a). Printed

constructs consisted of printed strands of 600 to 1,000 µm with pores of 200 to 400 µm in size (Figure 1b). Diffusion through the gelMA hydrogel occurred at >1,000 µm within minutes, as was determined by using a coloring dye (Figure S1). This observation indicates that the hydrogel allows an exchange of soluble compounds with molecular weight comparable or superior to the drugs used in this work, thus permitting exposure to the hydrogel-embedded organoids. Moreover, the shear thinning property of gelMA was unaffected by the presence of organoids in the hydrogel (Figure S1), as the trend in viscosity with increasing angular frequency was comparable to gelMA without organoids.

Cell viability in bioprinted constructs

Hepatic differentiation of ICOs was started directly after bioprinting using differentiation media. After 10 days of culture, morphology of the organoids was assessed using an HE staining. We observed that the organoids remained within the printed gelMA struts or aligned along the edge (Figure 1c) with an average diameter size of 48.2 ± 29.0 µm (Figure S2). Organoids were distributed evenly throughout the construct with an overall coverage area of 6.4 ± 0.4 % (Figure S2) of bioprinted struts. In order to assess if the printed constructs can be applied for long-term toxicity studies, we assessed the cell viability of organoids over time using an Alamar blue assay as well as a live-dead assay. The differentiated (non-proliferative) organoids remained viable over a period of 10 days (88 – 107% cell viability compared to printing day; Figure 1d) as determined using an Alamar blue assay, which is comparable to organoids plated in gelMA (non-printed). Fluorescence imaging of live/dead cells showed that the amount of viable cells is stable over time and individual dead cells, which are present on the first day after printing, decreased over time (Figure 1e), which is comparable to the plated control (data not shown).

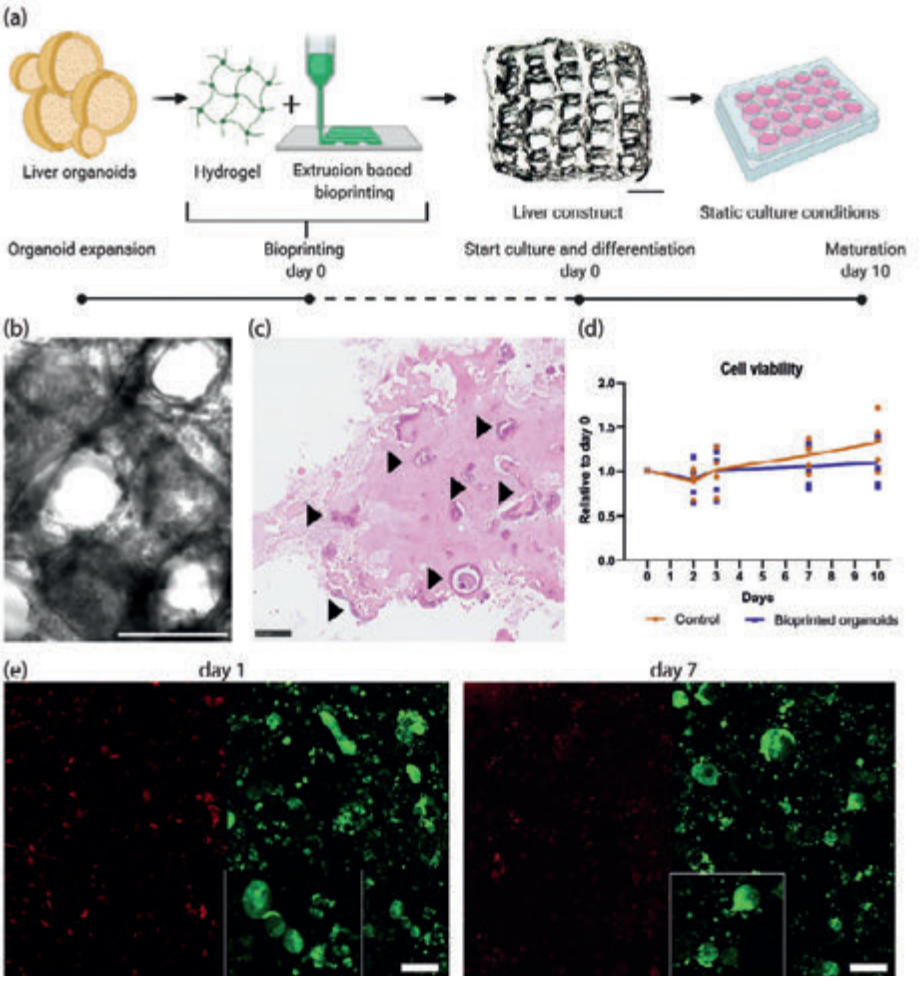

Figure 1. Bioprinting liver constructs. (a) Schematic overview of the experimental procedure for bioprinting liver constructs. Once expanded, liver organoids are encapsulated in hydrogel (gelMA). A porous construct was fabricated using extrusion-based bioprinting of the resulting bioink. The construct is cultured in organoid differentiation media, thus guiding organoids towards a hepatocyte-like phenotype. Scale bar = 1,000 µm. Created with BioRender.com (b) Brightfield image of the bioprinted liver construct. Scale bar = 1,000 µm. (c) HE staining of the bioprinted liver construct. Scale bar = 100 µm. Arrowheads indicate cystic organoid structures within printed struts. Scale bar = 100 µm, inserts are twofold higher magnification. (d) Cell viability of liver organoids in gelMA (5 donors) after plating (control; orange) and after printing (blue). Each dot represents the mean of a technical triplicate of a donor. (e) Representative image of the live/dead staining of liver organoids after printing at day 1 and 7 post-printing. Viable cells are stained in green, dead cells in red, image covers an entire printed strut.

Post-printing hepatic functionality

Hepatic differentiation of the organoids in gelMA droplets and extrusion-based bioprinted constructs was compared to that of organoids in in plated Matrigel cultures (day 10 of differentiation), by gene expression profiling and protein expression (immunofluorescence). As expected, gene expression profiling indicated a decrease of the stemness marker leucine-rich repeat-containing G-protein coupled receptor 5 (*LGR5*) compared to expansion conditions ($p<0.01$ for plated and printed organoids), and an increase of hepatic markers ATP-binding cassette super-family G member 2 (*G6PC*), bile salt export pump (*BSEP*), Glucose-6-Phosphatase Catalytic Subunit (*ABCG2*), cytochrome P450 3A4 (*CYP3A4*) in differentiation conditions compared to expansion conditions (Figure 2a). Expression levels of *albumin*, *G6PC*, *ABCG2*, and *CYP3A4* and cytochrome P450 2E1 (*CYP2E1*) show that the use of organoid technology includes donor-to-donor variation, with one of the donors showing low expression, whereas the other donors show increased expression levels in differentiation condition (Figure 2a). Overall, gelMA differentiating conditions (both printed constructs and plated controls) showed similar gene expression levels for the assessed hepatic markers compared to Matrigel. Immunofluorescence analysis (Figure 2b) showed that the cytoskeleton marker CK18 (cytokeratin 18) is present in bioprinted liver constructs (Figure S3). Expression of membrane marker E-cadherin and tight junction marker zonula occludens-1 (ZO-1; Figure S3) confirm that the bioprinted organoids retain an epithelial phenotype. Additionally, expression of hepatic markers HNF4α (hepatic nuclear factor 4 alpha), albumin, and argininosuccinate synthase (ASS) show differentiation towards hepatocytes. Expression of multi drug resistance protein 1 (MDR1), an apical transporter, shows polarization of liver organoids, allowing for transepithelial transport. Another characteristic of hepatocytes is glycogen storage. Glycogen can be hydrolyzed during a fasting state to generate glucose. Periodic acid-Schiff staining for glycogen shows that bioprinted organoids show glyocogen accumulation indicating hepatic function (Figure 2c).

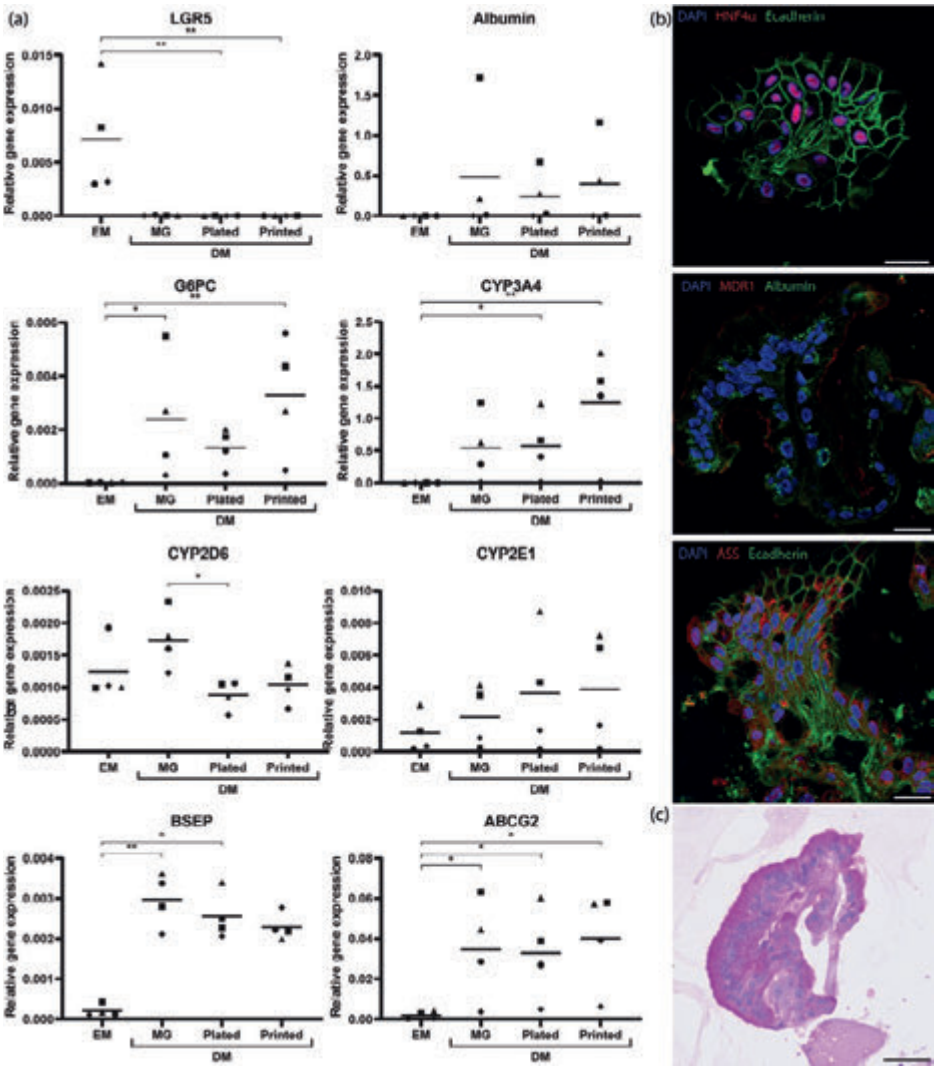

Figure 2. Functionality assessment in liver constructs. (a) Gene expression of liver organoids in Matrigel (MG; expansion (EM) and differentiation (DM) conditions), plated and printed in gelMA in differentiation conditions (DM). Each dot represents the mean of a technical triplicate of a donor. Relative gene expression was calculated using the reference genes GAPDH and RPS5 (ΔCt). LGR5, Leucine-rich repeat-containing G-protein coupled receptor 5; G6PC, ATP-binding cassette super-family G member 2; CYP2D6, Cytochrome P450 2D6; CYP3A4, Cytochrome P450 3A4; CYP2E1, Cytochrome P450 2E1; ABCG2, Glucose-6-Phosphatase Catalytic Subunit; BSEP, Bile salt export pump (b) Immunofluorescence staining in liver constructs. Scale bar = 25 μm. HNF4α, Hepatocyte nuclear factor 4 alpha; MDR1, Multidrug resistance protein 1; ASS, Argininosuccinate synthase (c) Glycogen accumulation in liver construct. Scale bar = 50 μm.

Toxicity in bioprinted constructs

As a proof-of-concept that the liver constructs can be applied to predict drug toxicity, we exposed bioprinted human organoids (5 donors) to the well-known hepatotoxic compound acetaminophen (APAP) on post-printing (differentiation) day 7 (72h to 30 mM). APAP can cause liver toxicity after biotransformation into its toxic metabolite N-acetyl-p-benzoquinone imine (NAPQI) by cytochrome P450 enzymes. Exposed organoids had a decreased cell viability to 21 – 45 % ($p<0.01$) after 72h of exposure compared to the start of exposure (Figure 3a), which is comparable to APAP toxicity observed in non-printed organoids (Figure S4). Fluorescence imaging of cell viability shows that after 72h of APAP exposure, the spherical shape of the organoids is disrupted indicating cellular stress (Figure 3b). Additionally, levels of damage marker miRNA-122 was also measured for four donors in the media. Levels of miRNA-122 seemed elevated compared to non-exposed organoids indicating leakage of miRNA-122 into the media (Figure 3c). Taken together, this data suggests that bioprinted organoids contain functional cytochrome P450 enzymes which were able to biotransform APAP into its toxic metabolite NAPQI.

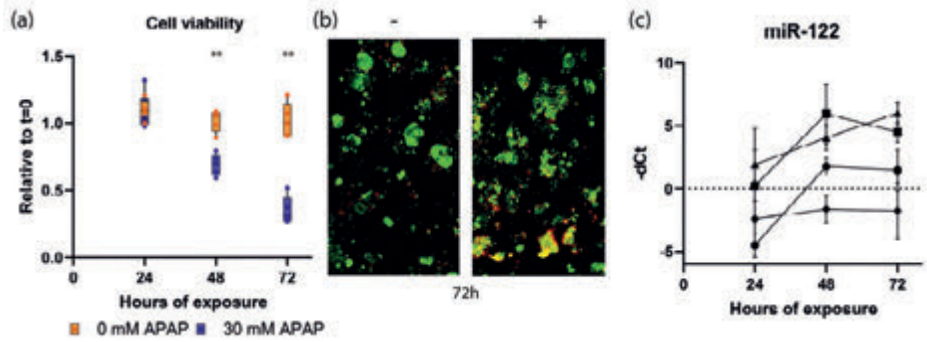

Figure 3. Acetaminophen (APAP) toxicity in bioprinted organoids. Exposure (72h to 30 mM APAP) started on day 7 post-printing with organoid-derived hepatocyte like cells. (a) Cell viability of bioprinted organoids exposed to APAP relative to the cell viability at start of exposure. Bioprinted organoids exposed to 0 mM APAP (control; orange) and 30 mM (blue). Each dot represents the mean of a technical triplicate of one donor (n=5). After 72h of exposure the cell viability of exposed organoids is significantly affected ($p<0.01$). (b) Live/dead staining of bioprinted organoids non-exposed (-, day 10 post-printing) and exposed to APAP for 72h (+, day 10 post-printing). Viable cells are stained in green, dead cells in red. (c) Medium-levels of microRNA-122. Data are expressed as log2 fold-change (-ΔCt) using the non-exposed samples as baseline. Each symbol, representing a different donor (n=4), and error bars represent the mean ± standard deviation.

DISCUSSION

The present study shows the potential application of hepatocyte-like cells derived from human intrahepatic cholangiocyte organoids (ICOs) for the bioprinting of drug responsive liver models. This enables the production of liver tissue constructs that are able to metabolize compounds relevant for pharmaceutical research. To obtain such models, an extrusion-based bioprinting strategy using an organoid-laden, gelatin-based bioink was established. Bioprinted hepatocyte-like cells from ICOs with a sustained metabolic activity provide possibilities for developing more advanced post-printing culture platforms, such as bioreactors and the incorporation of microfluidic devices, which will increase functional maturation, as well as standardized testing procedures [16,22,27]. Herein, it is demonstrated that hepatic functionality of differentiated ICOs in gelMA (plated and bioprinted) is comparable to regular Matrigel cultures. As a proof of principle to show the potential of bioprinted hepatocyte-like cells from ICOs to predict *in vitro* toxicity, bioprinted constructs were exposed to acetaminophen (APAP), a well-known hepatotoxic drug [28]. Donor-derived liver organoids are hollow cystic structures that express hepatic functionality once differentiated towards the hepatic lineage [20]. After differentiation, the hepatocyte-like cells are polarized as indicated by specific membrane transporters at either the apical or basolateral membrane. The observed polarization (MDR1), an apical membrane transporter, does mimic the native tissue in great detail and is important in the excretion of metabolites and transepithelial transport which can be measured in the media surrounding the bioprinted construct. In non-polarized 2D cultures such transport studies are not possible [29]. The donor-derived origin of the liver organoids was visible in our expression profile as not all donors showed similar expression levels, such as CYP3A4 and CYP2E1. Interindividual differences in metabolic gene expression profile may contribute to the sensitivity to hepatotoxic drugs [30], a feature that single-donor derived hepatic cell lines do not provide [12].

Additionally to toxicity screening, hepatocyte-like cells from ICOs also hold great promise for therapeutic applications due to their patient-derived origin. Next to iPSCs, it is one of the few models that allows for precision medicine approaches [27]. Tissue-derived epithelial organoids have been shown to exhibit patient-specific phenotypes *in vitro* [31], thereby enabling personalized testing of therapeutic applications. Disease modelling using patient derived liver organoids have been described for diseases such as Alagille syndrome and alpha-1 antitrypsin deficiency [20]. Moreover, patient-derived organoids have been show to allow for genetic repair by gene editing techniques [32] and are envisioned as a clinical therapy [33]. Next to the liver-derived organoids focused on in this paper, the described bioprinting strategy can also be used

in combination with tissue-derived organoids from other organs, including gall bladder, kidney, intestine and pancreas paving the way for more *in vitro* (disease) modelling opportunities [16,18,34].

Although hepatocyte-like cells from ICOs are a valuable tool for studying metabolism, even after differentiation some hepatic features are still lacking resulting in an immature phenotype. By bioprinting the biological resemblance of the *in vitro* system can be improved by applying precise patterning of organoids thereby permitting control over porosity and improved nutrient and waste exchange [35-37]. Here, we used extrusion-based bioprinting, which is an affordable technique in which a wide range of materials can be used [38,39]. The bioink (organoid-laden hydrogel pre-cursor) is pushed through a needle and is used to draw the desired 3D design layer-by-layer. Extrusion-based bioprinting could potentially cause organoid disruption due to shear stress at the nozzle. However, with the printing settings optimized in this study, viability of the hepatocyte-like cells from ICOs remained stable over time and comparable to non-printed controls.

Epithelial organoids are commonly cultured in the animal-derived and thermosensitive hydrogel Matrigel, which is advantageous for organoid growth and can be printed with a cooled print head [40]. However, while Matrigel has been well established to expand organoids in culture, using other 3D matrices during the organoid maturation steps has been proven to increase hepatic differentiation of liver organoids [41,42]. Furthermore, Matrigel shows considerable batch-to-batch variations, which represents a hurdle towards generation of highly standardized and scalable *in vitro* models for pharmaceutical research [43]. In our study, the main goal was to maintain a hepatic phenotype for subsequent testing, rather than proliferation and maintenance of undifferentiated phenotypes. Thus, we selected the widely used gelatin-derived hydrogel gelMA to prepare the printable bioinks. The modified methacryloyl groups in gelMA allow irreversible photocrosslinking and highly controllable stiffness of the hydrogel [38,43]. Furthermore, rheological analysis showed that the used gelMA concentration has shear thinning properties, which greatly facilitates stable extrusion while minimizing cell stress during printing [44,45]. Upon addition of organoids, the material still maintained its shear thinning properties. As the selected gelMA concentration is known to give rise to relatively soft hydrogels, typically in the range ≈5 kPa [46]. Pluronic-127 was used to temporarily support the desired grid-like structure before photocrosslinking [47] and the sacrificial filaments can also serve as a template to provide channels suitable to permit vascularization at a later stage [36]. The porosity of the current lattice shaped constructs already permit close proximity of the liver organoids to the media and nutrient supply. LAP was used

as photoinitiator for its cytocompatibility, herein demonstrated also when mixed with organoid-laden bioinks, and its potential to trigger crosslinking with visible light (~405 nm), which has been shown to permit hydrogel formation under mild and cell-friendly photo-exposure conditions [48]. Importantly, this is, to the best of our knowledge, the first report demonstrating the feasibility of bioprinting organoids derived from liver epithelium. Such liver organoids, forming lumen-rich structures, are more structurally fragile than dense spheroids and could potentially be susceptible to damage and disruption during extrusion through a nozzle. This study indicates the feasibility and safety of bioprinting such structures without hampering their functionality and constitutes a necessary preliminary step for future studies of more complex bioprinted architectures. Taken together, extrusion-based bioprinting using gelMA in combination with a sacrificial material provide a versatile strategy for the bioprinting of a porous construct that sustains organoid viability.

Extrusion-based bioprinting of hepatic structures has been shown before using different hepatic *in vitro* models, such as tumor-derived hepatic lines [35,36,49-51], (cryopreserved) PHHs [52,53], and human iPSCs [54,55]. Although all cell-types have hepatocyte features, the cellular organization of these bioprinted models is different compared to the bioprinted organoid constructs. Cells can be bioprinted as single cells [36,49-53,55], cellular aggregates that are forced to form (co-cultured) spheroids [35] or, in our case, as self-organizing organoids. Even though the size and level of organization of the cellular structures does not necessarily affect cell viability after bioprinting [56], it can have an effect on hepatic functionality [54] and contribute to cellular organization within prints. Extrusion-based bioprinted intestinal-derived organoids showed that specific patterning of the organoids can stimulate self-organization [57]. Here, liver organoids also reorganized within the bioprinted constructs and did not maintain their morphological characteristics as seen in Matrigel cultures. Even though there are morphological differences, the hepatic differentiation state in bioprinted constructs was similar compared to Matrigel. The high stability of the bioprinted organoids with respect to cell viability could also be due to intrinsic cell-binding motifs present in gelatin [58].

Next to the stability in viability and gene expression levels, histology and function are equally important. The current liver constructs do not fully recapitulate the native liver structure yet. We showed that liver organoids can be patterned via bioprinting, which provides the basis for future applications. Several important steps need to be taken to increase the complexity of the *in vitro* system which will lead to improved hepatic differentiation. This improved differentiation can be reached by co-culture with supporting liver cells [59,60] or vascular cells leading to a vascularized construct [36], or flow perfusion

[61,62], which can be applied to the bioprinted constructs [11]. The latter can be particularly beneficial, as recent studies have shown how *in vitro* zonation can be induced by flow perfusion [63,64]. The presence of Argininosuccinate synthetase (ASS, involved in urea cycle and mainly located in the periportal area) as well as the expression of CYP enzymes (mainly located in the perivenous area), suggests that hepatocyte-like cells from ICOs are not yet zonally oriented in the bioprinted constructs. In this study, we showed that hepatocyte-like cells from ICOs maintained high metabolic activity up to at least ten days after printing, allowing for post-printing exposure assays. The combination of bioprinting and ICOs provides possibilities to increase culture complexity to provide a more physiological relevant microenvironment and thereby potentially improve the hepatic differentiation state of the organoids.

Although several liver models have been developed for the determination of hepatic toxicity, almost all models have limitations that hamper their use in toxicity screening [8]. In this study, acetaminophen-induced toxicity was observed in the liver constructs over time, although used acetaminophen concentrations were relatively high compared to literature [35,65]. This is likely mainly due to the high level of the anti-oxidant glutathione present in the organoid differentiation medium which acts as an anti-oxidant and protects against APAP toxicity [66]. Additionally, expression levels of CYP2E1, which is mainly responsible for the formation of the toxic metabolite NAPQI (in addition CYP3A4 and CYP1A2 contribute to APAP metabolism, albeit to a lesser extent) [67], are only slightly increased in differentiated liver organoids compared to expanding conditions. Improved hepatic functionality, including CYP expression, can reinforce the predictive capacity for necrotic toxicity after formation of reactive metabolites [68,69]. With improvements of hepatic functionality of the organoids and the experimental setup, bioprinted liver organoids could result in a robust *in vitro* model to detect drug-induced effects. Acetaminophen toxicity is known to be predictable and dose-dependent as the formation of a toxic metabolite causes toxicity, however most drug-induced hepatic injury are less predictable and occur via different mechanisms [70]. By exposure of liver organoids to a selection of known hepatotoxic compounds with different toxicological mechanisms (for example formation of reactive metabolites, BSEP inhibition, mitochondrial impairment) the applicability of liver organoids in specific toxicological mechanisms can be established [71].

CONCLUSIONS

We aimed to develop a hepatic model that allowed spatial control using hepatocyte-like cells from ICOs and gelatin-based hydrogel as bioink. By bioprinting epithelial organoids we have taken the first step in the development

of a more complex, and hence more physiologically relevant, *in vitro* model system that allows the accurate predictions of drug-induced liver injury (DILI). This study provided the basis of a humanized testing platform for personalized medicine and/or drug screening based on the creation of liver constructs through bioprinting.

EXPERIMENTAL SECTION

Cells and culture conditions

Healthy liver biopsies were obtained during liver transplantation at the Erasmus Medical Center Rotterdam in accordance with the ethical standard of the institutional committee to use the tissue for research purposes (ethical approval number MEC 2014-060). The procedure was in accordance with the Helsinki Declaration of 1975 and informed consent in writing was obtained from each patient. Obtained human liver material was frozen down in Recovery Cell Freezing Medium for future experiments or used for organoid isolation directly. Organoid isolation was performed as follows: Tissue was chopped into small pieces and enzymatically digested with 0.125 mg mL^{-1} Type II collagenase and 0.125 mg mL^{-1} dispase in Dulbecco's Modified Eagle's Medium (DMEM) Glutamax supplemented with 0.01% (v/v) DNase I (Roche, Basel, Switzerland), 1% (v/v) fetal calf serum (FCS) and 1% (v/v) penicillin/streptomycin (P/S) at 37°C. Every hour, the supernatant was collected and fresh enzyme-supplemented media was added to the remaining tissue until only ducts and single cells were visible. Cells were washed with DMEM Glutamax (supplemented with 1% (v/v) FCS and 1% (v/v) P/S) and spun down at 453 g for 5 min. All components were obtained from Life Technologies (Carlsbad, CA, USA).

The cell suspension was cultured in Matrigel™ (Corning, New York, NY, USA) droplets in expansion medium (EM) until intrahepatic cholangiocyte organoids (ICOs) arise, as previously described [20]. In short, EM consisted of Advanced DMEM/F12 (Life Technologies) supplemented with 1% (v/v) penicillin-streptomycin (Life Technologies), 1% (v/v) GlutaMax (Life Technologies), 10 mM HEPES (4-(2-hydroxyethyl)-1-piperazineethanesulfonic acid, Life Technologies), 2% (v/v) B27 supplement without vitamin A (Invitrogen, Carlsbad, CA, USA), 1% (v/v) N2 supplement (Invitrogen), 10 mM nicotinamide (Sigma-Aldrich, St Louis, MO, USA), 1.25 mM N-acetylcysteine (Sigma-Aldrich), 10% (v/v) R-spondin-1 conditioned medium (the Rspo1-Fc-expressing cell line was a kind gift from Calvin J. Kuo), 10 µM forskolin (Sigma-Aldrich), 5 µM A83-01 (transforming growth factor beta inhibitor; Tocris Bioscience, Bristol, UK), 50 ng mL^{-1} EGF (Invitrogen), 25 ng mL^{-1} HGF (Peprotech, Rocky Hill, NJ, USA), 0.1 µg mL^{-1} FGF10 (Peprotech) and 10 nM recombinant human (Leu15)-gastrin I (Sigma-Aldrich). Media was changed twice a week. Passaging occurred every 7-10 days at ratios

ranging between 1:2 and 1:4. All cultures were kept in a humidified atmosphere of 95% air and 5% CO_2 at 37°C. Organoids were primed for differentiation with BMP7 (25 ng mL^{-1}, Peprotech) through spiking EM 3 days prior to shifting to differentiation medium (DM). DM consisted of EM without R-spondin-1, FGF10 and nicotinamide, supplemented with 100 ng mL^{-1} FGF19 (Peprotech), 500 nM A83-01 (Tocris Bioscience), 10 µM DAPT (Selleckchem, Munich, Germany), 25 ng mL^{-1} BMP-7 (Peprotech), and 30 µM dexamethasone (Sigma-Aldrich). Organoids were kept on DM up to 10 days.

Bioink preparation

Gelatin-methacryloyl (gelMA) was synthesized from gelatin-derived from porcine skin (Sigma-Aldrich) as previously described [72]. In short, 10% (w/v) gelatin in phosphate buffered saline (PBS) was reacted with 1:0.6 methacrylic anhydride (Sigma-Aldrich) at 50°C for 1h in order to form 80% degree of functionalization of the lysine residues. The excess of methacrylic anhydride was removed by centrifugation. The obtained gelMA solution was neutralized with NaOH and dialyzed against distilled water for 5 days, sterile-filtered, freeze-dried and stored at -20°C until further use.

The used photoinitiator in the bioink was lithium-phenyl-2,4,6-trimethylbenzoylphosphinate (LAP; Sigma-Aldrich) 0.2% (w/v) dissolved in DMEM/F12 (without phenol red, supplemented with 1% (v/v) penicillin-streptomycin, 1% (v/v) GlutaMax, 10 mM HEPES). Freeze-dried gelMA was dissolved (5% (w/v)) in the LAP-solution. The temperature of the gelMA solution was stabilized at 25°C prior to cell mixing. Organoids were mechanically fragmented and mixed with the gelMA bioink right before transferring to the bioprinting cartridge. The sacrificial material Pluronic®F-127 (Sigma-Aldrich) was dissolved in PBS (40% (w/v)) while incubating at 4°C under continuous agitation.

Rheological evaluation gelMA

The rheological properties of the hydrogel precursor solution were assessed using a DHR2 rheometer (TA Instruments, the Netherlands). To evaluate the hydrogels shear thinning properties, a stainless-steel flat plate (diameter = 20 mm) with a 200 µm plate-to-plate distance was used. gelMA in LAP-solution (65 µL of 5% (w/v); previously described) was loaded and the gels complex viscosity (Pa·S) was recorded at 25°C as a function of shear rate (0.01–100 rad s^{-1}) at a constant strain of 5% (n=3 for gelMA control, n=4 for cell-laden gelMA).

Compound diffusion in gelMA

A 5% (w/v) gelMA in 0.2% (w/v) LAP-solution was casted using a custom-designed PDMS mold and crosslinked for 10 minutes under 400 nm light exposure, to form cylindrical discs (diameter = 5 mm; height = 3 mm). To evaluate the diffusion rate of the crosslinked hydrogel construct, 10 µL of a green colored dye (MW = 534,3 – 561,7 g mol^{-1}; Singh Traders, Baambrugge, the Netherlands) was pipetted on top of the cylinder to create an even fluid layer over the top face surface of the hydrogel disc. After 1, 2, 4, 6, 8, 12, 16, 24, 32 minutes samples were removed from the mold (n=2 per time point). The migration of the dye through the gel over time was assessed using a stereomicroscope (Olympus SZ61 coupled with an Olympus DP70 digital camera; Olympus Soft Imaging Solutions GmbH, the Netherlands) by imaging cross-sections of the hydrogel cylinder at the indicated time points.

Bioprinting settings

The constructs were designed using a Computer Aided Design (CAD) software (BioCAD, RegenHU, Switzerland), and printed using an extrusion-based bioprinter (3D Discovery, RegenHU, Switzerland) in a sterile 5 cm Petri dish (ThermoFisher, Waltham, Massachusetts, USA). The constructs consist of horizontal strands of Pluronic®F-127 with 0.135 mm space between each strand. In between these supporting strands, the cell-laden gelMA was printed and photocrosslinked with an exposure of 45 seconds with blue-light (405 nm). Subsequent layers are printed in a layer-by-layer fashion, with a 90 degrees rotation in the filament orientation between each layer. Pluronic®F-127 was printed at a speed of 30 mm sec^{-1} at a pressure of 450-550 kPa. gelMA was printed at a speed of 15 mm sec^{-1} at a pressure of 15-30 kPa. The printhead containing the cell-laden gelMA bioink was equipped with a cooling device set to 25°C. The dispensing tip was a stainless steel 27G nozzle (length 6.35 mm; Nordson, Westlake, OH, USA) for both bioinks. After printing 10 layers, the printed construct is further photocrosslinked for 10 min in a custom-made curing box containing 400 nm LED lights (000214, Groenlicht, Geldrop, the Netherlands). Pluronic®F-127 was washed away with DMEM/F12 (without phenol red, supplemented with 1% (v/v) penicillin-streptomycin, 1% (v/v) GlutaMax, 10 mM HEPES) at 4°C resulting in porous cubical shaped constructs (approximately 5x5x2 mm lxwxh). Constructs were cultured in 24 well plates (ThermoFisher) under differentiating conditions (Differentiation Medium, DM) as described for a maximum of 10 days in a humidified atmosphere of 95% air and 5% CO_2 at 37°C.

Alamar Blue assay

Cell viability of the organoids (4 donors in technical triplicate) in printed constructs and plated controls (gelMA and Matrigel) was examined through an Alamar Blue assay (ThermoFisher), a resazurin-based solution that functions as a

cell health indicator. Briefly, the Alamar Blue reagent was diluted 1:10 in DMEM/F12 (phenol-red free). Cells were incubated for 2 h at 37°C. Subsequently, fluorescence intensity of the Alamar Blue solution was measured with a photospectrometer (Fluoroskan Ascent FL, ThermoFischer Scientific) at ex/em 544/570 nm.

Cell viability

Cell viability of printed and exposed organoids was visualized using a LIVE/DEAD Viability/Cytotoxicity Kit for mammalian cells (ThermoFisher, Catalog number: L3224). Samples were incubated with fluorescent dyes to detect live (Calcein-AM) and dead (Ethidium homodimer-1) cells. Samples were imaged using confocal laser scanning microscopy (SP8, Leica Microsystems, the Netherlands).

Gene expression

Prior to RNA isolation, gelMA hydrogels were broken down using QIAshredder columns according to the manufacturer's instructions (Qiagen, Hilden, Germany). RNA was isolated from liver organoids (4 donors (n=4), in triplicate) using 350 µL RNeasy lysis buffer directly added into one well of the 24 well plate followed by RNA extraction using the RNeasy micro Kit according to the manufacturer's instructions (Qiagen). cDNA synthesis was performed using iScript cDNA synthesis kit (Bio-Rad, Veenendaal, the Netherlands). Relative gene expression of selected genes was measured using RT-qPCR in a CFX-384 (Bio-Rad). Primer design, validation, RT-qPCR conditions, and data analysis was performed as previously described [73]. Normalization was performed using reference genes GAPDH and RPS5. Details of primers are listed in Table S1.

Immunofluorescence

Organoids (4 donors) were fixed in 4% (w/v) paraformaldehyde (PFA) with 0.1% (v/v) eosin and stored in 70% (v/v) EtOH at 4°C until further processing. Bioprinted constructs were placed in agarose before embedding to keep the constructs integrity during the histological processing. Samples were embedded in paraffin and cut into 4 µm sections. Sections were deparaffinized and rehydrated. After antigen retrieval (information per antibody in Table S2), a blocking step was performed using 10% (v/v) normal goat serum (Bio-Rad) in PBS for 30min at RT. Antibodies are listed in Table S2. Incubation with primary antibodies was performed overnight at 4°C. Secondary antibodies were incubated at room temperature for 1h. Nuclei were stained with DAPI (Sigma-Aldrich) diluted 2,000x in PBS. Washing steps were performed using a buffer of PBS with 0.1% Triton X-100 (Sigma-Aldrich) and 0.2% (w/v) Bovine Serum Albumin (Sigma). Slides were mounted using FluorSave (Merck-Millipore,

Burlington, MA, USA), and images were acquired using confocal microscopy (SP8, Leica Microsystems).

HE staining
Morphology and distribution of organoids in printed constructs (4 donors) was evaluated by hematoxylin and eosin (H&E) staining, scanned with slide scanner (Hamamatsu Photonics, Hamamatsu-city, Japan).

Acetaminophen toxicity
Acetaminophen (APAP; CAS 103-90-2, Sigma-Aldrich) was dissolved in differentiation medium as described above, using DMEM Glutamax with added factors as described for DM except Glutamax, NAC and B27. At day 7 of differentiation organoids were exposed to 30 mM APAP for 72h (4 donors, n=3), repeated dosing every 24h. Metabolic activity was examined at 24, 48 and 72h after start of exposure using the Alamar Blue assay. Medium was collected at 4, 24, 48 and 72h of exposure to examine levels of miRNA-122 in the medium.

Detection miRNA-122 in medium
Total RNA was extracted from assay medium (120 – 160 µL) using the miRNeasy Serum/Plasma Kit (Qiagen) following the manufacturer's instructions. miRNA-122 was reverse-transcribed using the miScript II RT Kit (Qiagen) according to the manufacturer's protocol. Normalization of qPCR data of printed samples was performed using spiked-in synthetic C. elegans miR-39 (miRNeasy Serum/Plasma Spike-In Control, Qiagen). Ce_miR-39_1 and H2_miR-122a_1 miScript Primer Assays (Qiagen) were used for qPCR. The qPCR was carried out in a CFX-384 (Bio-Rad). Calculations were performed as previously described [74]. Changes of miRNA levels in supernatants were determined by comparing the Ct values in the exposed samples in comparison to the control (non-exposed) samples and expressed as -ΔCt.

Statistical analysis
For the statistical analysis of metabolic activity data, the gene expression data and the effects of acetaminophen exposure, we applied the post-hoc comparison uncorrected Dunn's test using GraphPad Prism (version 8.3.0). Significance levels are * $p \leq 0.05$; ** $p \leq 0.01$ and *** $p \leq 0.001$.

FUNDING STATEMENT

This work is part of the research program Applied and Engineering Sciences with project number 15498, which is financed by the Dutch Research Council (NWO). R.L. acknowledges funding from the European Research Council (ERC)

under the European Union's Horizon 2020 research and innovation programme (grant agreement No. 949806).

AUTHOR CONTRIBUTIONS

Conceptualization, M.C.B., R.L., K.S. and B.S.; methodology, M.C.B., P.B.N, L.A.O., V.L., M.V., M.B.B., K.S., and Q.P.; investigation, M.C.B., P.B.N, L.A.O., and M.v.W.; resources, L.J.W.v.d.L.; visualization, M.C.B., P.B.N. and L.A.O.; supervision, R.L., N.I.K., and B.S.; writing—original draft preparation, M.C.B.; writing—review and editing, B.S., N.I.K., P.B.N., R.L., J.M., V.L., L.J.W.v.d.L., and K.S.; funding acquisition, J.M., N.I.K., and B.S. All authors have read and agreed to the published version of the manuscript.

CONFLICTS OF INTEREST

The authors declare no conflict of interest.

SUPPLEMENTARY MATERIALS

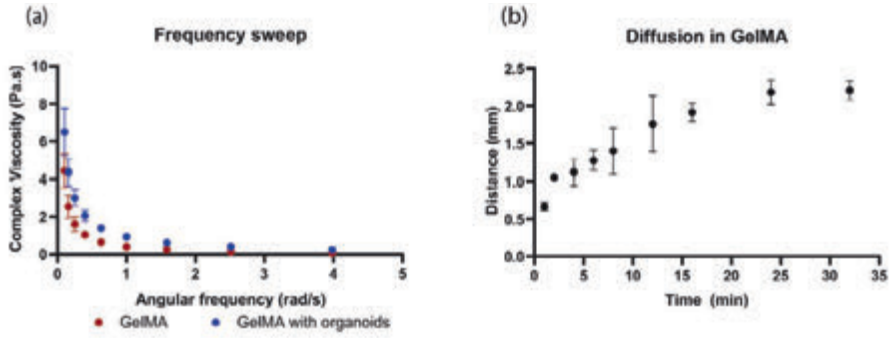

Figure S1. Characterization of (a) the frequency-depended behavior of viscosity in a 5% (w/v) gelMA ink with (blue) and without (red) organoids (n=3), and of (b) its capability to allow diffusion of solutes over time (n=4). Dots and error bars represent the average ± standard deviation.

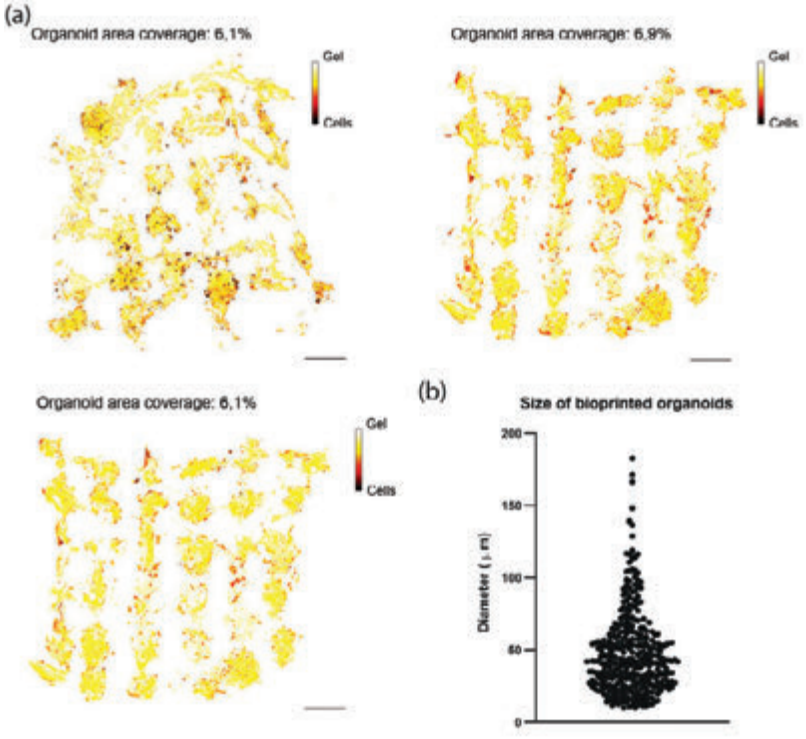

Figure S2. Area of coverage (a) and organoid diameter (b) of the bioprinted organoids. (a) Average area of coverage is 6.4 ± 0.4 % (n=3). Scale bar = 1,000 μm. Yellow: Hydrogel; Red: Cells. (b) The average diameter of bioprinted organoids is 48.2 ± 29.0 μm.

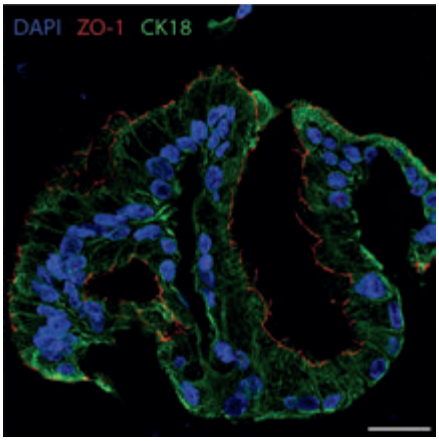

Figure S3. Immunofluorescence staining in liver constructs. Scale bar = 25 µm. ZO-1, Zonula occludens-1; CK18, Cytokeratin 18.

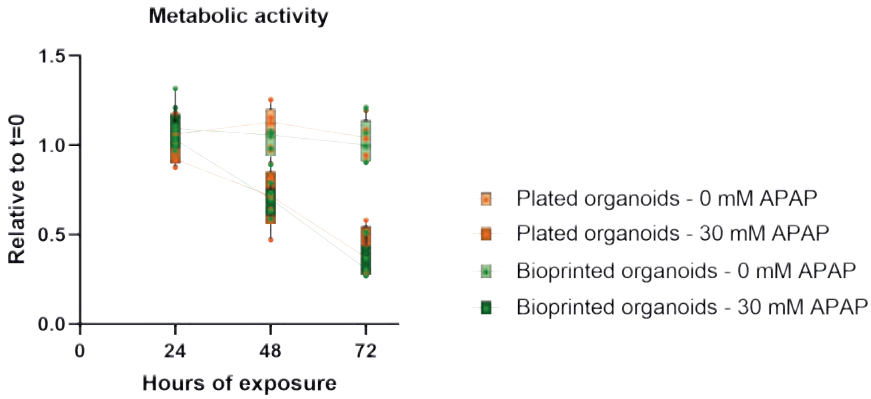

Figure S4. Metabolic activity of non-bioprinted (plated; orange) and bioprinted (green) liver organoids exposed to acetaminophen (APAP) relative to the metabolic activity at start of exposure (differentiation day 7 after plating/printing). Organoids exposed to 0 mM APAP (control; light colored box) and 30 mM (dark colored box). Each dot represents the mean of a technical triplicate of one donor (n=5).

Table S1. Primers used for quantitative PCR analysis.

Gene	Forward	Reverse
LGR5	GCAGTGTTCACCTTCCC	GGTCCACACTCCAATTCTG
ALB	GTTCGTTACACCAAGAAAGTACC	GACCACGGATAGATAGTCTTCTG
G6PC	CGTCTTTAAGTGGATTCTCTTTGG	GTCCAGTCTCACAGGTTACAG
CYP3A4	TGATGGTCAACAGCCTGTGCTGG	CCACTGGACCAAAAGGCCTCCG
CYP2D6	GAGGTGCTGAATGCTGTC	AGGTCATCCTGTGCTCAG
CYP2E1	GTACACAATGGACGGTATCACC	GGAGCTTCTCTTCGATCTCAG
ABCG2	CGAGTAAAACTGAAGAGTGGCTTT	CGAAGATTTGCCTCCACCT
BSEP	GTCATCTTGTGCTTCTTCCC	TCATTTGTAATCTGTCCCACCA

Table S2. Antibodies used for immunofluorescence analysis

Primary antibodies				
Antigen	**Source and cat. number**	**Raised in**	**Dilution**	**Antigen retrieval**
MDR1	Novus Bio NBP1-90291	rabbit	1:200	TE
CK18	Santa Cruz sc-51582	mouse	1:400	Pepsin
Albumin	Sigma Aldrich A6684	mouse	1:1,000	TE
ZO-1	Invitrogen 40-2300	rabbit	1:250	Pepsin
HNF4α	LS Biosciences LS-B969	rabbit	1:200	TE
ASS	Aviva System Biology ARP41366_T100	rabbit	1:300	Citrate
E-cadherin	BD Bioscience 610181	mouse	1:100	TE / Citrate

TE: 10 mM Tris, 1 mM EDTA, 0.5% Tween 20 in PBS at pH 9.0 for 30 min at 98°C.
Citrate: 10 mM citrate buffer at pH 6.0 for 30 min at 98 °C.
Pepsin: 0.4% (w/v) (Dako) in 0.2 M HCl for 20 min at 37 °C.

Secondary antibodies			
Antigen	**Source and cat. number**	**Raised in**	**Dilution**
Anti-mouse Alexa 488	Life Technologies #A11029	goat	1:200
Anti-rabbit Alexa 568	Life Technologies #A11036	goat	1:200

Secondary antibodies were diluted in Antibody Diluent (Dako).

REFERENCES

[1] Siramshetty, V.B.; Nickel, J.; Omieczynski, C.; Gohlke, B.O.; Drwal, M.N.; Preissner, R. WITHDRAWN - A Resource for Withdrawn and Discontinued Drugs. Nucleic Acids Res. **2016**, *44*, D1080-D1086.

[2] Lee, W.M. Drug-Induced Hepatotoxicity. N. Engl. J. Med. **2003**, 474-485.

[3] Ostapowicz, G.; Fontana, R.J.; Schi odt, F.V.; Larson, A.; Davern, T.J.; Han, S.H.B.; McCashland, T.M.; Shakil, O.A.; Hay, E.J.; Hynan, L. *et al.* Results of a Prospective Study of Acute Liver Failure at 17 Tertiary Care Centers in the United States. Ann. Intern. Med. **2002**, *137*, 947-955.

[4] McGill, M.R.; Jaeschke, H. Animal Models of Drug-Induced Liver Injury. Biochimica et Biophysica Acta - Molecular Basis of Disease **2019**, *1865*, 1031-1039.

[5] Ballet, F.c. Preventing Drug-Induced Liver Injury: How Useful are Animal Models? Digestive Diseases **2015**, *33*, 477-485.

[6] Olson, H.; Betton, G.; Robinson, D.; Thomas, K.; Monro, A.; Kolaja, G.; Lilly, P.; Sanders, J.; Sipes, G.; Bracken, W. *et al.* Concordance of the Toxicity of Pharmaceuticals in Humans and in Animals. Regulatory Toxicology and Pharmacology **2000**, *32*, 56-67.

[7] Gómez-Lechón, M.J.; Tolosa, L.; Conde, I.; Donato, M.T. Competency of Different Cell Models to Predict Human Hepatotoxic Drugs. Expert Opin. Drug Metab. Toxicol. **2014**, *10*, 1553-1568.

[8] Godoy, P.; Hewitt, N.J.; Albrecht, U.; Andersen, M.E.; Ansari, N.; Bhattacharya, S.; Bode, J.G.; Bolleyn, J.; Borner, C.; Böttger, J. *et al.* Recent Advances in 2D and 3D in Vitro Systems using Primary Hepatocytes, Alternative Hepatocyte Sources and Non-Parenchymal Liver Cells and their use in Investigating Mechanisms of Hepatotoxicity, Cell Signaling and ADME. Arch. Toxicol. **2013**, *87*, 1315-1530.

[9] Lauschke, V.M.; Shafagh, R.Z.; Hendriks, D.F.G.; Sundberg, M.I. 3 D Primary Hepatocyte Culture Systems for Analyses of Liver Diseases , Drug Metabolism , and Toxicity : Emerging Culture Paradigms and Applications. Biotechnology Journal **2019**, *14*, 1-12.

[10] Fraczek, J.; Bolleyn, J.; Vanhaecke, T.; Rogiers, V.; Vinken, M. Primary Hepatocyte Cultures for Pharmaco-Toxicological Studies: At the Busy Crossroad of various Anti-Dedifferentiation Strategies. Arch. Toxicol. **2013**, *87*, 577-610.

[11] Ruoß, M.; Vosough, M.; Konigsrainer, A.; Nadalin, S.; Wagner, S.; Sajadian, S.; Huber, D.; Heydari, Z.; Ehnert, S.; Hengstler, J.G. *et al.* Towards Improved Hepatocyte Cultures: Progress and Limitations. Food and Chemical Toxicology **2020**, *138*, 111188.

[12] Castell, J.V.; Jover, R.; Martínez-Jiménez, C.P.; Gómez-Lechón, M.J. Hepatocyte Cell Lines: Their use, Scope and Limitations in Drug Metabolism Studies. Expert Opinion on Drug Metabolism and Toxicology **2006**, *2*, 183-212.

[13] Hart, S.N.; Li, Y.; Nakamoto, K.; Subileau, E.A.; Steen, D.; Zhong, X.B. A Comparison of Whole Genome Gene Expression Profiles of HepaRG Cells and HepG2 Cells to Primary Human Hepatocytes and Human Liver Tissues. Drug Metab. Dispos. **2010**, *38*, 988-994.

[14] Ashraf, M.N.; Asghar, M.W.; Rong, Y.; Doschak, M.R.; Kiang, T.K.L. Advanced in Vitro HepaRG Culture Systems for Xenobiotic Metabolism and Toxicity Characterization. Eur. J. Drug Metab. Pharmacokinet. **2019**, *44*, 437-458.

[15] Zhou, S.F.; Liu, J.P.; Chowbay, B. Polymorphism of Human Cytochrome P450 Enzymes and its Clinical Impact. Drug Metab. Rev. **2009**, *41*, 89-295.
[16] Schutgens, F.; Rookmaaker, M.B.; Margaritis, T.; Rios, A.; Ammerlaan, C.; Jansen, J.; Gijzen, L.; Vormann, M.; Vonk, A.; Viveen, M. *et al.* Tubuloids Derived from Human Adult Kidney and Urine for Personalized Disease Modeling. Nat. Biotechnol. **2019**, *37*, 303-313.
[17] Marsee, A.; Roos, F.J.M.; Verstegen, M.M.A.; HPB Organoid Consortium; Gehart, H.; de Koning, E.; Lemaigre, F.; Forbes, S.J.; Peng, W.C.; Huch, M. *et al.* Building Consensus on Definition and Nomenclature of Hepatic, Pancreatic, and Biliary Organoids. Cell. Stem Cell. **2021**, *28*, 816-832.
[18] Sato, T.; Stange, D.E.; Ferrante, M.; Vries, R.G.J.; Van Es Johan, H.; Van Den Brink Stieneke; Van Houdt Winan, J.; Pronk, A.; Van Gorp Joost; Siersema, P.D. *et al.* Long-Term Expansion of Epithelial Organoids from Human Colon, Adenoma, Adenocarcinoma, and Barrett's Epithelium. Gastroenterology **2011**, *141*, 1762-1772.
[19] Planas-Paz, L.; Sun, T.; Pikiolek, M.; Cochran, N.R.; Bergling, S.; Orsini, V.; Yang, Z.; Sigoillot, F.; Jetzer, J.; Syed, M. *et al.* YAP, but Not RSPO-LGR4/5, Signaling in Biliary Epithelial Cells Promotes a Ductular Reaction in Response to Liver Injury. Cell. Stem Cell. **2019**, *25*, 39-53.e10.
[20] Huch, M.; Gehart, H.; van Boxtel, R.; Hamer, K.; Blokzijl, F.; Verstegen, M.M.; Ellis, E.; van Wenum, M.; Fuchs, S.A.; de Ligt, J. *et al.* Long-Term Culture of Genome-Stable Bipotent Stem Cells from Adult Human Liver. Cell **2015**, *160*, 299-312.
[21] Schneeberger, K.; Sánchez-Romero, N.; Ye, S.; van Steenbeek, F.G.; Oosterhoff, L.A.; Pla Palacin, I.; Chen, C.; van Wolferen, M.E.; van Tienderen, G.; Lieshout, R. *et al.* Large-Scale Production of LGR5-Positive Bipotential Human Liver Stem Cells. Hepatology **2020**, *72*, 257-270.
[22] Chen, C.; Soto-Gutierrez, A.; Baptista, P.M.; Spee, B. Biotechnology Challenges to in Vitro Maturation of Hepatic Stem Cells. Gastroenterology **2018**, *154*, 1258-1272.
[23] Underhill, G.H.; Khetani, S.R. Bioengineered Liver Models for Drug Testing and Cell Differentiation Studies. Cmgh **2018**, *5*, 426-439.e1.
[24] Schneeberger, K.; Spee, B.; Costa, P.; Sachs, N.; Clevers, H.; Malda, J. Converging Biofabrication and Organoid Technologies: The Next Frontier in Hepatic and Intestinal Tissue Engineering? Biofabrication **2017**, *9*.
[25] Lawlor, K.T.; Vanslambrouck, J.M.; Higgins, J.W.; Chambon, A.; Bishard, K.; Arndt, D.; Er, P.X.; Wilson, S.B.; Howden, S.E.; Tan, K.S. *et al.* Cellular Extrusion Bioprinting Improves Kidney Organoid Reproducibility and Conformation. Nature Materials **2020**.
[26] Levato, R.; Jungst, T.; Scheuring, R.G.; Blunk, T.; Groll, J.; Malda, J. From Shape to Function: The Next Step in Bioprinting. Adv Mater **2020**, *32*.
[27] Takahashi, T. Organoids for Drug Discovery and Personalized Medicine. Annu. Rev. Pharmacol. Toxicol. **2019**, *59*, 447-462.
[28] Jaeschke, H.; Bajt, M.L.; Ramachandran, A. 2.19 - Mechanisms of Acetaminophen Hepatotoxicity: Cell Death Signaling Mechanisms in Hepatocytes. In *Comprehensive Toxicology (Third Edition)*, Third Edition ed.; Charlene A. McQueen, Ed.; Elsevier: Oxford, 2018, pp. 460-482.
[29] Ramaiahgari, S.C.; Den Braver Michiel, W.; Herpers, B.; Terpstra, V.; Commandeur, J.N.M.; Van De Water Bob; Price, L.S. A 3D in Vitro Model of Differentiated HepG2 Cell Spheroids with Improved Liver-Like Properties for Repeated Dose High-Throughput Toxicity Studies. Arch. Toxicol. **2014**, *88*, 1083-1095.

[30] Utkarsh, D.; Loretz, C.; Li, A.P. In Vitro Evaluation of Hepatotoxic Drugs in Human Hepatocytes from Multiple Donors: Identification of P450 Activity as a Potential Risk Factor for Drug-Induced Liver Injuries. Chem. Biol. Interact. **2016**, *255*, 12-22.

[31] Kruitwagen, H.S.; Oosterhoff, L.A.; Vernooij, I.G.W.H.; Schrall, I.M.; van Wolferen, M.E.; Bannink, F.; Roesch, C.; van Uden, L.; Molenaar, M.R.; Helms, J.B. *et al.* Long-Term Adult Feline Liver Organoid Cultures for Disease Modeling of Hepatic Steatosis. Stem Cell Reports **2017**, *8*, 822-830.

[32] Schene, I.F.; Joore, I.P.; Oka, R.; Mokry, M.; van Vugt, A.H.M.; van Boxtel, R.; van der Doef, H.P.J.; van der Laan, L.J.W.; Verstegen, M.M.A.; van Hasselt, P.M. *et al.* Prime Editing for Functional Repair in Patient-Derived Disease Models. Nature Communications **2020**, *11*, 1-8.

[33] Sampaziotis, F.; Muraro, D.; Tysoe, O.C.; Sawiak, S.; Beach, T.E.; Godfrey, E.M.; Upponi, S.S.; Brevini, T.; Wesley, B.T.; Garcia-Bernardo, J. *et al.* Cholangiocyte Organoids can Repair Bile Ducts After Transplantation in the Human Liver. Science (New York, N.Y.) **2021**, *371*, 839-846.

[34] Roos, F.J.M.; Verstegen, M.M.A.; Mu\noz Albarinos Laura; Roest, H.P.; Poley, J.; Tetteroo, G.W.M.; IJzermans, J.N.M.; van der Laan, L.J.W. Human Bile Contains Cholangiocyte Organoid-Initiating Cells which Expand as Functional Cholangiocytes in Non-Canonical Wnt Stimulating Conditions. Frontiers in Cell and Developmental Biology **2021**, *8*, 1-12.

[35] Bhise, N.S.; Manoharan, V.; Massa, S.; Tamayol, A.; Ghaderi, M.; Miscuglio, M.; Lang, Q.; Zhang, Y.S.; Shin, S.R.; Calzone, G. *et al.* A Liver-on-a-Chip Platform with Bioprinted Hepatic Spheroids. Biofabrication **2016**, *8*.

[36] Massa, S.; Sakr, M.A.; Seo, J.; Bandaru, P.; Arneri, A.; Bersini, S.; Zare-Eelanjegh, E.; Jalilian, E.; Cha, B.H.; Antona, S. *et al.* Bioprinted 3D Vascularized Tissue Model for Drug Toxicity Analysis. Biomicrofluidics **2017**, *11*, 1-12.

[37] Grix, T.; Ruppelt, A.; Thomas, A.; Amler, A.; Noichl, B.P.; Lauster, R.; Kloke, L. Bioprinting Perfusion-Enabled Liver Equivalents for Advanced Organ-on-a-Chip Applications. Genes (Basel) **2018**, *9*, 176. doi: 10.3390/genes9040176.

[38] Klotz, B.J.; Gawlitta, D.; Rosenberg, A.J.W.P.; Malda, J.; Melchels, F.P.W. Gelatin-Methacryloyl Hydrogels: Towards Biofabrication-Based Tissue Repair. Trends Biotechnol. **2016**, *34*, 394-407.

[39] Ozbolat, I.T.; Hospodiuk, M. Current Advances and Future Perspectives in Extrusion-Based Bioprinting. Biomaterials **2016**, *76*, 321-343.

[40] Snyder, J.E.; Hamid, Q.; Wang, C.; Chang, R.; Emami, K.; Wu, H.; Sun, W. Bioprinting Cell-Laden Matrigel for Radioprotection Study of Liver by Pro-Drug Conversion in a Dual-Tissue Microfluidic Chip. Biofabrication **2011**, *3*.

[41] Krüger, M.; Oosterhoff, L.A.; van Wolferen, M.E.; Schiele, S.A.; Walther, A.; Geijsen, N.; De Laporte Laura; van der Laan, L.J.W.; Kock, L.M.; Spee, B. Cellulose Nanofibril Hydrogel Promotes Hepatic Differentiation of Human Liver Organoids. Advanced healthcare materials **2020**, e1901658.

[42] Klotz, B.J.; Oosterhoff, L.A.; Utomo, L.; Lim, K.S.; Vallmajo-Martin, Q.; Clevers, H.; Woodfield, T.B.F.; Rosenberg, A.J.W.P.; Malda, J.; Ehrbar, M. *et al.* A Versatile Biosynthetic Hydrogel Platform for Engineering of Tissue Analogues. Advanced Healthcare Materials **2019**, *8*.

[43] Benton, G.; Arnaoutova, I.; George, J.; Kleinman, H.K.; Koblinski, J. Matrigel: From Discovery and ECM Mimicry to Assays and Models for Cancer Research. Adv. Drug Deliv. Rev. **2014**, *79*, 3-18.

[44] Jungst, T.; Smolan, W.; Schacht, K.; Scheibel, T.; Groll, J.u. Strategies and Molecular Design Criteria for 3D Printable Hydrogels. Chem. Rev. **2016**, *116*, 1496-1539.

[45] Schwab, A.; Levato, R.; D'Este, M.; Piluso, S.; Eglin, D.; Malda, J. Printability and Shape Fidelity of Bioinks in 3D Bioprinting. Chem. Rev. **2020**, *120*, 11028-11055.

[46] Schuurman, W.; Levett, P.A.; Pot, M.W.; van Weeren, P.R.'.; Dhert, W.J.A.; Hutmacher, D.W.; Melchels, F.P.W.; Klein, T.J.; Malda, J. Gelatin-Methacrylamide Hydrogels as Potential Biomaterials for Fabrication of Tissue-Engineered Cartilage Constructs. Macromolecular Bioscience **2013**, *13*, 551-561.

[47] Levato, R.; Webb, W.R.; Otto, I.A.; Mensinga, A.; Zhang, Y.; van Rijen, M.; van Weeren, R.'.; Khan, I.M.; Malda, J. The Bio in the Ink: Cartilage Regeneration with Bioprintable Hydrogels and Articular Cartilage-Derived Progenitor Cells. Acta Biomaterialia **2017**, *61*, 41-53.

[48] Nguyen, A.K.; Goering, P.L.; Reipa, V.; Narayan, R.J. Toxicity and Photosensitizing Assessment of Gelatin Methacryloyl-Based Hydrogels Photoinitiated with Lithium Phenyl-2,4,6-Trimethylbenzoylphosphinate in Human Primary Renal Proximal Tubule Epithelial Cells. Biointerphases **2019**, *14*, 021007.

[49] Bertassoni, L.E.; Cardoso, J.C.; Manoharan, V.; Cristino, A.L.; Bhise, N.S.; Araujo, W.A.; Zorlutuna, P.; Vrana, N.E.; Ghaemmaghami, A.M.; Dokmeci, M.R. *et al.* Direct-Write Bioprinting of Cell-Laden Methacrylated Gelatin Hydrogels. Biofabrication **2014**, *6*.

[50] Hiller, T.; Berg, J.; Elomaa, L.; R ohrs, V.; Ullah, I.; Schaar, K.; Dietrich, A.C.; Al-Zeer, M.A.; Kurtz, A.; Hocke, A.C. *et al.* Generation of a 3D Liver Model Comprising Human Extracellular Matrix in an Alginate/Gelatin-Based Bioink by Extrusion Bioprinting for Infection and Transduction Studies. International Journal of Molecular Sciences **2018**, *19*, 1-17.

[51] Gori, M.; Giannitelli, S.M.; Torre, M.; Mozetic, P.; Abbruzzese, F.; Trombetta, M.; Traversa, E.; Moroni, L.; Rainer, A. Biofabrication of Hepatic Constructs by 3D Bioprinting of a Cell-Laden Thermogel: An Effective Tool to Assess Drug-Induced Hepatotoxic Response. Advanced Healthcare Materials **2020**, *2001163*, 1-11.

[52] Mazzocchi, A.; Devarasetty, M.; Huntwork, R.; Soker, S.; Skardal, A. Optimization of Collagen Type I-Hyaluronan Hybrid Bioink for 3D Bioprinted Liver Microenvironments. Biofabrication **2018**, *11*, 015003.

[53] Norona, L.M.; Nguyen, D.G.; Gerber, D.A.; Presnell, S.C.; LeCluyse, E.L. Modeling Compound-Induced Fibrogenesis in Vitro using Three-Dimensional Bioprinted Human Liver Tissues. Toxicological Sciences **2016**, *154*, 354-367.

[54] Goulart, E.; De Caires-Junior Luiz Carlos; Telles-Silva, K.A.; Araujo, B.H.S.; Rocco, S.A.; Sforca, M.; De Sousa Irene Layane; Kobayashi, G.S.; Musso, C.M.; Assoni, A.F. *et al.* 3D Bioprinting of Liver Spheroids Derived from Human Induced Pluripotent Stem Cells Sustain Liver Function and Viability in Vitro. Biofabrication **2020**, *12*.

[55] Faulkner-Jones, A.; Fyfe, C.; Cornelissen, D.J.; Gardner, J.; King, J.; Courtney, A.; Shu, W. Bioprinting of Human Pluripotent Stem Cells and their Directed Differentiation into Hepatocyte-Like Cells for the Generation of Mini-Livers in 3D. Biofabrication **2015**, *7*.

[56] Roche, C.D.; Sharma, P.; Ashton, A.W.; Jackson, C. Printability, Durability, Contractility and Vascular Network Formation in 3D Bioprinted Cardiac Endothelial Cells using Alginate-Gelatin Hydrogel. **2021**, *9*, 1-14.

[57] Brassard, J.A.; Nikolaev, M.; Hübscher, T.; Hofer, M.; Lutolf, M.P. Recapitulating Macro-Scale Tissue Self-Organization through Organoid Bioprinting. Nature Materials **2020**.

[58] Davidenko, N.; Schuster, C.F.; Bax, D.V.; Farndale, R.W.; Hamaia, S.; Best, S.M.; Cameron, R.E. Evaluation of Cell Binding to Collagen and Gelatin: A Study of the Effect of 2D and 3D Architecture and Surface Chemistry. J. Mater. Sci. Mater. Med. **2016**, *27*.

[59] Lee, H.; Chae, S.; Kim, J.Y.; Han, W.; Kim, J.; Choi, Y.; Cho, D. Cell-Printed 3D Liver-on-a-Chip Possessing a Liver Microenvironment and Biliary System. Biofabrication **2018**, *11*, 25001.

[60] Ma, X.; Yu, C.; Wang, P.; Xu, W.; Wan, X.; Lai, C.S.E.; Liu, J.; Koroleva-Maharajh, A.; Chen, S. Rapid 3D Bioprinting of Decellularized Extracellular Matrix with Regionally Varied Mechanical Properties and Biomimetic Microarchitecture. Biomaterials **2018**, *185*, 310-321.

[61] Bale, S.S.; Borenstein, J.T. Microfluidic Cell Culture Platforms to Capture Hepatic Physiology and Complex Cellular Interactions. Drug Metab. Disposition **2018**, *46*, 1638-1646.

[62] Foster, A.J.; Chouhan, B.; Regan, S.L.; Rollison, H.; Amberntsson, S.; Andersson, L.C.; Srivastava, A.; Darnell, M.; Cairns, J.; Lazic, S.E. *et al.* Integrated in Vitro Models for Hepatic Safety and Metabolism : Evaluation of a Human Liver-Chip and Liver Spheroid. Arch. Toxicol. **2019**, *93*, 1021-1037.

[63] Allen, J.W.; Khetani, S.R.; Bhatia, S.N. In Vitro Zonation and Toxicity in a Hepatocyte Bioreactor. Toxicological Sciences **2005**, *84*, 110-119.

[64] Ahn, J.; Ahn, J.; Yoon, S.; Nam, Y.S.; Son, M.; Oh, J. Human Three-Dimensional in Vitro Model of Hepatic Zonation to Predict Zonal Hepatotoxicity. **2019**, *5*, 1-15.

[65] Zhou, Y.; Shen, J.X.; Lauschke, V.M. Comprehensive Evaluation of Organotypic and Microphysiological Liver Models for Prediction of Drug-Induced Liver Injury. Frontiers in Pharmacology **2019**, *10*, 1-22.

[66] Xu, J.; Oda, S.; Yokoi, T. Cell-Based Assay using Glutathione-Depleted HepaRG and HepG2 Human Liver Cells for Predicting Drug-Induced Liver Injury. Toxicology in Vitro **2018**, *48*, 286-301.

[67] Yoon, E.; Babar, A.; Choudhary, M.; Kutner, M.; Pyrsopoulos, N. Acetaminophen-Induced Hepatotoxicity: A Comprehensive Update. J. Clin. Transl. Hepatol. **2016**, *4*, 131-142.

[68] Ribeiro, A.J.S.; Yang, X.; Patel, V.; Madabushi, R.; Strauss, D.G. Liver Microphysiological Systems for Predicting and Evaluating Drug Effects. Clin. Pharmacol. Ther. **2019**, *106*, 139-147.

[69] Lin, C.; Khetani, S.R. Advances in Engineered Liver Models for Investigating Drug-Induced Liver Injury. Biomed. Res. Int. **2016**, *2016*, 1829148.

[70] Goldring, C.; Norris, A.; Kitteringham, N.; Aleo, M.D.; Antoine, D.J.; Heslop, J.; Howell, B.A.; Ingelman-Sundberg, M.; Kia, R.; Kamalian, L. *et al.* Mechanism-Based Markers of Drug-Induced Liver Injury to Improve the Physiological Relevance and Predictivity of in Vitro Models. Applied In Vitro Toxicology **2015**, *1*, 175-186.

[71] Dragovic, S.; Vermeulen, N.P.E.; Gerets, H.H.; Hewitt, P.G.; Ingelman-Sundberg, M.; Park, B.K.; Juhila, S.; Snoeys, J.; Weaver, R.J. Evidence-Based Selection of Training Compounds for use in the Mechanism-Based Integrated Prediction of Drug-Induced Liver Injury in Man. Arch. Toxicol. **2016**, *90*, 2979-3003.

[72] Melchels, F.P.W.; Blokzijl, M.M.; Levato, R.; Peiffer, Q.C.; de Ruijter, M.; Hennink, W.E.; Vermonden, T.; Malda, J. Hydrogel-Based Reinforcement of 3D Bioprinted Constructs. Biofabrication **2016**, *8*, 035004-5090/8/3/035004.

[73] van Steenbeek, F.G.; Spee, B.; Penning, L.C.; Kummeling, A.; van Gils, I.H.M.; Grinwis, G.C.M.; van Leenen, D.; Holstege, F.C.P.; Vos-Loohuis, M.; Rothuizen, J. *et al.* Altered Subcellular Localization of Heat Shock Protein 90 is Associated with Impaired Expression of the Aryl Hydrocarbon Receptor Pathway in Dogs. PLoS ONE **2013**, *8*.

[74] Kroh, E.M.; Parkin, R.K.; Mitchell, P.S.; Tewari, M. Analysis of Circulating microRNA Biomarkers in Plasma and Serum using Quantitative Reverse Transcription-PCR (qRT-PCR). Methods **2010**, *50*, 298-301.

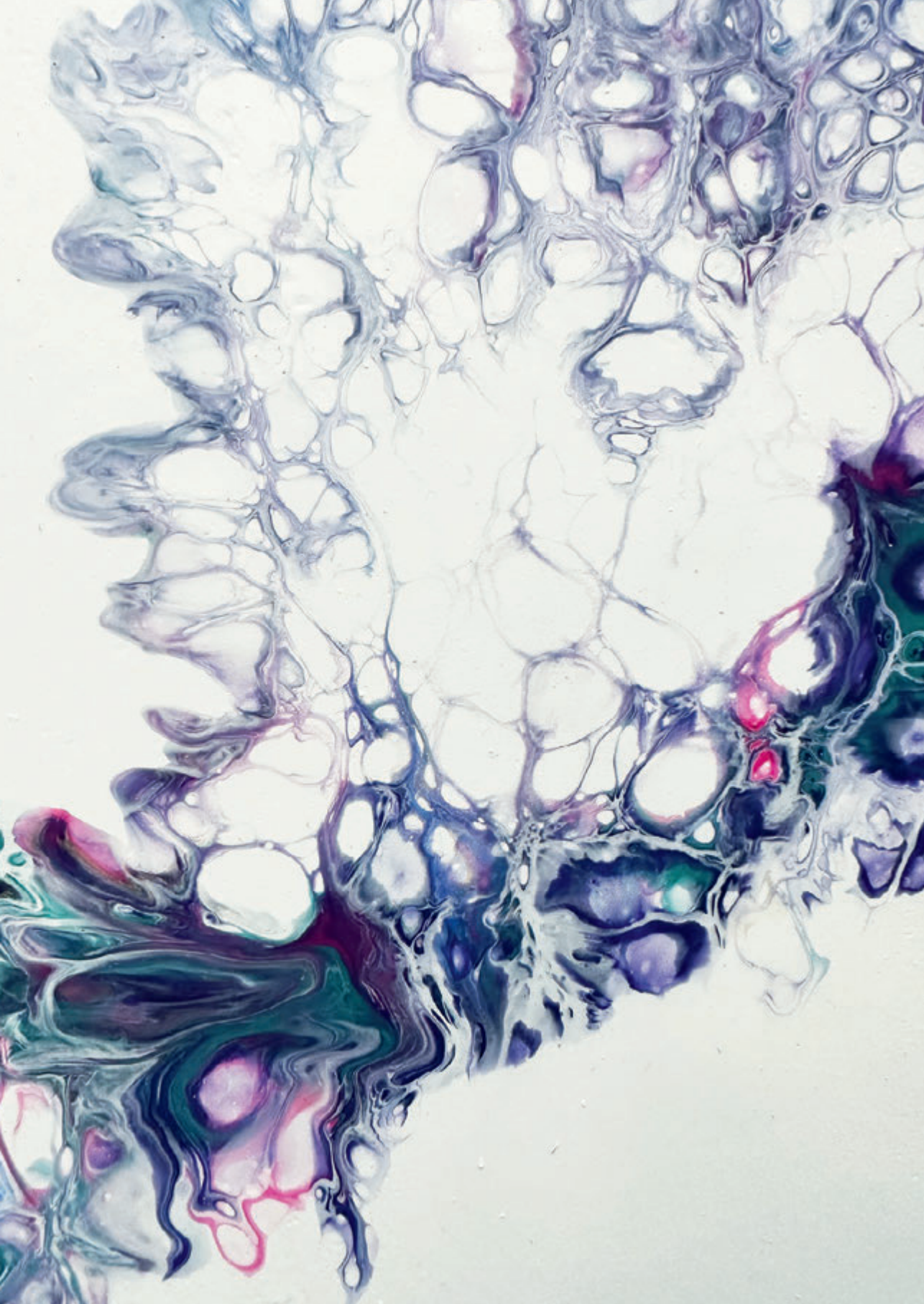

Volumetric Bioprinting of Organoids and Optically Tuned Hydrogels to Build Liver-Like Metabolic Biofactories

Paulina Nuñez Bernal[†,1], Manon C. Bouwmeester[†,2], Jorge Madrid-Wolff[3], Marc Falandt[2], Sammy Florczak[1], Nuria Ginés Rodriguez[1], Yang Li[1], Gabriel Größbacher[1], Roos-Anne Samsom[2], Monique van Wolferen[2], Luc J.W. van der Laan[4], Paul Delrot[5], Damien Loterie[5], Jos Malda[1,2], Christophe Moser[3], Bart Spee[2], Riccardo Levato[1,2]

1 Department of Orthopaedics, University Medical Center Utrecht, Regenerative Medicine Center Utrecht, 3584 CT Utrecht, The Netherlands
2 Department of Clinical Sciences, Faculty of Veterinary Medicine, Regenerative Medicine Center Utrecht, Utrecht University, 3584 CT Utrecht, The Netherlands
3 Laboratory of Applied Photonics Devices, École Polytechnique Fédéral Lausanne (EPFL), CH-1015 Lausanne, Switzerland
4 Department of Surgery, Erasmus MC Transplant Institute, University Medical Center Rotterdam, 3015 CN Rotterdam, The Netherlands
5 Readily3D SA, EPFL Innovation Park, Building A, CH-1015 Lausanne, Switzerland
† These authors contributed equally to this work.

Published in Advanced Materials (2022); 34(15):2110054. doi: 10.1002/adma.202110054

4

ABSTRACT

Organ- and tissue-level biological functions are intimately linked to microscale cell-cell interactions and to the overarching tissue architecture. Together, biofabrication and organoid technologies offer the unique potential to engineer multi-scale living constructs, with cellular microenvironments formed by stem cell self-assembled structures embedded in customizable bioprinted geometries. This study introduces the volumetric bioprinting of complex organoid-laden constructs, which capture key functions of the human liver. Volumetric bioprinting via optical tomography shaped organoid-laden gelatin hydrogels into complex centimeter-scale 3D structures in under 20 seconds. Optically-tuned bioresins enabled refractive index matching of specific intracellular structures, countering the disruptive impact of cell-mediated light scattering on printing resolution. This layerless, nozzle-free technique poses no harmful mechanical stresses on organoids, resulting in superior viability and morphology preservation post-printing. Bioprinted organoids underwent hepatocytic differentiation showing albumin synthesis, liver-specific enzyme activity, and remarkably acquired native-like polarization. Organoids embedded within low stiffness gelatins (<2 kPa) were bioprinted into mathematically-defined lattices with varying degrees of pore network tortuosity, and cultured under perfusion. These structures acted as metabolic biofactories in which liver-specific ammonia detoxification could be enhanced by the architectural profile of the constructs. This technology opens up new possibilities for regenerative medicine and personalized drug testing.

Keywords
Biofabrication; Volumetric additive manufacturing; Light-based 3D printing; Bioresin; Hydrogel

INTRODUCTION

Laboratory-made three-dimensional (3D) living constructs that fully retain the function of human tissues and organs remain a major hope for regenerative medicine and for the development of advanced *in vitro* models for drug discovery, toxicology testing and precision medicine [1,2]. Biofabrication approaches, thanks to their ability to precisely orchestrate the three-dimensional (3D) patterning of multiple types of cells and biomaterials, have great potential to generate key architectural elements that can instruct the emergence of native functionalities in engineered tissues [2]. To date, various bioprinting techniques, a subset of biofabrication approaches in which one or several cellular components are directly incorporated in an additive manufacturing process [3], have played a primary role in several proof-of-concept applications that showed the mimicry of salient organ functions *in vivo*, including in engineered ovaries [4], thyroid glands [5], and innervated skeletal muscle-like constructs [6]. The versatility and the freedom of design guaranteed by bioprinting technologies can be exploited both to generate anatomical-like as well as engineering-inspired architectures. While the exact degree of biomimicry that an engineered tissue should have right after the fabrication step is still a matter of debate, it is generally agreed that recapitulating every detail of physiological structures may not be needed, while providing cells with an environment to initiate and boost their own biological functionality is more important [4,5,7,8]. However, developing complex living structures of physiologically-relevant size (i.e., dimension above the centimeter-scale) that can favorably guide cell behavior remains a major challenge. In addition, while bioprinting excels at modulating the environment surrounding the printed cells, tissue morphogenesis events *in vivo* are primarily driven by cell-cell interactions and self-assembly at the microscale, and thus cannot be directly controlled in a bioprinting strategy. Thanks to the development of organoids, which are miniaturized 3D structures that express key organ-like behavior, harnessing such cell-driven organization *in vitro* has led to a major breakthrough in biomedical research [9]. Even though organoids can also be generated from differentiated primary cells, most of the systems developed up to now arise from stem cells (harvested from adult tissue, or induced pluripotent cells) [10]. Stem-cell derived systems are particularly promising due to their self-renewal capacity, helping to obtain sufficient organoid numbers for downstream applications, and due to the potential of the cells to differentiate into the multiple lineages that compose the tissue of reference [10]. However, organoid development in conventional tissue culture on Matrigel-like substrates is highly aleatory, offering no control over individual architecture, and resulting in sizes limited to the millimeter range.

In this work, we introduce a new, generalizable strategy for the light-driven volumetric bioprinting (VBP) of complex, functional organoid-laden constructs (Figure 1A). VBP is a layerless printing approach capable of printing positive and negative features (channels) at high resolutions (41.5 ± 2.9 μm and 104.0 ± 5.5 μm, respectively) (Figures 1B-C) and large-scale constructs previously achieving volumes of up to 4.14 cm^3 in less than 30 seconds [11]. Given the novelty of the technology and of its working principle, which relies on the precise delivery of multiple tomographic light projections onto a cell-laden photopolymer, little is still known on the interplay between the cells and the precisely patterned projected light as well as on the printability requirements that a biomaterial needs to fulfill. Thus, first we investigated a new technique to engineer the optical properties of cell-laden hydrogels for VBP and unraveled its impact on printing shape fidelity. Leveraging this knowledge, in the present study VBP is combined for the first time with organoids that exhibit a microscale multicellular structure. These are herein bioprinted into centimeter-scale structures with designed architectures that facilitate access to metabolites. To meet the large cell numbers required for the volumetric bioprinting process (in the range of tens of millions of cells, at the densities shown throughout this study), a dynamic spinner flask culture system is used to establish organoid structures from human tissue samples (Figure 1D). As a proof-of-concept, we demonstrate the fabrication of centimeter-scale hydrogel-based objects embedding human liver epithelial organoids, obtained from primary (stem) cells found in intrahepatic bile ducts [8]. Differently from dense aggregates obtained from differentiated hepatic cells, that do not usually acquire native microarchitectural features of the liver [12], these organoids are epithelial in nature, and form a cyst-like structure with an inner hollow lumen surrounded by a thin cell (mono)layer (Figure 1D) [13]. This specific organization is especially interesting since many liver functions are dependent on hepatocyte polarization, i.e., the directional transfer and secretion of compounds from and towards the apical or basolateral side of the cell. Importantly, since the specialized microarchitecture of the organoids can be easily compromised by mechanical stresses, a particular attention was placed on the ability of the printing process to preserve the self-organization of these biological building units. Thus, in this work epithelial liver organoids were selected to study how they can act as metabolically active biofactories, in which a prominent detoxification function of the liver can be modulated by the overall architecture of the construct, as defined via the volumetric printing process (Figure 1E).

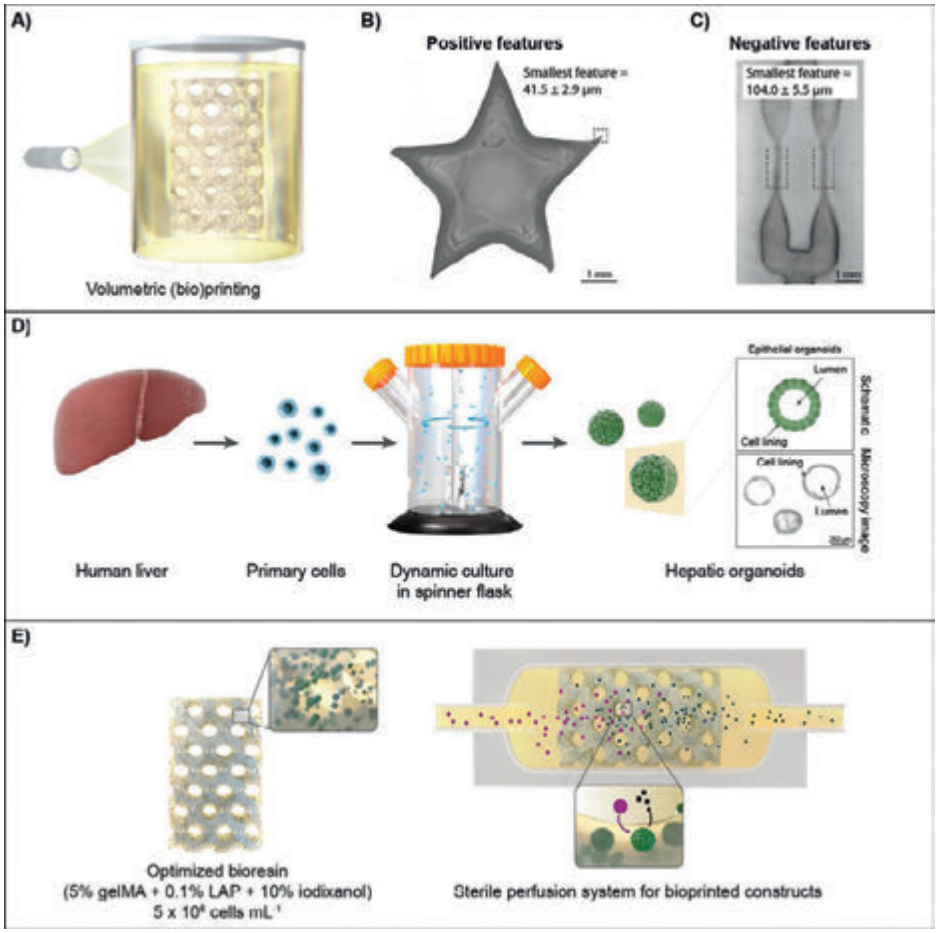

Figure 1. Overview of the high-resolution volumetric printing process and study design. A) Schematic representation of the volumetric printing process. B-C) Highest resolution prints of B) positive and C) fully perfusable negative features achieved with the 5% gelMA + 0.1% LAP bioresin used in this study (scale bars = 1 mm). Samples were imaged when being immersed in PBS directly after printing. D) Diagram of the hepatic organoid culture system, starting with human liver biopsies and isolation into single cells, which are then dynamically cultured in a spinner flask system to establish high yields of hollow epithelial organoid structures (microscopy image scale bar = 250 µm). E) Illustration of a complex, organoid-laden printed biofactory cultured under dynamic perfusion to enhance hepatic function, showing a representation of the breakdown of perfused compounds (purple circles) into metabolites (black squares).

RESULTS AND DISCUSSION

Volumetric bioprinting is an emerging light-based technology capable of sculpting cell-laden photoresponsive hydrogels - also termed bioresins - into 3D constructs of various sizes, ranging up to several cubic centimeters, and complex geometries in a layerless fashion [11]. Leveraging the principles of tomographic additive manufacturing [14,15], in VBP, a vat containing the bioresin is illuminated with visible light from multiple angles using a sequence of filtered backprojections of the object to be printed. While the light patterns address the whole build volume, the cumulative energy dose provided by the projections exceeds the bioresin's photocrosslinking threshold only in the geometry corresponding to the programmed object, thus building the whole construct at once. In this way, VBP yields centimeter-scale structures embedding microscale features in tens of seconds [11]. The rapid fabrication time and cell-friendly light doses are beneficial for preserving cell viability and functionality post-printing, whereas extensive printing times required to fabricate large parts can be of concern for conventional layer-by-layer manufacturing (i.e., extrusion- and lithographic-based methods) [16]. Moreover, via VBP, elements like overhangs, moving parts and convoluted porous networks typical of native tissues, can be easily recapitulated without the need for sacrificial or support materials, as previously reported reproducing the trabecular meshwork of cancellous bone [11].

As the first step towards the fabrication of organoid-laden structures, we investigated the impact of the optical properties of the bioresin on printing resolution, in particular the ability of the cell-laden material to homogenously transmit light. As opposed to extrusion-based bioprinting (EBB), in which printability is predominantly governed by the rheological properties of a bioink [17-20], in VBP and other light-based approaches, such as stereolithography and digital light processing, the printing resolution is defined primarily by the photopolymerization kinetics of the material, and by the ability to precisely control the spatial distribution of the light dose within the bioresin volume. While EBB of photocrosslinkable materials requires rapid polymerization kinetics as well to ensure construct stability, in VBP the latter is key in achieving highly accurate prints. This factor is largely dependent on the resolution of the light projection, the spatial coherence of the light source, the algorithm for generating the set of patterns (for a digital micromirror device, the optical resolution is given by the effective pixel size projected in the print volume), and the presence or absence of scattering elements. The latter is of particular relevance for bioprinting applications, since cells and many subcellular structures are capable of altering the path of incident light, either causing attenuation of ballistic photons or scattering, therefore affecting printing resolution. In

particular, scattered light will blur the projected tomographic images, causing an increase of the light dose in regions of the volume adjacent, but external to the part to be printed. Depending on the length of the scattering mean free path at a given wavelength (which is a measurement of the average distance between two consecutive scattering events, thus inversely proportional to the cell density [21]), this can result in off-target polymerization and loss of resolution. In addition, the ballistic light attenuation caused by scattering decreases the addressable size of the construct in the vial.

To investigate this effect, we printed a 5% w/v gelatin methacryloyl (gelMA)-based bioresin (Figure S1) supplemented with 0.1% w/v lithium phenyl-2,4,6-trimethylbenzoylphosphinate (LAP) as photoinitiator carrying either a single cell suspension of a well-known hepatic cell line (HepG2) (Figure 2A) or epithelial organoids derived from human liver (Figure 2B) in the form of a hollow disc with an S-shape filament (thickness = 500 µm) placed at its center (Figure S2). This specific size was selected to generate filaments that could completely embed the produced organoids, even though finer printing resolution are possible as shown before in Figures 1B and C, in which resolution superior to what shown with volumetric printing up to date has been demonstrated [14,15,22,23]. In an ideal print, both the thick border of the disc and the thinner filament, herein used as a benchmark to quantify the printing resolution, should solidify at the same time after receiving the same, optimal light dose. Exceeding this optimal dose will cause overcuring of the fine feature, thickening of the filament wall, and eventually clogging of the disc. At a low cell density ($1x10^6$ individual cells mL^{-1}) the bioresin is photocrosslinked at an exposure dose of 250 mJ cm^{-2}, and the fine features can be correctly resolved (at 312 mJ cm^{-2}) with both single HepG2 cells and organoids. At higher cell concentrations, the minimal light dose required for crosslinking single cell suspensions rises, and the slope of the dose-thickness curve rapidly increases, narrowing the ideal printing window. Consequently, with the currently available hardware and software, printing at high cell densities is possible (as previously shown with up to 10^7 articular cartilage progenitor cells mL^{-1}) [11]. However, this requires a fine empirical adjustment of the delivered dose, which is often impractical when cells are available in limited amounts. A similar trend was observed for organoid-laden bioresins, although the printing process yielded a larger printability window compared to what was observed with single cells, as loss of shape fidelity in reproducing the fine feature was observed only at $5x10^6$ cells mL^{-1} (Figure S3), a cell density selected for this investigation due to its already proven suitability for functional liver tissue engineering studies [24-33]. This result can be explained by the fact that liver organoids form cyst-like, hollow structures delimited by an epithelial cell monolayer [13]. Due to their relatively large size (~300µm), organoids have a longer scattering mean free path, compared to single cell

suspensions at any given equivalent cell concentration. Recent research efforts are introducing novel algorithms for tomographic printing that can correct for scattering events at the filtered projection-level, and thus ensure high resolution printing even in opaque media [34]. Although this has been only shown with resins carrying homogenously-sized particles so far [34], future translation to materials laden with cells, which have more complex light scattering profiles, will help expand the range of applications of VBP.

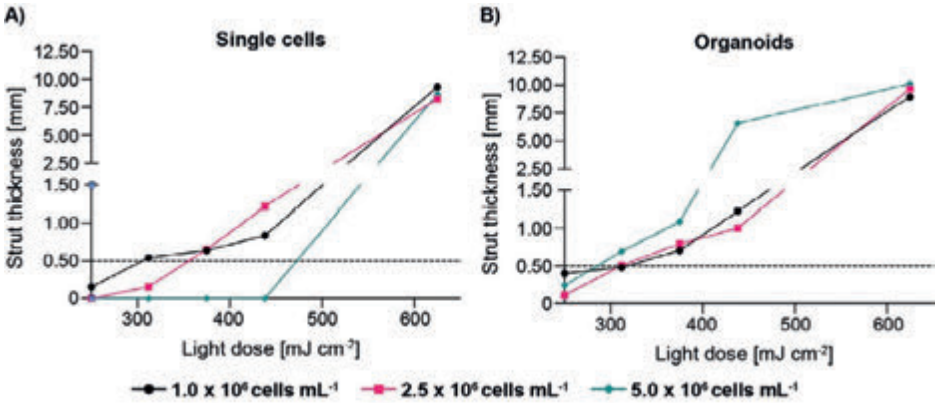

Figure 2. Effect of single cell and organoid density on volumetric bioprinting accuracy in absence of optical corrections. Fine feature thickness in constructs printed at increasing light doses (250 – 625 mJ cm^{-2}) with bioresins containing different densities of A) single cell and B) organoid (1 – 5 x 10^6 cells mL^{-1}). Dashed line represents the programmed feature dimension of the printed model (selected to be 500 µm to accommodate for the size of the printed organoids) (n = 3).

Cell-mediated scattering can also be addressed from the biomaterial-design perspective, by tuning the optical properties of the bioresin. In this study, we introduced a biocompatible and water-miscible refractive index matching compound, iodixanol, in order to modulate the optical performance of the gelMA-based bioresins (Figure 3A). Iodixanol was selected as it was proven not to harm cellular structures and tissue components, since this iodine, non-ionic compound has been applied for *in vivo* imaging [35], as contrast agent for x-ray imaging [36], and as an agent for the isolation of extracellular vesicles when preserving the integrity of membrane proteins is needed [37]. In principle, scattering-driven artefacts could be completely obviated, if the refractive index of the hydrogels matches that of the scattering element (i.e., the cells). However, cells are highly heterogeneous, composed of several subcellular structures each characterized by its own average refractive index (Table S1) [38]. Furthermore, different cell types and even individual cells within the same population have a unique light scattering fingerprint. Selected concentrations

of iodixanol could thus be tested to approximate the light refracting profile of key subcellular components that play a major role in light scattering at 405 nm (the wavelength used in the printer), which primarily includes the nucleus, contributing to increased ballistic light [38].

Supplementation with iodixanol successfully improved printing resolution both when using bioresins embedding single cells or liver organoids at $5x10^6$ cells mL^{-1} (Figure 3B), and it increased the refractive index of the bioresin in a concentration dependent manner, from 1.352 (pristine gelMA) up to 1.3783 at a 40% w/v (Figure 3C). The characterization of the angular light scattering profile in bioresins laden with single cells and organoids, supplemented with increasing iodixanol concentrations (Figure 3D, E), confirmed the experimentally found result that more optical power was directed in the forward direction. The extracellular refractive index change caused by the addition of iodixanol provides a better match to the overall refractive index of the organoids and thus light is less scattered, which is indicated quantitatively by a measured anisotropy coefficient closer to 1 (unity indicates no scattering). This effect was observed for both single cells and organoids. In terms of volumetric bioprinting, this made it possible to identify a working window for printing hepatocytic cells of 30% w/v iodixanol and organoids with as low as 10% w/v iodixanol (Figures 3F, S4, statistical analyses in Tables S2, S3). Importantly, the positive effect of the printing optimization via hydrogel optical tuning can be readily applied to produce thin features also when utilizing higher cell densities (herein tested with $1.5x10^7$ cells mL^{-1}). This was shown by printing star-shaped hydrogel structures with the smallest resolved points measuring 49.2 ± 8.4 µm and 50.5 ± 6.0 µm, when using single cells and organoids respectively, although the organoids, given their large size exceeding the minimum print resolution, may of course protrude from the gel in the proximity of the finest features (Figure S5). Notably, this approach for optical tuning of the biomaterials could potentially be combined with upcoming software-end based algorithms to further enhance printing resolution [34].

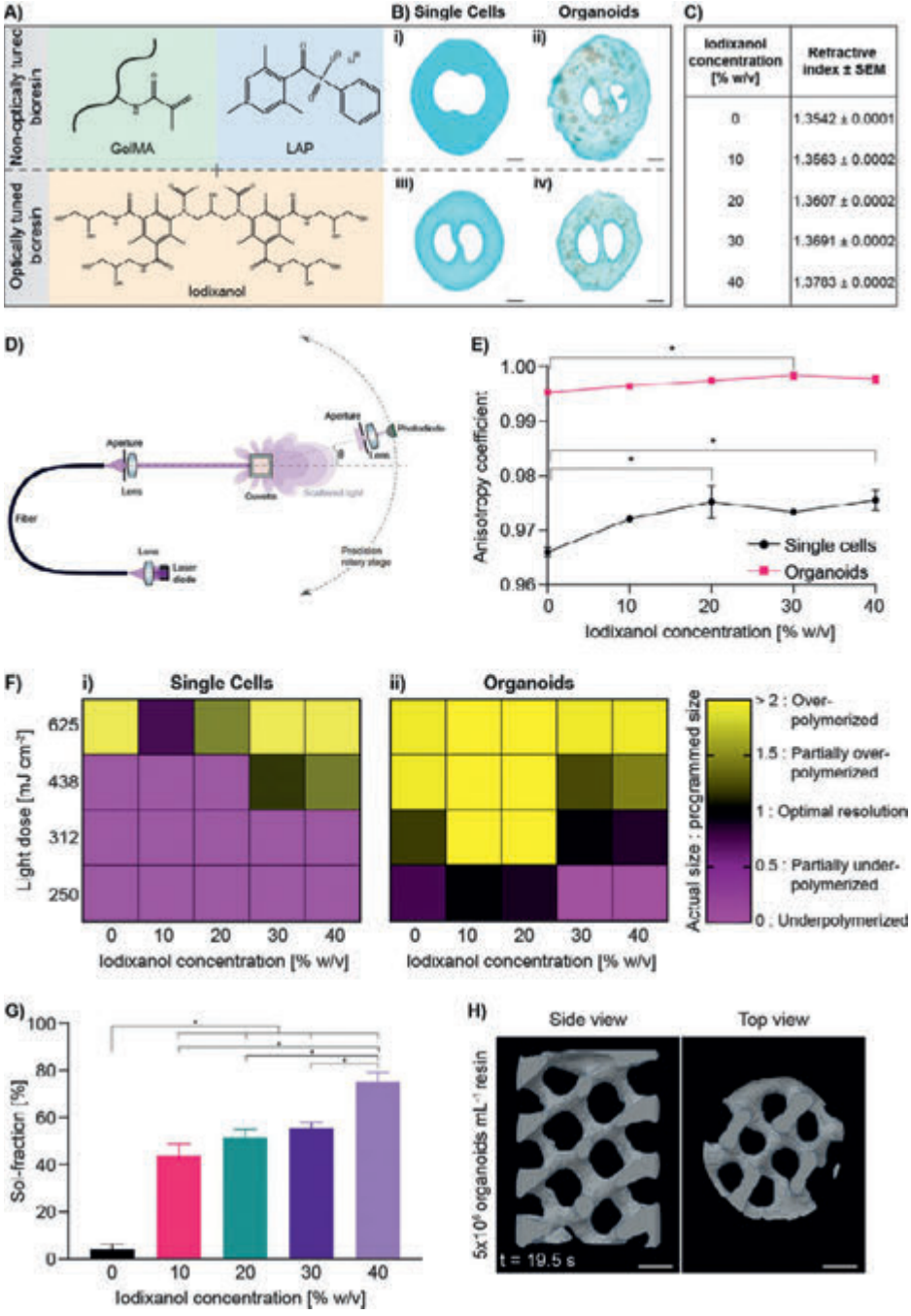

Figure 3. Enhancing volumetric bioprinting of single cells and hepatic organoids through bioresin optical tuning with iodixanol. A) Schematic of the bioresins used for volumetric bioprinting consisting of gelMA and LAP, supplemented with iodixanol to

optically tune the bioresin for enhanced printing accuracy in the presence of cellular structures. B) Stereomicroscopy images of i, ii) non-optically tuned bioresin and iii), iv) iodixanol-containing bioresins for printing single cells and organoids (scale bars = 1 mm). C) Refractive index of the pristine and optically-tuned bioresins (n = 3). D) Schematic of the light scattering measuring setup, and E) resulting anisotropy coefficient of different bioresin samples containing 5 x 10^6 mL^{-1} single cells and organoids and increasing iodixanol content (n = 3). F) Printability window of 5 x 10^6 mL^{-1} single cells and organoids represented by the ratio of the printed fine feature thickness to the programmed thickness (n = 3). G) Soluble fraction of gelMA samples containing increasing iodixanol concentrations (n = 3). H) Side and top view of cross-sections from the 3D reconstruction of a complex bioprinted gyroidal structure with the optimized bioresin formulation carrying 10% w/v iodixanol (scale bars = 2 mm). * = significant difference ($p < 0.05$).

It should be noted that, while these results apply to the liver cells tested in this study, such optimization of the refractive index of the bioresin is likely to result in a different optimal printing window when utilizing another cell population. From the chemico-physical point of view, iodixanol is intended as a fugitive additive, and it passively diffuses out of the hydrogel after crosslinking. Sol-fraction analysis revealed that in presence of iodixanol concentrations from 10 to 40% w/v, the sol fraction of the bioresins increased from 44.0 ± 4.7 % to 75.3 ± 3.9 %, whereas pristine gelMA showed lower values (4.2 ± 2.1 %) (Figure 3G). Such high values for the mass loss after 24h can be explained by the partial diffusion of the refractive index matching compound out of the gels, but also indicate that part of the additive, which forms a viscous solution at room temperature, is likely still trapped in the gel and may be released over a longer time frame. Thus, to minimize the presence of this extra component in the culture environment and ensure hydrogel stability for the subsequent prints embedding liver organoids, the bioresin formulation containing the lowest amount of iodixanol (10% w/v) was selected. This optimized, optically tuned bioresin composition made it possible to resolve complex 3D structures, such as gyroidal constructs (Figure 3H) printed in under 20 seconds (195 mJ cm^{-2}, 19.5 s printing time), which are otherwise not possible to bioprint with conventional extrusion methods, especially with soft materials needed for tissue culture.

Having identified a bioresin formulation for printing with high shape fidelity in presence of increasing cell concentrations, we further explored the advantages of combining VBP and organoid technology to create a bioengineered construct able to perform native-like liver function, given the critical role of the liver in maintaining systemic homeostasis. Notably, the distinguishing ability of liver epithelial organoids to capture micro-scale level architectures present in the liver, together with the fact that they can be readily obtained from individual patients and healthy donors via minimally invasive biopsies, holds potential for the development of advanced *in vitro* models for drug discovery and

toxicology in personalized medicine. Such new platforms are especially needed in biomedical research, as liver damage is a primary cause for post-marketing withdrawal of new drugs [39], a situation accentuated by the fact that current animal and cell culture models are insufficient to fully predict human physiology or donor-dependent responses [40,41]. The performance of liver organoids within the selected hydrogel upon bioprinting via VBP was investigated. Given the inherent challenge in replicating the multifaceted biosynthetic functions of native hepatocytes *in vitro*, we specifically analyzed i) the viability of the printed structures, and ii) the influence of the VBP on organoid microstructure and morphology, as a preliminary step to promote the differentiation and maturation capacity of the printed construct into hepatic-like structures.

The liver organoids used in this study were originally derived from adult stem cells positive for EpCAM and for leucine-rich repeat-containing G-protein coupled receptor 5 (LGR5) [13], obtained through expansion in a dynamic stirred bioreactor [42]. Recent works further probing the *in vivo* origin of these cells suggest that these cells may be intrahepatic cholangiocytes, which display bi-potent differentiation capacity [43]. These adult cells have already been demonstrated to maintain genomic stability over multiple passages [13], suggesting they can be an ideal source when high cell numbers are required for liver tissue engineering applications. As these hepatic organoids are available from donor tissues, they also have the potential for simulating a patient-specific response to drugs, as well as the production of catabolites or toxic compounds natively metabolized in the liver for drug discovery and toxicology studies, or serve as promising building blocks for whole organ engineering [44]. However, when freshly isolated and expanded, these cells do not normally display specific hepatocytic phenotype commitment [43]. The liver organoids obtained from these cells are typically expanded in presence of laminin-rich basal membrane extracts (i.e., Matrigel), in culture media cocktails that maintain them in a proliferative state. Their differentiation into hepatocytic structures is accompanied by an inhibition of proliferation and can be triggered by switching the media composition (key components being bone morphogenetic protein-7 and fibroblast growth factor-19) [42].[This process has also been shown to be greatly influenced by mechano-chemical stimuli provided by different biomaterials and culture conditions [45]. As a first step, it was paramount to assess how organoids in differentiation media respond to the milieu defined by the VBP process.

Thus, upon printing, liver organoid-laden hydrogels were cultured in differentiation media. First, it was confirmed that iodixanol had no detrimental effect on the metabolic activity of the organoids, even when used in concentrations up to 40% w/v. In particular, all the tomographically bioprinted

samples performed similarly to casted controls in absence of iodixanol, in which a slight decrement of resazurin reduction from day 1 to day 10 of culture was observed (Figure 4A). This was in line with what was previously observed for liver organoids cultured in differentiation conditions using other natural-origin hydrogels such as cellulose nanofibril-derived gels [46].

The evolution of the metabolic activity over 10 days was also assessed in further detail with the optimized bioresin supplemented with 10% w/v iodixanol. The performance of constructs obtained from cells from three adult donors, was evaluated comparing samples generated via VBP, EBB, and casted gelMA (with and without iodixanol) and Matrigel controls to assess the impact of different fabrication approaches and materials (Figure 4B, further statistical details in Figure S6). In all gelMA samples, the metabolic activity remained constant, whereas in the Matrigel control, a gradual increase was observed over the culture period. In the latter, this increment was accompanied by a higher amount of DNA in the samples (Table S4). This result is coherent with the notion that Matrigel is a favorable substrate for organoid proliferation [46].

Having demonstrated the cytocompatibility of the bioresin and of the printing process, an important objective was to evaluate if VBP could be used to preserve organoid structure, including the specific cell-cell contacts, tight junctions, and communication channels established during the organoid formation phase. During the expansion phase, organoids can reach millimeter-scale sizes, and in general, the growth to larger dimensions is regarded as an indicator of cell health [42]. As a light-based biofabrication technology, VBP does not subject cells to potentially harmful shear stresses that can instead be experienced in nozzle-based techniques [47]. Moreover, in extrusion-based bioprinting, nozzles typically displaying diameters 2-3 times larger than these organoid structures are required in order to avoid clogging [48], thus imposing a compromise on printing resolution. Alternatively, organoids need to be fragmented via mechanical or enzymatic disruption to enable seamless flow of the bioink during printing.

A LIVE/DEAD fluorescent staining post-printing revealed that organoids printed via VBP displayed superior viability (93.3 ± 1.4 %) and undisturbed average size (273.5 ± 49.9 μm) when compared to EBB (73.2 ± 1.2 % viability, 100.1 ± 14.2 μm average size) one day post-printing (Figure 4C, D, E). Such high viability, as demonstrated by the positive staining of Calcein AM into the cells lining the hollow organoid structures, was comparable or superior to casted gelMA and Matrigel controls. Notably, for all samples, it was found that most of the dead cells were single cells shed from the organoids, which appeared in higher numbers in the samples containing fragmented cells processed via EBB. This

significant difference in dead cell numbers between the VBP conditions and the other processing methods can likely be attributed to the fact that the nozzle-free nature of VBP allows for the maintenance of the structural integrity of the organoids by minimizing the shear stresses induced on these large structures through actions such as pipetting or extruding through a nozzle. The EBB samples, which show the lowest viability at day 1, exhibit high number of dead cells likely due to i) a high number of single cells resulting from the mechanical fragmentation of the organoids pre-printing that are not capable of reassembly when incorporated in the hydrogels, and ii) further organoid damage and breakdown into single cells and smaller fragments due to the shear stresses experienced during extrusion through the nozzle (Figure 4D). This is further supported by the significantly smaller organoid sizes observed in EBB samples during the differentiation period (Figure 4E). Casted organoids in gelMA and Matrigel on the other hand, only undergo shear stresses as the embedded organoids pass through the narrow pipette tip for controlled volume deposition for the casting process, instead of the extensive fragmentation of EBB-printed organoids. This is likely the reason for the significantly higher viability compared to the EBB condition. Over time, viability values reached comparable values (94.1 – 98.2 %) for all experimental groups and controls. This was predominantly due to the fact that dead cells are removed from the culture environment with each media exchange, paired with the preservation of the cell viability already discussed for the biomaterials used in this study. To date, organoid shaping via bioprinting has been demonstrated via extrusion of a suspension of single stem cells, which are then led to re-form into organoids post-printing [49]. Alternatively, biofabrication of pre-generated organoids has been prevalently performed via molding [50], individual spheroid dispensing [5], or robotic-assisted pick-and-place techniques [51]. Although yielding impressive results in terms of generating tissues with high cell content, these approaches are limited to relatively simple 3D geometries, and rely on the printing of thick filaments/spheroids with a 400-1000 µm diameter range to achieve simple tubular structures [5,49-51]. Complementing the possibilities granted by such strategies, the ability of VBP to print pristine, undamaged organoids offers an alternative to facilitate the free-form generation of intact organoid-laden constructs. Printing morphologically intact organoids can be advantageous for applications aiming to preserve the organoid pre-deposited ECM, given the increasing evidence that cells embedded in biomaterials alter their behavior via contact with the nascent, self-synthesized ECM [52]. Even though in the context of liver tissue engineering, hepatocytes alone have limited capacity to secrete extracellular matrix proteins, this could be relevant especially when incorporating other liver-specific cell types, such as stellate cells [53].

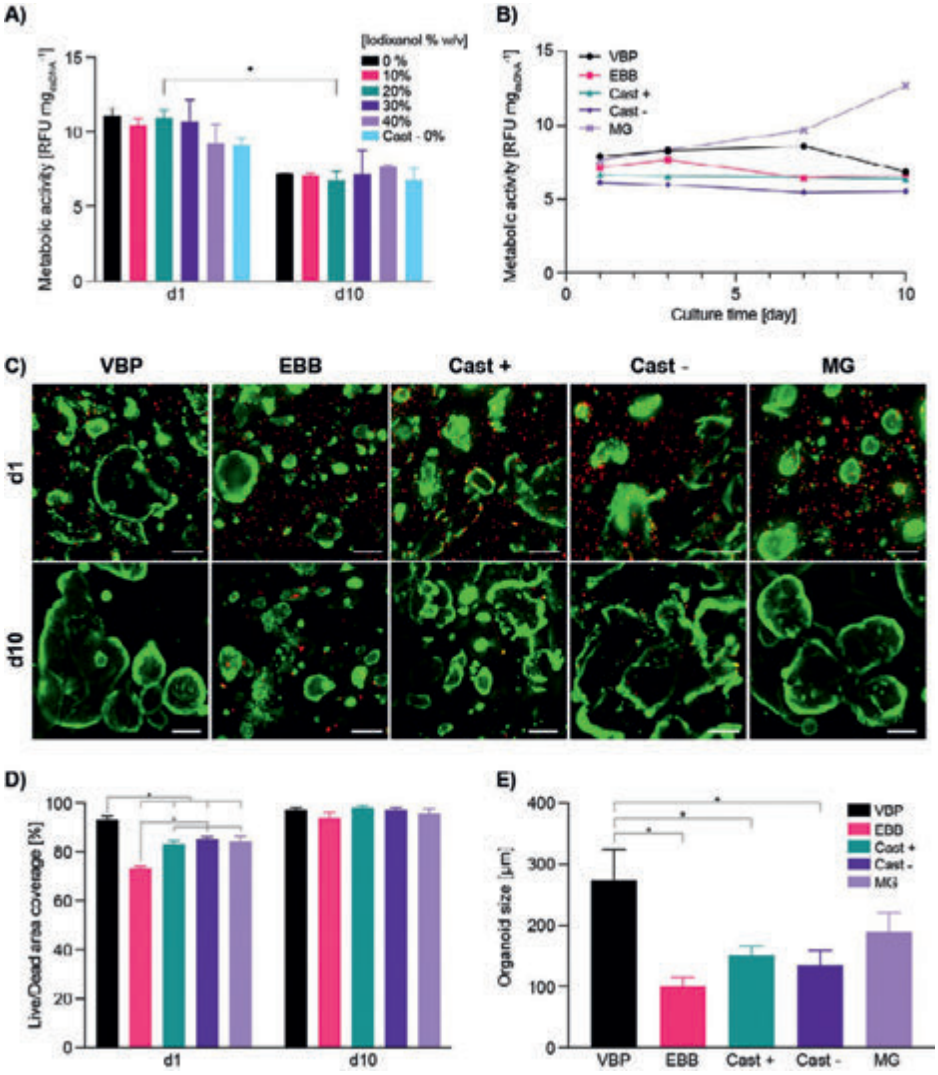

Figure 4. Viability of volumetrically bioprinted hepatic organoids. A) Metabolic activity of bioprinted organoids within bioresins with increasing iodixanol concentrations (0 – 40% w/v) over a 10-day differentiation period (n = 5). B) Metabolic activity (n = 5), C) Representative Live/Dead images (scale bars = 250 µm), D) Live to dead ratio area (n = 3) coverage, and E) Average organoid sizes (n = 60) of VBP- and EBB-printed organoids with the optically tuned bioresin (gelMA + 10 % w/v iodixanol), casted gelMA samples with (Cast +) and without 10% w/v iodixanol (Cast -) and casted Matrigel (MG) samples over a 10-day differentiation period. * = significant difference ($p < 0.05$).

Next, the expression of key hepatocyte differentiation markers was investigated (Figure 5). Organoids from all experimental groups showed comparable levels of cytochrome 3A4 activity (which appeared significantly elevated in Matrigel-

based cultures vs. EBB samples) normalized over the total protein content of the sample (Figure 5A), as well as gene expression levels of the same cytochrome and albumin (Figure 5B, C). In addition, all samples showed comparable normalized levels of various liver transaminases, such as aspartate transaminase (ASAT, involved in amino acid metabolism), gamma-glutamyl transferase (GGT, involved in drug and xenobiotic detoxification)nand glutamate dehydrogenase (GLDH, involved in the urea cycle) (Figure S7). The presence of such markers indicates the successful commitment towards a hepatocyte-like phenotype in VBP, EBB, and the casted controls, while only in the volumetrically bioprinted group this result was also paired with higher cell viability after printing. The evident donor-dependent variability observed in the expression levels indicate that liver organoids as *in vitro* models are better suited for personalized medicine applications or to establish bio-banks e.g., to study drug susceptibility on patient groups with similar genetic make-up, as already proposed for other tissue types [54].

Immunofluorescence analysis of volumetrically bioprinted organoids within the optimized gelMA-based bioresin also revealed the intracellular presence of the hepatocyte markers hepatocyte nuclear factor 4 alpha (HNF4α), E-cadherin, high-expression of albumin and tight junction protein-1 (ZO-1) (Figures 5D, E, F), as well as the absence of the cholangiocyte marker cytokeratin 19 (CK19) [42], underlining the acquisition of a hepatocyte-like phenotype. Organoid morphology and glycogen storage was also visualized in all experimental groups though hematoxylin and eosin (H&E) and periodic acid-Schiff (PAS) stainings (Figure S8). Extrusion-based printed samples and casted controls also showed similar patterns, albeit with some key differences. In particular, the VBP samples clearly showed a significantly higher degree organoid polarization, with the formation of an apical side in the cyst lumen for the highest percentage of organoids (73.9 ± 1.8 %), as evidenced by the localized expression of multidrug resistance protein 1 (MDR1) [55]. Organoid polarization is an indicator of maturation and an important feature to study the directional uptake, transport and eventual secretion of metabolites present in the native liver, which is not observed in cell lines under conventionally established culture conditions (i.e., standard 2D culture of single liver cell lines, primary cells or 3D spheroid cultures). Moreover, while MDR1 was also detected in EBB and casted gelMA controls (but not in Matrigel), quantitative analysis of the polarized organoids showed significantly impaired polarization in these groups (12.1 ± 1.2 % for EBB, 36.9 ± 3.0 % and 36.5 ± 3.6 % 7 or the cast+ and cast- samples respectively) as opposed to VBP-printed organoids (Figure 5E, Figure S9, Figure S10). This significant difference between VBP-printed organoids and EBB and casted controls could be attributed to the fact that in VBP, structural integrity of the organoids is not disrupted during the printing process and seemingly results in

the rapid acquisition of polarity markers when the differentiation process begins. Instead, EBB and casted organoids undergo shear stresses and fragmentation during their respective fabrication processes, and have to reassemble once they have been embedded in viscous hydrogels, a condition that may impair the onset of polarity across all organoids, as suggested by our results. These findings are also supported by the comparable trends observed in organoid viability post-fabrication (Figure 4), in which, much like for MDR1 polarization, EBB showed the lowest values, followed by the milder casting process. In addition, Matrigel controls were also negative for MDR1, and notably also for albumin, even if the marker was present at a gene expression level, indicating no synthesis of this protein and indicative of a well-known common mismatch in molecular biology between mRNA levels and actual protein expression [56-58]. This result, paired with the previous finding of enhanced metabolic activity over time, further underlines how Matrigel is an ideal substrate for organoid proliferation. On the other hand, for hepatocytic differentiation, other hydrogels including gelMA as shown in this study, appear to provide a more suitable 3D environment [45,46,59]. While the exact mechanism by which gelMA facilitates organoid differentiation remains to be elucidated, previous studies with other RGD-modified polyethyleneglycol hydrogels have identified stiffness values in the range between 1-2 kPa as beneficial for organoid growth and differentiation [45]. Conversely, the same hydrogels in softer or stiffer formulation lead to inferior organoid yield and expression of liver fibrosis markers, respectively [45]. Interestingly, gelMA-iodixanol bioresins yielded gels with compressive moduli of 1.73 ± 0.09 kPa, nearly identical to the Matrigel compressive modulus (1.72 ± 0.09 kPa), suggesting that mechanosensing may indeed be a contributing element to the enhanced organoid differentiation, and the biological cues provided by the gelatin-derived gelMA resin may be a key factor in creating a more permissive environment for differentiation compared to the proliferative enhancement observed in Matrigel culture systems. These soft gels are also likely a consequence of the higher sol-fraction after crosslinking, since unmodified gelMA prepared at the same prepolymer concentration with no optical tuning resulted in stiffer gels (5.04 ± 0.10 kPa) (Figure S11). Notably, both gelMA resins were shown to remain biodegradable after the photocrosslinking process, as found upon exposure to a collagenase-laden media [60], an essential characteristic of biocompatible materials used in the field of tissue engineering (Figure S12).

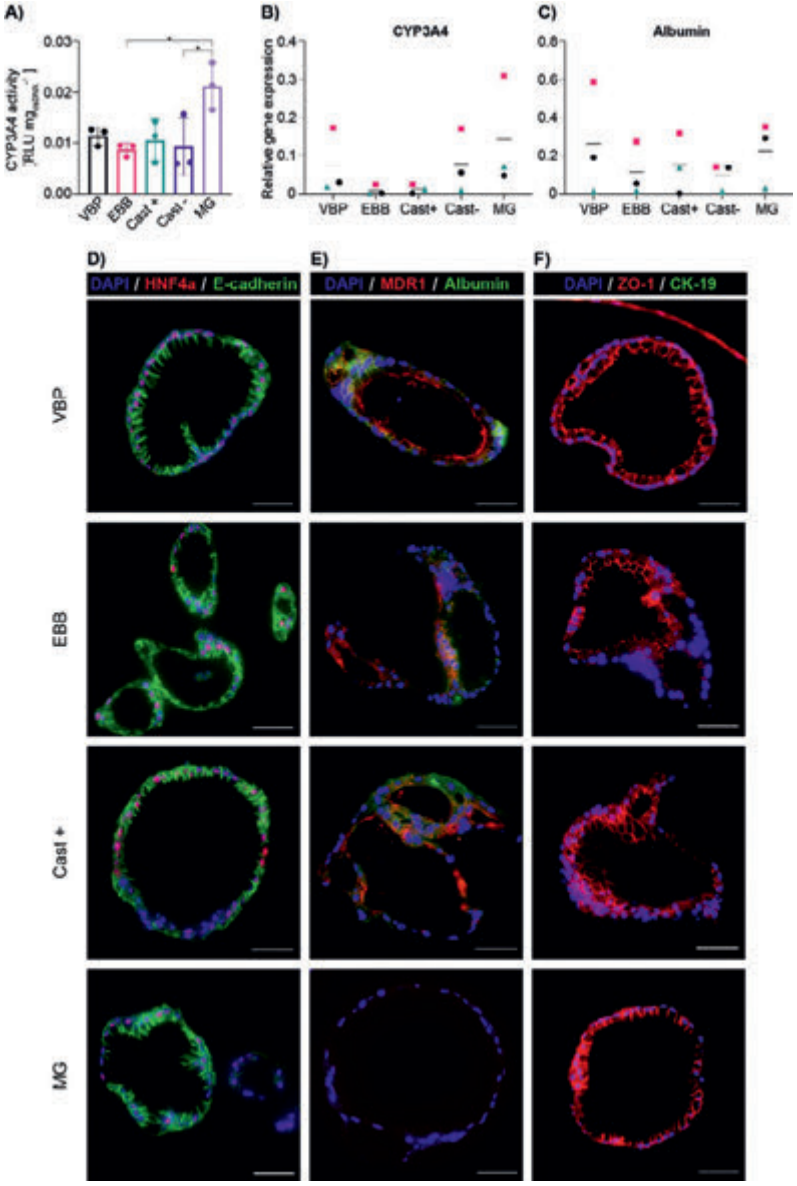

Figure 5. Liver-specific markers in volumetrically bioprinted hepatic organoids. A) CYP3A4 activity and relative gene expression of B) CYP3A4 and C) albumin in VBP- and EBB-printed organoids with the optically tuned bioresin, casted gelMA samples with (Cast +) and without 10% w/v iodixanol (Cast -) and casted Matrigel (MG) samples after a 10-day differentiation period (n = 3). Representative fluorescence images of liver-specific and organoid polarization markers D) HNF4α and E-cadherin, E) MDR1 and albumin, and F) CK19 and ZO-1 in the VBP, EBB, Cast + and MG conditions after 10 days of hepatic differentiation. Scale bars = 50 µm. Individual data points shown for 3 different donors (N = 3).* = significant difference ($p < 0.05$).

Upon confirming that VBP samples in optically tuned gelMA bioresins provide a suitable environment for liver organoid differentiation, we investigated the potential of bioprinting to modulate the functionality of the organoid-laden constructs, when cultured in a dynamic perfusion setting. At first, we selected a series of 3D objects with convoluted pore distribution from a pool of mathematically defined triple periodic minimal surface structures. This class of geometries is well-known in the field of tissue engineering, as lattices belonging to this family have been investigated to produce mechanical metamaterials [61], to maximize cell seeding in polymeric scaffolds [62], and to promote *in vivo* bone ingrowth in biomaterials-based implants [63], among other applications. Specifically, we selected three lattice structures with interconnected porosity: Schwarz D, Schwarz G and Schwarz P [64-67]. At a comparable volume (between 383.17 and 394.25 mm^3), these structures show a decrease in surface area to volume ratio (from 2.05 to 1.88 mm^{-1}), and decreasing average tortuosity of the porous network (from 1.32 to 1.04) respectively (Figure S13, Supplementary Table S5). Thus, the choice of these structures provide the possibility to modulate key geometrical parameters, and, under perfusion, the flow profile within the porous construct, that are paramount for the interaction between the embedded cells and the solutes within the culture media, without significantly altering the cell content and cell density. Therefore, these architectures offer an ideal platform and proof-of-concept to study the effect of the geometry imposed by the printing process on the functionality of the embedded cells. Notably, such complex geometries are in general extremely difficult to reproduce at high resolution with extrusion technologies, especially when soft hydrogels are used as carrier materials. Hydrogel-based gyroidal structures can instead be easily printed with digital light projection bioprinting techniques, although generally requiring extended printing times that scale linearly with the height of the construct [68].

However, printing similar convoluted structures in cell-friendly processing times and at the same time ensuring shape fidelity when using soft, cell-friendly hydrogels like the gelMA-iodixanol bioresin tested in this study remains a major challenge in the field of biofabrication. Via VBP, we could successfully generate all three Schwarz structures laden with organoids, and the construct could maintain their shape when retrieved from the printing environment and immersed in aqueous media. To facilitate handling and permit a seamless coupling of the constructs with a fluidic circuit for perfusion culture, we modified the design of the lattices. These were encased in a hydrogel made fluidic chamber, equipped with an entry and an exit port, to which plastic microfluidic tubing could be coupled. The modified design could be reproducibly printed, with a printing time ranging from 14 to 15.5 seconds, depending on the geometry (Figure 6A, Supplementary Videos V1, 2, 3). When compared to

the extensive printing times that would be needed to fabricate these same centimeter-scale structures under optimal printing conditions (between 24.7 – 34.0 minutes, even when using the easily printable and high-shape fidelity ink Pluronic F127, Figure S14), the extremely rapid printing speed offered by VBP pose a promising advantage to overcome the detrimental effects on cell functionality that have been previously observed over extended printing times [16]. Given the high-speed printing achieved with VBP, these structures could also be printed for high-throughput analysis in a matter of minutes (Figure S15). The system was first perfused with a constant flow of buffered solution supplemented with fluorescent microspheres to evaluate the flow profile within the structures. Tracking of the trajectory of the beads confirmed that these particles followed a nearly straight path in the Schwarz P lattice, as opposed to an increasingly wavy path in the other geometries (Figure 6B, Supplementary Videos V4, 5, 6). This was quantitatively proven by the significantly larger trajectory amplitudes exhibited by the Schwarz D structure (0.214 ± 0.098 mm) compared to the G and P architectures (0.157 ± 0.109 and 0.077 ± 0.105 mm respectively, Figure S16). Given the constant flow rate (1.5 μL min^{-1}) imposed by the pump connected to the system and a smaller equivalent cross-sectional area along the flow pathway within more convoluted lattice in the Schwarz D, the average particle speed in this system was the highest (0.416 ± 0.009 mm s^{-1}), whereas the lowest speed was found for the Schwarz P lattice (0.241 ± 0.009) (Figure 6C). Thus, the Schwarz D and P geometries, that showed the most marked differences in terms of flow profile, were printed embedding liver organoids, and conditioned in differentiation media, prior to being connected to the perfusion system for 24 hours.

Figure 6. Modulating hepatic organoid function through volumetric bioprinting of mathematically-derived lattices with differing flow properties. A) Complex, perfusable architectures were successfully printed within seconds with an adjusted lattice design that enables coupling to microfluidic tubing as shown in the i-iii) STL models of the i) Schwarz D, ii) Schwarz G and iii) Schwarz P architectures. iv-vi) 3D reconstructions from μCT scans and vii-ix) macro-photographs showing the different complex and interconnected pore networks exhibited by the Schwarz iv,vii) D, v,viii) G, and vi,ix) P structures (scale bars = 2 mm). B) These complex architectures were shown to modulate the flow trajectory of microspheres moving through the Schwarz i) D, ii) G and iii) P prints, as well as the C) average speed of the flowing particles (n = 485 – 1210). D) Albumin secretion and E) GLDH levels of organoids embedded in Schwarz D and P architectures, after 24 hours of continuous perfusion (n = 4 – 8). F) Sterile perfusion setup, which enabled perfusion of differentiation medium supplemented with 1.5 mM NH_4Cl through complex architectures and resulted in differing G) total NH_4Cl elimination compared to statically cultured cylindrical control samples and H) architecture-dependent NH_4Cl elimination rates (n=4 – 8). * = significant difference ($p < 0.05$).

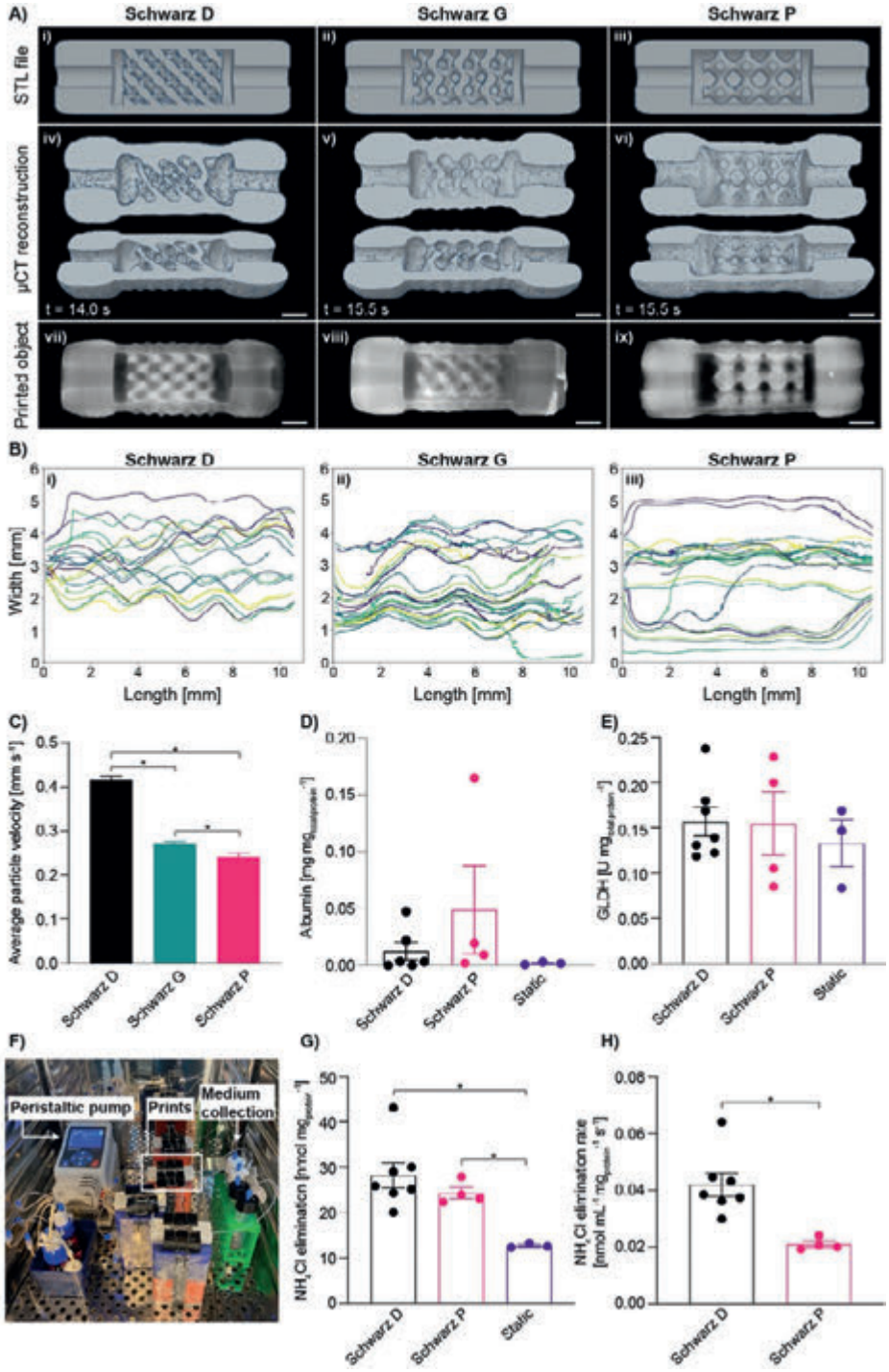
A)
Schwarz D
Schwarz G
Schwarz P
STL file
µCT reconstruction
Printed object
t = 14.0 s
t = 15.5 s
t = 15.5 s
B)
Width [mm]
Length [mm]
C)
Average particle velocity [mm s⁻¹]
D)
Albumin [ng mg⁻¹]
E)
GLDH [U mg⁻¹]
Static
F)
Peristaltic pump
Prints
Medium collection
G)
NH4Cl elimination [nmol mg⁻¹]
H)
NH4Cl elimination rate [nmol mL⁻¹ mg⁻¹ s⁻¹]

During this time, the culture media was collected to measure the secretion of albumin and of the liver specific enzyme GLDH, which is a key player in protein catabolism, ammonia production, and in the generation of substrates for the synthesis of ATP (Figure 6D, E, F) [69]. Albumin levels secreted over a 24 hour period of continuous flow perfusion were highest in the Schwarz P structure (0.061 ± 0.051 mg $mg_{total\ protein}^{-1}$) compared to Schwarz D (0.013 ± 0.008 mg $mg_{total\ protein}^{-1}$) and static controls (0.002 ± 0.001 mg $mg_{total\ protein}^{-1}$) (Figure 6D). The total albumin production (3.40 ± 1.75 and 17.00 ± 13.03 μg mL^{-1} for Schwarz D and P, respectively, Table S6) exhibited by the complex printed structures was also superior to previously reported experimental results from liver-like constructs, where albumin values range from ~0.004, ~0.3, and ~0.6 μg mL^{-1}, over longer medium collection periods of 7 – 10 days [46,70-72]. Taking into account the total volume of medium collected in our perfusable system (~28 mL), these highly complex VBP-printed biofactories outperform previous tissue engineering attempts in terms of albumin production. As for GLDH, printed and static constructs exhibited similar enzyme levels (Figure 6E). Most notably, the organoid-laden bioprinted lattices were able to actively remove ammonia from the media injected in the perfusion chamber (Figure 6G), a key function normally performed by the liver through the urea cycle. Ammonia detoxification was significantly higher under perfusion culture (33.5 ± 5.8 and 24.3 ± 1.4 nmol $mg_{total\ protein}^{-1}$ for Schwarz D and P, respectively) when compared to static controls (12.7 ± 0.3 nmol $mg_{total\ protein}^{-1}$), suggesting that the applied flow promotes organoid function, possibly due to stimuli provided by the fluid shear stresses on the gelMA-embedded organoids. Previous studies using perfusion systems in combination with liver cell lines [73], stem cells [25], and differentiated primary cells [28] have shown enhanced liver-like functions in smaller-scale systems. In addition, fluid flow-induced shear stresses have demonstrated to enhance organoid maturation in different tissue engineering and organ-on-a-chip applications (i.e., kidney) [74], further supporting the hypothesis that shear stimuli also played a role in our system. Importantly, in Schwarz D samples, due to the higher flow velocity compared to the Schwarz P lattice, ammonia molecules have a shorter residency time within the construct (24.0 vs. 41.5 s). Yet, ammonia elimination also occurred at a significantly faster rate, indicating that the ammonia detoxification capacity of the bioprinted organoids can be effectively boosted by the accurate selection of the architecture imposed to the organoid-laden hydrogel, in this case, using a highly convoluted, tortuous structure like the Schwarz D construct (Figure 6H). While it can be inferred that part of this modulation of the biological functionality in response to the engineered geometry can be due to an improved surface area available for exchange of solutes, it is also likely that the design-driven enhancement in diffusion could directly stimulate the encapsulated liver organoids. It should also be noted that, given the design of these constructs, organoids were also

present in the casing with connectors placed around the lattices, and these additions to the Schwarz structures were identical for all three architectures. Nevertheless, the variation in geometry imparted in the central part of the object was sufficient to observe a difference in terms of cell behavior during culture. In the context of our *in vitro* system, these mathematically defined lattices were shown to offer unique potential to control the fluid flow within the pores and to modulate the communication between the bioprinted organoids and solutes found in the media, leading to a modulatory effect on ammonia detoxification. Moreover, it is important to remark that, although in this specific study focused on bioprinting for *in vitro* 3D culture applications, and thus *in vivo* regenerative medicine applications go beyond the scope of this work, such user designable, bioprinted structures that can maximize the ability of the cells to interact with the surrounding nutrients and signals could have valuable applications also for producing transplantable grafts. Overall, these results underline the importance of architectural cues in the design of advanced tissue engineered and biofabricated constructs.

CONCLUSIONS

In summary, the first phase of the study takes fundamental steps to unravel the effects of different cellular components (single cells and organoids) on the volumetric printing process, namely due to the cell-mediated light scattering and its effect on printing resolution. Using this knowledge, an optically tuned, gelatin-based bioresin was successfully developed and was able to reduce scattering through refractive index matching of specific intracellular components. This strategy is versatile, and could be potentially applied to resins used for volumetric additive manufacturing which use other photocrosslinking chemistries besides methacryloly-based, such as thiolene step growth [75]. This development allowed high resolution volumetric bioprinting with increasing cell densities, and provides important knowledge on the ideal design requirements for the development of next-generation bioresins for VBP. In combination with more advanced tomographic algorithms, multi-material and multi-cellular printing approaches can be more easily established in order to increase the overall complexity of volumetrically printed architectures. Using the liver as a model tissue platform, this study demonstrated the ability to harness the advantages of both VBP and organoid technology in a single approach that resulted in the fabrication of multi-scale biofactories capable of guiding tissue-specific functions. Liver-derived organoids were successfully printed at high densities and demonstrated maintained viability and hepatic function compared to extrusion printed and casted controls. The layerless fabrication approach employed by VBP resulted in increased organoid viability post-printing, and enabled the preservation of organoid morphology and polarity compared

to controls. The soft, organoid-laden bioresin was successfully sculpted into highly convoluted, mathematically-derived structures with distinct structural properties. Successful printing of these cell-laden structures in under 20 seconds and establishment of a sterile perfusion chamber allowed the printed organoids to act as biofactories capable of modulating liver-specific ammonia detoxification depending on the printed architecture. These findings demonstrate the close relationship between the shape of the constructs and their resulting biological functionality, further underlining the potential of biofabrication for advancing tissue engineering. This study, therefore, opens up new possibilities for the future development of self-sustaining biofactories that are able to carry out a wide variety to tissue-specific functions. Overall, the combination of the ultra-fast VBP process with organoid technology holds great potential for the development of advanced regenerative medicine approaches and *in vitro* model development for fundamental biology research, personalized drug screening and disease modelling.

EXPERIMENTAL SECTION

Materials

GelMA (93.5% DoF) was synthesized as previously reported [76], and used as a 5% w/v solution in phosphate buffered saline (PBS). Lithium phenyl(2,4,6-trimethylbenzoyl)phosphinate (LAP, Tokyo Chemical Industry, Japan) was added at 0.1% (w/v) as a photoinitiator to induce a photocrosslinking reaction. To perform optical tuning of the cell-laden bioresin, the gelMA and LAP solution was supplemented with different concentrations (0 – 40% w/v) of iodixanol (OptiPrep™; StemCell Technologies, Canada).

Volumetric Bioprinting Procedure

Volumetric bioprinting of different structures was achieved using a Tomolite printer (Readily3D, Switzerland). For bioprinting, single cells and hepatic organoids were embedded in different gelMA bioresins at densities of 1 – 1.5 x 10^7 cells per mL and placed in Ø10 mm cylindrical borosilicate glass vials. The bioresin-filled vials were placed at 4° C to elicit thermal gelation and prevent cell sedimentation throughout the printing process. Briefly, the printing process is induced by a laser beam at 405 nm directed onto a digital micromirror device (DMD) that is modulated into tomographic projections. These projections are then imaged into the printing vials. The projections were calculated using a commercial software (Apparite, Readily3D, Switzerland) taking into account the material properties of the resin and the printing vials. The average light intensity before the printing container was 9.98 mW cm^{-2} during printing. Further details concerning the tomographic printing process can be found in literature [11,15]. Post-printing, the printer vials were heated to 37 °C to melt the unpolymerized

bioresin, and samples were washed with prewarmed PBS. For the printing optimization experiments, prints at different light doses were performed, by modulating the exposure time. Successful crosslinking was appreciated for doses at which the every intended feature object could be resolved and the print did not redissolve when heating the bioresin. Finally, the as-printed parts underwent 5 min of additional crosslinking in 0.1% w/v LAP in PBS solution in a CL-1000 Ultraviolet Crosslinker (λ = 365 nm; UVP, USA).

Hepatic Organoid Establishment, Expansion and Differentiation

Healthy liver biopsies were obtained during liver transplantation at the Erasmus Medical Center Rotterdam in accordance with the ethical standard of the institutional committee to use the tissue for research purposes (ethical approval number MEC 2014-060). The procedure was in accordance with the Helsinki Declaration of 1975 and informed consent in writing was obtained from each patient. Disposable 125-mL spinner flasks (Corning, USA) were inoculated with 5 x 10^6 of the collected single cells in 20 mL expansion medium (EM), including 10% v/v Matrigel™ (Matrigel; Corning, New York, NY, USA) to increase organoid yield as previously described [42]. Rotation speed was set to 85 rpm. Every 2-3 days, new medium was added to the spinner flasks. After a 14-day expansion period, organoids were collected for printing and passaged into a new spinner flask. To assess the size of the organoids, aliquots from the spinner flasks were taken at the end of the culture time and imaged with an optical microscope, measuring the diameter of at least 150 organoids per spinner flask. In order to match the printed cell densities to the single cell conditions, aliquots of the organoid suspension were mechanically fragmented and trypsinized into single cells, and were subsequently counted using an automatic cell counter. Post-printing, organoid-laden structures were cultured in hepatic differentiation media (DM) for 10 days. For single cell studies, HepG2 cell line was used, (ATCC nr. HB-8065) and cultured in T175 culture flasks in HEPG2 expansion medium, which was replenished twice a week. All cultures were kept in a humidified atmosphere of 95% air and 5% CO_2 at 37°C. Details of the cell isolation protocol from liver biopsies and of the culture media components are reported in the Supporting Information.

Stereomicroscopy and Computed Tomography for Print Evaluation

Macroscopic images of cell- and organoid-laden structures were acquired using an Olympus SZ61 stereomicroscope coupled with an Olympus DP70 digital camera (Olympus Soft Imaging Solutions GmbH, The Netherlands). Zoomed in images were cropped and pasted over a black background to eliminate background reflections. μCT scans were performed with a Quantum FX μCT (voxel size = 15 μm^3, 90 kV tube voltage, 200 μA current, and 26 seconds of

scan time, Perkin Elmer, USA). 3D reconstructions were generated with the 3D viewer plugin in Image J (n = 3 - 6).

Refractive Index and Measurements of Scattering Phase Function of Cell Suspensions

The refractive index of bioresins with different iodixanol concentrations (n = 3) was measured with an Abbe refractometer (2WAJ, Optika, Italy). The scattering properties of the hydrogels were measured with a custom-made apparatus, as depicted in figure 3D. The principle of the setup is similar to that introduced by Hunt and Huffman [77]. The apparatus setup and anisotropy coefficient calculations are detailed in the Supporting Information.

Metabolic Activity and Viability of Bioprinted and Cast Organoids

Cylindrical organoid-laden constructs (5 x 10^6 cells mL^{-1}; 5 mm diameter x 2 mm height) were produced through i) volumetric bioprinting (170 mJ cm^{-2}, 17.0 s printing time) with and without iodixanol (0 – 40 % w/v), ii) extrusion-based bioprinting with a pneumatic-driven system (25 G stainless steel nozzle, temperature = 21 °C, pressure = 0.03 MPa, 3DDiscovery, REGENHU, Switzerland), iii) casting of the gelMA bioresin with and without idodixanol (10 % w/v) and crosslinking for 15 minutes in a CL-1000 Ultraviolet Crosslinker (λ = 365 nm; UVP, USA) and iv) casting in Matrigel droplets, thermally crosslinked at 37°C for 20 minutes. Importantly, EBB-printed organoids had to be mechanically fragmented using a P200 pipette tip in order to prevent nozzle clogging prior to the fabrication step. Samples were cultured in organoid differentiation medium for 10 days, which was refreshed every two days. Metabolic activity (n = 5) was measured with a resazurin assay (resazurin sodium salt, Alfa Aesar, Germany) and normalized by double-stranded DNA content per sample quantified using a Picogreen Quant-iT assay (Thermo Fischer Scientific, The Netherlands) after 1, 3, 7 and 10 days. Cell viability was evaluated using a LIVE/DEAD assay (Calcein, ethidium homodimer, Thermo Fischer Scientific, The Netherlands) after 1, 3 and 10 days (n = 3), imaged by a Thunder imaging system (Leica Microsystems, Germany). For each measurement in the printing/casting comparisons, 3 donors were evaluated (N = 3).

Hepatic Functionality Assessment of Bioprinted/Casted Constructs

CYP3A4 activity in organoids at day 10 of differentiation was quantified using the P450-Glo CYP3A4 Assay (Promega, USA) according to the manufacturer's instructions. CYP3A4 levels were normalized to DNA amount in the samples determined with a picogreen assay (n = 3). Gene expression of liver-specific markers (CYP3A4 and albumin) was quantified through RT-qPCR (Bio-Rad, The Netherlands) at day 10 of differentiation (n = 3). Liver-specific and polarization marker expression upon hepatic differentiation (HNF4α, ZO-1, MDR1, CK19

and E-cadherin) were visualized through immunofluorescent stainings and imaged using a Thunder imaging system (Leica Microsystems, Germany) (n = 3). Details of the qPCR protocol primers and of the immunohistochemical procedures are reported in the Supporting Information. Liver transaminase and GLDH present in organoid-laden constructs and secreted albumin in the culture medium were measured with the clinical chemistry analyzer Beckman AU680 (Beckman Coulter, USA) using standard protocols (n = 3). Values were normalized to total protein content quantified through a micro-BCA protein assay kit (ThermoFischer Scientific, The Netherlands).

Fluorescent beads tracking through complex printed structures

Printed Schwarz D, G and P strcutures were placed in a custom-made PDMS mold and connected to a syringe pump using FA microfluidic tubing (IDEX Health&Science, OD 1.6 mm, ID 0.75 mm). Green fluorescent polyethylene microspheres (125 – 150 µm diameter; Cospheric, USA) were perfused through the printed structures at a flow rate of 20 µL min^{-1} (n = 3). Videos of microsphere flow through the printed constructs were recorded using a custom-made imaging system (Supporting Information). The particle trajectories were calculated from the acquired videos with the Crocker and Grier algorithm [78], using trackpy v0.5.0 (https://zenodo.org/record/4682814). The particles identified in each video frame were linked into trajectories using a proximity criterion. Mean particle speeds were calculated as averages between each trajectory start and end point, where the contribution of each trajectory to the overall mean speed was weighed by the trajectory length. The amplitude was calculated on a subset of the oscillations within the trajectories shown in Figure 6Bi-iii (n = 50-80). Local minima and maxima values were identified in the trajectory y positions. Amplitude was calculated as half of the distance in the direction orthogonal to the main direction of the flow from a maximum to the subsequent minimum. All code used for video analysis is available at: https://github.com/VictorOnink/Particle-Trajectory-Analysis.

Ammonia Elimination Assay in a Sterile Perfusion Setup

Organoid-laden, volumetrically bioprinted Schwarz D and P structures (5 x 10^6 cells mL^{-1}, 200 mJ cm^{-2}, 20.0 s printing time; n = 8 and 4 respectively) were cultured with differentiation medium for 10 days under static conditions. After 10 days the structures were transferred to a sterile flow perfusion chamber (Supplementary information) and perfused with DM supplemented with 1.5 mM ammonium chloride (NH_4Cl) for 24 hours under continuous flow of 20 µL min^{-1}. The fluidic chambers were cultured in sterile conditions at 37 °C , and medium was collected for 24 hours. Ammonium chloride concentrations in the collected medium were determined using the Urea/Ammonia Assay Kit (Megazyme, Ireland). Medium samples were decolored using activated

carbon (Merck, Germany). Static controls consisted of volumetrically printed non-porous cylinders (diameter 6 mm x 17 mm height) cultured under static conditions (n = 3). Media supplemented with 1.5 mM NH_4Cl that was incubated for 24 hours without cells was used to determine the initial concentration (n = 3). Total ammonium chloride elimination and elimination rate were normalized to the total protein content.

Statistics

Results were reported as mean ± standard error of the mean (SEM). Statistical analysis was performed using GraphPad Prism 9.0 (GraphPad Software, USA). Comparisons between experimental groups were assessed via one or two-way ANOVAs, followed by *post hoc* Bonferroni correction to test differences between groups. When normality could not be assumed, non-parametric tests were performed. Differences were found to be significant when $p < 0.05$.

ACKNOWLEDGEMENTS

The authors would like to thank D.J. Hall from Carbon and Neon for his support with scientific illustrations, V. Onink for his assistance with the particle tracking analysis, C. Spiegel for her help with editing, Dr. K. Schneeberger and Dr. M. Pietribiasi for the fruitful discussions.

FUNDING STATEMENT

This project received funding from the European Research Council (ERC) under the European Union's Horizon 2020 research and innovation programme (grant agreement No. 949806, VOLUME-BIO) and from the European's Union's Horizon 2020 research and innovation programme under grant agreement No 964497 (ENLIGHT). R.L and J.M acknowledge the funding from the ReumaNederland (LLP-12, LLP22, and 19-1-207 MINIJOINT) and the Gravitation Program "Materials Driven Regeneration", funded by the Netherlands Organization for Scientific Research (024.003.013). R.L. also acknowledges funding from the NWA-Ideeëngenerator programme of the Netherlands Organization for Scientific Research (NWA.1228.192.105). M.B. and B.S. acknowledge funding from the research program Applied and Engineering Sciences with project number 15498, which is financed by the Netherlands Organization for Scientific Research. J.M.W and C.M acknowledge funding from the Swiss National Science Foundation: "Light based Volumetric printing in scattering resins" (n°200021_196971).

CONFLICT OF INTEREST

Dr. P. Delrot and Dr. D. Loterie are shareholders and employees of Readily3D SA. Prof. C. Moser is a shareholder of Readily3D SA. All the other co-authors declare no conflicts of interest.

AUTHOR CONTRIBUTIONS

P.N.B. and M.B. contributed equally to this work.

SUPPLEMENTARY MATERIALS

Supplementary Figures

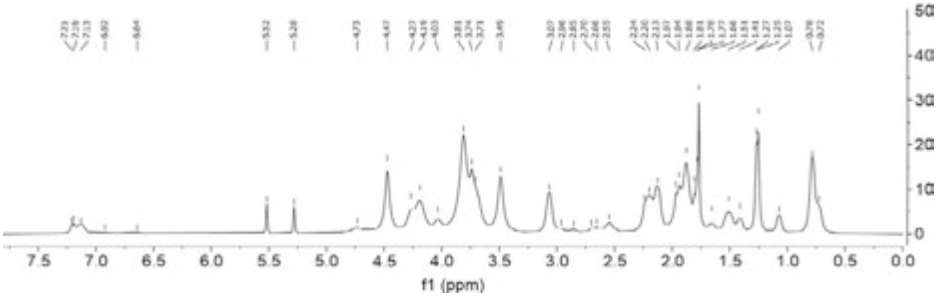

Figure S1. Proton nuclear magnetic resonance (^{1}H-NMR) spectrum of synthesized gelatin methacryloyl in D_2O. ^{1}H NMR (400 MHz, d_2o) δ 7.24 – 7.10 (m, 3H), 5.52 (s, 1H), 5.28 (s, 1H), 4.73 (s, 2H), 4.47 (s, 9H), 4.27 (s, 3H), 4.19 (s, 8H), 4.03 (s, 2H), 3.81 (s, 24H), 3.72 (d, *J* = 13.3 Hz, 9H), 3.49 (s, 9H), 3.07 (s, 6H), 2.55 (s, 3H), 2.22 (d, *J* = 17.1 Hz, 8H), 2.13 (s, 6H), 1.95 (d, *J* = 11.6 Hz, 7H), 1.88 (s, 13H), 1.78 (d, *J* = 6.4 Hz, 8H), 1.51 (s, 4H), 1.41 (s, 2H), 1.26 (d, *J* = 6.7 Hz, 10H), 1.07 (s, 2H), 0.78 (s, 10H).

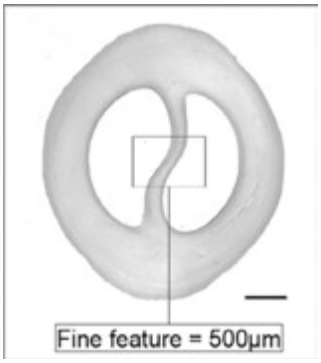

Figure S2. Simple structure to measure printing resolution. Oval shaped structure with a curved inner strut representing a fine feature of 500 µm thickness. This structure was used to assess printing resolution with cell-laden bioresins containing different cell densities and concentrations of iodixanol. Scale bar = 2 mm.

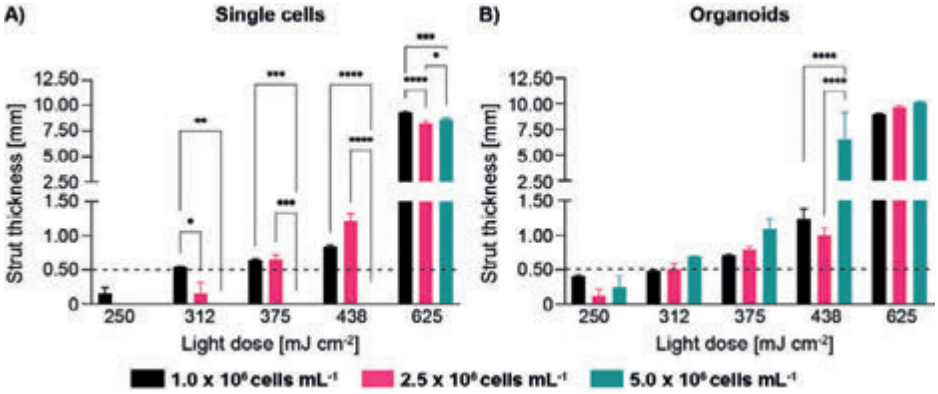

Figure S3. Printing accuracy of bioresins with increasing cell densities in absence of optical corrections (including SEM). Fine feature thickness in constructs printed at increasing light doses (250 – 625 mJ cm^{-2}) with bioresins containing different A) single cell and B) organoid densities (1 – 5 x 10^6 cells mL^{-1}) (n = 3). Statistically significant differences are represented with an *.

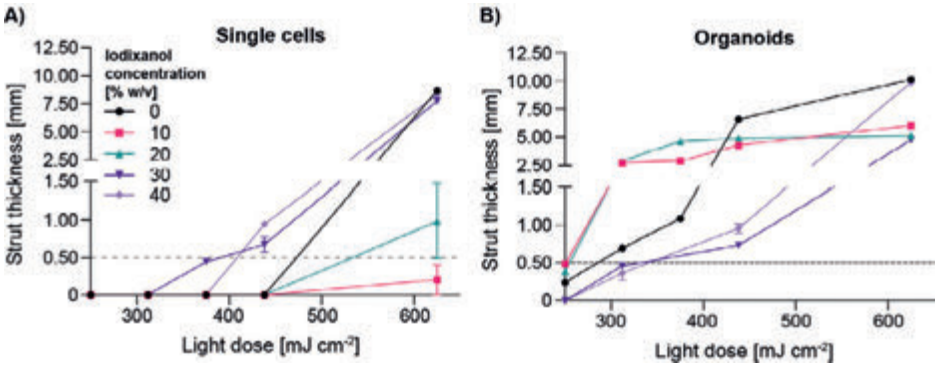

Figure S4. Printing accuracy of bioresins with increasing iodixanol concentrations (including SEM). Fine feature thickness in constructs printed with 5 x 10^6 A) single cells and B) organoids mL^{-1} at increasing light doses (250 – 625 mJ cm^{-2}) with bioresins containing different iodixanol concentrations (0 – 40 % w/v) (n = 3).

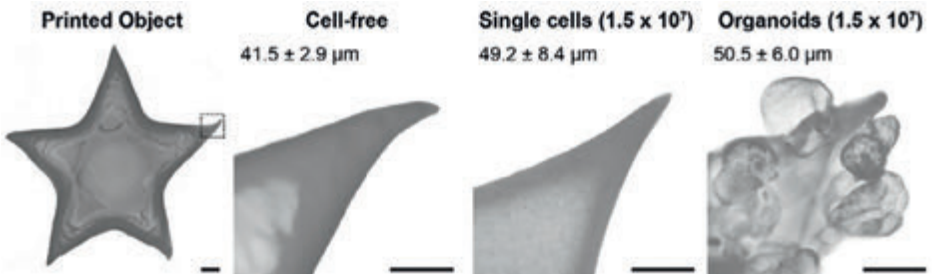

Figure S5. High-resolution printing with high single cell and organoid densities. Stereomicroscopy images showing the printing of a star-shaped construct, zooming in on the fine feature points of the stars containing no cells, 1.5 x 10^7 cells mL^{-1}, printed as single cells and as organoids (scale bar = 500 µm). The measurements reported in the panels refer to the width at the tips of the stars.

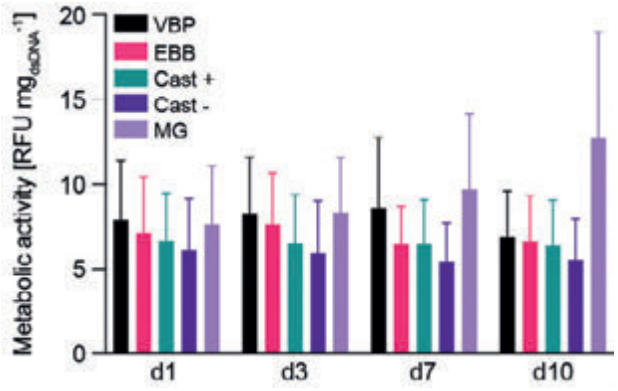

Figure S6. Metabolic activity of printed and casted organoids during hepatic differentiation (including SEM). Metabolic activity of VBP- and EBB-printed organoids with the optically tuned bioresin (gelMA + 10 % w/v iodixanol), casted gelMA samples with (Cast +) and without iodixanol (Cast -) and casted Matrigel (MG) samples over the 10-day differentiation period (n = 3).

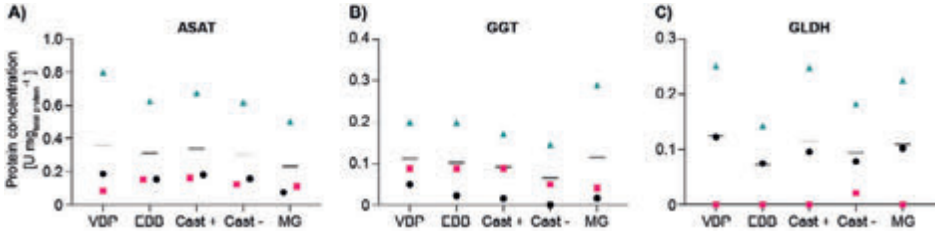

Figure S7. Liver transaminases levels in bioprinted and casted organoid-laden samples upon hepatic differentiation. Levels of A) ASAT, B) GGT and C) GLDH in cell lysates of VBP- and EBB-printed organoids with the optically tuned bioresin (gelMA + 10 % w/v iodixanol), casted gelMA samples with (Cast+) and without iodixanol (Cast-) and casted Matrigel (MG) samples after the 10-day differentiation period (n = 3).

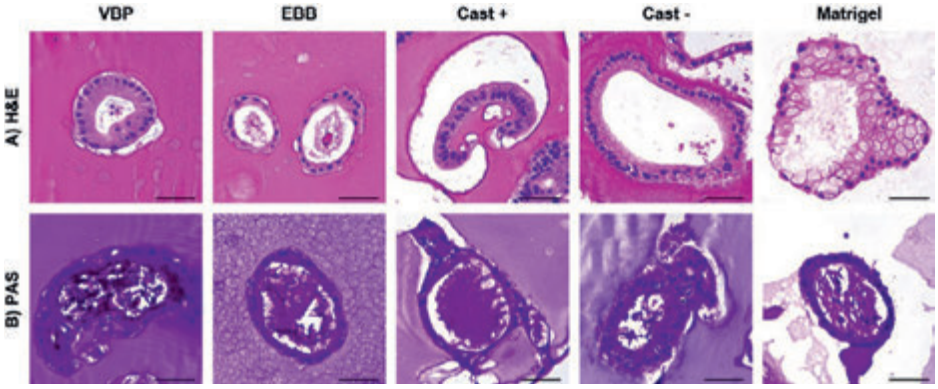

Figure S8. H&E and PAS staining of bioprinted and casted organoid-laden samples after hepatic differentiation. Histological images showing A) H&E staining and B) PAS staining of VBP- and EBB-printed organoids with the optically tuned bioresin (gelMA + 10 % w/v iodixanol), casted gelMA samples with (Cast+) and without iodixanol (Cast-) and casted Matrigel (MG) samples after the 10-day differentiation period.

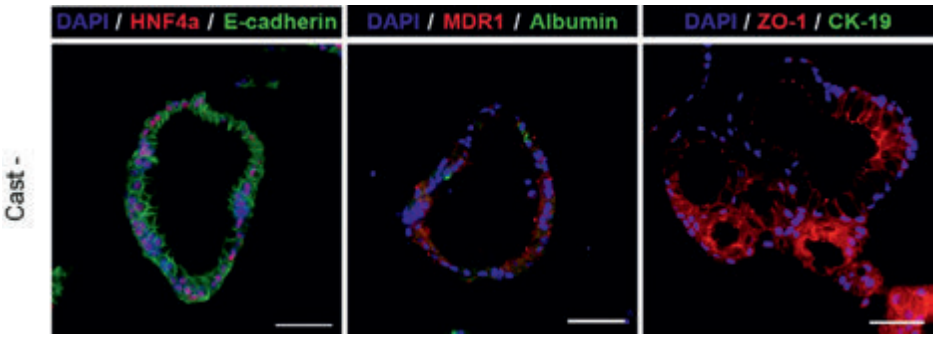

Figure S9. Liver-specific markers in the cast samples not supplemented with iodixanol. Representative fluorescence images of liver-specific and organoid polarization HNF4α and E-cadherin, MDR1 and albumin, and CK19 and ZO-1 in the Cast- condition after 10 days of hepatic differentiation. Scale bars = 50 µm. Individual data points shown for 3 different donors (N = 3).* = significant difference ($p < 0.05$).

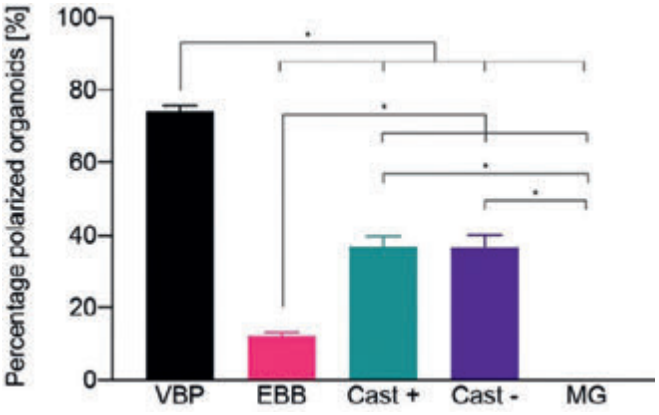

Figure S10. Quantitative analysis of organoid polarization based on luminal MDR1 expression between different fabrication strategies: VBP, EBB, and casted gelMA (with and without iodixanol) and Matrigel. (n = 160 – 255). * = significant difference ($p < 0.05$).

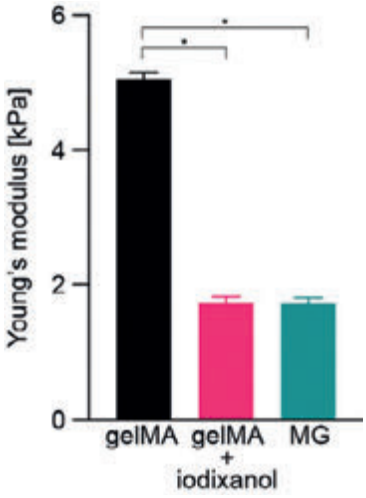

Figure S11. Compression modulus of gelMA samples without and with (10% w/v) iodixanol and Matrigel control samples. (n = 3). Statistically significant differences are represented with an *.

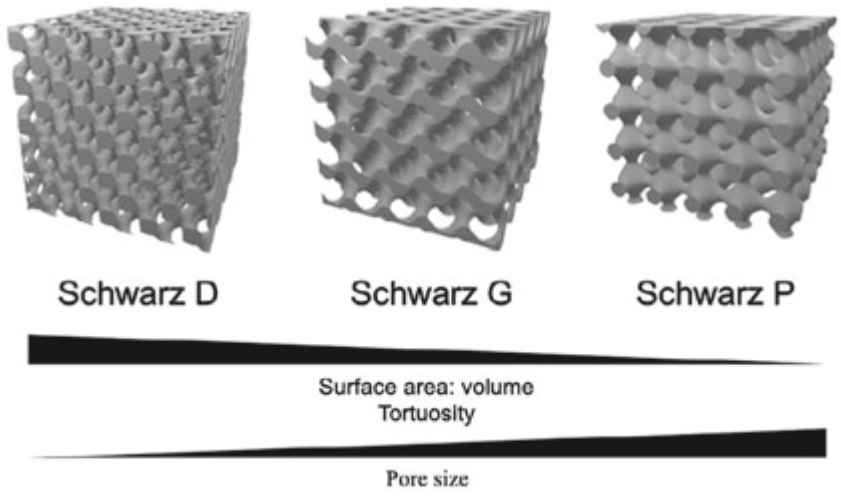

Figure S12. Mathematically-derived triply periodic minimal surface structures with distinct structural properties. STL models of the selected complex architectures Schwarz D, G and P, outlining their different surface area to volume ratio, tortuosity and pore sizes.

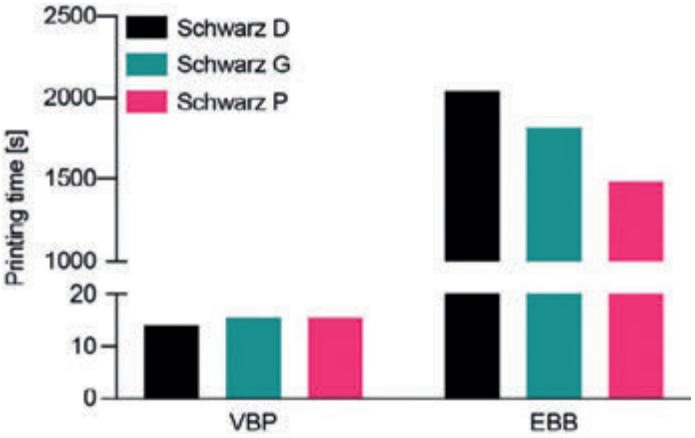

Figure S13. Printing times of Schwarz structures using different bioprinting approaches. Printing times (s) for Schwarz D, G and P structures as shown in figure 6A i-iii. VBP prints were performed with the optically tuned gelMA-based bioresin, while EBB prints, given the challenge in printing free-standing volumetric structures with such a soft material, were instead printed with a model bioink, Pluronic F-127.

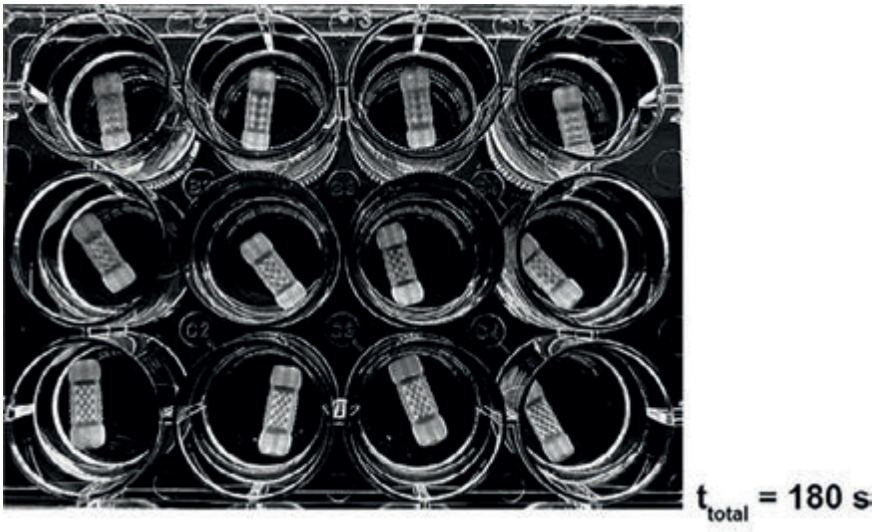

Figure S14. High-throughput printing of highly complex, perfusable structures within minutes. Twelve volumetrically printed constructs of complex architectures (Schwarz D, G and P) each measuring 1.7 cm in length and 6 mm in diameter with perfusable inlets printed in 180 s for high-throughput analysis of organoid activity.

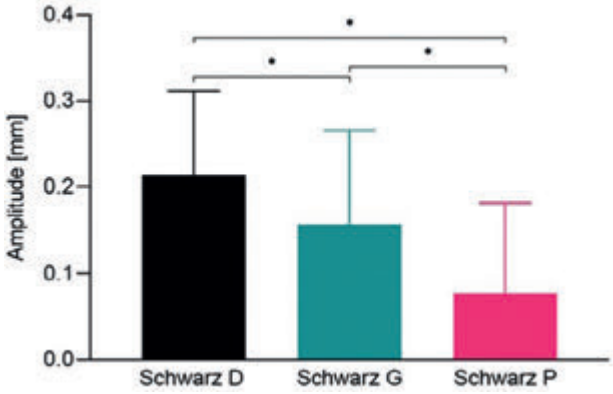

Figure S15. Bead trajectory analysis in different Schwarz architectures. Amplitude of the bead trajectories during perfusion at 1.5 µL min^{-1} of Schwarz D, G and P structures (n = 50 – 80). Statistically significant differences are represented with an *.

SUPPLEMENTARY TABLES

Table S1. Refractive index of different cellular organelles. Modified from Liu *et al.,* 2016 [38].

Organelles / intracellular matter	Refractive index
Cytosol	1.360 – 1.390
Nucleus	1.355 – 1.365
Nucleolus	1.375 – 1.385
Mitochondria	1.400 – 1.420
Lysosome	1.600

Table S2. Two-way ANOVA, multiple comparisons analysis results of feature size measurements for single cells at different iodixanol concentrations.

Supplementary Table S2 can be found in the online version of this manuscript.

Table S3. Two-way ANOVA, multiple comparisons analysis results of feature size measurements for organoids at different iodixanol concentrations.

Supplementary Table S3 can be found in the online version of this manuscript.

Table S4. dsDNA content of organoid-laden samples fabricated with different approaches. Total dsDNA content in: VBP- and EBB-printed organoids with the optically tuned bioresin (gelMA + 10 % w/v iodixanol), casted gelMA samples with (Cast+) and without iodixanol (Cast-) and casted Matrigel (MG) samples after a 10-day differentiation period.

Fabrication method	dsDNA content [mg sample^{-1}]
VBP	1.45 ± 0.28
EBB	1.46 ± 0.06
Cast+	1.25 ± 0.06
Cast-	1.13 ± 0.19
MG	2.03 ± 0.22

Table S5. Structural and dimensional properties of mathematically-derived Schwarz structures.

Structure	Volume (mm^3)	SA : V (mm^{-1})	Tortuosity
Schwarz D	394.25	2.05	1.32
Schwarz G	383.17	1.98	1.05
Schwarz P	390.86	1.88	1.04

Table S6. Secreted albumin levels in bioprinted structures. Total albumin production of hepatic organoids printed into different architectures during 24 hours of sterile perfusion at 20 µL min^{-1}.

Architecture	Albumin production over 24 hrs [µg mL^{-1}± SEM]
Schwarz D	3.40 ± 1.75
Schwarz P	17.00 ± 13.03
Cylinder (static)	1.17 ± 0.47

Table S7. Primers used for quantitative PCR analysis.

Gene	Forward sequence	Reverse sequence
CYP3A4	TGATGGTCAACAGCCTGTGCTGG	CCACTGGACCAAAAGGCCTCCG
ALB	GTTCGTTACACCAAGAAAGTACC	GACCACGGATAGATAGTCTTCTG

Table S8. Primary antibodies used for immunofluorescence analysis

Antigen	Source and cat. number	Raised in	Dilution*	Antigen retrieval*
HNFα	LS Biosciences LS-B969	Rabbit	1:200	TE
E-cadherin	BD Bioscience 610181	Mouse	1:400	TE
ZO-1	Invitrogen 40-2300	Rabbit	1:200	TE
CK-19	Abcam Ab15463	Rabbit	1:500	TE
MDR1	Novus Bio NBP1-90291	Rabbit	1:200	TE
Albumin	Sigma A6684	Mouse	1:1000	TE

*TE: 10 mM Tris, 1 mM EDTA, 0.5% Tween 20 in PBS at pH 9.0 for 30 min at 98°C.

Table S9. Secondary antibodies used for immunofluorescence analysis

Antigen	Source and cat. number	Raised in	Dilution*
Anti-mouse Alexa 488	Life Technologies A11029	Goat	1:200
Anti-mouse Alexa 568	Life Technologies A11036	Goat	1:200

*Secondary antibodies were diluted in Antibody Diluent (Dako).

SUPPLEMENTARY VIDEOS

Video V1. Sequence of μCT sections of a volumetrically printed Schwarz D structure with perfusable inlet and outlet.

Video V2. Sequence of μCT sections of a volumetrically printed Schwarz G structure with perfusable inlet and outlet.

Video V3. Sequence of μCT sections of a volumetrically printed Schwarz P structure with perfusable inlet and outlet.

Video V4. Fluorescent microspheres being perfused through a volumetrically printed Schwarz D structure.

Video V5. Fluorescent microspheres being perfused through a volumetrically printed Schwarz G structure.

Video V6. Fluorescent microspheres being perfused through a volumetrically printed Schwarz P structure.

SUPPLEMENTARY METHODS

GelMA Characterization

^{1}H NMR spectrum was measured on an Agilent 400 MR-NMR spectrometer (Agilent Technologies, USA) at 400 MHz in D_2O at 50° C. The degree of functionalization of the synthesized gelMA was measured using a 2,4,6-trinitrobenzenesulfonic acid (TNBSA, 5% w/v, Sigma, The Netherlands) in H_2O solution to quantify free primary amines before and after methacryloyl substitution. For the sol-fraction analysis, cylindrical constructs (6 mm diameter x 2 mm height) were printed with bioresins containing different concentrations of iodixanol (n = 3; 0 – 40% w/v) and the mass loss of the resulting structures was assessed as previously described [67].

Cell Isolation From Liver Biopsies

Liver biopsies (obtained during liver transplantation at the Erasmus Medical Center Rotterdam with ethical approval number MEC 2014-060) were chopped into small pieces and enzymatically digested with 0.125 mg mL^{-1} Type II collagenase and 0.125 mg mL^{-1} dispase in Dulbecco's Modified Eagle's Medium (DMEM) Glutamax supplemented with 0.01% (v/v) DNase I (Roche, Basel, Switzerland), 1% (v/v) fetal calf serum (FCS) and 1% (v/v) penicillin/streptomycin (P/S) at 37°C. Every hour, the supernatant was collected and fresh enzyme-supplemented media was added to the remaining tissue until only ducts and single cells were visible. Single cells were washed with DMEM Glutamax (supplemented with 1% (v/v) FCS and 1% (v/v) P/S) and spun down at 453 g for 5 min. All components were obtained from Life Technologies (Carlsbad, CA, USA).

Organoid Expansion and Differentiation Medium

Expansion medium (EM) consisted of Advanced DMEM/F12 (Life Technologies) supplemented with 1% (v/v) penicillin-streptomycin (Life Technologies), 1% (v/v) GlutaMax (Life Technologies), 10 mM HEPES (Life Technologies), 2% (v/v) B27 supplement without vitamin A (Invitrogen, Carlsbad, CA, USA), 1% (v/v) N2 supplement (Invitrogen), 10 mM nicotinamide (Sigma-Aldrich, St Louis, MO, USA), 1.25 mM N-acetylcysteine (Sigma-Aldrich), 10% (v/v) Rspondin-1 conditioned medium (the Rspo1-Fc-expressing cell line was a kind gift from Calvin J. Kuo), 10 µM forskolin (Sigma-Aldrich), 5 µM A83-01 (transforming growth factor beta inhibitor; Tocris Bioscience, Bristol, UK), 50 ng mL^{-1} EGF (Invitrogen), 25 ng mL^{-1} HGF (Peprotech, Rocky Hill, NJ, USA), 0.1 µg mL^{-1} FGF10 (Peprotech) and 10 nM recombinant human (Leu15)-gastrin I (Sigma-Aldrich). Differentiation medium (DM) consisted of EM without R-spondin-1, FGF10 and nicotinamide, supplemented with 100 ng mL^{-1} FGF19 (Peprotech), 500 nM A83-01 (Tocris Bioscience), 10 µM DAPT (Selleckchem, Munich, Germany),

25 ng mL^{-1} BMP-7 (Peprotech), and 30 μM dexamethasone (Sigma-Aldrich). The characterization of the micro-scale morphology of the organoids both in expansion and differentiation media via transmission electron microscopy has been extensively investigated and reported previously [79].

HepG2 Expansion Medium
DMEM + GlutaMAX (Gibco, 31966, The Netherlands) supplemented with fetal bovine serum (FBS, 10% v/v, Gibco, 10270, The Netherlands) and penicillin/streptomycin (1%, Gibco, The Netherlands).

Measurement of Scattering Phase Function of Cell Suspensions
In the apparatus, light from a laser diode at 405 nm (HL40033G, Ushio, Japan) is condensed by an aspherical lens (C671-TME405, Thorlabs, USA) into a multimode optical fiber (WF 70×70/115/200/400N, CeramOptec, Germany). Then, a lens (AC254-030-A-ML, Thorlabs) collimates the light at the output of the fiber. An aperture placed right after the lens limits the extension of the outgoing beam to 1 mm. The light is sent straight onto a 2 mm thick square quartz cuvette (CV10Q7FA, Thorlabs). The thickness of the cuvette was chosen so that only single scattering events were present in the hydrogel. Light scattered from the sample is collected by a photodiode (SM05PD3A, Thorlabs). The photodiodes rotate along a circumference of r = 250 mm by means of a precision rotational stage (X-RSW60A-E03, Zaber, Canada). The cuvette is held static on top of the center of the circumference. The signal from the photodiode is amplified (PDA200C, Thorlabs) and digitized by a data acquisition device (USB-6003, National Instruments, USA) and recorded in a computer. A MATLAB code controls and synchronizes the laser, the rotational stage, and the data acquisition device to acquire intensities 5 times at every angle with an angular resolution of 0.05° between 0° and 20° (scattered light beyond this angle was 3 orders of magnitude less intense than at θ = 10°, and thus approached to zero). A python code is used to process and convert the raw measured currents on the photodiode into light intensities, and to calculate scattering properties from them. For each hydrogel, we report the anisotropy coefficient *g*, which is the expected value of the scattering angle (*n* = 3) [80].

$$g = \langle cos\theta \rangle$$

$$g = \int_0^{\pi} p(\theta)\cos(\theta)2\pi\sin(\theta)d\theta$$

Mechanical Analysis of Samples With and Without Iodixanol
Compressive properties of casted bioresin cylinders (6 mm x 2 mm height) with 0 and 10% w/v iodixanol were assessed in an uniaxial, indentation-based compression test with a Dynamic Mechanical Analyzer (DMA Q800, TA Instruments, The Netherlands), equipped with a cylindrical flat piston (diameter = 2 mm). Samples were subjected to a strain ramp of –20 %/min strain rate to –30 % deformation (n = 5). Young's modulus was calculated as the slope of the stress/strain curve in the 10–15% strain range.

Enzymatic Degradation Assay
To assess the enzymatic degradation of photocrosslinked resins used in this study, photocrosslinked 5% w/v gelMA and 5% w/v gelMA + 10% w/v iodixanol (cylindrical samples, diameter = 6 mm , height = 2 mm) were swollen in PBS overnight and subsequently incubated at 37°C in a 0.2% w/v solution of collagenase type II in Dulbecco's modified Eagle Medium (DMEM, 31966, Gibco, The Netherlands), supplemented with 10% v/v heat-inactivated fetal bovine serum (FBS Gibco, The Netherlands), and 1% v/v penicillin and streptomycin (Life Technologies, The Netherlands). Samples were removed from the enzymatic solution at different time points (10, 25, 35, 45, and 60 min, n = 3 per time point), and the mass was measured and compared to that of the hydrogels before collagenase incubation as previously described [60].

Gene Expression Analysis
Prior to RNA isolation, GelMA hydrogels were broken down using QIAshredder columns according to the manufacturer's instructions (Qiagen, Hilden, Germany). RNA was isolated from organoids (3 donors, n = 3) using 350 µL RNeasy lysis buffer directly added into one well of the 24 well plate followed by RNA extraction using the RNeasy micro Kit according to the manufacturer's instructions (Qiagen). cDNA synthesis was performed using iScript cDNA synthesis kit (Bio-Rad, Veenendaal, the Netherlands). Relative gene expression of selected genes was measured using RT-qPCR in a CFX-384 (Bio-Rad). Primer design, validation, RT-qPCR conditions, and data analysis was performed as previously described (primer sequences are detailed in Supplementary Table S7) [81]. Normalization was performed using reference gene 60S ribosomal protein L19 (RPL19).

Albumin Secretion
To determine organoid albumin secretion medium was collected during the differentiation period of 10 days to examine total albumin secretion (n = 3). The culture medium was collected and concentrated using Amicon Ultra centrifugal filters (Amicon, Germany). The concentration of albumin was then determined

using a DxC-600 Beckman chemistry analyzer (Beckman Coulter, USA). Values were normalized for total protein content.

Liver Transaminase Levels

Enzyme activity levels were determined by lysing the samples (3 donors, $n = 3$) with Milli-Q water (Merck, Millipore, Burlington, MA, USA). Subsequently, aspartate transaminase (ASAT), gamma-glutamyl transferase (GGT) and glutamate dehydrogenase (GLDH) were measured with the clinical chemistry analyzer Beckman AU680 (Beckman Coulter, USA) using standard protocols. Values were normalized for total protein content.

Immunofluorescence

Cell-laden discs (3 donors , $n = 3$) were fixed in 4% (w/v) paraformaldehyde (PFA) and stored in 70% (v/v) EtOH at 4°C until further processing. Samples were embedded in paraffin and cut into 5 µm sections. Sections were deparaffinized and rehydrated. After antigen retrieval (information per antibody in Supplementary Table S8), a blocking step was performed using 10% v/v normal goat serum (Bio-Rad) in PBS for 30min at RT. Antibodies are listed in Supplementary Table S8. Incubation with primary antibodies was performed overnight at 4°C. Secondary antibodies were incubated at room temperature for 1h (listed in Supplementary Table S9). Nuclei were stained with DAPI (Sigma-Aldrich) diluted 2,000x in PBS. Washing steps were performed using a buffer of PBS with 0.1% v/v Triton X-100 (Sigma-Aldrich) and 0.2% w/v Bovine Serum Albumin (Sigma, The Netherlands). Slides were mounted using FluorSave (Merck-Millipore, USA), and images were acquired using a Thunder imaging system (Leica Microsystems, Germany).

Extrusion-Based Printing Attempt of Schwarz Structures

Schwarz D, G and P structures encased in a perfusable chamber as shown in Figure 6A i-iii were printed with a pneumatic-driven system (27 G stainless steel nozzle, temperature = 21 °C, pressure = 0.2 MPa, feed rate = 25 mm s^{-1}, 3DDiscovery, REGENHU, Switzerland) using model in Pluronic F-127 (Sigma-Aldrich, The Netherlands). Support structures were printed with the same material under the same printing parameters to ensure the structure was successfully printed and remained stable. Printing time was recorded for comparison to VBP printing times.

Fluorescent Microsphere Imaging in Perfusable System

The fluorescent microspheres were illuminated using a 405nm laser source (USHIO HL40033G) driven at 500±50 mW. The beam was first collimated using a f=6.33mm 0.68NA mounted aspheric lens (Thorlabs C330TMD-A) then passed through an engineered square diffuser (Thorlabs ED1-S20-MD). This produced

a homogenously illuminated surface with a square, top-hat illumination profile under which the samples were placed. A monochromatic camera (Basler a2A1920-160umPRO) with a 25mm lens (Basler C125-2522-5M-P f25mm) and 455nm longpass filter (Thorlabs FGL455) was used to perform the imaging. The longpass filter acted to reduce the background signal of the laser illumination, such as not to overwhelm the emission signal of the excited microspheres.

Sterile Perfusion System for Assessment of Organoid Ammonia Elimination

Volumetrically printed constructs were assembled into custom-made PDMS mold fitted in a custom-designed Polylactic acid (PLA) flow chamber prepared by Ultimaker S3 FDM 3D printer (Ultimaker, The Netherlands). For a leakproof flow chamber, the PFA microfluidic tubing (IDEX Health&Science, OD 1.6 mm, ID 0.75 mm) was guided through the side walls of the chamber and the hollow inlet/outlet printed within the hydrogel construct, followed by applying UV crosslinkable glue (Norland Optical Adhesive NOA 63; Norland Products, USA) around the connection between the PDMS mold and the tubing under 5 min UV exposure with a handheld lamp (λ = 365 nm; Vilber Lourmat, Eberhardzell, Germany) solely on the connection zone. A 4-channel peristaltic pump (ISMATEC Regio ICC, 12 rollers, 3-stop tubing ID 2.54 mm) was applied to perfuse 4 flow chambers independently at the flow rate of 20 µL min^{-1} per chamber for 24 hours within an incubator. An inlet reservoir of organoid differentiation medium (DM) supplemented with 1.5 mM of ammonium chloride was closed with a solvent cap (Diba Industries, 3*1/4”-28 UNF, GL32) which connected two PFA tubing for perfusion plus one syringe filter (0.2 mm) to prevent both particulate contamination and the evaporation of medium. The PFA tubing both from the flow chamber inlet and the solvent caps was fitted with the pumping tubing via a 1/4”-28 barbed adapter (IDEX Health&Science) coupled with a standard union (P-620, IDEX Health&Science), and the PFA tubing from the flow chamber outlet was connected to a microfluidic reservoir adapter (Elveflow, 2/4 port) which collected the fluid from each chamber towards individual 50 mL falcon tubes.

REFERENCES

[1] Mironov, V.; Trusk, T.; Kasyanov, V.; Little, S.; Swaja, R.; Markwald, R. Biofabrication: A 21st Century Manufacturing Paradigm. Biofabrication , *1*, 022001-5082/1/2/022001. Epub 2009 Jun 10.

[2] Levato, R.; Jungst, T.; Scheuring, R.G.; Blunk, T.; Groll, J.; Malda, J. From Shape to Function: The Next Step in Bioprinting. Adv Mater **2020**, *32*.

[3] Groll, J.; Boland, T.; Blunk, T.; Burdick, J.A.; Cho, D.; Dalton, P.D.; Derby, B.; Forgacs, G.; Li, Q.; Mironov, V.A. *et al.* Biofabrication: Reappraising the Definition of an Evolving Field. Biofabrication **2016**, *8*, 013001-5090/8/1/013001.

[4] Laronda, M.M.; Rutz, A.L.; Xiao, S.; Whelan, K.A.; Duncan, F.E.; Roth, E.W.; Woodruff, T.K.; Shah, R.N. A Bioprosthetic Ovary Created using 3D Printed Microporous Scaffolds Restores Ovarian Function in Sterilized Mice. Nat. Commun. **2017**, *8*, 15261.

[5] Bulanova, E.A.; Koudan, E.V.; Degosserie, J.; Heymans, C.; Pereira, F.D.; Parfenov, V.A.; Sun, Y.; Wang, Q.; Akhmedova, S.A.; Sviridova, I.K. *et al.* Bioprinting of a Functional Vascularized Mouse Thyroid Gland Construct. Biofabrication **2017**, *9*, 034105-5090/aa7fdd.

[6] Kim, J.H.; Kim, I.; Seol, Y.; Ko, I.K.; Yoo, J.J.; Atala, A.; Lee, S.J. Neural Cell Integration into 3D Bioprinted Skeletal Muscle Constructs Accelerates Restoration of Muscle Function. Nat. Commun. **2020**, *11*, 1025-9.

[7] Martin, I.; Malda, J.; Rivron, N.C. Organs by Design: Can Bioprinting Meet Self-Organization? Curr. Opin. Organ. Transplant. **2019**, *24*, 562-567.

[8] Lewis, P.L.; Green, R.M.; Shah, R.N. 3D-Printed Gelatin Scaffolds of Differing Pore Geometry Modulate Hepatocyte Function and Gene Expression. Acta Biomater. **2018**, *69*, 63-70.

[9] Clevers, H. Modeling Development and Disease with Organoids. Cell **2016**, *165*, 1586-1597.

[10] Kim, J.; Koo, B.; Knoblich, J.A. Human Organoids: Model Systems for Human Biology and Medicine. Nat. Rev. Mol. Cell Biol. **2020**, *21*, 571-584.

[11] Bernal, P.N.; Delrot, P.; Loterie, D.; Li, Y.; Malda, J.; Moser, C.; Levato, R. Volumetric Bioprinting of Complex Living-Tissue Constructs within Seconds. Adv Mater **2019**, *31*, e1904209.

[12] Harrison, S.P.; Baumgarten, S.F.; Verma, R.; Lunov, O.; Dejneka, A.; Sullivan, G.J. Liver Organoids: Recent Developments, Limitations and Potential. Front. Med. **2021**, *8*, 574047.

[13] Huch, M.; Gehart, H.; van Boxtel, R.; Hamer, K.; Blokzijl, F.; Verstegen, M.M.; Ellis, E.; van Wenum, M.; Fuchs, S.A.; de Ligt, J. *et al.* Long-Term Culture of Genome-Stable Bipotent Stem Cells from Adult Human Liver. Cell **2015**, *160*, 299-312.

[14] Kelly, B.E.; Bhattacharya, I.; Heidari, H.; Shusteff, M.; Spadaccini, C.M.; Taylor, H.K. Volumetric Additive Manufacturing Via Tomographic Reconstruction. Science **2019**, *363*, 1075-1079.

[15] Loterie, D.; Delrot, P.; Moser, C. High-Resolution Tomographic Volumetric Additive Manufacturing. Nat. Commun. **2020**, *11*, 852-4.

[16] de Ruijter, M.; Ribeiro, A.; Dokter, I.; Castilho, M.; Malda, J. Simultaneous Micropatterning of Fibrous Meshes and Bioinks for the Fabrication of Living Tissue Constructs. Adv. Healthc. Mater. **2019**, *8*, e1800418.

[17] Schwab, A.; Levato, R.; D'Este, M.; Piluso, S.; Eglin, D.; Malda, J. Printability and Shape Fidelity of Bioinks in 3D Bioprinting. Chem. Rev. **2020**, *120*, 11028-11055.

[18] Ribeiro, A.J.S.; Yang, X.; Patel, V.; Madabushi, R.; Strauss, D.G. Liver Microphysiological Systems for Predicting and Evaluating Drug Effects. Clin. Pharmacol. Ther. **2019**, *106*, 139-147.

[19] Paxton, N.; Smolan, W.; Böck, T.; Melchels, F.; Groll, J.; Jungst, T. Proposal to Assess Printability of Bioinks for Extrusion-Based Bioprinting and Evaluation of Rheological Properties Governing Bioprintability. Biofabrication **2017**, *9*, 044107-5090/aa8dd8.

[20] Echalier, C.; Levato, R.; Mateos-Timoneda, M.; Castaño, O.; Déjean, S.; Garric, X.; Pinese, C.; Noël, D.; Engel, E.; Martinez, J. *et al.* Modular Bioink for 3D Printing of Biocompatible Hydrogels: Sol–gel Polymerization of Hybrid Peptides and Polymers. RSC Adv. **2017**, *7*, 12231-12235.

[21] Arjmand, P.; Katz, O.; Gigan, S.; Guillon, M. Three-Dimensional Broadband Light Beam Manipulation in Forward Scattering Samples. Opt. Express **2021**, *29*, 6563-6581.

[22] Rizzo, R.; Ruetsche, D.; Liu, H.; Zenobi-Wong, M. Optimized Photoclick (Bio)Resins for Fast Volumetric Bioprinting. Adv Mater **2021**, *33*, e2102900.

[23] Loterie, D.; Delrot, P.; Moser, C. Volumetric 3D Printing of Elastomers by Tomographic Back-Projections. Preprint **2018**.

[24] Rebelo, S.P.; Costa, R.; Estrada, M.; Shevchenko, V.; Brito, C.; Alves, P.M. HepaRG Microencapsulated Spheroids in DMSO-Free Culture: Novel Culturing Approaches for Enhanced Xenobiotic and Biosynthetic Metabolism. Arch. Toxicol. **2015**, *89*, 1347-1358.

[25] Starokozhko, V.; Hemmingsen, M.; Larsen, L.; Mohanty, S.; Merema, M.; Pimentel, R.C.; Wolff, A.; Emnéus, J.; Aspegren, A.; Groothuis, G. *et al.* Differentiation of Human-Induced Pluripotent Stem Cell Under Flow Conditions to Mature Hepatocytes for Liver Tissue Engineering. J. Tissue Eng. Regen. Med. **2018**, *12*, 1273-1284.

[26] Christoffersson, J.; Aronsson, C.; Jury, M.; Selegård, R.; Aili, D.; Mandenius, C. Fabrication of Modular Hyaluronan-PEG Hydrogels to Support 3D Cultures of Hepatocytes in a Perfused Liver-on-a-Chip Device. Biofabrication **2018**, *11*, 015013-5090/aaf657.

[27] Kehtari, M.; Zeynali, B.; Soleimani, M.; Kabiri, M.; Seyedjafari, E. Fabrication of a Co-Culture Micro-Bioreactor Device for Efficient Hepatic Differentiation of Human Induced Pluripotent Stem Cells (hiPSCs). Artif. Cells Nanomed Biotechnol. **2018**, *46*, 161-170.

[28] Esch, M.B.; Prot, J.; Wang, Y.I.; Miller, P.; Llamas-Vidales, J.R.; Naughton, B.A.; Applegate, D.R.; Shuler, M.L. Multi-Cellular 3D Human Primary Liver Cell Culture Elevates Metabolic Activity Under Fluidic Flow. Lab. Chip **2015**, *15*, 2269-2277.

[29] Bertassoni, L.E.; Cardoso, J.C.; Manoharan, V.; Cristino, A.L.; Bhise, N.S.; Araujo, W.A.; Zorlutuna, P.; Vrana, N.E.; Ghaemmaghami, A.M.; Dokmeci, M.R. *et al.* Direct-Write Bioprinting of Cell-Laden Methacrylated Gelatin Hydrogels. Biofabrication **2014**, *6*.

[30] Mazzocchi, A.; Devarasetty, M.; Huntwork, R.; Soker, S.; Skardal, A. Optimization of Collagen Type I-Hyaluronan Hybrid Bioink for 3D Bioprinted Liver Microenvironments. Biofabrication **2018**, *11*, 015003.

[31] Taymour, R.; Kilian, D.; Ahlfeld, T.; Gelinsky, M.; Lode, A. 3D Bioprinting of Hepatocytes: Core-Shell Structured Co-Cultures with Fibroblasts for Enhanced Functionality. Sci. Rep. **2021**, *11*, 5130-6.

[32] Lee, H.; Han, W.; Kim, H.; Ha, D.; Jang, J.; Kim, B.S.; Cho, D. Development of Liver Decellularized Extracellular Matrix Bioink for Three-Dimensional Cell Printing-Based Liver Tissue Engineering. Biomacromolecules **2017**, *18*, 1229-1237.
[33] Hong, S.; Song, J.M. A 3D Cell Printing-Fabricated HepG2 Liver Spheroid Model for High-Content in Situ Quantification of Drug-Induced Liver Toxicity. Biomater. Sci. **2021**, *9*, 5939-5950.
[34] Madrid-Wolff, J.; Boniface, A.; Loterie, D.; Delrot, P.; Moser, C. Controlling Light in Scattering Materials for Volumetric Additive Manufacturing. Adv. Sci. **2022**, *9*, e2105144.
[35] Boothe, T.; Hilbert, L.; Heide, M.; Berninger, L.; Huttner, W.B.; Zaburdaev, V.; Vastenhouw, N.L.; Myers, E.W.; Drechsel, D.N.; Rink, J.C. A Tunable Refractive Index Matching Medium for Live Imaging Cells, Tissues and Model Organisms. Elife **2017**, *6*, 10.7554/eLife.27240.
[36] Pouran, B.; Arbabi, V.; Bleys, R.L.; René van Weeren, P.; Zadpoor, A.A.; Weinans, H. Solute Transport at the Interface of Cartilage and Subchondral Bone Plate: Effect of Micro-Architecture. J. Biomech. **2017**, *52*, 148-154.
[37] Zonneveld, M.I.; van Herwijnen, M.J.C.; Fernandez-Gutierrez, M.M.; Giovanazzi, A.; de Groot, A.M.; Kleinjan, M.; van Capel, T.M.M.; Sijts, A.J.A.M.; Taams, L.S.; Garssen, J. *et al.* Human Milk Extracellular Vesicles Target Nodes in Interconnected Signalling Pathways that Enhance Oral Epithelial Barrier Function and Dampen Immune Responses. J. Extracell Vesicles **2021**, *10*, e12071.
[38] Liu, P.Y.; Chin, L.K.; Ser, W.; Chen, H.F.; Hsieh, C.; Lee, C.; Sung, K.; Ayi, T.C.; Yap, P.H.; Liedberg, B. *et al.* Cell Refractive Index for Cell Biology and Disease Diagnosis: Past, Present and Future. Lab. Chip **2016**, *16*, 634-644.
[39] Lee, W.M. Drug-Induced Hepatotoxicity. N. Engl. J. Med. **2003**, *349*, 474-485.
[40] Olson, H.; Betton, G.; Robinson, D.; Thomas, K.; Monro, A.; Kolaja, G.; Lilly, P.; Sanders, J.; Sipes, G.; Bracken, W. *et al.* Concordance of the Toxicity of Pharmaceuticals in Humans and in Animals. Regulatory Toxicology and Pharmacology **2000**, *32*, 56-67.
[41] den Braver-Sewradj, S.P.; den Braver, M.W.; Baze, A.; Decorde, J.; Fonsi, M.; Bachellier, P.; Vermeulen, N.P.E.; Commandeur, J.N.M.; Richert, L.; Vos, J.C. Direct Comparison of UDP-Glucuronosyltransferase and Cytochrome P450 Activities in Human Liver Microsomes, Plated and Suspended Primary Human Hepatocytes from Five Liver Donors. Eur. J. Pharm. Sci. **2017**, *109*, 96-110.
[42] Schneeberger, K.; Sánchez-Romero, N.; Ye, S.; van Steenbeek, F.G.; Oosterhoff, L.A.; Pla Palacin, I.; Chen, C.; van Wolferen, M.E.; van Tienderen, G.; Lieshout, R. *et al.* Large-Scale Production of LGR5-Positive Bipotential Human Liver Stem Cells. Hepatology **2020**, *72*, 257-270.
[43] Marsee, A.; Roos, F.J.M.; Verstegen, M.M.A.; HPB Organoid Consortium; Gehart, H.; de Koning, E.; Lemaigre, F.; Forbes, S.J.; Peng, W.C.; Huch, M. *et al.* Building Consensus on Definition and Nomenclature of Hepatic, Pancreatic, and Biliary Organoids. Cell. Stem Cell. **2021**, *28*, 816-832.
[44] Schneeberger, K.; Spee, B.; Costa, P.; Sachs, N.; Clevers, H.; Malda, J. Converging Biofabrication and Organoid Technologies: The Next Frontier in Hepatic and Intestinal Tissue Engineering? Biofabrication **2017**, *9*.
[45] Sorrentino, G.; Rezakhani, S.; Yildiz, E.; Nuciforo, S.; Heim, M.H.; Lutolf, M.P.; Schoonjans, K. Mechano-Modulatory Synthetic Niches for Liver Organoid Derivation. Nat. Commun. **2020**, *11*, 3416-0.

[46] Krüger, M.; Oosterhoff, L.A.; van Wolferen, M.E.; Schiele, S.A.; Walther, A.; Geijsen, N.; De Laporte Laura; van der Laan, L.J.W.; Kock, L.M.; Spee, B. Cellulose Nanofibril Hydrogel Promotes Hepatic Differentiation of Human Liver Organoids. Advanced healthcare materials **2020**, e1901658.

[47] Blaeser, A.; Duarte Campos, D.F.; Puster, U.; Richtering, W.; Stevens, M.M.; Fischer, H. Controlling Shear Stress in 3D Bioprinting is a Key Factor to Balance Printing Resolution and Stem Cell Integrity. Adv. Healthc. Mater. **2016**, *5*, 326-333.

[48] Levato, R.; Visser, J.; Planell, J.A.; Engel, E.; Malda, J.; Mateos-Timoneda, M.A. Biofabrication of Tissue Constructs by 3D Bioprinting of Cell-Laden Microcarriers. Biofabrication , *6*, 035020-5082/6/3/035020. Epub 2014 Jul 22.

[49] Brassard, J.A.; Nikolaev, M.; Hübscher, T.; Hofer, M.; Lutolf, M.P. Recapitulating Macro-Scale Tissue Self-Organization through Organoid Bioprinting. Nature Materials **2020**.

[50] Liu, Y.; Dabrowska, C.; Mavousian, A.; Strauss, B.; Meng, F.; Mazzaglia, C.; Ouaras, K.; Macintosh, C.; Terentjev, E.; Lee, J. *et al.* Bio-Assembling Macro-Scale, Lumenized Airway Tubes of Defined Shape Via Multi-Organoid Patterning and Fusion. Adv. Sci. **2021**, *8*, 2003332.

[51] Daly, A.C.; Davidson, M.D.; Burdick, J.A. 3D Bioprinting of High Cell-Density Heterogeneous Tissue Models through Spheroid Fusion within Self-Healing Hydrogels. Nat. Commun. **2021**, *12*, 753-2.

[52] Ferreira, S.A.; Motwani, M.S.; Faull, P.A.; Seymour, A.J.; Yu, T.T.L.; Enayati, M.; Taheem, D.K.; Salzlechner, C.; Haghighi, T.; Kania, E.M. *et al.* Bi-Directional Cell-Pericellular Matrix Interactions Direct Stem Cell Fate. Nat. Commun. **2018**, *9*, 4049-4.

[53] Ouchi, R.; Togo, S.; Kimura, M.; Shinozawa, T.; Koido, M.; Koike, H.; Thompson, W.; Karns, R.A.; Mayhew, C.N.; McGrath, P.S. *et al.* Modeling Steatohepatitis in Humans with Pluripotent Stem Cell-Derived Organoids. Cell. Metab. **2019**, *30*, 374-384.e6.

[54] Sachs, N.; de Ligt, J.; Kopper, O.; Gogola, E.; Bounova, G.; Weeber, F.; Balgobind, A.V.; Wind, K.; Gracanin, A.; Begthel, H. *et al.* A Living Biobank of Breast Cancer Organoids Captures Disease Heterogeneity. Cell **2018**, *172*, 373-386.e10.

[55] Schulze, R.J.; Schott, M.B.; Casey, C.A.; Tuma, P.L.; McNiven, M.A. The Cell Biology of the Hepatocyte: A Membrane Trafficking Machine. J. Cell Biol. **2019**, *218*, 2096-2112.

[56] Vogel, C.; Marcotte, E.M. Insights into the Regulation of Protein Abundance from Proteomic and Transcriptomic Analyses. Nat. Rev. Genet. **2012**, *13*, 227-232.

[57] Maier, T.; Güell, M.; Serrano, L. Correlation of mRNA and Protein in Complex Biological Samples. FEBS Lett. **2009**, *583*, 3966-3973.

[58] de Sousa Abreu, R.; Penalva, L.O.; Marcotte, E.M.; Vogel, C. Global Signatures of Protein and mRNA Expression Levels. Mol. Biosyst **2009**, *5*, 1512-1526.

[59] Ye, S.; Boeter, J.W.B.; Mihajlovic, M.; van Steenbeek, F.G.; van Wolferen, M.E.; Oosterhoff, L.A.; Marsee, A.; Caiazzo, M.; van der Laan, L.J.W.; Penning, L.C. *et al.* A Chemically Defined Hydrogel for Human Liver Organoid Culture. Adv. Funct. Mater. **2020**, *30*, 2000893.

[60] Levato, R.; Lim, K.S.; Li, W.; Asua, A.U.; Peña, L.B.; Wang, M.; Falandt, M.; Bernal, P.N.; Gawlitta, D.; Zhang, Y.S. *et al.* High-Resolution Lithographic Biofabrication of Hydrogels with Complex Microchannels from Low-Temperature-Soluble Gelatin Bioresins. Mater. Today Bio **2021**, *12*, 100162.

[61] Callens, S.J.P.; Arns, C.H.; Kuliesh, A.; Zadpoor, A.A. Decoupling Minimal Surface Metamaterial Properties through Multi-Material Hyperbolic Tilings. Adv. Funct. Mater. **2021**, *31*, 2101373.

[62] Melchels, F.P.W.; Tonnarelli, B.; Olivares, A.L.; Martin, I.; Lacroix, D.; Feijen, J.; Wendt, D.J.; Grijpma, D.W. The Influence of the Scaffold Design on the Distribution of Adhering Cells After Perfusion Cell Seeding. Biomaterials **2011**, *32*, 2878-2884.

[63] Paré, A.; Charbonnier, B.; Tournier, P.; Vignes, C.; Veziers, J.; Lesoeur, J.; Laure, B.; Bertin, H.; De Pinieux, G.; Cherrier, G. *et al.* Tailored Three-Dimensionally Printed Triply Periodic Calcium Phosphate Implants: A Preclinical Study for Craniofacial Bone Repair. ACS Biomater. Sci. Eng. **2020**, *6*, 553-563.

[64] Kapfer, S.C.; Hyde, S.T.; Mecke, K.; Arns, C.H.; Schröder-Turk, G.E. Minimal Surface Scaffold Designs for Tissue Engineering. Biomaterials **2011**, *32*, 6875-6882.

[65] Femmer, T.; Kuehne, A.J.C.; Wessling, M. Estimation of the Structure Dependent Performance of 3-D Rapid Prototyped Membranes. Chem. Eng. J. **2015**, *273*, 438-445.

[66] Jung, Y.; Torquato, S. Fluid Permeabilities of Triply Periodic Minimal Surfaces. Phys. Rev. E. Stat. Nonlin Soft Matter Phys. **2005**, *72*, 056319.

[67] Thomas, N.; Sreedhar, N.; Al-Ketan, O.; Rowshan, R.; Abu Al-Rub, R.K.; Arafat, H. 3D Printed Triply Periodic Minimal Surfaces as Spacers for Enhanced Heat and Mass Transfer in Membrane Distillation. Desalination **2018**, *443*, 256-271.

[68] Lim, K.S.; Levato, R.; Costa, P.F.; Castilho, M.D.; Alcala-Orozco, C.R.; van Dorenmalen, K.M.A.; Melchels, F.P.W.; Gawlitta, D.; Hooper, G.J.; Malda, J. *et al.* Bio-Resin for High Resolution Lithography-Based Biofabrication of Complex Cell-Laden Constructs. Biofabrication **2018**, *10*, 034101-5090/aac00c.

[69] Plaitakis, A.; Kalef-Ezra, E.; Kotzamani, D.; Zaganas, I.; Spanaki, C. The Glutamate Dehydrogenase Pathway and its Roles in Cell and Tissue Biology in Health and Disease. Biology (Basel) **2017**, *6*, 11.

[70] Hong, G.; Kim, J.; Oh, H.; Yun, S.; Kim, C.M.; Jeong, Y.; Yun, W.; Shim, J.; Jang, I.; Kim, C. *et al.* Production of Multiple Cell-Laden Microtissue Spheroids with a Biomimetic Hepatic-Lobule-Like Structure. Adv Mater **2021**, *33*, e2102624.

[71] Kang, D.; Hong, G.; An, S.; Jang, I.; Yun, W.; Shim, J.; Jin, S. Bioprinting of Multiscaled Hepatic Lobules within a Highly Vascularized Construct. Small **2020**, *16*, e1905505.

[72] Cuvellier, M.; Ezan, F.; Oliveira, H.; Rose, S.; Fricain, J.; Langouët, S.; Legagneux, V.; Baffet, G. 3D Culture of HepaRG Cells in GelMa and its Application to Bioprinting of a Multicellular Hepatic Model. Biomaterials **2021**, *269*, 120611.

[73] Kim, Y.; Asif, A.; Chethikkattuveli Salih, A.R.; Lee, J.; Hyun, K.; Choi, K. Gravity-Based Flow Efficient Perfusion Culture System for Spheroids Mimicking Liver Inflammation. Biomedicines **2021**, *9*, 1369.

[74] Homan, K.A.; Gupta, N.; Kroll, K.T.; Kolesky, D.B.; Skylar-Scott, M.; Miyoshi, T.; Mau, D.; Valerius, M.T.; Ferrante, T.; Bonventre, J.V. *et al.* Flow-Enhanced Vascularization and Maturation of Kidney Organoids in Vitro. Nat. Methods **2019**, *16*, 255-262.

[75] Cook, C.C.; Fong, E.J.; Schwartz, J.J.; Porcincula, D.H.; Kaczmarek, A.C.; Oakdale, J.S.; Moran, B.D.; Champley, K.M.; Rackson, C.M.; Muralidharan, A. *et al.* Highly Tunable Thiol-Ene Photoresins for Volumetric Additive Manufacturing. Adv Mater **2020**, *32*, e2003376.

[76] Lim, K.S.; Abinzano, F.; Bernal, P.N.; Albillos Sanchez, A.; Atienza-Roca, P.; Otto, I.A.; Peiffer, Q.C.; Matsusaki, M.; Woodfield, T.B.F.; Malda, J. *et al.* One-Step Photoactivation of a Dual-Functionalized Bioink as Cell Carrier and Cartilage-Binding Glue for Chondral Regeneration. Adv. Healthc. Mater. **2020**, *9*, e1901792.

[77] Hunt, A.J.; Huffman, D.R. A New Polarization-modulated Light Scattering Instrument. Rev. Sci. Instrum. **2003**, *44*, 1753-1762.

[78] Crocker, J.C.; Grier, D.G. When Like Charges Attract: The Effects of Geometrical Confinement on Long-Range Colloidal Interactions. Phys. Rev. Lett. **1996**, *77*, 1897-1900.

[79] Lehmann, V.; Schene, I.F.; Ardisasmita, A.I.; Liv, N.; Veenendaal, T.; Klumperman, J.; van der Doef, H.P.J.; Verkade, H.J.; Verstegen, M.M.A.; van der Laan, L.J.W. *et al.* The Potential and Limitations of Intrahepatic Cholangiocyte Organoids to Study Inborn Errors of Metabolism. J. Inherit. Metab. Dis. **2022**, *45*, 353-365.

[80] Fukutomi, D.; Ishii, K.; Awazu, K. Highly Accurate Scattering Spectra of Strongly Absorbing Samples obtained using an Integrating Sphere System by Considering the Angular Distribution of Diffusely Reflected Light. Lasers Med. Sci. **2015**, *30*, 1335-1340.

[81] van Steenbeek, F.G.; Spee, B.; Penning, L.C.; Kummeling, A.; van Gils, I.H.M.; Grinwis, G.C.M.; van Leenen, D.; Holstege, F.C.P.; Vos-Loohuis, M.; Rothuizen, J. *et al.* Altered Subcellular Localization of Heat Shock Protein 90 is Associated with Impaired Expression of the Aryl Hydrocarbon Receptor Pathway in Dogs. PLoS ONE **2013**, *8*.

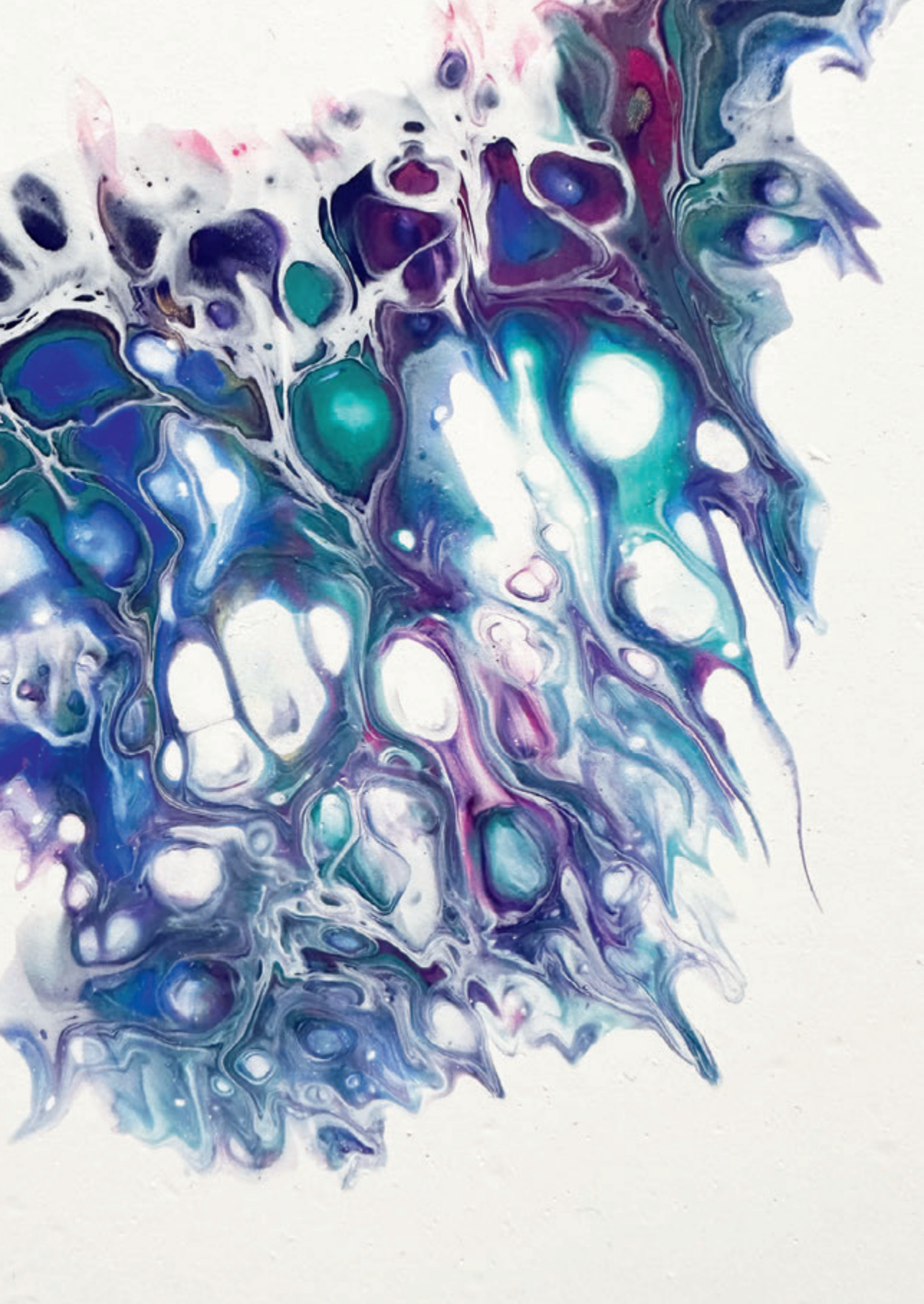

Establishment of a tailor-made bioreactor for dynamic culture of bioprinted hepatic constructs

M.C. Bouwmeester[1], Y. Tao[1], N.A. van Heck[1], T. Walraven[1], P. Nuñez Bernal[2], D. Wanders[3], R. Levato[1,2], B. Spee[1]

1 Department of Clinical Sciences, Faculty of Veterinary Medicine, Utrecht University, Utrecht, the Netherlands.
2 Department of Orthopaedics, University Medical Center Utrecht, Utrecht University, Utrecht, The Netherlands.
3 LifeTec Group BV, Eindhoven, The Netherlands.

5

ABSTRACT

Recently developed three-dimensional hepatic *in vitro* systems have improved functionality compared to conventional two-dimensional cultures. These more physiological relevant models range from 3D culture methods to more advanced bioreactors with dynamic flow. Here, a tailor-made perfusion bioreactor was developed to provide media flow to bioprinted hepatic constructs under standardized conditions. The bioreactor allows for automated media replenishment and provides continuous flow which mimics the *in vivo* situation. Medium samples can be taken without the need to disturb circulation and thereby introduce temperature fluctuations. The hepatic constructs inside the bioreactor are volumetric bioprinted structures containing intrahepatic cholangiocyte organoids (ICOs) which are differentiated towards their hepatic phenotype. ICOs are patient-derived cells with a potential in regenerative medicine and disease modelling. Results indicate that media flow in the bioreactor could maintain and perfuse bioprinted constructs. Although a trend of increased expression of hepatic markers albumin, cytochrome P450 3A4 (CYP3A4) and Multi Resistance Protein 2 (MRP2) was observed in perfused constructs compared to static controls, further experiments including more ICO donors are needed to confirm these findings. The use of the tailor-made bioreactor showed to be a suitable system for construct perfusion and, with adjustments including fluid flow optimizations, this setup allows for high-content mechanistic studies.

Keywords
Liver organoids; bioreactor; bioengineering; hepatic *in vitro* model; dynamic culture

INTRODUCTION

Over the years, *in vitro* culture technology has progressed from conventional two-dimensional (2D) towards more physiological relevant three-dimensional (3D) cultures [1,2]. The *in vivo* microenvironment is highly complex and dynamic, and recapitulation *in vitro* has been shown to increase cellular functionality [3-6]. Approaches to create more physiological relevant cultures range from 3D culture methods, such as spheroids and organoids, to more advanced culture techniques involving 3D bioprinting, co-culture of multiple cell types and/or incorporation of extracellular matrix [7,8]. More importantly, by adding physiological fluid flow, the dynamic nature of the natural microenvironment is further mimicked leading to improved cellular function [9-11] and can stimulate maturation of differentiating stem cells [12-14] and improve vascularization in constructs [15,16].

The development of bioreactor technology provides a setting to create such dynamic cultures providing mechanical stimulation of cells, as well as nutrient supply and metabolites removal, under standardized conditions [17-20]. A wide variety of bioreactor types exist, ranging from microfluidic (organ-on-a) chip devices, to macro-scaled bioreactor designs with different properties, such as complexity, material choice, or flow direction [21]. These bioreactor specific features guide their application. Chip devices have been described for high-throughput approaches, such as toxicity testing, and are, due to material choice, suitable for imaging studies [22,23]. Other setups can serve as high-content (low-throughput) models for non-targeted purposes, e.g., omics screening to unravel disease mechanisms [24].

In this chapter, a tailor-made bioreactor is described that is compatible with the previously reported volumetric and extrusion-based bioprinted hepatic constructs to provide flow perfusion [25,26]. The constructs contain hepatic differentiated intrahepatic cholangiocyte organoids (ICOs) of which the potential in disease modelling and regenerative medicine is described [27-29]. ICOs are bipotential and can be differentiated to cholangiocyte- and hepatocyte-lineage, can be maintained for a long time while maintaining genetic stability [30]. Bioprinting procedures themselves did not improve hepatic maturation state of the ICOs [25,26], however the importance of the architectural design of the constructs on cellular functionality was shown and short-term exposure of bioprinted constructs in a lab-made perfusion chamber showed improved functionality on ammonia detoxification [26]. Dynamic conditions of hepatic *in vitro* models mimic the hemodynamics in hepatic sinusoids and several papers confirmed that exposing stem-cell derived hepatocytes to shear stress forces through fluid flow improves their hepatic maturation status [12,17,31-34]. Next

to this, it is described that unidirectional flow, as applied in this system, is superior over bidirectional flow and adding a closed loop system would mimic hepatic circulation as it occurs in the human body [35]. Running in circulation also allows for repeated dose testing, and providing flow is suggested to allow chronic exposure studies, reflecting more loosely in the *in vivo* situation [36]. The bioreactor is made of the inert material polyether ether ketone (PEEK) in order to prevent from binding of chemicals, such as drugs, toxicants and compounds supplied into the perfusion media. This unwanted effect would lead to inaccurate concentrations of parent compound and/or metabolites which are vital when performing exposure studies [37,38]. These toxicity studies are one of the potential applications of hepatic *in vitro* models since the liver is the major organ involved in drug metabolism [39-41]. Overall, this novel bioreactor that can hold a bioprinted liver construct and allows dynamic flow will improve liver function and standardize (long-term) measurements, a much needed hepatic liver model.

EXPERIMENTAL SECTION

Organoid culture and functional assays

Intrahepatic cholangiocyte organoids (ICOs) are liver-derived organoids that are expanded *in vitro* and can be differentiated towards their hepatocyte- and cholangiocyte-lineage. In this study, ICOs are differentiated towards hepatocyte-like organoids, hereafter called liver organoids. Details on the establishment of ICO culture and culture procedure is described in the Supplemental Experimental Procedures. In this study two organoid donors are used. Details on assays regarding metabolic activity of the organoids and gene expression levels of hepatic maturation markers are described in the Supplemental Experimental Procedures.

Bioprinting liver constructs

Organoid-laden constructs were bioprinted as previously described [26]. In short, gelatin-methacrylol (gelMA) was prepared from gelatine-derived from porcine skin (Sigma-Aldrich, St Louis, MO, USA) as previously reported and it was used as a 5% (w/v) solution in phosphate-buffered saline [42]. GelMA was supplemented with 0.1% (w/v) of the photoinitiator lithium phenyl(2,4,6-trimethylbenzoyl)phosphinate (LAP; Tokyo Chemical Industry, Tokyo, Japan) and 10% (v/v) iodixanol (OptiPrep; StemCell Technologies, Vancouver, Canada). Organoids were taken up in the gelMA at a density of 5 million cells per mL. The bioink was transferred to cylindrical borosilicate glass vials, hereafter referred to as printing vials. The printing vials were placed on ice to induce gelation in order to prevent cell sedimentation during the bioprinting procedure.

Volumetric bioprinting of constructs was performed using a Tomolite printer (Readily 3D, Lausanne, Switzerland). The bioprinter projects tomographic images onto the printing vials at a wavelength of 405 nm. These projections were calculated using the Apparite software (Readily3D) taking into account parameters such as the material properties of the printing vials and the bioink. Constructs were printed in a Schwarz D structure using a light dose of 250 mJ/cm^2 (printing time: 20.0s). After printing, the printing vials were heated to 37 °C to melt the unpolymerized bioink, which was subsequently washed away with pre-warmed phosphate-buffered saline.

Static pre-culture of the volumetric bioprinted organoid-laden constructs in differentiation medium (DM) in a standard 6 well culture plate (ThermoFisher, Waltham, Massachusetts, USA) was performed overnight prior to the perfusion experiment. As measure for cell viability, metabolic activity of the bioprinted constructs was measured using the AlamarBlue assay (as described in Supplemental Experimental Procedures) and then the constructs were transferred to a perfusion bioreactor chamber.

Perfusion setup

The proposed bioreactor and flow perfusion system was designed by LifeTec Group (Eindhoven, the Netherlands) and Utrecht University for providing a continuous flow to the bioprinted liver constructs [43]. The perfusion system, depicted schematically in Figure 1, is composed of: (1) a polyether ether ketone (PEEK) bioreactor with polycarbonate lid, (2) a rollerpump (Ismatec IPC-N, Masterflex, Gelsenkirchen, Germany) with the ability for low speed pumping using Tygon® tubing (Ismatec, LMT-55, 2-stop, 0.19 mm ID; Masterflex) and multiple systems in parallel with a modular setup; (3) a heat exchanger, (4) an air bubble trap (Elveflow, Paris, France), and (5) two media containers, one for fresh media and one for waste media. The bioreactor, air bubble trap and heat exchanger are placed inside the incubator. The flow perfusion system is designed in such a way, that medium can be refreshed without the need to detach the system. Reversing the flow direction enables to refresh the medium in the perfusion system, as medium will be pumped from the fresh media container towards the waste media container, the bioreactor is excluded from this circulation by the use of one way valves (Figure 1B and 1C). In this study this media refreshment option is not used, as liver constructs were only cultured for 7 days.

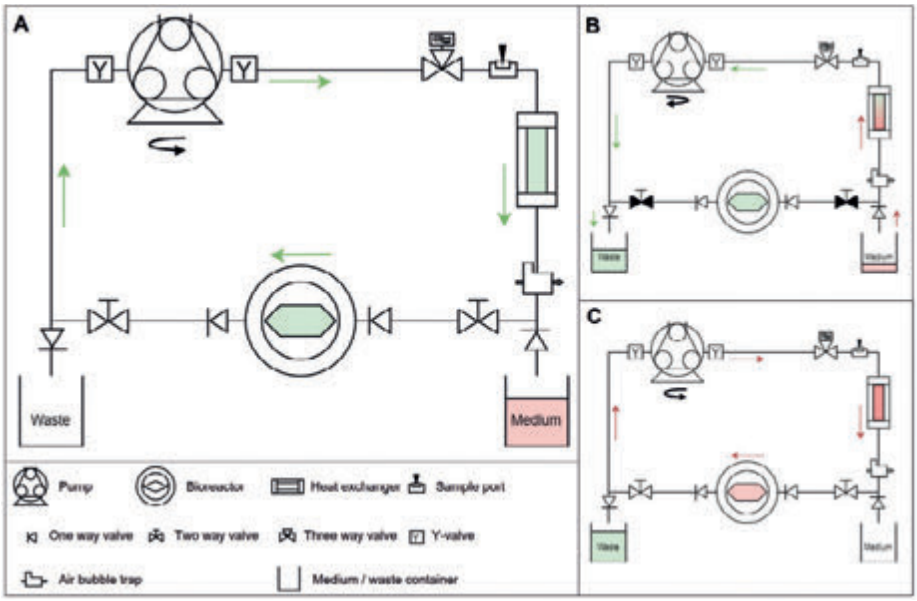

Figure 1. Schematic representation of flow perfusion system. A) Regular flow. B) Reverse flow direction leading to media refreshment. Black coloured two-way valve represent closed valve. C) Flow back to original direction leading to regular flow with refreshed media.

The bioreactor consists of two compatible and screwable parts: the PEEK bioreactor with a chamber (dimensions lxwxh 8x6x6 mm for the rectangular part, total length from inlet to outlet 12.3 mm) for the construct and a polycarbonate lid (Figure 2A). The bioreactor was designed to be easily milled from PEEK, a high-performance semi-crystalline thermoplastic, with limited curvature that can be reproduced with high precision. PEEK has strong mechanical properties with a high resistance to fatigue and wear due to reuse (including sterilisation) and flow. The square chamber has triangular ends to equalise the pressure of the fluid before the media enters the construct. For loading, bioprinted constructs were placed in the bioreactor while it was submerged in DMEM media to limit air bubbles in the chamber. The beforementioned one way valves right before and after the bioreactor allow the system and bioreactor with the construct to be filled separately. The PEEK bioreactor is equipped with an inlet and outlet channels with screw threads. Watertightness is achieved by a silicone O-ring at both the inlet, outlet and around the chamber (Figure 2A). Bioreactors were placed in stainless steel holders which were organized in a modular system (Figure 2C) which are placed in a 20 degree angle to minimize potential pockets of air in the bioreactor. The total volume of the system is 17 – 20 mL including 12 – 14.5 mL dead volume in the tubing. The media containers can hold up to

120 mL. The constructs were perfused with hepatic differentiation medium (DM) at a flow rate of 50 µl/min. The flow rate was determined based on previous papers [17,32-34,44-46].

Polycarbonate parts (heat exchanger, medium and waste containers, lid of bioreactor) were vapor polished with dichloromethane to make them see-through and enable monitoring parameters such as construct integrity and medium colour during perfusion. Tygon® tubing (1/16 inch inner diameter) was used. An injection port was placed right before the heat exchanger to take medium samples during perfusion without disturbing the flow.

As a control, three additional constructs were transferred to separate T25 culture flasks and suspended in 17 mL DM and referred to as static controls. Static and perfused constructs were incubated at 5% CO_2 and 37 °C for 7 days. Due to one day of static overnight culture in both conditions, the total hepatic differentiation time of the ICOs was 8 days.

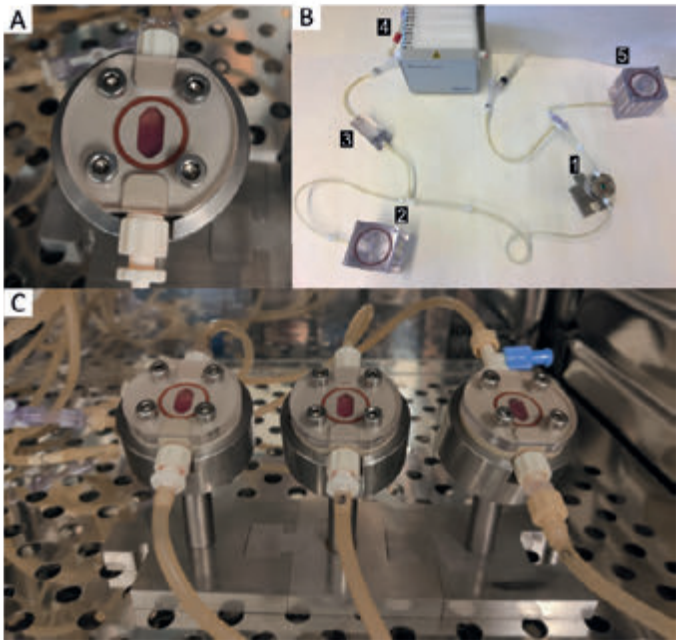

Figure 2. Bioreactor and perfusion system. A) Polyether ether ketone (PEEK) bioreactor with polycarbonate lid with volumetric bioprinted construct inside. B) Perfusion setup. 1 bioreactor; 2 medium container; 3 heat exchanger; 4 pump; 5 waste container. Air bubble trap is not included in this picture. C) Three bioreactors in a modular system during the perfusion experiment.

RESULTS

The bioreactor setup was maintained under continuous flow for 7 days. To avoid contamination of the system as much as possible, the tailor-made bioreactor and all other parts of the perfusion system were autoclaved, except for the connecting parts which were ethanol disinfected and allowed to dry in air under sterile conditions. The system was assembled in a flow biosafety cabinet using sterilized forceps. Due to the use of forceps, connections may be unproperly sealed leading to leakages, as observed in several experiments. Therefore, the number of connectors in the system was reduced. Cell-free experiments showed that high speed perfusion (540 µL/min) resulted in construct flush out, but at the chosen speed (50 µL/min) constructs stayed intact as long as the chamber contained minimal air bubbles. Pressure build-up and bubble formation can lead to construct disintegration, as observed in previous experiments (data not shown), however incorporation of the air bubble trap solved this issue.

Intrahepatic cholangiocyte organoids (ICOs) were expanded in a spinner flask culture up to 3 weeks in order to obtain enough cells for bioprinting multiple constructs (12.5 million cells/bioprinting procedure). Liver constructs were directly after the bioprinting procedure placed in hepatic differentiation medium (day -1 of perfusion). The next day, constructs were placed in the bioreactors (day 0 of perfusion). For one of the two donors, one construct was lost due to leakages as a result of incorrect position of one of the O-rings. Therefore, shown data represents a technical duplicate for one and a technical triplicate for the other donor.

Metabolic activity of liver organoids in the constructs was measured on day 0 of perfusion and at day 7 of perfusion as a measure for viability (Figure 3). At day 7, the viability of liver organoids in perfused constructs was 60% (58 – 63%) relative to day 0. In the static controls, the average viability was 84% (80 – 88%) at day 7 relative to day 0.

In both perfused and static cultured constructs the gene expression levels of hepatic marker albumin, hepatic transporter multi resistance protein 2 (MRP2) and major cytochrome P450 (CYP) enzyme 3A4 were examined as markers for hepatic maturation state of the liver organoids. Although no significant differences were observed between perfused constructs and static controls, the expression of *ALB*, *MRP2* and *CYP3A4* showed increased expression in the perfused constructs compared to static controls (Figure 3). Inclusion of more organoid donors is needed to be able to study significance of the effect.

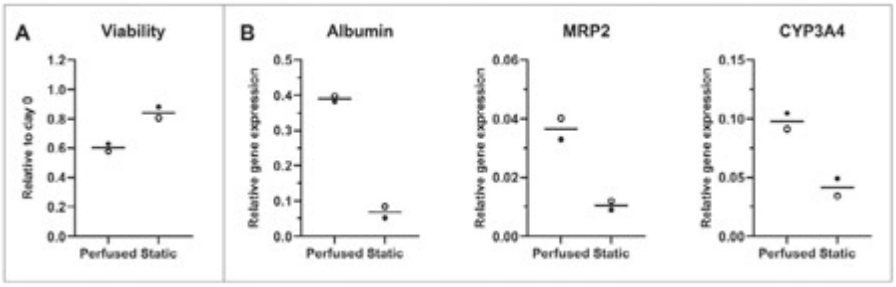

Figure 3. Viability and gene expression levels of liver organoids in bioprinted constructs in perfused and static condition. Constructs were kept in culture for 7 days. A) Metabolic activity of liver organoids, as a measure for cell viability, at day 7 relative to day 0. C) Gene expression levels of liver organoids at day 7. Relative gene expression was calculation using the reference genes *RPS5* and *RPL13A* (ΔCt). MRP2, Multi Resistance Protein 2; CYP3A4, Cytochrome P450 3A4. Each dot per condition (perfused/static) represents a technical duplicate (closed dot) or triplicate (open dot) of an organoid donor.

DISCUSSION

Bioengineering advances are bridging the gap between *in vitro* systems and the *in vivo* situation by incorporating features such as organ's architectural characteristics, cellular patterning and fluidics. Here, we describe a tailor-made bioreactor system for (volumetric) bioprinted hepatic constructs to guide towards a standardized perfused system. Additionally, the effect of flow perfusion on viability and hepatic differentiation of liver organoids was shown. Liver organoids are a valuable hepatic model in disease modelling and for regenerative medicine purposes [27,47]. A more advanced *in vitro* culture system can improve the hepatic functionality of liver organoids and thereby open new possibilities to their application in disease modelling and regenerative medicine.

The bioreactor system was tailor-made for the previous reported bioprinted hepatic constructs [43]. This bioreactor can be considered a macro-scaled system which is convenient for signal sensitivity [45,48-52]. Such model is rather high-content than high-throughput, which is not feasible due to its size and the required high cell numbers. High-content screenings are usually non-targeted and focused on gaining biological knowledge, e.g., to unravel disease mechanisms. The opaque characteristics of the bottom half of the bioreactor, made from PEEK, hamper accurate monitoring of the construct and for example live imaging readouts which could be considered a limitation. Though the polycarbonate lid accommodated the observation of the construct, the advantage of PEEK is the ability to reuse it continuously after autoclaving

it and, more importantly, its inert nature [53,54]. This is different from, for example, the often used PDMS which is known to bind chemicals depending on their physicochemical properties. PDMS is highly flexible in design [55-57], while the PEEK bioreactor in this study is milled and recent 3D printing approaches are described [58,59]. Suggestions for technical optimizations include reducing medium volume in the system to increase the medium-cell ratio and improve signal sensitivity, and/or automated control over medium parameters, such as a pressure sensor right before the chamber [60-62].

Current flow speed was based on literature [17,32-34,44-46], however the optimal flow speed for this bioreactor system in combination with the bioprinted liver organoids needs to be determined. Moreover, fluidic modeling can give more insight in flow behavior inside the bioreactor and if the shear stress that cells experience cells is in an *in vivo*-relevant range (0.1 – 0.5 dyne/cm^2) [34,44,63]. A trend was observed in the gene expression levels of albumin, CYP3A4 and MRP2 in perfused constructs compared to static controls, however this needs to be confirmed by using multiple organoid donors to determine the effect of media flow and establish the optimal flow speed. The continuous flow in the current system enables controlled medium flow and gradient formation, which is not possible in gravity driven devices [35]. In the liver sinusoids, an oxygen gradient exists which contributes to the zonal orientation of cells [64,65]. This is of interest for the liver organoids as their current (static) zonal orientation is indistinct [66] and it determines expression of specific hepatic features, e.g., higher CYP expression in pericentral area of the liver [67,68]. Additionally, the system allows for modular expansion of the number of bioreactors which can reduce inter-experimental variations and improve statistical power as more samples can be included. More complete characterization of the bioreactor system will lead to improved standardization and thereby greater experimental reproducibility and more precise comparison.

Alongside practical steps of improvement, further recapitulation of the *in vivo* liver architecture could be implemented and thereby improve hepatic maturation of the cells *in vitro* [69-71]. Approaches range from a graded microenvironment to mimic hepatic zonation [52,72-77], incorporation of cellular interaction of hepatocyte(-like cell)s with non-parenchymal liver cells [10,78-80] or vascularization [16,79,81]. This chamber can serve as maturation chamber for bioengineered hepatic *in vitro* constructs in order to mature towards tissue analogs for transplantation purposes [82-84] or in-depth mechanistic studies, e.g., high-content screenings to unravel disease mechanisms [63,85,86].

CONCLUSIONS

In this study, we developed a tailor-made bioreactor for previous described bioprinted hepatic constructs to allow for perfusion in a unidirectional flow. Preliminary data suggested increased expression of hepatic markers, however further technical and biological adjustments need to be explored and applied to determine the optimal culture setup and the effect of flow on hepatic function of the ICOs. This proof-of-concept study is paving the way towards a more complex *in vitro* model combining liver organoids and biofabrication with a potential in regenerative medicine and tissue engineering.

AUTHOR CONTRIBUTIONS

Conceptualization: MB, BS. Methodology: MB, DW. Experimental work: MB, TW, YT, NH, PNB. Data analysis: MB, YT, NH. Writing original draft: MB. Review and editing: TW, YT, NH, PNB, DW, RL, BS.

ACKNOWLEDGEMENTS

Figure 1 is created with draw.io.

SUPPLEMENTAL EXPERIMENTAL PROCEDURES

Cell culture

Intrahepatic cholangiocyte organoids (ICOs) were isolated from healthy liver biopsies, which were obtained during liver transplantation at the Erasmus Medical Center Rotterdam in accordance with the ethical standard of the institutional committee to use the tissue for research purposes (ethical approval number MEC 2014-060). The procedure was in accordance with the Helsinki Declaration of 1975 and informed consent in writing was obtained from each patient. Obtained human liver material was frozen down in Recovery Cell Freezing Medium for future experiments or used for organoid isolation directly. Organoid isolation is previously described [87].

Obtained cells were cultured in Matrigel™ (Matrigel; Corning, New York, NY, USA) until intrahepatic cholangiocyte organoids (ICOs) formed as previously described [30]. Cells received expansion medium (EM) consisting of Advanced DMEM/F12 (Life Technologies, Carlsbad, CA, USA) supplemented with 1% (v/v) penicillin-streptomycin (Life Technologies), 1% (v/v) GlutaMax (Life Technologies), 10 mM HEPES (Life Technologies), 2% (v/v) B27 supplement without vitamin A (Invitrogen, Carlsbad, CA, USA), 1% (v/v) N2 supplement (Invitrogen), 10 mM nicotinamide (Sigma-Aldrich, St Louis, MO, USA), 1.25 mM

N-acetylcysteine (Sigma-Aldrich), 2% (v/v) recombinant human R-spondin-3 (Qkine, Cambridge, UK), 10 µM forskolin (Sigma-Aldrich), 5 µM A83-01 (Tocris Bioscience, Bristol, UK), 50 ng/mL EGF (Invitrogen), 25 ng/mL HGF (Peprotech, Rocky Hill, NJ, USA), 0.1 µg/mL FGF10 (Peprotech), and 10 nM recombinant human (Leu15)-Gastrin I (Sigma-Aldrich). Media was refreshed twice a week and ICOs were passaged every 7 to 10 days at ratios ranging from 1:2 to 1:4. Cells were stored in a humidified atmosphere of 5% CO_2 at 37 °C.

For large scale production of organoids prior to the bioprinting procedure, ICOs were expanded in disposable spinner flasks (Corning) as previously described [87]. In short, spinner flasks were inoculated with 100,000 cells/mL EM containing 5% (v/v) Matrigel and were placed on a magnetic stir-plate with a rotation speed of 85 rpm. After 20 days of expansion with media addition every 2 to 3 days, ICOs were collected prior to the bioprinting procedure. To determine cell amounts, an aliquot of ICOs was mechanically and enzymatically (with TrypLE Express Enzyme; Life Technologies) disassociated into single cells and counted using the automatic Corning Cell counter (CytoSMART, Skillman, NJ, USA).

Bioprinted ICOs were hepatic differentiated, hereafter called liver organoids. Hepatic differentiation media (DM) consisted of EM without R-spondin-3, FGF10, and nicotinamide, and was supplemented with 100 ng/mL FGF19 (Peprotech), 500 nM A83-01 (Tocris Bioscience), 10 µM DAPT (Selleckchem, Munich, Germany), 25 ng/mL BMP-7 (Peprotech, and 30 µM dexamethasone (Sigma-Aldrich).

Cell viability

As a measure for cell viability, metabolic activity was measured using the resazurin-based AlamarBlue Cell Viability Reagent (Invitrogen). Resazurin is a non-toxic compound which function as a cell health-indicator. Briefly, the AlamarBlue Cell Viability Reagent was diluted 1:10 in Advanced DMEM/F12 without phenol red (Life Technologies), and cells were incubated for two to four hours at 37 °C. Absorbance was measured after incubation at ex/em 544/570 nm using a spectrophotometer.

Gene expression analysis

All materials used for RNA isolation were obtained from Qiagen (Hilden, Germany). For ICOs cultured in Matrigel droplets, RNeasy lysis buffer was added directly to the well. RNA isolation of these samples was performed using the RNeasy micro kit according to the manufacturer's instructions. Prior to RNA isolation of bioprinted constructs, constructs were disrupted using QIAshredder columns. RNA isolation was continued using the RNeasy mini kit according to

the manufacturer's instructions. RNA concentration were determined using the DS-11 spectrophotometer (DeNovix, Wilmington, DE, USA). cDNA synthesis was performed using the iScript cDNA synthesis kit (Bio-Rad, Veenendaal, the Netherlands). Relative gene expression of genes of interests were measured using RT-qPCR in a CFX-384 (Bio-Rad). Details of primers can be found in Table S1.

Table S1. Primer details

Gene	Forward primer	Reverse primer
RPS5	TGCAGGATTACATTGCAGTG	CATCATGGAGTTAGTGAGGC
RPL13A	GTGAAGGCATCAACATTTCTG	GATAGGCAAACTTTCTTGTAGG
MRP2	GCCAACTTGTGGCTGTGATAGG	ATCCAGGACTGCTGTGGGACAT
CYP3A4	TTTTGTCCTACCATAAGGGCTTT	CACAGGCTGTTGACCATCAT
ALB	GTTCGTTACACCAAGAAAGTACC	GACCACGGATAGATAGTCTTCTG

REFERENCES

[1] Cacciamali, A.; Villa, R.; Dotti, S. 3D Cell Cultures: Evolution of an Ancient Tool for New Applications. Front. Physiol. **2022**, *13*, 836480.

[2] Milner, E.; Ainsworth, M.; McDonough, M.; Stevens, B.; Buehrer, J.; Delzell, R.; Wilson, C.; Barnhill, J. Emerging Three-Dimensional Hepatic Models in Relation to Traditional Two-Dimensional in Vitro Assays for Evaluating Drug Metabolism and Hepatoxicity. Medicine in Drug Discovery **2020**, *8*, 100060.

[3] Jensen, C.; Teng, Y. Is it Time to Start Transitioning from 2D to 3D Cell Culture? Front. Mol. Biosci. **2020**, *7*, 33.

[4] Xie, Y.; Yao, J.; Jin, W.; Ren, L.; Li, X. Induction and Maturation of Hepatocyte-Like Cells in Vitro: Focus on Technological Advances and Challenges. Front. Cell. Dev. Biol. **2021**, *9*, 765980.

[5] Yun, C.; Kim, S.H.; Jung, Y. Current Research Trends in the Application of in Vitro Three-Dimensional Models of Liver Cells. Pharmaceutics **2022**, *15*, 54.

[6] Leal, F.; Zeiringer, S.; Jeitler, R.; Costa, P.F.; Roblegg, E. A Comprehensive Overview of Advanced Dynamic in Vitro Intestinal and Hepatic Cell Culture Models. Tissue Barriers **2023**, 2163820.

[7] Bassi, G.; Grimaudo, M.A.; Panseri, S.; Montesi, M. Advanced Multi-Dimensional Cellular Models as Emerging Reality to Reproduce in Vitro the Human Body Complexity. Int. J. Mol. Sci. **2021**, *22*, 1195.

[8] Guagliano, G.; Volpini, C.; Briatico-Vangosa, F.; Cornaglia, A.I.; Visai, L.; Petrini, P. Toward 3D-Bioprinted Models of the Liver to Boost Drug Development. Macromol. Biosci. **2022**, *22*, e2200264.

[9] Kang, H.K.; Sarsenova, M.; Kim, D.; Kim, M.S.; Lee, J.Y.; Sung, E.; Kook, M.G.; Kim, N.G.; Choi, S.W.; Ogay, V. *et al.* Establishing a 3D in Vitro Hepatic Model Mimicking Physiologically Relevant to in Vivo State. Cells **2021**, *10*, 1268. doi: 10.3390/cells10051268.

[10] Esch, M.B.; Prot, J.; Wang, Y.I.; Miller, P.; Llamas-Vidales, J.R.; Naughton, B.A.; Applegate, D.R.; Shuler, M.L. Multi-Cellular 3D Human Primary Liver Cell Culture Elevates Metabolic Activity Under Fluidic Flow. Lab. Chip **2015**, *15*, 2269-2277.

[11] Jung, D.J.; Byeon, J.H.; Jeong, G.S. Flow Enhances Phenotypic and Maturation of Adult Rat Liver Organoids. Biofabrication **2020**, *12*, 045035-5090/abb538.

[12] Starokozhko, V.; Hemmingsen, M.; Larsen, L.; Mohanty, S.; Merema, M.; Pimentel, R.C.; Wolff, A.; Emnéus, J.; Aspegren, A.; Groothuis, G. *et al.* Differentiation of Human-Induced Pluripotent Stem Cell Under Flow Conditions to Mature Hepatocytes for Liver Tissue Engineering. J. Tissue Eng. Regen. Med. **2018**, *12*, 1273-1284.

[13] Tao, T.; Wang, Y.; Chen, W.; Li, Z.; Su, W.; Guo, Y.; Deng, P.; Qin, J. Engineering Human Islet Organoids from iPSCs using an Organ-on-Chip Platform. Lab. Chip **2019**, *19*, 948-958.

[14] Cho, A.; Jin, Y.; An, Y.; Kim, J.; Choi, Y.S.; Lee, J.S.; Kim, J.; Choi, W.; Koo, D.; Yu, W. *et al.* Microfluidic Device with Brain Extracellular Matrix Promotes Structural and Functional Maturation of Human Brain Organoids. Nat. Commun. **2021**, *12*, 4730-5.

[15] Homan, K.A.; Gupta, N.; Kroll, K.T.; Kolesky, D.B.; Skylar-Scott, M.; Miyoshi, T.; Mau, D.; Valerius, M.T.; Ferrante, T.; Bonventre, J.V. *et al.* Flow-Enhanced Vascularization and Maturation of Kidney Organoids in Vitro. Nat. Methods **2019**, *16*, 255-262.

[16] Dellaquila, A.; Le Bao, C.; Letourneur, D.; Simon-Yarza, T. In Vitro Strategies to Vascularize 3D Physiologically Relevant Models. Adv. Sci. (Weinh) **2021**, *8*, e2100798.
[17] Kehtari, M.; Zeynali, B.; Soleimani, M.; Kabiri, M.; Seyedjafari, E. Fabrication of a Co-Culture Micro-Bioreactor Device for Efficient Hepatic Differentiation of Human Induced Pluripotent Stem Cells (hiPSCs). Artif. Cells Nanomed Biotechnol. **2018**, *46*, 161-170.
[18] Wikswo, J.P. The Relevance and Potential Roles of Microphysiological Systems in Biology and Medicine. Exp. Biol. Med. (Maywood) **2014**, *239*, 1061-1072.
[19] Azizgolshani, H.; Coppeta, J.R.; Vedula, E.M.; Marr, E.E.; Cain, B.P.; Luu, R.J.; Lech, M.P.; Kann, S.H.; Mulhern, T.J.; Tandon, V. *et al.* High-Throughput Organ-on-Chip Platform with Integrated Programmable Fluid Flow and Real-Time Sensing for Complex Tissue Models in Drug Development Workflows. Lab. Chip **2021**, *21*, 1454-1474.
[20] Bircsak, K.M.; DeBiasio, R.; Miedel, M.; Alsebahi, A.; Reddinger, R.; Saleh, A.; Shun, T.; Vernetti, L.A.; Gough, A. A 3D Microfluidic Liver Model for High Throughput Compound Toxicity Screening in the OrganoPlate®. Toxicology **2021**, *450*, 152667.
[21] Hoyle, H.W.; Stenger, C.M.L.; Przyborski, S.A. Design Considerations of Benchtop Fluid Flow Bioreactors for Bio-Engineered Tissue Equivalents in Vitro. Biomater. Biosyst **2022**, *8*, 100063.
[22] Monteduro, A.G.; Rizzato, S.; Caragnano, G.; Trapani, A.; Giannelli, G.; Maruccio, G. Organs-on-Chips Technologies - A Guide from Disease Models to Opportunities for Drug Development. Biosens. Bioelectron. **2023**, *231*, 115271.
[23] Dalsbecker, P.; Beck Adiels, C.; Goksör, M. Liver-on-a-Chip Devices: The Pros and Cons of Complexity. Am. J. Physiol. Gastrointest. Liver Physiol. **2022**, *323*, G188-G204.
[24] Pieters, V.M.; Co, I.L.; Wu, N.C.; McGuigan, A.P. Applications of Omics Technologies for Three-Dimensional in Vitro Disease Models. Tissue Eng. Part C. Methods **2021**, *27*, 183-199.
[25] Bouwmeester, M.C.; Bernal, P.N.; Oosterhoff, L.A.; van Wolferen, M.E.; Lehmann, V.; Vermaas, M.; Buchholz, M.; Peiffer, Q.C.; Malda, J.; van der Laan, L.J.W. *et al.* Bioprinting of Human Liver-Derived Epithelial Organoids for Toxicity Studies. Macromol. Biosci. **2021**, *21*, e2100327.
[26] Bernal, P.N.; Bouwmeester, M.; Madrid-Wolff, J.; Falandt, M.; Florczak, S.; Rodriguez, N.G.; Li, Y.; Größbacher, G.; Samsom, R.; van Wolferen, M. *et al.* Volumetric Bioprinting of Organoids and Optically Tuned Hydrogels to Build Liver-Like Metabolic Biofactories. Adv Mater **2022**, *34*, e2110054.
[27] Prior, N.; Inacio, P.; Huch, M. Liver Organoids: From Basic Research to Therapeutic Applications. Gut **2019**, *68*, 2228-2237.
[28] Nuciforo, S.; Heim, M.H. Organoids to Model Liver Disease. JHEP Rep. **2020**, *3*, 100198.
[29] Lancaster, M.A.; Huch, M. Disease Modelling in Human Organoids. Dis. Model. Mech. **2019**, *12*, dmm039347. doi: 10.1242/dmm.039347.
[30] Huch, M.; Gehart, H.; van Boxtel, R.; Hamer, K.; Blokzijl, F.; Verstegen, M.M.; Ellis, E.; van Wenum, M.; Fuchs, S.A.; de Ligt, J. *et al.* Long-Term Culture of Genome-Stable Bipotent Stem Cells from Adult Human Liver. Cell **2015**, *160*, 299-312.

[31] Takeishi, K.; Collin de l'Hortet, A.; Wang, Y.; Handa, K.; Guzman-Lepe, J.; Matsubara, K.; Morita, K.; Jang, S.; Haep, N.; Florentino, R.M. *et al.* Assembly and Function of a Bioengineered Human Liver for Transplantation Generated Solely from Induced Pluripotent Stem Cells. Cell. Rep. **2020**, *31*, 107711.

[32] Du, Y.; Li, N.; Yang, H.; Luo, C.; Gong, Y.; Tong, C.; Gao, Y.; Lü, S.; Long, M. Mimicking Liver Sinusoidal Structures and Functions using a 3D-Configured Microfluidic Chip. Lab. Chip **2017**, *17*, 782-794.

[33] Nishii, K.; Brodin, E.; Renshaw, T.; Weesner, R.; Moran, E.; Soker, S.; Sparks, J.L. Shear Stress Upregulates Regeneration-Related Immediate Early Genes in Liver Progenitors in 3D ECM-Like Microenvironments. J. Cell. Physiol. **2018**, *233*, 4272-4281.

[34] Rashidi, H.; Alhaque, S.; Szkolnicka, D.; Flint, O.; Hay, D.C. Fluid Shear Stress Modulation of Hepatocyte-Like Cell Function. Arch. Toxicol. **2016**, *90*, 1757-1761.

[35] Ehrlich, A.; Duche, D.; Ouedraogo, G.; Nahmias, Y. Challenges and Opportunities in the Design of Liver-on-Chip Microdevices. Annu. Rev. Biomed. Eng. **2019**, *21*, 219-239.

[36] Mueller, D.; Tascher, G.; Müller-Vieira, U.; Knobeloch, D.; Nuessler, A.K.; Zeilinger, K.; Heinzle, E.; Noor, F. In-Depth Physiological Characterization of Primary Human Hepatocytes in a 3D Hollow-Fiber Bioreactor. J. Tissue Eng. Regen. Med. **2011**, *5*, 207.

[37] Proença, S.; Escher, B.I.; Fischer, F.C.; Fisher, C.; Grégoire, S.; Hewitt, N.J.; Nicol, B.; Paini, A.; Kramer, N.I. Effective Exposure of Chemicals in in Vitro Cell Systems: A Review of Chemical Distribution Models. Toxicol. In. Vitro. **2021**, *73*, 105133.

[38] Dimitrijevic, D.; Fabian, E.; Nicol, B.; Funk-Weyer, D.; Landsiedel, R. Toward Realistic Dosimetry in Vitro: Determining Effective Concentrations of Test Substances in Cell Culture and their Prediction by an in Silico Mass Balance Model. Chem. Res. Toxicol. **2022**.

[39] Lauschke, V.M.; Shafagh, R.Z.; Hendriks, D.F.G.; Sundberg, M.I. 3D Primary Hepatocyte Culture Systems for Analyses of Liver Diseases , Drug Metabolism , and Toxicity : Emerging Culture Paradigms and Applications. Biotechnology Journal **2019**, *14*, 1-12.

[40] Yadav, J.; El Hassani, M.; Sodhi, J.; Lauschke, V.M.; Hartman, J.H.; Russell, L.E. Recent Developments in in Vitro and in Vivo Models for Improved Translation of Preclinical Pharmacokinetics and Pharmacodynamics Data. Drug Metab. Rev. **2021**, *53*, 207-233.

[41] Ribeiro, A.J.S.; Yang, X.; Patel, V.; Madabushi, R.; Strauss, D.G. Liver Microphysiological Systems for Predicting and Evaluating Drug Effects. Clin. Pharmacol. Ther. **2019**, *106*, 139-147.

[42] Melchels, F.P.W.; Blokzijl, M.M.; Levato, R.; Peiffer, Q.C.; de Ruijter, M.; Hennink, W.E.; Vermonden, T.; Malda, J. Hydrogel-Based Reinforcement of 3D Bioprinted Constructs. Biofabrication **2016**, *8*, 035004-5090/8/3/035004.

[43] Bernal, P.N.; Delrot, P.; Loterie, D.; Li, Y.; Malda, J.; Moser, C.; Levato, R. Volumetric Bioprinting of Complex Living-Tissue Constructs within Seconds. Adv Mater **2019**, *31*, e1904209.

[44] Schepers, A.; Li, C.; Chhabra, A.; Seney, B.T.; Bhatia, S. Engineering a Perfusable 3D Human Liver Platform from iPS Cells. Lab. Chip **2016**, *16*, 2644-2653.

[45] Sphabmixay, P.; Raredon, M.S.B.; Wang, A.J.; Lee, H.; Hammond, P.T.; Fang, N.X.; Griffith, L.G. High Resolution Stereolithography Fabrication of Perfusable Scaffolds to Enable Long-Term Meso-Scale Hepatic Culture for Disease Modeling. Biofabrication **2021**, *13*, 10.1088/1758-5090/ac23aa.

[46] Domansky, K.; Inman, W.; Serdy, J.; Dash, A.; Lim, M.H.M.; Griffith, L.G. Perfused Multiwell Plate for 3D Liver Tissue Engineering. Lab. Chip **2010**, *10*, 51-58.
[47] He, C.; Lu, D.; Lin, Z.; Chen, H.; Li, H.; Yang, X.; Yang, M.; Wang, K.; Wei, X.; Zheng, S. *et al.* Liver Organoids, Novel and Promising Modalities for Exploring and Repairing Liver Injury. Stem Cell. Rev. Rep. **2022**, 1-13.
[48] Liu, J.; Li, C.; Cheng, S.; Ya, S.; Gao, D.; Ding, W. Large-Scale High-Density Culture of Hepatocytes in a Liver Microsystem with Mimicked Sinusoid Blood Flow. J. Tissue Eng. Regen. Med. **2018**, *12*, 2266-2276.
[49] Xie, M.; Sun, Y.; Wang, J.; Fu, Z.; Pan, L.; Chen, Z.; Fu, J.; He, Y. Thermo-Sensitive Sacrificial Microsphere-Based Bioink for Centimeter-Scale Tissue with Angiogenesis. Int. J. Bioprint **2022**, *8*, 599.
[50] Grebenyuk, S.; Abdel Fattah, A.R.; Kumar, M.; Toprakhisar, B.; Rustandi, G.; Vananroye, A.; Salmon, I.; Verfaillie, C.; Grillo, M.; Ranga, A. Large-Scale Perfused Tissues Via Synthetic 3D Soft Microfluidics. Nat. Commun. **2023**, *14*, 193-1.
[51] Banaeiyan, A.A.; Theobald, J.; Paukštyte, J.; Wölfl, S.; Adiels, C.B.; Goksör, M. Design and Fabrication of a Scalable Liver-Lobule-on-a-Chip Microphysiological Platform. Biofabrication **2017**, *9*, 015014-5090/9/1/015014.
[52] Wesseler, M.F.; Taebnia, N.; Harrison, S.; Youhanna, S.; Preiss, L.C.; Kemas, A.M.; Vegvari, A.; Mokry, J.; Sullivan, G.J.; Lauschke, V.M. *et al.* 3D Microperfusion of Mesoscale Human Microphysiological Liver Models Improves Functionality and Recapitulates Hepatic Zonation. Acta Biomater. **2023**.
[53] Briem, D.; Strametz, S.; Schröder, K.; Meenen, N.M.; Lehmann, W.; Linhart, W.; Ohl, A.; Rueger, J.M. Response of Primary Fibroblasts and Osteoblasts to Plasma Treated Polyetheretherketone (PEEK) Surfaces. J. Mater. Sci. Mater. Med. **2005**, *16*, 671-677.
[54] Noiset, O.; Schneider, Y.J.; Marchand-Brynaert, J. Adhesion and Growth of CaCo2 Cells on Surface-Modified PEEK Substrata. J. Biomater. Sci. Polym. Ed. **2000**, *11*, 767-786.
[55] Cao, U.M.N.; Zhang, Y.; Chen, J.; Sayson, D.; Pillai, S.; Tran, S.D. Microfluidic Organ-on-A-Chip: A Guide to Biomaterial Choice and Fabrication. Int. J. Mol. Sci. **2023**, *24*, 3232. doi: 10.3390/ijms24043232.
[56] Zhou, J.; Ellis, A.V.; Voelcker, N.H. Recent Developments in PDMS Surface Modification for Microfluidic Devices. Electrophoresis **2010**, *31*, 2-16.
[57] Abbasi, F.; Mirzadeh, H.; Katbab, A. Modification of Polysiloxane Polymers for Biomedical Applications: A Review. Polym. Int. **2023**, *50*, 1279-1287.
[58] Arif, M.F.; Kumar, S.; Varadarajan, K.M.; Cantwell, W.J. Performance of Biocompatible PEEK Processed by Fused Deposition Additive Manufacturing. Mater Des **2018**, *146*, 249-259.
[59] Xie, M.; Sun, Y.; Wang, J.; Fu, Z.; Pan, L.; Chen, Z.; Fu, J.; He, Y. Thermo-Sensitive Sacrificial Microsphere-Based Bioink for Centimeter-Scale Tissue with Angiogenesis. Int. J. Bioprint **2022**, *8*, 599.
[60] Mou, L.; Mandal, K.; Mecwan, M.M.; Hernandez, A.L.; Maity, S.; Sharma, S.; Herculano, R.D.; Kawakita, S.; Jucaud, V.; Dokmeci, M.R. *et al.* Integrated Biosensors for Monitoring Microphysiological Systems. Lab. Chip **2022**, *22*, 3801-3816.
[61] Sung, J.H.; Shuler, M.L. Prevention of Air Bubble Formation in a Microfluidic Perfusion Cell Culture System using a Microscale Bubble Trap. Biomed. Microdevices **2009**, *11*, 731-738.

[62] Gharib, G.; Bütün, İ; Muganlı, Z.; Kozalak, G.; Namlı, İ; Sarraf, S.S.; Ahmadi, V.E.; Toyran, E.; van Wijnen, A.J.; Koşar, A. Biomedical Applications of Microfluidic Devices: A Review. Biosensors (Basel) **2022**, *12*, 1023. doi: 10.3390/bios12111023.
[63] Kammerer, S. Three-Dimensional Liver Culture Systems to Maintain Primary Hepatic Properties for Toxicological Analysis in Vitro. Int. J. Mol. Sci. **2021**, *22*, 10214.
[64] Jungermann, K.; Kietzmann, T. Oxygen: Modulator of Metabolic Zonation and Disease of the Liver. Hepatology **2000**, *31*, 255-260.
[65] Cunningham, R.P.; Porat-Shliom, N. Liver Zonation - Revisiting Old Questions with New Technologies. Front. Physiol. **2021**, *12*, 732929.
[66] Ardisasmita, A.I.; Schene, I.F.; Joore, I.P.; Kok, G.; Hendriks, D.; Artegiani, B.; Mokry, M.; Nieuwenhuis, E.E.S.; Fuchs, S.A. A Comprehensive Transcriptomic Comparison of Hepatocyte Model Systems Improves Selection of Models for Experimental Use. Commun. Biol. **2022**, *5*, 1094-9.
[67] Allen, J.W.; Khetani, S.R.; Bhatia, S.N. In Vitro Zonation and Toxicity in a Hepatocyte Bioreactor. Toxicological Sciences **2005**, *84*, 110-119.
[68] Kietzmann, T. Metabolic Zonation of the Liver: The Oxygen Gradient Revisited. Redox Biol. **2017**, *11*, 622-630.
[69] Paradiso, A.; Volpi, M.; Rinoldi, C.; Celikkin, N.; Contessi Negrini, N.; Bilgen, M.; Dallera, G.; Pierini, F.; Costantini, M.; Święszkowski, W. *et al.* In Vitro Functional Models for Human Liver Diseases and Drug Screening: Beyond Animal Testing. Biomater. Sci. **2022**.
[70] Monckton, C.P.; Brown, G.E.; Khetani, S.R. Latest Impact of Engineered Human Liver Platforms on Drug Development. APL. Bioeng. **2021**, *5*, 031506.
[71] Chen, C.; Soto-Gutierrez, A.; Baptista, P.M.; Spee, B. Biotechnology Challenges to in Vitro Maturation of Hepatic Stem Cells. Gastroenterology **2018**, *154*, 1258-1272.
[72] Lee-Montiel, F.T.; George, S.M.; Gough, A.H.; Sharma, A.D.; Wu, J.; DeBiasio, R.; Vernetti, L.A.; Taylor, D.L. Control of Oxygen Tension Recapitulates Zone-Specific Functions in Human Liver Microphysiology Systems. Exp. Biol. Med. (Maywood) **2017**, *242*, 1617-1632.
[73] Matsumoto, S.; Safitri, A.R.; Danoy, M.; Maekawa, T.; Kinoshita, H.; Shinohara, M.; Sakai, Y.; Fujii, T.; Leclerc, E. Investigation of the Hepatic Respiration and Liver Zonation on Rat Hepatocytes using an Integrated Oxygen Biosensor in a Microscale Device. Biotechnol. Prog. **2019**, *35*, e2854.
[74] Kang, Y.B.A.; Eo, J.; Mert, S.; Yarmush, M.L.; Usta, O.B. Metabolic Patterning on a Chip: Towards in Vitro Liver Zonation of Primary Rat and Human Hepatocytes. Sci. Rep. **2018**, *8*, 8951-6.
[75] Tonon, F.; Giobbe, G.G.; Zambon, A.; Luni, C.; Gagliano, O.; Floreani, A.; Grassi, G.; Elvassore, N. In Vitro Metabolic Zonation through Oxygen Gradient on a Chip. Sci. Rep. **2019**, *9*, 13557-6.
[76] Ahn, J.; Ahn, J.; Yoon, S.; Nam, Y.S.; Son, M.; Oh, J. Human Three-Dimensional in Vitro Model of Hepatic Zonation to Predict Zonal Hepatotoxicity. **2019**, *5*, 1-15.
[77] Li, X.; George, S.M.; Vernetti, L.; Gough, A.H.; Taylor, D.L. A Glass-Based, Continuously Zonated and Vascularized Human Liver Acinus Microphysiological System (vLAMPS) Designed for Experimental Modeling of Diseases and ADME/TOX. Lab. Chip **2018**, *18*, 2614-2631.
[78] Choi, Y.Y.; Seok, J.; Kim, D. Flow-Based Three-Dimensional Co-Culture Model for Long-Term Hepatotoxicity Prediction. Micromachines (Basel) **2019**, *11*, 36. doi: 10.3390/mi11010036.

[79] Janani, G.; Priya, S.; Dey, S.; Mandal, B.B. Mimicking Native Liver Lobule Microarchitecture in Vitro with Parenchymal and Non-Parenchymal Cells using 3D Bioprinting for Drug Toxicity and Drug Screening Applications. ACS Appl. Mater. Interfaces **2022**, *14*, 10167-10186.

[80] Baze, A.; Parmentier, C.; Hendriks, D.F.G.; Hurrell, T.; Heyd, B.; Bachellier, P.; Schuster, C.; Ingelman-Sundberg, M.; Richert, L. Three-Dimensional Spheroid Primary Human Hepatocytes in Monoculture and Coculture with Nonparenchymal Cells. Tissue Eng. Part C. Methods **2018**, *24*, 534-545.

[81] Dame, K.; Ribeiro, A.J. Microengineered Systems with iPSC-Derived Cardiac and Hepatic Cells to Evaluate Drug Adverse Effects. Exp. Biol. Med. (Maywood) **2021**, *246*, 317-331.

[82] Kryou, C.; Leva, V.; Chatzipetrou, M.; Zergioti, I. Bioprinting for Liver Transplantation. Bioengineering (Basel) **2019**, *6*, 95.

[83] Ogoke, O.; Maloy, M.; Parashurama, N. The Science and Engineering of Stem Cell-Derived Organoids-Examples from Hepatic, Biliary, and Pancreatic Tissues. Biol. Rev. Camb. Philos. Soc. **2021**, *96*, 179-204.

[84] Antarianto, R.D.; Mahmood, A.; Giselvania, A.; Asri Dewi, A.A.P.; Gustinanda, J.; Pawitan, J.A. Inventing Engineered Organoids for End-Stage Liver Failure Patients. J. Mol. Histol. **2022**, *53*, 611-621.

[85] Serras, A.S.; Rodrigues, J.S.; Cipriano, M.; Rodrigues, A.V.; Oliveira, N.G.; Miranda, J.P. A Critical Perspective on 3D Liver Models for Drug Metabolism and Toxicology Studies. Front. Cell. Dev. Biol. **2021**, *9*, 626805.

[86] Kukla, D.A.; Khetani, S.R. Bioengineered Liver Models for Investigating Disease Pathogenesis and Regenerative Medicine. Semin. Liver Dis. **2021**, *41*, 368-392.

[87] Schneeberger, K.; Sánchez-Romero, N.; Ye, S.; van Steenbeek, F.G.; Oosterhoff, L.A.; Pla Palacin, I.; Chen, C.; van Wolferen, M.E.; van Tienderen, G.; Lieshout, R. *et al.* Large-Scale Production of LGR5-Positive Bipotential Human Liver Stem Cells. Hepatology **2020**, *72*, 257-270.

Summary and general discussion

6

The liver plays a crucial role in drug metabolism, and is therefore susceptible to drug induced injury. Drug induced liver injury (DILI) is a major cause for discontinuation of drug development and post-marketing drug withdrawal [1]. Traditionally, the safety of novel drugs is determined using animal models. Significant interspecies differences in the expression and function of drug metabolism enzymes and transporters, however, hamper the accurate prediction of hepatotoxicity potential and pharmacokinetics in patients [2,3]. A shift towards human cell-based models tackles the issue of interspecies differences, while at the same time replacing and reducing animal tests in safety evaluations [4,5]. In order to perform reliable hepatoxicity and pharmacokinetic prediction *in vitro*, hepatic models need to exhibit morphological and functional features similar to *in vivo*.

Intrahepatic cholangiocyte organoids (ICOs) are patient liver-derived adult stem cells which are cultured as self-organizing hollow 3D structures [6]. ICOs can be differentiated towards their cholangiocyte-like or hepatocyte-like lineage [6,7], where in this thesis the hepatic differentiated ICOs are used and are described as liver organoids hereafter. The goal of this thesis was to explore liver organoids as an alternative *in vitro* model for hepatotoxicity testing. As hepatic functionality can be promoted *in vitro* by providing *in vivo*-like micro-environmental cues [8], such as more complex architectural design or the application of dynamic culture, this thesis also aimed to improve the hepatic functionality of liver organoids by recapitulating the *in vivo* situation. To this end, the combination of biofabrication techniques, such as bioprinting and application of flow perfusion, with liver organoids was studied.

The research questions of this thesis are:

1. What is the potential of liver organoids as *in vitro* model for toxicity testing? (**Chapter 2**)
2. Can the hepatic functionality of liver organoids be improved by creating an *in vivo*-like culture environment using bioprinting techniques and flow perfusion? (**Chapter 3**, **4** and **5**)

The results, opportunities, challenges, and future perspectives of the studies included in this thesis are discussed in this chapter.

DRUG METABOLISM IN LIVER ORGANOIDS

The applicability of liver organoids as *in vitro* hepatotoxicity model to reflect the liver's function and mechanisms upon drug-induced Injury was examined in **Chapter 2**. Expression levels of genes involved in drug metabolism and hepatic

transporters in organoids (both in expansion and in hepatic differentiation conditions) were compared to liver, primary human hepatocytes (PHHs) and HepaRG cells. Gene expression levels of phase I enzymes, including major cytochrome P450 (CYP) enzymes CYP3A4, CYP2B6, CYP2C9 and CYP2D6, improved upon differentiation. However, although expression levels of some CYP enzymes, like CYP3A4 and CYP2C9, were comparable to HepaRGs, expression levels were still lower compared to PHHs. Additionally, CYP and UGT activity was examined by measuring metabolite formation of enzyme specific substrates. The observed CYP3A4 activity, the CYP enzyme responsible for metabolism of most therapeutic categories [9,10], in liver organoids seemed donor-dependent and showed comparable activity to PHHs for one donor. Gene expression levels of phase II enzymes in liver organoids also improved upon differentiation, and exceeded expression levels of PHHs for some genes involved in phase II metabolism (e.g., UGT2B11, UGT2B15, SULT1C2 and SULT1B1). UGT activity data showed complete depletion of the UGT substrate, however only partial formation of the measured metabolite was observed, which suggests formation of alternative metabolites. Together with relative high expression levels of certain phase II enzymes, these observations suggest that liver organoids express a different composition of enzymes in phase II metabolism compared to PHHs and HepaRGs. This is important because reactive metabolites formed in phase I metabolism are usually counteracted by phase II metabolism [11]. Further characterization of phase II drug metabolism in liver organoids, for instance using a phase II specific substrate cocktail, can give insights in liver organoids' phase II activity [12,13]. Although gene expression levels and enzyme activity represented interdonor differences, expanding the donor set is needed to be able to confirm and quantify interdonor variations. Additional (genotypic) profiling of the organoids could provide insight in interindividual differences in drug response [14-17].

SENSITIVITY OF LIVER ORGANOIDS TO HEPATOTOXICANTS

The applicability of liver organoids as an *in vitro* hepatotoxicity model was further explored by testing their sensitivity to five well-known hepatotoxicants (i.e., acetaminophen, diclofenac, perhexiline, troglitazone and valproic acid) in **Chapter 2**. The median effect concentrations (EC50s) for diclofenac, perhexiline, and troglitazone were comparable between liver organoids, PHHs and HepaRGs. EC50s for valproic acid were comparable between liver organoids and PHHs, however lower compared to HepaRGs. The determined EC50s in liver organoids for acetaminophen were five-fold higher than those in PHHs and HepaRGs, which may be explained by differences in media composition between the hepatic models and/or higher activity of alternative metabolism pathways in liver organoids, as mentioned before. More specifically,

alternative phase II metabolism can lead to increased formation of glucuronide and sulfate metabolites instead of the toxic metabolite NAPQI [18,19]. The cytotoxic potency of acetaminophen to extrusion-based bioprinted liver organoids (studied in **Chapter 3**) was less compared to liver organoids cultured under standard conditions, which may in part be explained by the retention of acetaminophen by the hydrogel reducing the concentration available to cause toxicity in cells [20] and/or the use of different organoid donors in **Chapters 2** and **3**. The comparison of sensitivity to hepatotoxicants between different hepatic cell models can be improved by determining the cell associated or intracellular concentration that is available to be taken up by the cells in the system [20-23]. To further illustrate the potential of liver organoids in toxicity testing *in vitro*, future studies should include a more extended compound set and biomarkers of hepatotoxicity (e.g., lipid accumulation) to characterize the applicability domain of liver organoids [24]. The compounds tested in **Chapter 2** induce hepatotoxicity via various mechanisms and exposure to subtoxic concentrations could provide insight in the liver organoids' potential to reveal the different mechanisms of hepatotoxicity. Although the expression levels of certain genes involved in specific hepatotoxicity pathways, such as bile salt export pump important in the onset of cholestasis, show relatively low expression in liver organoids, further optimization of microenvironmental cues, e.g., medium composition, could lead to improved hepatic functionality.

INCREASING CULTURE COMPLEXITY USING BIOENGINEERING TECHNIQUES

Improving hepatic maturation of cells *in vitro* can be accomplished by increasing the *in vivo*-like culture environment [8]. In **Chapter 3** and **4**, two different bioprinting techniques were applied to the organoid culture in order to create constructs with a more complex architecture.

Volumetric and extrusion-based bioprinting

Extrusion-based bioprinting (EBB) is a well-established technique, whereas volumetric bioprinting (VBP) was only recently established [25]. In both techniques, liver organoids are mixed in a photo-crosslinkable gelatin-based hydrogel, gelMA, which forms a so-called bioink or bioresin. In the EBB technique, described in **Chapter 3**, this bioink is loaded into a printing cartridge, whereafter it is extruded via a needle in the desired position. The bioprinted construct is generated layer-by-layer which requires rapid polymerization kinetics to ensure construct stability, in addition, to the support provided by a second (sacrificial) hydrogel. VBP, described in **Chapter 4**, is a light-based technique in which a spinning container with the bioresin (hydrogel with cells) is illuminated with visible light from multiple angles using a sequence of filtered

back projections of the object to be printed. In this way, constructs with complex geometries of various sizes can be printed within seconds in a layerless fashion. The bioink formulation for VBP was optimized to be able to print with high shape fidelity in presence of cellular 3D structures in high cell concentrations. The precise positioning of the bioink by EBB allows for the preparation of the amount of bioink needed for a bioprinted construct, where for VBP, a relatively large volume of excess bioink is required. Consequently, larger amounts of organoids are needed for VBP prints and although organoid expansion in stirred bioreactors is an efficient method to generate large numbers of organoids [26], donor-dependent inconsistency, such as cell growth and/or mucus formation, makes the generation of large amounts of organoids challenging. In addition, exact quantification of cell numbers based on single cells is hindered by the cellular 3D structures which, in turn, could hamper the standardization of the technique [27].

The ability of controlled positioning by EBB allows for multi-material and/or -cellular constructs in a specific composition [28], where VBP is currently based on generating a construct containing a single bioresin. Implementation of multi-materials enables bioprinting multiple cell types in distinct design and location and thereby more *in vivo*-like structures can be created. The bioprinting field and the field of hydrogels are rapidly emerging [29-31], so novel (adaptations of) bioprinting techniques will likely be developed by the time this thesis is printed, such as the ability to volumetrically bioprint with dual bioresins or to rapidly replace hydrogels during printing.

Post-printing viability and functionality

Bioprinting techniques offer the opportunity to create structures recapitulating the complex liver architecture and/or enabling vascularization, which have been described to improve hepatic functionality [8,32]. The combination of these techniques with organoid culture is challenging due to their (hollow) 3D cellular structure, which could increase the incidence of nozzle clogging in the case of EBB or light scattering in VBP. Viability and hepatic functionality of the extrusion-based and volumetrically bioprinted liver organoids was examined after 10 days of hepatic differentiation and compared to liver organoids in conventional Matrigel™ (Matrigel) culture and cast (non-printed) controls. Cellular viability was restored in all conditions. However, the volumetric bioprinted liver organoids showed superior viability compared to the other conditions (EBB, Matrigel, cast controls). Hepatic functionality was examined by gene expression levels of hepatic markers, which were stable after the bioprinting procedures compared to non-printed controls. Additionally, protein expression of hepatic markers (i.e., HNF4α, MDR1, and albumin) in bioprinted liver organoids was examined as readout for hepatic functionality, and showed the presence of

these hepatic markers for both bioprinting techniques. Volumetric bioprinted organoids showed most prominent polarization of liver organoids by the apical expression of hepatic transporter MDR1, which can be explained by the nozzle/pipette tip-free generation of the constructs and therefore avoiding organoid structure disruption. Signal quantification of MDR1 expression is needed to identify if there is a significant difference and additional export studies should show actual activity of the transporters [7,33]. Taken together, liver organoids retained viability and functionality post-printing for both techniques. This opens ways to create structures with complex designs and specific cellular positioning which can further improve hepatic functionality of our liver organoids.

Dynamic culture of bioprinted structures

Next to the architectural structures that can be provided by bioprinting innovations, application of dynamic culture has been described to improve hepatic maturation [34-38]. In **Chapter 4**, three different volumetric bioprinted lattices showed different flow trajectory and flow speed of microspheres. Based on this data, the two structures with most distinct flow profile were perfused for 24h in a home-made bioreactor. Liver organoids in the perfused constructs were tested on their hepatic functionality by measurement of hepatic key features, such as albumin secretion and ammonia elimination. Although albumin secretion was comparable between both structure types and between dynamic and static conditions, a significant difference was observed in ammonia elimination between perfused conditions and the static control. Moreover, the ammonia elimination rate was significantly different between the two structure types, which emphasizes the importance of construct architecture and choice of design.

The architectural design showing highest ammonia elimination rate was selected for perfusion in the tailored-made bioreactor described in **Chapter 5**. The tailor-made polyether ether ketone (PEEK) bioreactor with polycarbonate lid consisted of screwable parts and o-rings, which enabled a proper sterilization process and ensured tight connections. The system design enabled automatic media refreshment and sample ports to take media samples, allowing minimal disturbance of the perfused culture. An air bubble trap was included to limit bubble formation inside the bioreactor, which potentially can lead to disintegration of the construct. As proof-of-concept, two organoid donors were volumetrically bioprinted and constructs were placed in the bioreactor chamber under submerged circumstances to prevent bubble formation and perfused for 7 days under hepatic differentiation conditions. Hepatic functionality of perfused liver organoids was studied by gene expression levels of hepatic markers albumin, CYP3A4 and hepatic transporter Multi Resistance Protein 2 (MRP2). Elevated gene expression levels of albumin, CYP3A4 and MRP2

were observed in liver organoids in perfused constructs compared to the static controls, although not statistically significant. Repeated experiments with multiple donors and an extended set of functional readouts, as well as exploration of different flow speeds, are needed to decidedly study the effect of flow on viability and hepatic maturation of liver organoids. Moreover, exploring viability and functionality of liver organoids cultured for a longer period of time will provide the basis for subtoxic and/or chronic exposure studies in the future [39]. Taken together, we developed a tailor-made perfused culture system with the potential to provide a standardized dynamic culture to bioengineered constructs within an *in vivo*-like environment.

FURTHER *IN VIVO* RECAPITULATION

Other advances to stimulate hepatic maturation *in vitro* by mimicking the hepatic *in vivo* environment include enhanced structural resemblance to the liver's architecture, incorporation of other cell types and micro-environmental cues to improve *in vitro* hepatic functionality (Figure 1) [40-42]. The liver's unique architecture is arranged into hexagonal spatial units, called lobules, and its vasculature system is essential for nutrient and gas exchange. Bioprinting enables the creation of cell-laden constructs that allow vascularization and thereby improve hepatic functionality [30,43,44]. The architectural designs of structures range from mathematical architectures, as applied to the work described in this thesis, to constructs with lobular structures that further mimics the liver's microphysiology [45-49]. *In vivo*, this unique organization generates a graded microenvironment enabling various metabolic functions to occur in localized zones of the lobule [50]. For example, urea synthesis predominantly occurs at the periportal area, while xenobiotic metabolism occurs predominantly in the pericentral area. Acetaminophen-induced liver injury is therefore located in the pericentral area, as well as the development of steatosis since enzymes involved in liver synthesis are also predominantly expression in this region [51]. The zonal orientation of liver organoids is yet indistinct [52], however by applying gradients of oxygen or other modulators, such as hormones and inducers, cells could be guided towards hepatic zonation *in vitro* [53-56].

Moreover, cellular interaction of hepatocyte(-like cell)s *in vitro* with non-parenchymal liver cells, such as stellate cells or Kupffer cells can further improve hepatic functionality of the culture [38,57,58]. Although *in vivo*-like expression and functionality of the liver is desired for the prediction of human safety, the presence of immune cells in hepatic *in vitro* systems is of particular interest due to their role in idiosyncratic DILI, or specifically immune-mediated DILI [59-61]. Specific multicellular disposition can be realized by the use of multi-material bioprinting which enables graded composition and properties [62,63].

Environmental cues are also key to support and promote hepatic functionality from stem cell derived hepatocytes [64]. These can be provided by the media composition, which is usually supplemented with growth factors and components to aid viability and the state of hepatic maturation [8], or extracellular matrix (ECM) surrounding hepatocyte(-like cell)s which *in vivo* provides biomechanical and biochemical cues required for hepatic functionality and homeostasis [65,66]. Hydrogels can supply these functions *in vitro*, e.g., by the use of naturally-derived (from plants or animals) materials, such as Matrigel, gelatin-based or decellularized materials, or by the use of synthetic biomaterials [31,67,68]. Although naturally-derived hydrogels have advantages over synthetic hydrogels in mimicking the *in vivo* ECM and binding affinity to cells, synthetic materials are chemically defined and are tunable to precisely control stiffness and/or cell-matrix interaction [67,69,70]. In the case of biofabrication advances, the selected hydrogel must meet several additional features (e.g., printability, shape stability, degradability, and biocompatibility) next to the biological criteria [62,63,71,72].

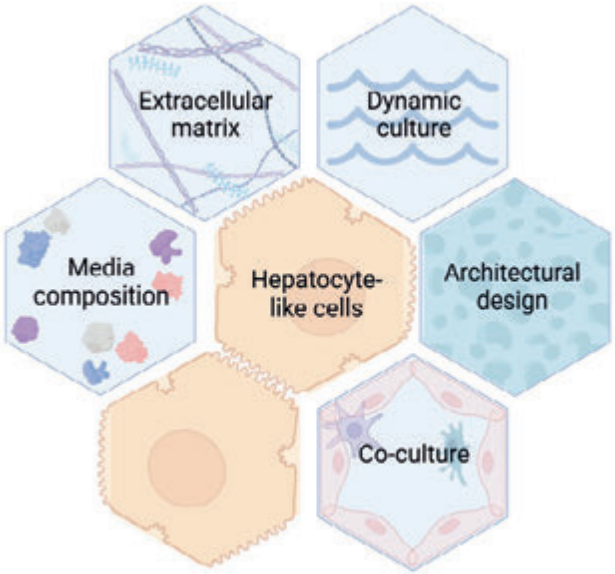

Figure 1. Approaches to create an *in vivo*-like liver environment in order to improve hepatic maturation *in vitro*.

HEPATIC CELL MODELS

Next to *in vivo*-like micro-environmental guidance and support, the choice of hepatocyte(-like cell)s is essential for the level of hepatic maturation that can

be reached *in vitro* [73]. Primary human hepatocytes (PHHs) are traditionally considered the gold standard in *in vitro* toxicity testing due to their hepatic functionality, yet several alternative hepatic models, such as hepatic cell lines, Upcyte hepatocytes, induced pluripotent stem-cell-derived hepatocytes (iPSC-Heps) and liver organoids, overcome the shortcomings of PHH culture (Table 1) [74]. Nowadays, 2D monolayer cultures are no longer considered standard culture conditions, as developed 3D culture methods (e.g., spheroids or hydrogel-enriched cultures) showed delayed dedifferentiation and/or improved hepatic maturation levels and are well-established [74-78]. Developments in novel hepatic culture methodologies are ongoing, resulting in, among others, primary human hepatocytes with reinforced proliferation capacity or adult-hepatocyte derived organoids (HepOrgs), which have been described for human fetal and adult mouse liver but are still under development for human adult liver [79-84]. The development of innovative culture methodologies requires proper characterization to learn about their advantages and limitations compared to existing models (including valid reference models). Although omics-based comparisons between different models are informative to identify the level of hepatic functionality or specific pathway activity [52,85-87], additional functional assays (with similar experimental set-up) can provide more thorough assessment and improved comparison of specific functions of the different models [88,89]. The knowledge gained on specific characteristics of the models can facilitate the choice of the appropriate hepatic cell model for specific applications [73,81], such as expression of specific pathways, life span for chronic exposure studies, or suitability for genetic manipulation. Another desired specification is the compatibility with high-throughput screenings. In fact, due to recent biotechnological advancements also more complex culture methods, such as spheroids, organoids and bioprinted models, are applicable in a high-throughput fashion [90-96].

Table 1. Main characteristics of human *in vitro* hepatic models: a qualitative assessment.

	PHHs*	HepG2*	HepaRG*	iPSCs-Heps*	Upcytes*	Liver organoids
Availability	+	+++	+++	++	++	++
Low costs	-	+++	+	-	+	-
Ease of use	++	+++	++[1]	+[1]	++	+[1]
Proliferation/Life span	-	+++	+++	+++	++[2]	++
Donor variation	++	-	-	+++	++	+++
Albumin synthesis	+++	+	++	+	+++	+
Urea production	+++	+	-	+	+++	+[3]
Glycogen storage	+++	+++	+++	+++	+++	ND[4]
Phase I enzymes	+++	-	++[5]	+	++	+
Phase II enzymes	+++	-	+++	+	++	+[6]

Adapted from Kammerer, 2021 [74]. [1] Differentiation procedure required; [2] Not immortalized; [3] Based on comparison described by Ardisasmita *et al.*, 2022 [52]; [4] Glycogen presence is not quantified compared to other models; [5] Poor metabolizer for CYP2D6; [6] Based on hydroxycoumarin metabolism only as described in Chapter 2. PHHs: Primary human hepatocytes; iPSC-heps: induced pluripotent stem-cell-derived hepatocytes; Upcytes: Upcyte hepatocytes; Liver organoids: Hepatic differentiated intrahepatic cholangiocyte organoids. Qualitative assessment: (-): absent; (+): low/poor; (++): intermediate/moderate; (+++): high/good; ND: Not enough data available. *in conventional 2D culture.

THE APPLICATION OF LIVER ORGANOIDS

In this thesis, the first characterization steps needed to assess the potential of liver organoids as *in vitro* toxicity model were performed (**Chapter 2**). Further elucidation of specific mechanisms, however, is needed, such as phase II metabolism or DILI pathways. A recent comparative transcriptomics study underlined that the current (general) hepatic maturation state of liver organoids needs improvement compared to PHHs, HepG2s and iPSC-Heps [52]. Previously mentioned advances in biofabrication and/or micro-environmental cues, like adjustments in media composition suggested in this comparative study [52], can more effectively guide the liver-derived liver organoids to their hepatic maturation state and thereby broaden their applicability as a model.

Although the hepatic phenotype of other hepatic cell models, at this point, is more *in vivo*-like than of liver organoids (Table 1), liver organoids do provide unique features, such as the polarized morphology of their hollow 3D structures which can be an opportunity for transporter (induction/inhibition) studies. Moreover, the donor-derived origin of liver organoids, and other stem-cell derived models such as iPSC-Heps, permits reflection the human population by providing interindividual phenotypic and genotypic variations [97]. Also in disease modelling this is of particular interest, as liver organoids have been shown to be a valuable model because they recapitulate features of human disease and capture patient heterogeneity [98-101]. In the case of idiosyncratic DILI, although patient-derived models can be valuable in its mechanistic understanding [102,103], data collection from patient cohorts to find biomarkers and/or (genetic) patterns together with sophisticated *in silico* or artificial intelligence approaches allow for new strategies to enhance iDILI evaluation [104,105]. Although iPSC-Heps and liver organoids both have a donor-derived origin, iPSC-Heps require the time-consuming procedure of transgenic reprogramming as they are derived from non-hepatic donor cells and require a minimum of six weeks to create [106], whereas for liver organoid establishment, an invasive procedure is needed to acquire primary liver tissue. In the case of personalized medicine, the need for a tissue biopsy or time of establishment of the model can be a criterion that guides the choice for a specific model. The combination of patient-derived cells with biofabrication advances, as described for liver organoids in **Chapter 3**, **4** and **5**, open ways to create tissue analogs *in vitro* to unravel disease phenotypes and mechanisms and potentially create transplantable constructs [107-109]. Additionally, the role of stem cell-derived models in personalized medicine is rising, although several challenges, including improved *in vitro* maturation, standardized procedures and biobanking of cells, must be overcome [100,110,111].

ALTERNATIVE MODELS TO ANIMAL TESTING

The worldwide movement away from the traditionally used animal testing in the preclinical phase [112-114] is emphasized by, among other initiatives, the EU's ban on animal testing for cosmetics and the adjustment of the US FDA Modernization Act ending the mandate to require animals in preclinical testing and thereby paving the way to the use of alternative models [115,116]. Alternative models to animal testing, such as *in silico* and modelling tools, omics approaches, and (advanced) *in vitro* assays, allow for a human-based safety assessment based on biological pathways or targets [117]. The mechanistic information generated by these so-called new approach methodologies (NAMs) can be mapped into adverse outcome pathways (AOPs) and AOP networks [118-120]. AOPs describe a sequential chain of causally linked events at different levels of biological organization that lead to an adverse health outcome. Tiered approaches are described to combine different assays and models to be able to provide the measures of changes to these key events within such described AOP [121,122], as no single *in vitro* model can assess human safety alone. A set of well-characterized *in vitro* models, next to other NAMs, with varying cell sources and culture complexity can be used in a multistep manner to study specific toxicity mechanisms, so-called integrated approaches to testing and assessment (IATA) [123]. Conventional 2D cultures could provide high-throughput lower tiered assays, where higher tiered approaches can include the previously described advanced culture technologies providing *in vitro* tissue analogs whether or not in multi-organ fashion [124]. The bioprinted liver organoids, as described in **Chapter 3** and **4**, pave the way towards such tissue analog model once culture complexity is increased, e.g., by co-culture with different cell types, and hepatic maturation is facilitated by a perfusion chamber as described in **Chapter 5**. The choice of (the grade of complexity of) an *in vitro* model is guided by the question which it aims to answer [125,126].

STANDARDIZATION OF *IN VITRO* MODELS

Thorough characterization is essential in the development of *in vitro* models to identify their strengths and limitations compared to other models, and therefore for their application in safety assessment. Models and conditions under which data is generated must adhere to standards to ensure that data quality is reliable and reproducible [127]. Guidance documents such as Guidance Document on Good In Vitro Method Practices (GIVIMP) and Good Cell Culture Practice (GCCP) aim to reduce uncertainties by standardization and promote confidence in *in vitro* methods [128-131]. These documents address key aspects of good *in vitro* practice and thereby enhance the reliability of *in vitro* outcomes [132], including procedures for storing and handling samples,

defining and describing standard operating procedures, method of assessment, and reporting results. In addition, the importance of the choice of materials and reagents is stressed with a focus on animal-derived materials. Apart from ethical considerations, the use of animal-derived media components or extracellular matrices, such as hydrogels, can lead to inconsistency of microenvironmental cues, of which the importance is stressed above, as a result of batch-to-batch differences and therefore can result in quality issues. Awareness on animal-free *in vitro* models is rising [113,133-136], resulting in major advances to develop alternatives including well-defined synthetic hydrogels, recombinant factors/proteins, and alternatives to medium components with animal origin, such as fetal bovine serum or bovine serum albumin [137-142].

The previous mentioned GCCP was recently updated following developments in culture methods including stem cell-derived models and microphysiological systems [143,144], where main additional considerations were genomic stability, ethical considerations and training of personnel. Recent publications showed that working under standardized conditions improved data quality and reproducibility for stem cell-derived models [145,146]. In the case of liver organoids, the shift towards animal-free, commercialized media instead of lab-made media could limit interlaboratory (and inter-personnel) differences resulting in more consistent functionality of the organoids and reliable interlaboratory comparisons. More specifically, for our liver organoids a commercial media is developed which not only maintain the organoids, but also improve hepatic function compared to our lab-made media (Hepaticult, Stem Cell Technologies). Furthermore, synthetic alternatives to Matrigel as extracellular matrix can enhance reproducibility and their clinical application [140,141], however at this point it is the favorable substrate for organoid proliferation. One candidate would be the synthetic hydrogel polyisocyanide (PIC) tested in our research group which maintained organoid proliferation when cultured with high concentrations of laminins [147]. Recent advancements in tissue-derived organoid cultures stressed their clinical applications and possibilities towards standardized and validated culture procedures [148-150].

Microphysiological systems and/or the combination of cells with biotechnology advances are not yet discussed in the GCCP, however they are expected to bring a greater reproducibility due to automatization steps [151,152]. As developments of culture methodologies and biotechnology advances are rising, it is suggested to implement GIVIMP requirements during development to improve the quality of the methodology and generated data, and possibly enhance the efficiency of validation studies and stimulate regulatory acceptance [132,153,154].

One of the described points of attention for microphysiological systems is device design (for example material choice) [143], which is essential in standardization of the model and therefore also for the generation of reliable data. The choice of materials and the presence of culture components can affect the *in vitro* disposition of a chemical, as is shown in **Chapter 2** where Matrigel presence and/or medium components affects chemical depletion. Another example is the frequent use of polydimethylsiloxane (PDMS) in microphysiological systems which is prone to chemical binding, therefore the material of choice for the bioreactor in **Chapter 5** was PEEK, although less flexible in design than PDMS, an inert material [155-158]. Complex *in vitro* systems introduce extra components to which chemicals can bind, depending on their physicochemical properties, and therefore demand for knowledge on *in vitro* disposition of chemicals in order to generate usable and reliable data, e.g., for computational modelling of the *in vivo* effect [159-161]. Computational models for *in vitro in vivo* extrapolation (IVIVE) take physiological parameters, like blood flow rates or chemical-specific binding affinities, into account to translate cell assays to human exposure, therefore inaccurate *in vitro* data can result in over-/underestimation of the effect [20,22].

TOWARDS REGULATORY ACCEPTANCE OF ALTERNATIVE MODELS

Next to challenges in data interpretation and integration of advanced *in vitro* methods, the implementation of such alternative models in safety assessment and their regulatory use is another hurdle to take [162,163]. Validation of these novel approaches encompass assessment of, among others, intra-test and interlaboratory variability, repeatability, and reproducibility, as well as accuracy (e.g., sensitivity and specificity) [164]. As validation of alternative models using animal data as reference could be biased, renewed approaches of validation need to be developed (e.g., incorporating human biological relevance)[165]. Moreover, non-validated methods and high quality data generated in peer-reviewed scientific literature could be relevant for safety assessment, especially if available validated assays do not assess specific pathways [166]. Guidelines, like GIVIMP, are essential to stress requirements regarding standardized culture environments and generate high quality data [146]. Additional guidance on the generation of data (e.g., biological readouts) essential for integration in human safety assessment will be informative, especially for scientific researchers from different fields of expertise. Next to generation of standardized and relevant data, following FAIR (Findable, Accessible, Interoperable, Reusable) data principles by default facilitate the accessibility and use of such data in safety assessment [167,168].

Although regulatory acceptance has been provided for several NAMs, it is expected that more methodologies will be accepted in the future [169]. Confidence in these novel approaches is required for an actual shift towards NAMs in safety assessment [162]. At some point, newly developed substances or chemicals need to be assessed within the novel frameworks using NAMs without available animal data. Together with other approaches, such as omics technologies and artificial intelligence [170-172], confidence in alternative models to animal testing in human safety assessment can be boosted. It is clear that the focus of the scientific community is more on the problem of reliability when conducting safety assessments, whereas politics are more focused on the ethical problem. This discrepancy needs to be addressed in the future. Therefore, input and involvement of different stakeholders, such as industry and regulatory bodies, is needed to align and move the field forward together.

CONCLUDING REMARKS

In this thesis, an important first step has been taken towards characterization of liver organoids as an *in vitro* toxicity model focusing on their drug metabolism capabilities (**Chapter 2**). The combination of liver organoids with biofabrication approaches open ways to further improve the hepatic maturation state of the cells, e.g., by bioprinting and applying flow as demonstrated in **Chapter 3**, **4**, and **5**. These techniques, among other approaches, provide tools to create more complex *in vivo*-like models with increased hepatic functionality. The application of patient-derived liver organoids in disease modelling is widely described, and the combination with biofabrication approaches facilitates the recapitulation of *in vivo* complexity and improved understanding of disease etiology. Moreover, the use of patient-derived cells opens the possibility for personalized medicine approaches, and developments in the field of biofabrication lead to promising clinical applications, such as *in situ* bioprinting [173]. These emerging technologies can bring together high-content models and high-throughput screening by facilitating applications of complex (e.g., bioprinted) models in compound/drug screens [92,94,96]. Bioengineered microphysiological relevant *in vitro* models can create (high-content) tissue analogs to bridge between animal models and simplistic *in vitro* models. Given the current wave of next generation risk assessment approaches, the research described in this thesis plays a crucial role in the shift towards human-relevant models for liver toxicity.

REFERENCES

[1] Alempijevic, T.; Zec, S.; Milosavljevic, T. Drug-Induced Liver Injury: Do we Know Everything? World J. Hepatol. **2017**, *9*, 491-502.

[2] Turpeinen, M.; Ghiciuc, C.; Opritoui, M.; Tursas, L.; Pelkonen, O.; Pasanen, M. Predictive Value of Animal Models for Human Cytochrome P450 (CYP)-Mediated Metabolism: A Comparative Study in Vitro. Xenobiotica **2007**, *37*, 1367-1377.

[3] Hammer, H.; Schmidt, F.; Marx-Stoelting, P.; Pötz, O.; Braeuning, A. Cross-Species Analysis of Hepatic Cytochrome P450 and Transport Protein Expression. Arch. Toxicol. **2021**, *95*, 117-133.

[4] Zink, D.; Chuah, J.K.C.; Ying, J.Y. Assessing Toxicity with Human Cell-Based in Vitro Methods. Trends Mol. Med. **2020**, *26*, 570-582.

[5] Krewski, D.; Acosta, D.,Jr; Andersen, M.; Anderson, H.; Bailar, J.C.,3rd; Boekelheide, K.; Brent, R.; Charnley, G.; Cheung, V.G.; Green, S.,Jr *et al.* Toxicity Testing in the 21st Century: A Vision and a Strategy. J. Toxicol. Environ. Health B Crit. Rev. **2010**, *13*, 51-138.

[6] Huch, M.; Gehart, H.; van Boxtel, R.; Hamer, K.; Blokzijl, F.; Verstegen, M.M.; Ellis, E.; van Wenum, M.; Fuchs, S.A.; de Ligt, J. *et al.* Long-Term Culture of Genome-Stable Bipotent Stem Cells from Adult Human Liver. Cell **2015**, *160*, 299-312.

[7] Wang, Z.; Faria, J.; van der Laan, L.J.W.; Penning, L.C.; Masereeuw, R.; Spee, B. Human Cholangiocytes Form a Polarized and Functional Bile Duct on Hollow Fiber Membranes. Front. Bioeng. Biotechnol. **2022**, *10*, 868857.

[8] Xie, Y.; Yao, J.; Jin, W.; Ren, L.; Li, X. Induction and Maturation of Hepatocyte-Like Cells in Vitro: Focus on Technological Advances and Challenges. Front. Cell. Dev. Biol. **2021**, *9*, 765980.

[9] Zanger, U.M.; Schwab, M. Cytochrome P450 Enzymes in Drug Metabolism: Regulation of Gene Expression, Enzyme Activities, and Impact of Genetic Variation. Pharmacol. Ther. **2013**, *138*, 103-141.

[10] Iversen, D.B.; Andersen, N.E.; Dalgård Dunvald, A.; Pottegård, A.; Stage, T.B. Drug Metabolism and Drug Transport of the 100 most Prescribed Oral Drugs. Basic Clin. Pharmacol. Toxicol. **2022**, *131*, 311-324.

[11] Gan, J.; Ma, S.; Zhang, D. Non-Cytochrome P450-Mediated Bioactivation and its Toxicological Relevance. Drug Metab. Rev. **2016**, *48*, 473-501.

[12] Kasteel, E.E.J.; Darney, K.; Kramer, N.I.; Dorne, J.L.C.M.; Lautz, L.S. Human Variability in Isoform-Specific UDP-Glucuronosyltransferases: Markers of Acute and Chronic Exposure, Polymorphisms and Uncertainty Factors. Arch. Toxicol. **2020**, *94*, 2637-2661.

[13] den Braver-Sewradj, S.P.; den Braver, M.W.; Baze, A.; Decorde, J.; Fonsi, M.; Bachellier, P.; Vermeulen, N.P.E.; Commandeur, J.N.M.; Richert, L.; Vos, J.C. Direct Comparison of UDP-Glucuronosyltransferase and Cytochrome P450 Activities in Human Liver Microsomes, Plated and Suspended Primary Human Hepatocytes from Five Liver Donors. Eur. J. Pharm. Sci. **2017**, *109*, 96-110.

[14] Mennecozzi, M.; Landesmann, B.; Palosaari, T.; Harris, G.; Whelan, M. Sex Differences in Liver Toxicity-do Female and Male Human Primary Hepatocytes React Differently to Toxicants in Vitro? PLoS One **2015**, *10*, e0122786.

[15] Zhou, S.F.; Liu, J.P.; Chowbay, B. Polymorphism of Human Cytochrome P450 Enzymes and its Clinical Impact. Drug Metab. Rev. **2009**, *41*, 89-295.

[16] Wang, C.W.; Preclaro, I.A.C.; Lin, W.H.; Chung, W.H. An Updated Review of Genetic Associations with Severe Adverse Drug Reactions: Translation and Implementation of Pharmacogenomic Testing in Clinical Practice. Front. Pharmacol. **2022**, *13*, 886377.
[17] Cao, X.; Durairaj, P.; Yang, F.; Bureik, M. A Comprehensive Overview of Common Polymorphic Variants that Cause Missense Mutations in Human CYPs and UGTs. Biomed. Pharmacother. **2019**, *111*, 983-992.
[18] Yoon, E.; Babar, A.; Choudhary, M.; Kutner, M.; Pyrsopoulos, N. Acetaminophen-Induced Hepatotoxicity: A Comprehensive Update. J. Clin. Transl. Hepatol. **2016**, *4*, 131-142.
[19] Court, M.H.; Zhu, Z.; Masse, G.; Duan, S.X.; James, L.P.; Harmatz, J.S.; Greenblatt, D.J. Race, Gender, and Genetic Polymorphism Contribute to Variability in Acetaminophen Pharmacokinetics, Metabolism, and Protein-Adduct Concentrations in Healthy African-American and European-American Volunteers. J. Pharmacol. Exp. Ther. **2017**, *362*, 431-440.
[20] Proença, S.; Escher, B.I.; Fischer, F.C.; Fisher, C.; Grégoire, S.; Hewitt, N.J.; Nicol, B.; Paini, A.; Kramer, N.I. Effective Exposure of Chemicals in in Vitro Cell Systems: A Review of Chemical Distribution Models. Toxicol. In. Vitro. **2021**, *73*, 105133.
[21] Kang, H.K.; Sarsenova, M.; Kim, D.; Kim, M.S.; Lee, J.Y.; Sung, E.; Kook, M.G.; Kim, N.G.; Choi, S.W.; Ogay, V. *et al.* Establishing a 3D in Vitro Hepatic Model Mimicking Physiologically Relevant to in Vivo State. Cells **2021**, *10*, 1268. doi: 10.3390/cells10051268.
[22] Dimitrijevic, D.; Fabian, E.; Nicol, B.; Funk-Weyer, D.; Landsiedel, R. Toward Realistic Dosimetry in Vitro: Determining Effective Concentrations of Test Substances in Cell Culture and their Prediction by an in Silico Mass Balance Model. Chem. Res. Toxicol. **2022**.
[23] Correia, C.; Ferreira, A.; Santos, J.; Lapa, R.; Yliperttula, M.; Urtti, A.; Vale, N. New in Vitro-in Silico Approach for the Prediction of in Vivo Performance of Drug Combinations. Molecules **2021**, *26*, 4257. doi: 10.3390/molecules26144257.
[24] Dragovic, S.; Vermeulen, N.P.E.; Gerets, H.H.; Hewitt, P.G.; Ingelman-Sundberg, M.; Park, B.K.; Juhila, S.; Snoeys, J.; Weaver, R.J. Evidence-Based Selection of Training Compounds for use in the Mechanism-Based Integrated Prediction of Drug-Induced Liver Injury in Man. Arch. Toxicol. **2016**, *90*, 2979-3003.
[25] Bernal, P.N.; Delrot, P.; Loterie, D.; Li, Y.; Malda, J.; Moser, C.; Levato, R. Volumetric Bioprinting of Complex Living-Tissue Constructs within Seconds. Adv Mater **2019**, *31*, e1904209.
[26] Schneeberger, K.; Sánchez-Romero, N.; Ye, S.; van Steenbeek, F.G.; Oosterhoff, L.A.; Pla Palacin, I.; Chen, C.; van Wolferen, M.E.; van Tienderen, G.; Lieshout, R. *et al.* Large-Scale Production of LGR5-Positive Bipotential Human Liver Stem Cells. Hepatology **2020**, *72*, 257-270.
[27] Bergin, C.J.; Benoit, Y.D. Protocol for Serial Organoid Formation Assay using Primary Colorectal Cancer Tissues to Evaluate Cancer Stem Cell Activity. STAR Protoc. **2022**, *3*, 101218.
[28] Ozbolat, I.T.; Hospodiuk, M. Current Advances and Future Perspectives in Extrusion-Based Bioprinting. Biomaterials **2016**, *76*, 321-343.
[29] Zandrini, T.; Florczak, S.; Levato, R.; Ovsianikov, A. Breaking the Resolution Limits of 3D Bioprinting: Future Opportunities and Present Challenges. Trends Biotechnol. **2023**, *41*, 604-614.

[30] Lv, W.; Zhou, H.; Aazmi, A.; Yu, M.; Xu, X.; Yang, H.; Huang, Y.Y.S.; Ma, L. Constructing Biomimetic Liver Models through Biomaterials and Vasculature Engineering. Regen. Biomater. **2022**, *9*, rbac079.

[31] Ye, S.; Boeter, J.W.B.; Penning, L.C.; Spee, B.; Schneeberger, K. Hydrogels for Liver Tissue Engineering. Bioengineering (Basel) **2019**, *6*, 59.

[32] Guagliano, G.; Volpini, C.; Briatico-Vangosa, F.; Cornaglia, A.I.; Visai, L.; Petrini, P. Toward 3D-Bioprinted Models of the Liver to Boost Drug Development. Macromol. Biosci. **2022**, *22*, e2200264.

[33] Rizki-Safitri, A.; Gupta, N.; Hiratsuka, K.; Kobayashi, K.; Zhang, C.; Ida, K.; Satlin, L.M.; Morizane, R. Live Functional Assays Reveal Longitudinal Maturation of Transepithelial Transport in Kidney Organoids. Front. Cell. Dev. Biol. **2022**, *10*, 978888.

[34] Starokozhko, V.; Hemmingsen, M.; Larsen, L.; Mohanty, S.; Merema, M.; Pimentel, R.C.; Wolff, A.; Emnéus, J.; Aspegren, A.; Groothuis, G. *et al.* Differentiation of Human-Induced Pluripotent Stem Cell Under Flow Conditions to Mature Hepatocytes for Liver Tissue Engineering. J. Tissue Eng. Regen. Med. **2018**, *12*, 1273-1284.

[35] Esch, M.B.; Prot, J.; Wang, Y.I.; Miller, P.; Llamas-Vidales, J.R.; Naughton, B.A.; Applegate, D.R.; Shuler, M.L. Multi-Cellular 3D Human Primary Liver Cell Culture Elevates Metabolic Activity Under Fluidic Flow. Lab. Chip **2015**, *15*, 2269-2277.

[36] Kim, Y.; Asif, A.; Chethikkattuveli Salih, A.R.; Lee, J.; Hyun, K.; Choi, K. Gravity-Based Flow Efficient Perfusion Culture System for Spheroids Mimicking Liver Inflammation. Biomedicines **2021**, *9*, 1369.

[37] Jung, D.J.; Byeon, J.H.; Jeong, G.S. Flow Enhances Phenotypic and Maturation of Adult Rat Liver Organoids. Biofabrication **2020**, *12*, 045035-5090/abb538.

[38] Choi, Y.Y.; Seok, J.; Kim, D. Flow-Based Three-Dimensional Co-Culture Model for Long-Term Hepatotoxicity Prediction. Micromachines (Basel) **2019**, *11*, 36. doi: 10.3390/mi11010036.

[39] Donato, M.T.; Gallego-Ferrer, G.; Tolosa, L. In Vitro Models for Studying Chronic Drug-Induced Liver Injury. International Journal of Molecular Sciences **2022**, *23*.

[40] Telles-Silva, K.A.; Pacheco, L.; Komatsu, S.; Chianca, F.; Caires-Júnior, L.C.; Araujo, B.H.S.; Goulart, E.; Zatz, M. Applied Hepatic Bioengineering: Modeling the Human Liver using Organoid and Liver-on-a-Chip Technologies. Front. Bioeng. Biotechnol. **2022**, *10*, 845360.

[41] Yun, C.; Kim, S.H.; Jung, Y. Current Research Trends in the Application of in Vitro Three-Dimensional Models of Liver Cells. Pharmaceutics **2022**, *15*, 54.

[42] Bassi, G.; Grimaudo, M.A.; Panseri, S.; Montesi, M. Advanced Multi-Dimensional Cellular Models as Emerging Reality to Reproduce in Vitro the Human Body Complexity. Int. J. Mol. Sci. **2021**, *22*, 1195.

[43] Dellaquila, A.; Le Bao, C.; Letourneur, D.; Simon-Yarza, T. In Vitro Strategies to Vascularize 3D Physiologically Relevant Models. Adv. Sci. (Weinh) **2021**, *8*, e2100798.

[44] Anthon, S.G.; Valente, K.P. Vascularization Strategies in 3D Cell Culture Models: From Scaffold-Free Models to 3D Bioprinting. Int. J. Mol. Sci. **2022**, *23*, 14582. doi: 10.3390/ijms232314582.

[45] Cui, J.; Wang, H.; Zheng, Z.; Shi, Q.; Sun, T.; Huang, Q.; Fukuda, T. Fabrication of Perfusable 3D Hepatic Lobule-Like Constructs through Assembly of Multiple Cell Type Laden Hydrogel Microstructures. Biofabrication **2018**, *11*, 015016-5090/aaf3c9.

[46] Grix, T.; Ruppelt, A.; Thomas, A.; Amler, A.; Noichl, B.P.; Lauster, R.; Kloke, L. Bioprinting Perfusion-Enabled Liver Equivalents for Advanced Organ-on-a-Chip Applications. Genes (Basel) **2018**, *9*, 176. doi: 10.3390/genes9040176.

[47] Janani, G.; Priya, S.; Dey, S.; Mandal, B.B. Mimicking Native Liver Lobule Microarchitecture in Vitro with Parenchymal and Non-Parenchymal Cells using 3D Bioprinting for Drug Toxicity and Drug Screening Applications. ACS Appl. Mater. Interfaces **2022**, *14*, 10167-10186.

[48] Sphabmixay, P.; Raredon, M.S.B.; Wang, A.J.; Lee, H.; Hammond, P.T.; Fang, N.X.; Griffith, L.G. High Resolution Stereolithography Fabrication of Perfusable Scaffolds to Enable Long-Term Meso-Scale Hepatic Culture for Disease Modeling. Biofabrication **2021**, *13*, 10.1088/1758-5090/ac23aa.

[49] Ya, S.; Ding, W.; Li, S.; Du, K.; Zhang, Y.; Li, C.; Liu, J.; Li, F.; Li, P.; Luo, T. *et al.* On-Chip Construction of Liver Lobules with Self-Assembled Perfusable Hepatic Sinusoid Networks. ACS Appl. Mater. Interfaces **2021**, *13*, 32640-32652.

[50] Kietzmann, T. Metabolic Zonation of the Liver: The Oxygen Gradient Revisited. Redox Biol. **2017**, *11*, 622-630.

[51] Cunningham, R.P.; Porat-Shliom, N. Liver Zonation - Revisiting Old Questions with New Technologies. Front. Physiol. **2021**, *12*, 732929.

[52] Ardisasmita, A.I.; Schene, I.F.; Joore, I.P.; Kok, G.; Hendriks, D.; Artegiani, B.; Mokry, M.; Nieuwenhuis, E.E.S.; Fuchs, S.A. A Comprehensive Transcriptomic Comparison of Hepatocyte Model Systems Improves Selection of Models for Experimental Use. Commun. Biol. **2022**, *5*, 1094-9.

[53] Kang, Y.B.A.; Eo, J.; Mert, S.; Yarmush, M.L.; Usta, O.B. Metabolic Patterning on a Chip: Towards in Vitro Liver Zonation of Primary Rat and Human Hepatocytes. Sci. Rep. **2018**, *8*, 8951-6.

[54] Lee-Montiel, F.T.; George, S.M.; Gough, A.H.; Sharma, A.D.; Wu, J.; DeBiasio, R.; Vernetti, L.A.; Taylor, D.L. Control of Oxygen Tension Recapitulates Zone-Specific Functions in Human Liver Microphysiology Systems. Exp. Biol. Med. (Maywood) **2017**, *242*, 1617-1632.

[55] Matsumoto, S.; Safitri, A.R.; Danoy, M.; Maekawa, T.; Kinoshita, H.; Shinohara, M.; Sakai, Y.; Fujii, T.; Leclerc, E. Investigation of the Hepatic Respiration and Liver Zonation on Rat Hepatocytes using an Integrated Oxygen Biosensor in a Microscale Device. Biotechnol. Prog. **2019**, *35*, e2854.

[56] Tonon, F.; Giobbe, G.G.; Zambon, A.; Luni, C.; Gagliano, O.; Floreani, A.; Grassi, G.; Elvassore, N. In Vitro Metabolic Zonation through Oxygen Gradient on a Chip. Sci. Rep. **2019**, *9*, 13557-6.

[57] Bhushan, A.; Senutovitch, N.; Bale, S.S.; McCarty, W.J.; Hegde, M.; Jindal, R.; Golberg, I.; Berk Usta, O.; Yarmush, M.L.; Vernetti, L. *et al.* Towards a Three-Dimensional Microfluidic Liver Platform for Predicting Drug Efficacy and Toxicity in Humans. Stem Cell. Res. Ther. **2013**, *4 Suppl 1*, S16.

[58] Baze, A.; Parmentier, C.; Hendriks, D.F.G.; Hurrell, T.; Heyd, B.; Bachellier, P.; Schuster, C.; Ingelman-Sundberg, M.; Richert, L. Three-Dimensional Spheroid Primary Human Hepatocytes in Monoculture and Coculture with Nonparenchymal Cells. Tissue Eng. Part C. Methods **2018**, *24*, 534-545.

[59] Girish, C.; Sanjay, S. Role of Immune Dysfunction in Drug Induced Liver Injury. World J. Hepatol. **2021**, *13*, 1677-1687.

[60] Gerussi, A.; Natalini, A.; Antonangeli, F.; Mancuso, C.; Agostinetto, E.; Barisani, D.; Di Rosa, F.; Andrade, R.; Invernizzi, P. Immune-Mediated Drug-Induced Liver Injury: Immunogenetics and Experimental Models. Int. J. Mol. Sci. **2021**, *22*, 4557. doi: 10.3390/ijms22094557.

[61] Tasnim, F.; Huang, X.; Lee, C.Z.W.; Ginhoux, F.; Yu, H. Recent Advances in Models of Immune-Mediated Drug-Induced Liver Injury. Front. Toxicol. **2021**, *3*, 605392.
[62] Ravanbakhsh, H.; Karamzadeh, V.; Bao, G.; Mongeau, L.; Juncker, D.; Zhang, Y.S. Emerging Technologies in Multi-Material Bioprinting. Adv Mater **2021**, *33*, e2104730.
[63] Ashammakhi, N.; Ahadian, S.; Xu, C.; Montazerian, H.; Ko, H.; Nasiri, R.; Barros, N.; Khademhosseini, A. Bioinks and Bioprinting Technologies to make Heterogeneous and Biomimetic Tissue Constructs. Mater. Today Bio **2019**, *1*, 100008.
[64] Chen, C.; Soto-Gutierrez, A.; Baptista, P.M.; Spee, B. Biotechnology Challenges to in Vitro Maturation of Hepatic Stem Cells. Gastroenterology **2018**, *154*, 1258-1272.
[65] Stowers, R.S. Advances in Extracellular Matrix-Mimetic Hydrogels to Guide Stem Cell Fate. Cells Tissues Organs **2022**, *211*, 703-720.
[66] Nicolas, J.; Magli, S.; Rabbachin, L.; Sampaolesi, S.; Nicotra, F.; Russo, L. 3D Extracellular Matrix Mimics: Fundamental Concepts and Role of Materials Chemistry to Influence Stem Cell Fate. Biomacromolecules **2020**, *21*, 1968-1994.
[67] Cruz-Acuña, R.; García, A.J. Synthetic Hydrogels Mimicking Basement Membrane Matrices to Promote Cell-Matrix Interactions. Matrix Biol. **2017**, *57-58*, 324-333.
[68] Zhang, X.; Chen, X.; Hong, H.; Hu, R.; Liu, J.; Liu, C. Decellularized Extracellular Matrix Scaffolds: Recent Trends and Emerging Strategies in Tissue Engineering. Bioact. Mater. **2021**, *10*, 15-31.
[69] Zhang, Y.; Zegers, M.M.P.; Nagelkerke, A.; Rowan, A.E.; Span, P.N.; Kouwer, P.H.J. Tunable Hybrid Matrices Drive Epithelial Morphogenesis and YAP Translocation. Adv. Sci. (Weinh) **2020**, *8*, 2003380.
[70] Brovold, M.; Almeida, J.I.; Pla-Palacín, I.; Sainz-Arnal, P.; Sánchez-Romero, N.; Rivas, J.J.; Almeida, H.; Dachary, P.R.; Serrano-Aulló, T.; Soker, S. *et al.* Naturally-Derived Biomaterials for Tissue Engineering Applications. Adv. Exp. Med. Biol. **2018**, *1077*, 421-449.
[71] Ji, S.; Guvendiren, M. Recent Advances in Bioink Design for 3D Bioprinting of Tissues and Organs. Front. Bioeng. Biotechnol. **2017**, *5*, 23.
[72] Fatimi, A.; Okoro, O.V.; Podstawczyk, D.; Siminska-Stanny, J.; Shavandi, A. Natural Hydrogel-Based Bio-Inks for 3D Bioprinting in Tissue Engineering: A Review. Gels **2022**, *8*, 179. doi: 10.3390/gels8030179.
[73] Xu, Q. Human Three-Dimensional Hepatic Models: Cell Type Variety and Corresponding Applications. Front. Bioeng. Biotechnol. **2021**, *9*, 730008.
[74] Kammerer, S. Three-Dimensional Liver Culture Systems to Maintain Primary Hepatic Properties for Toxicological Analysis in Vitro. Int. J. Mol. Sci. **2021**, *22*, 10214.
[75] Bell, C.C.; Lauschke, V.M.; Vorrink, S.U.; Palmgren, H.; Duffin, R.; Andersson, T.B.; Ingelman-Sundberg, M. Transcriptional, Functional, and Mechanistic Comparisons of Stem Cell-Derived Hepatocytes, HepaRG Cells, and Three-Dimensional Human Hepatocyte Spheroids as Predictive in Vitro Systems for Drug-Induced Liver Injury. Drug Metab. Dispos. **2017**, *45*, 419-429.
[76] Godoy, P.; Hewitt, N.J.; Albrecht, U.; Andersen, M.E.; Ansari, N.; Bhattacharya, S.; Bode, J.G.; Bolleyn, J.; Borner, C.; Böttger, J. *et al.* Recent Advances in 2D and 3D in Vitro Systems using Primary Hepatocytes, Alternative Hepatocyte Sources and Non-Parenchymal Liver Cells and their use in Investigating Mechanisms of Hepatotoxicity, Cell Signaling and ADME. Arch. Toxicol. **2013**, *87*, 1315-1530.

[77] Gunness, P.; Mueller, D.; Shevchenko, V.; Heinzle, E.; Ingelman-Sundberg, M.; Noor, F. 3D Organotypic Cultures of Human HepaRG Cells: A Tool for in Vitro Toxicity Studies. Toxicol. Sci. **2013**, *133*, 67-78.

[78] Luckert, C.; Schulz, C.; Lehmann, N.; Thomas, M.; Hofmann, U.; Hammad, S.; Hengstler, J.G.; Braeuning, A.; Lampen, A.; Hessel, S. Comparative Analysis of 3D Culture Methods on Human HepG2 Cells. Arch. Toxicol. **2017**, *91*, 393-406.

[79] Hu, H.; Gehart, H.; Artegiani, B.; LÖpez-Iglesias, C.; Dekkers, F.; Basak, O.; van Es, J.; Chuva de Sousa Lopes, S.M.; Begthel, H.; Korving, J. *et al.* Long-Term Expansion of Functional Mouse and Human Hepatocytes as 3D Organoids. Cell **2018**, *175*, 1591-1606.e19.

[80] Wang, Z.; Li, W.; Jing, H.; Ding, M.; Fu, G.; Yuan, T.; Huang, W.; Dai, M.; Tang, D.; Zeng, M. *et al.* Generation of Hepatic Spheroids using Human Hepatocyte-Derived Liver Progenitor-Like Cells for Hepatotoxicity Screening. Theranostics **2019**, *9*, 6690-6705.

[81] Collins, S.D.; Yuen, G.; Tu, T.; Budzinska, M.A.; Spring, K.; Bryant, K.; Shackel, N.A. In Vitro Models of the Liver: Disease Modeling, Drug Discovery and Clinical Applications. In *Hepatocellular Carcinoma*.; Tirnitz-Parker, J.E.E., Ed.: Brisbane (AU), 2019.

[82] Garcia-Llorens, G.; Martínez-Sena, T.; Pareja, E.; Tolosa, L.; Castell, J.V.; Bort, R. A Robust Reprogramming Strategy for Generating Hepatocyte-Like Cells Usable in Pharmaco-Toxicological Studies. Stem Cell. Res. Ther. **2023**, *14*, 94-w.

[83] Peng, W.C.; Kraaier, L.J.; Kluiver, T.A. Hepatocyte Organoids and Cell Transplantation: What the Future Holds. Exp. Mol. Med. **2021**, *53*, 1512-1528.

[84] Zhang, K.; Zhang, L.; Liu, W.; Ma, X.; Cen, J.; Sun, Z.; Wang, C.; Feng, S.; Zhang, Z.; Yue, L. *et al.* In Vitro Expansion of Primary Human Hepatocytes with Efficient Liver Repopulation Capacity. Cell. Stem Cell. **2018**, *23*, 806-819.e4.

[85] Hart, S.N.; Li, Y.; Nakamoto, K.; Subileau, E.A.; Steen, D.; Zhong, X.B. A Comparison of Whole Genome Gene Expression Profiles of HepaRG Cells and HepG2 Cells to Primary Human Hepatocytes and Human Liver Tissues. Drug Metab. Dispos. **2010**, *38*, 988-994.

[86] Gupta, R.; Schrooders, Y.; Hauser, D.; van Herwijnen, M.; Albrecht, W.; Ter Braak, B.; Brecklinghaus, T.; Castell, J.V.; Elenschneider, L.; Escher, S. *et al.* Comparing in Vitro Human Liver Models to in Vivo Human Liver using RNA-Seq. Arch. Toxicol. **2021**, *95*, 573-589.

[87] Kvist, A.J.; Kanebratt, K.P.; Walentinsson, A.; Palmgren, H.; O'Hara, M.; Björkbom, A.; Andersson, L.C.; Ahlqvist, M.; Andersson, T.B. Critical Differences in Drug Metabolic Properties of Human Hepatic Cellular Models, Including Primary Human Hepatocytes, Stem Cell Derived Hepatocytes, and Hepatoma Cell Lines. Biochem. Pharmacol. **2018**, *155*, 124-140.

[88] Vinken, M.; Hengstler, J.G. Characterization of Hepatocyte-Based in Vitro Systems for Reliable Toxicity Testing. Arch. Toxicol. **2018**, *92*, 2981-2986.

[89] Tabernilla, A.; Dos Santos Rodrigues, B.; Pieters, A.; Caufriez, A.; Leroy, K.; Van Campenhout, R.; Cooreman, A.; Gomes, A.R.; Arnesdotter, E.; Gijbels, E. *et al.* In Vitro Liver Toxicity Testing of Chemicals: A Pragmatic Approach. Int. J. Mol. Sci. **2021**, *22*, 5038. doi: 10.3390/ijms22095038.

[90] Xiao, R.; Lv, T.; Tu, X.; Li, P.; Wang, T.; Dong, H.; Tu, P.; Ai, X. An Integrated Biomimetic Array Chip for Establishment of Collagen-Based 3D Primary Human Hepatocyte Model for Prediction of Clinical Drug-Induced Liver Injury. Biotechnol. Bioeng. **2021**, *118*, 4687-4698.

[91] Shinozawa, T.; Kimura, M.; Cai, Y.; Saiki, N.; Yoneyama, Y.; Ouchi, R.; Koike, H.; Maezawa, M.; Zhang, R.; Dunn, A. *et al.* High-Fidelity Drug-Induced Liver Injury Screen using Human Pluripotent Stem Cell-Derived Organoids. Gastroenterology **2021**, *160*, 831-846.e10.

[92] Li, X.; Fu, G.; Zhang, L.; Guan, R.; Tang, P.; Zhang, J.; Rao, X.; Chen, S.; Xu, X.; Zhou, Y. *et al.* Assay Establishment and Validation of a High-Throughput Organoid-Based Drug Screening Platform. Stem Cell. Res. Ther. **2022**, *13*, 219-3.

[93] Ramaiahgari, S.C.; Den Braver Michiel, W.; Herpers, B.; Terpstra, V.; Commandeur, J.N.M.; Van De Water Bob; Price, L.S. A 3D in Vitro Model of Differentiated HepG2 Cell Spheroids with Improved Liver-Like Properties for Repeated Dose High-Throughput Toxicity Studies. Arch. Toxicol. **2014**, *88*, 1083-1095.

[94] Maloney, E.; Clark, C.; Sivakumar, H.; Yoo, K.; Aleman, J.; Rajan, S.A.P.; Forsythe, S.; Mazzocchi, A.; Laxton, A.W.; Tatter, S.B. *et al.* Immersion Bioprinting of Tumor Organoids in Multi-Well Plates for Increasing Chemotherapy Screening Throughput. Micromachines (Basel) **2020**, *11*, 208. doi: 10.3390/mi11020208.

[95] Kang, S.; Kimura, M.; Shrestha, S.; Lewis, P.; Lee, S.; Cai, Y.; Joshi, P.; Acharya, P.; Liu, J.; Yang, Y. *et al.* A Pillar and Perfusion Plate Platform for Robust Human Organoid Culture and Analysis. bioRxiv **2023**.

[96] Wang, Y.; Jeon, H. 3D Cell Cultures Toward Quantitative High-Throughput Drug Screening. Trends Pharmacol. Sci. **2022**, *43*, 569-581.

[97] Lynch, S.; Pridgeon, C.S.; Duckworth, C.A.; Sharma, P.; Park, B.K.; Goldring, C.E.P. Stem Cell Models as an in Vitro Model for Predictive Toxicology. Biochem. J. **2019**, *476*, 1149-1158.

[98] Nuciforo, S.; Heim, M.H. Organoids to Model Liver Disease. JHEP Rep. **2020**, *3*, 100198.

[99] Sun, X.; Kong, D.; Zhao, J.; Faber, K.N.; Xia, Q.; He, K. Liver Organoids: Established Tools for Disease Modeling and Drug Development. Hepatol. Commun. **2023**, *7*, e0105. doi: 10.1097/HC9.0000000000000105. eCollection 2023 Apr 1.

[100] Zhou, Z.; Cong, L.; Cong, X. Patient-Derived Organoids in Precision Medicine: Drug Screening, Organoid-on-a-Chip and Living Organoid Biobank. Front. Oncol. **2021**, *11*, 762184.

[101] Lancaster, M.A.; Huch, M. Disease Modelling in Human Organoids. Dis. Model. Mech. **2019**, *12*, dmm039347. doi: 10.1242/dmm.039347.

[102] Stern, S.; Wang, H.; Sadrieh, N. Microphysiological Models for Mechanistic-Based Prediction of Idiosyncratic DILI. Cells **2023**, *12*, 1476. doi: 10.3390/cells12111476.

[103] Villanueva-Badenas, E.; Donato, M.T.; Tolosa, L. Mechanistic Understanding of Idiosyncratic Drug-Induced Hepatotoxicity using Co-Cultures of Hepatocytes and Macrophages. Antioxidants (Basel) **2023**, *12*, 1315. doi: 10.3390/antiox12071315.

[104] Segovia-Zafra, A.; Di Zeo-Sánchez, D.E.; López-Gómez, C.; Pérez-Valdés, Z.; García-Fuentes, E.; Andrade, R.J.; Lucena, M.I.; Villanueva-Paz, M. Preclinical Models of Idiosyncratic Drug-Induced Liver Injury (iDILI): Moving Towards Prediction. Acta Pharm. Sin. B. **2021**, *11*, 3685-3726.

[105] Wang, X.; Xu, X.; Tong, W.; Liu, Q.; Liu, Z. DeepCausality: A General AI-Powered Causal Inference Framework for Free Text: A Case Study of LiverTox. Front. Artif. Intell. **2022**, *5*, 999289.

[106] Castro-Viñuelas, R.; Sanjurjo-Rodríguez, C.; Piñeiro-Ramil, M.; Rodríguez-Fernández, S.; López-Baltar, I.; Fuentes-Boquete, I.; Blanco, F.J.; Díaz-Prado, S. Tips and Tricks for Successfully Culturing and Adapting Human Induced Pluripotent Stem Cells. Mol. Ther. Methods Clin. Dev. **2021**, *23*, 569-581.

[107] Nikokiraki, C.; Psaraki, A.; Roubelakis, M.G. The Potential Clinical use of Stem/Progenitor Cells and Organoids in Liver Diseases. Cells **2022**, *11*, 1410. doi: 10.3390/cells11091410.
[108] Ajmal, L.; Ajmal, S.; Ajmal, M.; Nawaz, G. Organ Regeneration through Stem Cells and Tissue Engineering. Cureus **2023**, *15*, e34336.
[109] Takeishi, K.; Collin de l'Hortet, A.; Wang, Y.; Handa, K.; Guzman-Lepe, J.; Matsubara, K.; Morita, K.; Jang, S.; Haep, N.; Florentino, R.M. *et al.* Assembly and Function of a Bioengineered Human Liver for Transplantation Generated Solely from Induced Pluripotent Stem Cells. Cell. Rep. **2020**, *31*, 107711.
[110] Boers, S.N.; van Delden, J.J.; Clevers, H.; Bredenoord, A.L. Organoid Biobanking: Identifying the Ethics: Organoids Revive Old and Raise New Ethical Challenges for Basic Research and Therapeutic Use. EMBO Rep. **2016**, *17*, 938-941.
[111] Takebe, T.; Wells, J.M.; Helmrath, M.A.; Zorn, A.M. Organoid Center Strategies for Accelerating Clinical Translation. Cell. Stem Cell. **2018**, *22*, 806-809.
[112] Nuwer, R. US Agency Seeks to Phase Out Animal Testing. Nature **2022**.
[113] Neuhaus, W.; Reininger-Gutmann, B.; Rinner, B.; Plasenzotti, R.; Wilflingseder, D.; De Kock, J.; Vanhaecke, T.; Rogiers, V.; Jírová, D.; Kejlová, K. *et al.* The Rise of Three Rs Centres and Platforms in Europe. Altern. Lab. Anim. **2022**, *50*, 90-120.
[114] van Meer, P.; Theunissen, P.; van den Hoorn, T.; Herberts, C.; van der Laan, J.W. Animal-Free Applications in the Development of Cell-Based Therapies. Br. J. Clin. Pharmacol. **2021**, *87*, 2425-2427.
[115] European Commission. Regulation (EC) no 1223/2009 of the European Parliament and of the Council of 30 November 2009 on Cosmetic Products. . **2009**.
[116] US Congress. FDA Modernization Act 2.0. **2022**.
[117] Punt, A.; Bouwmeester, H.; Blaauboer, B.J.; Coecke, S.; Hakkert, B.; Hendriks, D.F.G.; Jennings, P.; Kramer, N.I.; Neuhoff, S.; Masereeuw, R. *et al.* New Approach Methodologies (NAMs) for Human-Relevant Biokinetics Predictions. Meeting the Paradigm Shift in Toxicology Towards an Animal-Free Chemical Risk Assessment. ALTEX **2020**, *37*, 607-622.
[118] Thomas, R.S.; Philbert, M.A.; Auerbach, S.S.; Wetmore, B.A.; Devito, M.J.; Cote, I.; Rowlands, J.C.; Whelan, M.P.; Hays, S.M.; Andersen, M.E. *et al.* Incorporating New Technologies into Toxicity Testing and Risk Assessment: Moving from 21st Century Vision to a Data-Driven Framework. Toxicol. Sci. **2013**, *136*, 4-18.
[119] Leist, M.; Ghallab, A.; Graepel, R.; Marchan, R.; Hassan, R.; Bennekou, S.H.; Limonciel, A.; Vinken, M.; Schildknecht, S.; Waldmann, T. *et al.* Adverse Outcome Pathways: Opportunities, Limitations and Open Questions. Arch. Toxicol. **2017**, *91*, 3477-3505.
[120] Escher, S.E.; Partosch, F.; Konzok, S.; Jennings, P.; Luijten, M.; Kienhuis, A.; de Leeuw, V.; Reuss, R.; Lindemann, K.; Bennekou, S.H. Development of a Roadmap for Action on New Approach Methodologies in Risk Assessment. EFSA Supporting Publications **2022**, *19*, 7341E.
[121] Weaver, R.J.; Blomme, E.A.; Chadwick, A.E.; Copple, I.M.; Gerets, H.H.J.; Goldring, C.E.; Guillouzo, A.; Hewitt, P.G.; Ingelman-Sundberg, M.; Jensen, K.G. *et al.* Managing the Challenge of Drug-Induced Liver Injury: A Roadmap for the Development and Deployment of Preclinical Predictive Models. Nat. Rev. Drug Discov. **2020**, *19*, 131-148.
[122] Serras, A.S.; Rodrigues, J.S.; Cipriano, M.; Rodrigues, A.V.; Oliveira, N.G.; Miranda, J.P. A Critical Perspective on 3D Liver Models for Drug Metabolism and Toxicology Studies. Front. Cell. Dev. Biol. **2021**, *9*, 626805.

[123] OECD. OECD Series on Testing and Assessment no. 260: Guidance Document on the use of Adverse Outcome Pathways in Developing Integrated Approaches to Testing and Assessment (IATA). **2016**.
[124] Pamies, D.; Hartung, T. 21st Century Cell Culture for 21st Century Toxicology. Chem. Res. Toxicol. **2017**, *30*, 43-52.
[125] Kyffin, J.A.; Sharma, P.; Leedale, J.; Colley, H.E.; Murdoch, C.; Mistry, P.; Webb, S.D. Impact of Cell Types and Culture Methods on the Functionality of in Vitro Liver Systems - A Review of Cell Systems for Hepatotoxicity Assessment. Toxicol. In. Vitro. **2018**, *48*, 262-275.
[126] Yang, S.; Ooka, M.; Margolis, R.J.; Xia, M. Liver Three-Dimensional Cellular Models for High-Throughput Chemical Testing. Cell. Rep. Methods **2023**, *3*, 100432.
[127] Hirsch, C.; Schildknecht, S. In Vitro Research Reproducibility: Keeping Up High Standards. Front. Pharmacol. **2019**, *10*, 1484.
[128] Pamies, D.; Leist, M.; Coecke, S.; Bowe, G.; Allen, D.G.; Gstraunthaler, G.; Bal-Price, A.; Pistollato, F.; de Vries, R.B.M.; Hogberg, H.T. *et al.* Guidance Document on Good Cell and Tissue Culture Practice 2.0 (GCCP 2.0). ALTEX **2022**, *39*, 30-70.
[129] Hartung, T.; Balls, M.; Bardouille, C.; Blanck, O.; Coecke, S.; Gstraunthaler, G.; Lewis, D.; ECVAM Good Cell Culture Practice Task Force. Good Cell Culture Practice. ECVAM Good Cell Culture Practice Task Force Report 1. Altern. Lab. Anim. **2002**, *30*, 407-414.
[130] Coecke, S.; Balls, M.; Bowe, G.; Davis, J.; Gstraunthaler, G.; Hartung, T.; Hay, R.; Merten, O.; Price, A.; Schechtman, L. *et al.* Guidance on Good Cell Culture Practice. a Report of the Second ECVAM Task Force on Good Cell Culture Practice. Altern. Lab. Anim. **2005**, *33*, 261-287.
[131] OECD. OECD Series on Testing and Assessment: Guidance Documents on Good in Vitro Method Practices (GIVIMP). **2018**.
[132] Ulrey, A.; Kolle, S.; Landsiedel, R.; Hill, E. How a GIVIMP Certification Program can Increase Confidence in in Vitro Methods. ALTEX **2021**, *38*, 316-318.
[133] Cassotta, M.; Bartnicka, J.J.; Pistollato, F.; Parvatam, S.; Weber, T.; D'Alessandro, V.; Bastos, L.F.; Coecke, S. A Worldwide Survey on the use of Animal-Derived Materials and Reagents in Scientific Experimentation. Eng. Life. Sci. **2022**, *22*, 564-583.
[134] Oredsson, S.; Coecke, S.; van der Valk, J.; Vinken, M. What is Understood by "Animal-Free Research"? Toxicol. In. Vitro. **2019**, *57*, 143-144.
[135] Singh, B.; Abdelgawad, M.E.; Ali, Z.; Bailey, J.; Budyn, E.; Civita, P.; Clift, M.J.D.; Connelly, J.T.; Constant, S.; Hittinger, M. *et al.* Towards More Predictive, Physiological and Animal-Free in Vitro Models: Advances in Cell and Tissue Culture 2020 Conference Proceedings. Altern. Lab. Anim. **2021**, *49*, 93-110.
[136] Naik, N.N.; Vadloori, B.; Poosala, S.; Srivastava, P.; Coecke, S.; Smith, A.; Akhtar, A.; Roper, C.; Radhakrishnan, S.; Bhyravbhatla, B. *et al.* Advances in Animal Models and Cutting-Edge Research in Alternatives: Proceedings of the Third International Conference on 3Rs Research and Progress, Vishakhapatnam, 2022. Altern. Lab. Anim. **2023**, 2611929231180428.
[137] van der Valk, J.; Bieback, K.; Buta, C.; Cochrane, B.; Dirks, W.G.; Fu, J.; Hickman, J.J.; Hohensee, C.; Kolar, R.; Liebsch, M. *et al.* Fetal Bovine Serum (FBS): Past - Present - Future. ALTEX **2018**, *35*, 99-118.

[138] Sekine, K.; Ogawa, S.; Tsuzuki, S.; Kobayashi, T.; Ikeda, K.; Nakanishi, N.; Takeuchi, K.; Kanai, E.; Otake, Y.; Okamoto, S. *et al.* Generation of Human Induced Pluripotent Stem Cell-Derived Liver Buds with Chemically Defined and Animal Origin-Free Media. Sci. Rep. **2020**, *10*, 17937-1.
[139] Hua, Y.; Yoshimochi, K.; Li, J.; Takekita, K.; Shimotsuma, M.; Li, L.; Qu, X.; Zhang, J.; Sawa, Y.; Liu, L. *et al.* Development and Evaluation of a Novel Xeno-Free Culture Medium for Human-Induced Pluripotent Stem Cells. Stem Cell. Res. Ther. **2022**, *13*, 223-z.
[140] Aisenbrey, E.A.; Murphy, W.L. Synthetic Alternatives to Matrigel. Nat. Rev. Mater. **2020**, *5*, 539-551.
[141] Kozlowski, M.T.; Crook, C.J.; Ku, H.T. Towards Organoid Culture without Matrigel. Commun. Biol. **2021**, *4*, 1387-8.
[142] Duarte, A.C.; Costa, E.C.; Filipe, H.A.L.; Saraiva, S.M.; Jacinto, T.; Miguel, S.P.; Ribeiro, M.P.; Coutinho, P. Animal-Derived Products in Science and Current Alternatives. Biomater. Adv. **2023**, *151*, 213428.
[143] Pamies, D.; Bal-Price, A.; Chesné, C.; Coecke, S.; Dinnyes, A.; Eskes, C.; Grillari, R.; Gstraunthaler, G.; Hartung, T.; Jennings, P. *et al.* Advanced Good Cell Culture Practice for Human Primary, Stem Cell-Derived and Organoid Models as Well as Microphysiological Systems. ALTEX **2018**, *35*, 353-378.
[144] Pamies, D.; Bal-Price, A.; Simeonov, A.; Tagle, D.; Allen, D.; Gerhold, D.; Yin, D.; Pistollato, F.; Inutsuka, T.; Sullivan, K. *et al.* Good Cell Culture Practice for Stem Cells and Stem-Cell-Derived Models. ALTEX **2017**, *34*, 95-132.
[145] Tigges, J.; Bielec, K.; Brockerhoff, G.; Hildebrandt, B.; Hübenthal, U.; Kapr, J.; Koch, K.; Teichweyde, N.; Wieczorek, D.; Rossi, A. *et al.* Academic Application of Good Cell Culture Practice for Induced Pluripotent Stem Cells. ALTEX **2021**, *38*, 595-614.
[146] Molina-Ruiz, F.J.; Introna, C.; Bombau, G.; Galofre, M.; Canals, J.M. Standardization of Cell Culture Conditions and Routine Genomic Screening Under a Quality Management System Leads to Reduced Genomic Instability in hPSCs. Cells **2022**, *11*, 1984. doi: 10.3390/cells11131984.
[147] Ye, S.; Boeter, J.W.B.; Mihajlovic, M.; van Steenbeek, F.G.; van Wolferen, M.E.; Oosterhoff, L.A.; Marsee, A.; Caiazzo, M.; van der Laan, L.J.W.; Penning, L.C. *et al.* A Chemically Defined Hydrogel for Human Liver Organoid Culture. Adv. Funct. Mater. **2020**, *30*, 2000893.
[148] Vonk, A.M.; van Mourik, P.; Ramalho, A.S.; Silva, I.A.L.; Statia, M.; Kruisselbrink, E.; Suen, S.W.F.; Dekkers, J.F.; Vleggaar, F.P.; Houwen, R.H.J. *et al.* Protocol for Application, Standardization and Validation of the Forskolin-Induced Swelling Assay in Cystic Fibrosis Human Colon Organoids. STAR Protoc. **2020**, *1*, 100019.
[149] Bose, S.; Clevers, H.; Shen, X. Promises and Challenges of Organoid-Guided Precision Medicine. Med. **2021**, *2*, 1011-1026.
[150] Dossena, M.; Piras, R.; Cherubini, A.; Barilani, M.; Dugnani, E.; Salanitro, F.; Moreth, T.; Pampaloni, F.; Piemonti, L.; Lazzari, L. Standardized GMP-Compliant Scalable Production of Human Pancreas Organoids. Stem Cell. Res. Ther. **2020**, *11*, 94-2.
[151] Jain, P.; Kathuria, H.; Dubey, N. Advances in 3D Bioprinting of Tissues/Organs for Regenerative Medicine and in-Vitro Models. Biomaterials **2022**, *287*, 121639.
[152] Lam, E.H.Y.; Yu, F.; Zhu, S.; Wang, Z. 3D Bioprinting for Next-Generation Personalized Medicine. Int. J. Mol. Sci. **2023**, *24*, 6357. doi: 10.3390/ijms24076357.

[153] Bas, A.; Burns, N.; Gulotta, A.; Junker, J.; Drasler, B.; Lehner, R.; Aicher, L.; Constant, S.; Petri-Fink, A.; Rothen-Rutishauser, B. Understanding the Development, Standardization, and Validation Process of Alternative in Vitro Test Methods for Regulatory Approval from a Researcher Perspective. Small **2021**, *17*, e2006027.

[154] Nitsche, K.S.; Müller, I.; Malcomber, S.; Carmichael, P.L.; Bouwmeester, H. Implementing Organ-on-Chip in a Next-Generation Risk Assessment of Chemicals: A Review. Arch. Toxicol. **2022**, *96*, 711-741.

[155] Zhou, J.; Ellis, A.V.; Voelcker, N.H. Recent Developments in PDMS Surface Modification for Microfluidic Devices. Electrophoresis **2010**, *31*, 2-16.

[156] Cao, U.M.N.; Zhang, Y.; Chen, J.; Sayson, D.; Pillai, S.; Tran, S.D. Microfluidic Organ-on-A-Chip: A Guide to Biomaterial Choice and Fabrication. Int. J. Mol. Sci. **2023**, *24*, 3232. doi: 10.3390/ijms24043232.

[157] Briem, D.; Strametz, S.; Schröder, K.; Meenen, N.M.; Lehmann, W.; Linhart, W.; Ohl, A.; Rueger, J.M. Response of Primary Fibroblasts and Osteoblasts to Plasma Treated Polyetheretherketone (PEEK) Surfaces. J. Mater. Sci. Mater. Med. **2005**, *16*, 671-677.

[158] Noiset, O.; Schneider, Y.J.; Marchand-Brynaert, J. Adhesion and Growth of CaCo2 Cells on Surface-Modified PEEK Substrata. J. Biomater. Sci. Polym. Ed. **2000**, *11*, 767-786.

[159] El-Masri, H.; Paul Friedman, K.; Isaacs, K.; Wetmore, B.A. Advances in Computational Methods Along the Exposure to Toxicological Response Paradigm. Toxicol. Appl. Pharmacol. **2022**, *450*, 116141.

[160] Jaroch, K.; Jaroch, A.; Bojko, B. Cell Cultures in Drug Discovery and Development: The Need of Reliable in Vitro-in Vivo Extrapolation for Pharmacodynamics and Pharmacokinetics Assessment. J. Pharm. Biomed. Anal. **2018**, *147*, 297-312.

[161] Zhang, Q.; Li, J.; Middleton, A.; Bhattacharya, S.; Conolly, R.B. Bridging the Data Gap from in Vitro Toxicity Testing to Chemical Safety Assessment through Computational Modeling. Front. Public. Health. **2018**, *6*, 261.

[162] Burden, N.; Clift, M.J.D.; Jenkins, G.J.S.; Labram, B.; Sewell, F. Opportunities and Challenges for Integrating New in Vitro Methodologies in Hazard Testing and Risk Assessment. Small **2021**, *17*, e2006298.

[163] Westmoreland, C.; Bender, H.J.; Doe, J.E.; Jacobs, M.N.; Kass, G.E.N.; Madia, F.; Mahony, C.; Manou, I.; Maxwell, G.; Prieto, P. *et al.* Use of New Approach Methodologies (NAMs) in Regulatory Decisions for Chemical Safety: Report from an EPAA Deep Dive Workshop. Regul. Toxicol. Pharmacol. **2022**, *135*, 105261.

[164] OECD. OECD Series on Testing and Assessment no. 34: Guidance Document on the Validation and International Acceptance of New Or Updates Test Methods for Hazard Assessment. **2005**.

[165] van der Zalm, A.J.; Barroso, J.; Browne, P.; Casey, W.; Gordon, J.; Henry, T.R.; Kleinstreuer, N.C.; Lowit, A.B.; Perron, M.; Clippinger, A.J. A Framework for Establishing Scientific Confidence in New Approach Methodologies. Arch. Toxicol. **2022**, *96*, 2865-2879.

[166] Zgheib, E.; Kim, M.J.; Jornod, F.; Bernal, K.; Tomkiewicz, C.; Bortoli, S.; Coumoul, X.; Barouki, R.; De Jesus, K.; Grignard, E. *et al.* Identification of Non-Validated Endocrine Disrupting Chemical Characterization Methods by Screening of the Literature using Artificial Intelligence and by Database Exploration. Environ. Int. **2021**, *154*, 106574.

[167] Krans, N.A.; Ammar, A.; Nymark, P.; Willighagen, E.L.; Bakker, M.I.; Quik, J.T.K. FAIR Assessment Tools: Evaluating use and Performance. NanoImpact **2022**, *27*, 100402.
[168] Zare Jeddi, M.; Virgolino, A.; Fantke, P.; Hopf, N.B.; Galea, K.S.; Remy, S.; Viegas, S.; Mustieles, V.; Fernandez, M.F.; von Goetz, N. *et al.* A Human Biomonitoring (HBM) Global Registry Framework: Further Advancement of HBM Research Following the FAIR Principles. Int. J. Hyg. Environ. Health **2021**, *238*, 113826.
[169] EURL ECVAM. Tracking System for Alternative Methods Towards Regulatory Acceptance.
[170] Lee, H. Engineering in Vitro Models: Bioprinting of Organoids with Artificial Intelligence. Cyborg Bionic Syst. **2023**, *4*, 0018.
[171] Luechtefeld, T.; Hartung, T. Computational Approaches to Chemical Hazard Assessment. ALTEX **2017**, *34*, 459-478.
[172] Brockmeier, E.K.; Hodges, G.; Hutchinson, T.H.; Butler, E.; Hecker, M.; Tollefsen, K.E.; Garcia-Reyero, N.; Kille, P.; Becker, D.; Chipman, K. *et al.* The Role of Omics in the Application of Adverse Outcome Pathways for Chemical Risk Assessment. Toxicol. Sci. **2017**, *158*, 252-262.
[173] Yang, Y.; Yu, Z.; Lu, X.; Dai, J.; Zhou, C.; Yan, J.; Wang, L.; Wang, Z.; Zang, J. Minimally Invasive Bioprinting for in Situ Liver Regeneration. Bioact. Mater. **2023**, *26*, 465-477.

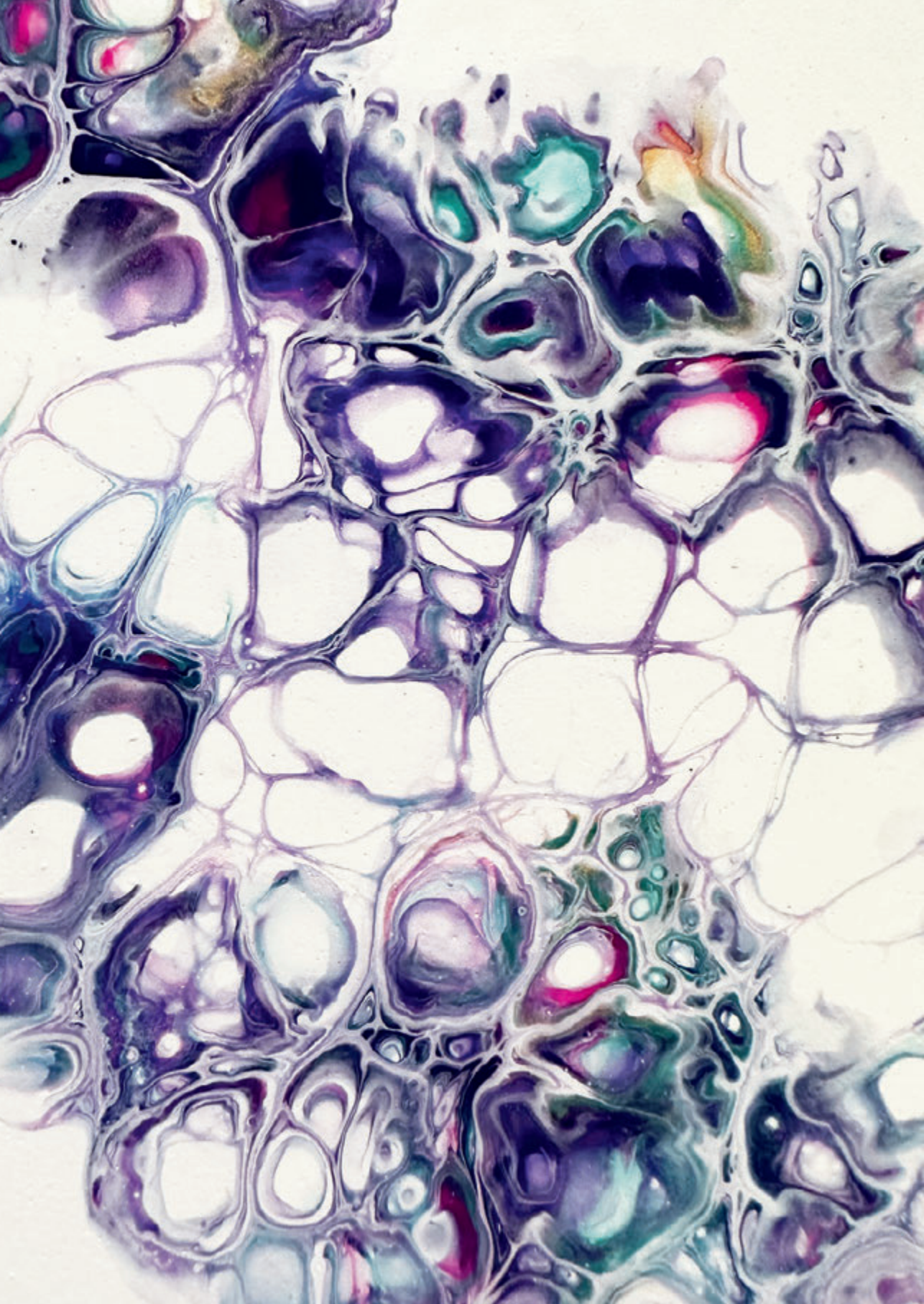

Addendum

A

NEDERLANDSE SAMENVATTING

De lever is belangrijk voor het omzetten van lichaamsvreemde stoffen, bijvoorbeeld medicijnen en chemische stoffen, zodat deze stoffen gemakkelijker door het lichaam kunnen worden uitgescheiden. In dit proces van biotransformatie worden giftige stoffen onschadelijk gemaakt, maar er kunnen ook juist schadelijke afbraakstoffen (metabolieten) worden gevormd. Hierom is de lever gevoelig voor schade veroorzaakt door lichaamsvreemde stoffen.

Het testen van de veiligheid van nieuwe medicijnen en chemische stoffen voor de mens wordt veelal in proefdieren uitgevoerd. Door verschillen tussen mens en dier is dit niet altijd accuraat. Er is een verandering gaande naar alternatieve methoden om risicobeoordeling uit te kunnen voeren voor de veiligheid van deze stoffen. Daarnaast draagt deze transitie er aan bij om het gebruik van proefdieren te verminderen. Nieuwe methoden zijn, onder andere, gebaseerd op het gebruik van computermodellen (*in silico*) of celmodellen (*in vitro*).

In dit proefschrift worden leverorganoïden gebruikt als *in vitro* model. Om leverorganoïden te maken, worden cellen verkregen uit menselijke donorlevers en worden deze gekweekt als drie-dimensionale (3D) structuren in een hydrogel: organoïden. Deze organoïden kunnen door de samenstelling van het kweekmedium gestuurd worden om te differentiëren naar cholangiocyten (galgangcellen) of hepatocyten (levercellen). Een van de voordelen van leverorganoïden is dat ze, in tegenstelling tot veel andere *in vitro* levermodellen, afkomstig zijn van verschillende donoren en daardoor ook het verschil in biotransformatie tussen mensen onderzocht kan worden. Daarbij worden deze organoïden beschouwd als waardevol model voor het ontrafelen van ziekte mechanismen.

In **Hoofdstuk 2** van dit proefschrift is het genexpressie profiel van die enzymen betrokken zijn in biotransformatie processen onderzocht in zowel leverorganoïden, als in een veelgebruikte hepatische cellijn (HepaRG) en primaire hepatocyten. Ook zijn deze drie celsystemen blootgesteld aan stoffen waarvan bekend is dat ze levertoxiciteit veroorzaken. De resultaten beschreven in Hoofdstuk 2 laten zien dat sommige belangrijke biotransformatie enzymen in leverorganoïden vergelijkbaar tot expressie komen als in HepaRG en/of primaire hepatocyten, maar dat de activiteit van sommige enzymen lager was ten opzichte van HepaRG en/of primaire hepatocyten. Daarnaast is aangetoond dat de schadelijkheid van sommige stoffen goed te voorspellen is in leverorganoïden, maar van andere stoffen (nog) niet, zoals wel in primaire hepatocyten. Verder onderzoek naar de activiteit van eiwitten betrokken in biotransformatie processen in leverorganoïden en blootstelling van

leverorganoïden aan een uitgebreidere selectie stoffen kunnen bijdragen aan het specificeren van de mogelijke toepassingen van leverorganoïden voor het testen van levertoxiciteit. Daarnaast kan het verbeteren van de hepatische functionaliteit van de organoïden, en daarmee het verbeteren van biotransformatie processen, meehelpen om de potentie van leverorganoïden in het voorspellen van toxiciteit van lichaamsvreemde stoffen te vergroten.

Door leverorganoïden te kweken in een omgeving die lijkt op wat cellen in de menselijke lever ervaren kan de functionaliteit van leverorganoïden (en daarmee de biotransformatie van stoffen) worden verbeterd. Geavanceerde technieken, zogeheten biofabricage technieken, zoals het 3D-printen van cellen (bioprinten) in complexe structuren, kunnen een lever-achtige omgeving creëren. In **Hoofdstuk 3** en **Hoofdstuk 4** van dit proefschrift is aangetoond dat de combinatie van leverorganoïden en verschillende bioprinttechnieken mogelijkheden biedt tot het maken van een complexere omgeving die de functionaliteit van leverorganoïden verbeterd. De printtechniek beschreven in Hoofdstuk 3 is gebaseerd op extrusie. Bij deze technieken zitten organoïden in een hydrogel in de cartridge van de printer en wordt deze bio-inkt met luchtdruk door een naald geperst en op de juiste positie geprint. Deze techniek biedt de mogelijkheid tot het precies positioneren van de hydrogel met cellen en door het gebruik van meerdere cartridges kunnen verschillende celtypen worden gecombineerd. Echter zijn ondersteunende structuren nodig bij het printen van complexere ontwerpen en kunnen de 3D organoïden structuren breken doordat ze door een dunne naald worden gedrukt. In Hoofdstuk 4 wordt de combinatie van leverorganoïden met volumetrisch bioprinten beschreven. Ook in deze techniek zijn de organoïden opgenomen in een hydrogel (de bio-inkt) in een glazen cartridge. De cartridge wordt in de printer van meerdere kanten met licht beschenen en, door de lichtgevoelige eigenschappen van de hydrogel, ontstaat er een construct op het snijvlak van de lichtstralen. Deze naaldvrije printtechniek is vriendelijker voor de cellen en kan complexe ontwerpen printen in tientallen seconden zonder ondersteunende structuren. Ontwikkelingen om te kunnen printen met verschillende materialen en verschillende celtypen tegelijk zijn nog gaande. In dit proefschrift is aangetoond dat het bioprinten van leverorganoïden mogelijk is met verschillende technieken en resulteert in levende en functionerende organoïden. De resultaten beschreven in Hoofdstuk 3 en 4 banen een weg naar de ontwikkeling van complexe ontwerpen met (lever) organoïden die bij kunnen dragen in studies naar leverschade door lichaamsvreemde stoffen of als ziektemodel.

Het dynamische kweken van de geprinte constructen kan de omgeving die cellen in de menselijke lever ervaren verder nabootsen en is beschreven om de functionaliteit van leverorganoïden te verbeteren. In Hoofdstuk 4 is

aangetoond dat perfusie (24 uur) van de geprinte organoïden constructen resulteert in verhoogde uitscheiding van ammoniak, hier gebruikt als marker voor lever functionaliteit. Daarnaast is in **Hoofdstuk 5** de ontwikkeling van een op maat gemaakte kweekkamer beschreven. Deze kweekkamer staat continue perfusie van geprinte constructen toe, vergelijkbaar met de bloedstroom in de menselijke lever. Daarnaast is het vervangen van het kweekmedium geautomatiseerd en is het mogelijk om mediummonsters te nemen zonder de circulatie te verstoren. De resultaten in Hoofdstuk 5 laten zien dat constructen 7 dagen kunnen worden geperfuseerd en dat organoïden blijven leven. Hoewel er aanwijzingen zijn voor verhoogde hepatische functionaliteit van de leverorganoïden, is verder onderzoek, met meerdere eindpunten en organoïden van verschillende donoren, nodig. Andere vervolgstappen zijn het optimaliseren van de perfusie snelheid en het vergroten van de complexiteit van de constructen, bijvoorbeeld door het gebruik van andere celtypen uit de lever. Samengevat, de ontwikkelde kweekkamer is geschikt voor het perfuseren van geprinte constructen en daarmee biedt het mogelijkheden voor studies naar gedetailleerde werkingsmechanismen van, bijvoorbeeld, leverschade.

In dit proefschrift is een stap gezet in het karakteriseren van leverorganoïden als *in vitro* model voor het testen van levertoxiciteit. De combinatie van leverorganoïden met biofabricage technieken, zoals bioprinten en het toepassen van perfusie, baant een weg naar verbeterde hepatische functionaliteit en vergroot daarmee de toepassing van donor-verkregen leverorganoïden. Ontwikkelingen in de werkvelden gefocust op organoïden en biofabricage kunnen een brug slaan tussen proefdieren en simplistische *in vitro* modellen. Gezien de huidige transitie naar het gebruik van *in vitro* en *in silico* methoden in risicobeoordeling, dragen de resultaten beschreven in dit proefschrift bij aan deze verschuiving naar alternatieve modellen voor levertoxiciteit.

PHD PORTFOLIO

	Year	Workload (ECTS)
General courses		
Writing a scientific paper	2018	2.0
Achieving your goals and performing more successfully during your PhD	2019	1.0
Illustrator	2020	0.6
Responsible conduct of research: how to do it right?	2021	0.4
Specific courses: Post-graduate Education in Toxicology		
Molecular Toxicology	2019	1.5
Cell Toxicology	2019	1.5
Medical en Forensic Toxicology	2019	2.0
Pathobiology and Toxicological Pathology	2020	1.5
Organ Toxicology	2020	1.5
Ecotoxicology	2021	3.0
Risk Communication	2021	1.5
Legal and Regulatory Toxicology	2021	1.5
Seminars, workshops and masterclasses		
Symposium Pharmaceutical Toxicology, Amsterdam.	2019	0.3
Summerschool JRC: Non-Animal Approaches in Science, Ispra, Italy.	2019	1.0

	Year	Workload (ECTS)
Presentations at conferences		
Nederlandse Vereniging van Toxicology, Hilversum. Oral presentation.	2018	0.6
Veterinary Science Day, Bunnik. Poster presentation.	2018	0.3
Nederlandse Vereniging van Toxicology, Ede. Pitch and poster presentation.	2019	0.6
Veterinary Science Day, online. Poster presentation.	2020	0.3
Nederlandse Vereniging van Toxicology, Ede. Poster presentation.	2022	0.3
Digestive Disease Days, Veldhoven. Pitch presentation.	2023	0.3
Visited conferences no presentation		
Dutch Liver Retreat, Spier.	2018 - 2020	1.8
International Society of Stem Cell Research, Amsterdam.	2019	0.3
Teaching activities		
Practical activity (bachelor Biology, summerschool RM; 5x)		
Workshop toxicokinetics (bachelor Biology; 3x)		
Supervision research proposal (bachelor Biology)		
Supervision writing assignment (master Biofabrication; 2x)		
Supervision 9-month research internships (2 students)		
Supervision 2-weeks internship (bachelor Biology; 3x)		
Other activities		
Veterinary Science Day, organizing committee	2019	
Video for Corning Life Sciences *Upscaling of Liver Organoids using Corning® Disposable Spinner Flasks*		
Video for One Medicine Utrecht		
Awards		
Finalist Young Hepatologist Award 2023		

LIST OF PUBLICATIONS

Bouwmeester, M.C., Bernal, P.N., Oosterhoff, L.A., van Wolferen, M.E., Lehmann, V., Vermaas, M., Buchholz, M., Peiffer, Q.C., Malda, J., van der Laan, L.J.W., Kramer, N.I., Schneeberger, K., Levato, R., Spee, B. (2021) Bioprinting of Human Liver-Derived Epithelial Organoids for Toxicity Studies. *Macromol Biosci,* 21 (12).

Bernal, P.N.*, **Bouwmeester, M.C.***, Madrid-Wolff, J., Falandt, M., Florczak, S., Ginés Rodriguez, N., Li, Y., Gröβbacher, G., Samsom, R.A., van Wolferen, M., van der Laan, L.J.W., Delrot, P., Loterie, D., Malda, J., Moser, C., Spee, B., Levato, R. (2022) Volumetric Bioprinting of Organoids and Optically Tuned Hydrogels to Build Liver-Like Metabolic Biofactories. *Adv Mat* 34 (15). *contributed equally

Bouwmeester, M.C., Tao, Y., Proença, S., van Steenbeek, F.G., Samsom, R.A., Nijmeijer, S.M., Sinnige, T., van der Laan, L.J.W., Legler, J., Schneeberger, K., Kramer, N.I., Spee, B. (2023) Drug Metabolism of Hepatocyte-Like Organoids and Their Applicability in In Vitro Toxicity Testing. *Molecules*, 28(2), 621.

DANKWOORD

Bij het schrijven van dit dankwoord bedacht ik me pas op hoe grote rol theetjes, koffietjes en taartjes speelden door de jaren heen. Een theetje wordt niet zonder reden 'a hug in a cup' genoemd, dat kon ik soms wel gebruiken. Maar met goed gezelschap smaken ze nog beter. Daarom wil ik de volgende mensen graag bedanken.

Mijn co-promotor, **dr. Bart Spee**, beste Bart. Grappig dat Hans jou eerder kende dan ik jou, niet wetende dat ik ooit bij jou terecht zou komen. Dankjewel voor het vertrouwen dat je had in dit project en in mij, terwijl ik dat zelf weleens kwijt was. Dankjewel voor het stroomlijnen van mijn gedachtegang ("MAND") en helpen keuzes maken ("ok, zal ik kiezen?"). Dankje voor je openheid, bereikbaarheid en voor jouw oplossingsgerichtheid. Ik ben blij dat jij mijn co-promotor was!

Mijn co-promotor, **dr. Nynke Kramer**, beste Nynke. Mijn eerste stage tijdens mijn master was bij jou. Ik raakte geïnspireerd door *in vitro* toxicologie, en werd zelfs enthousiast over *in vitro* kinetiek (!). Het tox-gedeelte van mijn PhD kwam vooral in de laatste twee jaar, maar ik ben blij met ons contact tijdens mijn hele PhD. Dankjewel voor de cappuccino's in het Johanna, en vooral voor jouw gedrevenheid en enthousiasme!

Mijn promotor, **prof.dr. Juliette Legler**, beste Juliette. Toen we samenwerkten aan het zebravis paper in 2014 was het toch ondenkbaar (vond ik tenminste) dat je ooit mijn promotor zou zijn. Dankjewel dat je wilde instappen in het 3e jaar van mijn PhD traject, ik ben erg blij dat je er de laatste twee jaar bij betrokken was. Enthousiast, maar ook kritisch. We komen elkaar vast weer tegen in het endocrien veld!

Graag wil ik de leden van **de leescommissie**, prof.dr. Martin van den Berg, prof.dr. Pedro Baptista, prof.dr. Roos Masereeuw, prof.dr. Bernds Helms en dr. Anne Kienhuis, hartelijk bedanken voor het beoordelen van mijn proefschrift.

Ook dank ik de **LIVeCon groep** bestaande uit prof.dr. Niels Geijsen, dr. Sabine Fuchs, prof.dr. Jos Malda, dr. Riccardo Levato, dr. Farzin Pourfarzad, Dave Wanders en José Willemse. Bedankt voor jullie kritische vragen en inzichten tijdens onze halfjaarlijkse meetings die mijn onderzoek weer verder hielpen.

A big thank you to all (ex-)STEAM-members for their interest, support and just for being around. A special thanks to: **Adam**, I enjoyed our meetings in my last year. Thanks for your input and critical notes. **Ary**, I admire your drive. Proud

of what you accomplished in the last couple of years! All the best for you! **FrankvS**, dankjewel voor je flauwe grappen en nuchtere adviezen. **Kerstin**, wat een powervrouw ben jij! Ik vond het heel fijn dat jij er was met jouw nuchtere kijk maar kritische blik en het delen van dezelfde granny hobbies (haken en bloemen zaaien) en interesses (Paleis voor een prikkie). **Lisa**, ik vond het jammer dat je pas vlak voordat ik weg was bij ons in de groep kwam, het had me leuk geleken om samen te werken! **Loes**, super leuk om elkaar na onze bachelor weer tegen te komen op het JDV. Mijn experimentele en emotionele steun en toeverlaat in drie jaar van mijn PhD. Jouw hulp met bioprinten in 2e jaar kwam als geroepen. Dank voor het delen van alle ~30-ers dillema's en kwaaltjes, wedding en baby vibes. Je bent een topper! **Louis**, bedankt voor het delen van al je biologische kennis en hersenspinsels. **Marjolein**, gezellig dat je een aantal jaar bleef plakken bij onze groep. Heel veel succes in Eindhoven! **Monique**, bedankt voor jouw experimentele support en koffiemomentjes met chocola. **Roos-Anne**, dankjewel voor jouw gezelligheid en support – altijd in voor een theetje of gewoon om samen door RMCU te hobbelen. We komen gauw weer kijken op de boerderij! **Shicheng**, we started with the two of us in the same office. After the move to RMCU, we stayed buddies. Thanks for cheering me up, thanks for all the cookies and chocolate on our shared shelf in times of hunger or PhD-frustrations (we agreed to bring both cookies, but I forgot to bring them most of the times and also ate them most of the times), thanks your motivational words ("you cry AGAIN?") and feeding my organoids in the weekends. I'm proud of you! **Vivian**, fijn dat jij me kwam vergezellen op ons project, het bleek een goede match. Dank voor alle cappuccino's en warme choco's, chocolademuffins, moestuinpraat en wederzijdse peptalks – dank voor het samen trotseren van de academische wereld. Dankjewel dat je mijn paranymf bent! Shicheng and Vivian, thanks for the PhTeas at the end of our journey which were very valuable. **Yu**, I've spent my first Mother's day with you plating hepatocytes and you brought me flowers. You're such a sweetheart and thoughtful person. I am sure that your positive mindset will bring you far. I would love to see how you bring the bioreactor project further. All the best for you! **Zhenguo**, you're such a happy person, thanks for cheering me up! Good luck with finishing up! Thanks to my students: **Maj-Britt**, je was al begonnen met je stage voordat ik met mijn PhD was begonnen: Een vliegende start voor mij, want jij ging als een speer. Dankjewel voor alles wat je me geleerd hebt over het bioprinten. **Tom**, ik had me geen andere en betere student kunnen wensen in mijn laatste jaar. Veel gelachen, soms dacht ik "Tohommm….", maar vaak kwam het toch goed. Veel succes met jouw PhD!

Dankjewel **Dave** voor jouw hulp met het perfusie systeem. Jouw technische inzichten en ideeën waren super nuttig. Ik vond het gezellig om met een koffie over de bioreactor te kletsen. Thanks **Riccardo**, **Paulina**, and other members

of Levato lab for the support regarding printing with the RegenHU, thoughts on GelMA, photocrosslinking, blue lights etc. Riccardo, thanks for inspiring, thinking out of the box, and to think in possibilities. Paulina, thanks for letting me mix our bioinks with 'chocolate sprinkles' while you focused on the rest of the VBP-printing procedure and talk about dogs and hamsters. It was a pleasure to work on the bioprinting papers with you! Thank you members of the ATX-group, specifically **Emma**, **Susana**, **Sandra**, **Theo**. Dank jullie wel voor de brainstorm sessies, jullie input en dat ik me welkom voelde ook al kwam ik maar af en toe aanwaaien. Emma, je weet wat je wil en gaat recht op je doel af! Dankjewel voor onze theetjes. Susana, I envy your curiosity and enthusiasm. Thanks for our cocktail-discussions. Sandra, dankjewel voor je experimentele kennis en support in de experimenten met HepaRGs. Theo, dankjewel voor je interesse, adviezen die ik soms nodig had zonder dat ik het wist, en jouw LCMS skills. Dankjewel collega DGK PhDers **Maya**, **Francis**, **Michelle**, **Lisanne**, **Josette**, **Jet**, **Thomas**, **Eva**, **Qingwu**, dat jullie er waren om even te zeuren, goede resultaten te delen, of gewoon even tegenaan te kletsen. Ook andere collega's van DGK en/of RMCU, waaronder **Adel**, **Saskia**, **Lianne**, **FrankR**, **Jeanette**, **Deepani**, **VivianN**, **Murillo**, bedankt voor jullie gezelligheid en hulp waar nodig!

Collega's van VTS (RIVM): dank jullie voor jullie interesse en support tijdens de laatste loodjes! Ik vind het super fijn om weer terug te zijn. Ook wil ik **dr. Leo van der Ven** bedanken voor de motivatie en zijn interesse door de jaren heen.

Evelyne, dankjewel voor de taartjes bij MAMS. Ik vond het zo fijn dat jij net wat beter dan ik de weg wist op het SciencePark: dank voor het meegaan als ik de weg niet wist. Dankjewel voor de maandag-telefoontjes tijdens het schrijven van mijn discussie, die waren super motiverend. Ik ben zo blij dat jij mijn paranimf bent! **Loes** en **Joost**, we begonnen ooit tegelijk aan onze master en jaren later beklommen we samen the Storr. Ik ben blij dat we nog steeds contact hebben! **Claudia**, zo dichtbij in het JDV gebouw en toch zagen we elkaar soms weken (maanden) niet. Maar het idee dat je in de buurt was, vond ik altijd prettig. Ik bewonder hoe jij je dromen najaagt! **Marjolein**, **Lisanne** en de boys, dank jullie voor jullie interesse tijdens de wijntjes en etentjes. Marjo, dankjewel voor de taxi op maandagavonden in mijn tweede en derde jaar. Sit back and relax, en luisteren naar jouw geklets, wat wil je nog meer. Lies, onze treinritjes naar huis waren erg gezellig, dan waren we zo in Apeldoorn. Nu met drie kleine hupsies erbij, level-up! **Jody** en **Viola**: best friends. Wetende dat jullie er zijn, voor een luisterend oor, schaterlach, lief advies of gewoon een theetje, is genoeg. Ik hoop dat dit nog lang zo blijft. Jeut, dankje voor jouw muziekinvloed, R&B bleek perfecte muziek voor tijdens het schrijven.

De Graven, lieve schoonfamilie, dank jullie voor de getoonde interesse! In het bijzonder Henk, die kritische vragen stelde, waardoor ik soms juist wel/niet aan mijn onderzoek ging twijfelen. In het bijzonder Klaas en Gerrit, die, hoewel uit een totaal ander veld, toch met mij PhD experience konden delen. **Emiel**, Eem, mijn grote broer. Hoewel we op beeld hebben dat je me vroeger van een biels duwde, voelde ik me later altijd gesteund door jou. Dankjewel daarvoor! **Iris**, gezellig dat jij er bij bent! Op naar nog heel veel high tea's. Lieve **pap** en **mam**, dank jullie wel dat jullie er altijd zijn. Voor zomaar even een kopje koffie tussen het thuiswerken door, een warme prak, een klusje in huis, even 'kleppen', of een middagje voor Millie zorgen. Jullie support tijdens mijn PhD en jullie vertrouwen in mij betekent heel veel.

Lieve **Hans**, dream hubby, dankjewel voor het aan mij denken als ik dat zelf niet deed. Dank voor het motiveren (onder lichte dwang) en jouw vertrouwen in mij. Ik ben trots op jou! En op jou lieve **Millie**. Zonder dat je het weet heb je zoveel bijgedragen aan het afronden van dit proefschrift; ik kon opeens efficiënter werken, wetende dat ik je 's middags op moest halen. Ik houd zo van jullie!

CURRICULUM VITAE
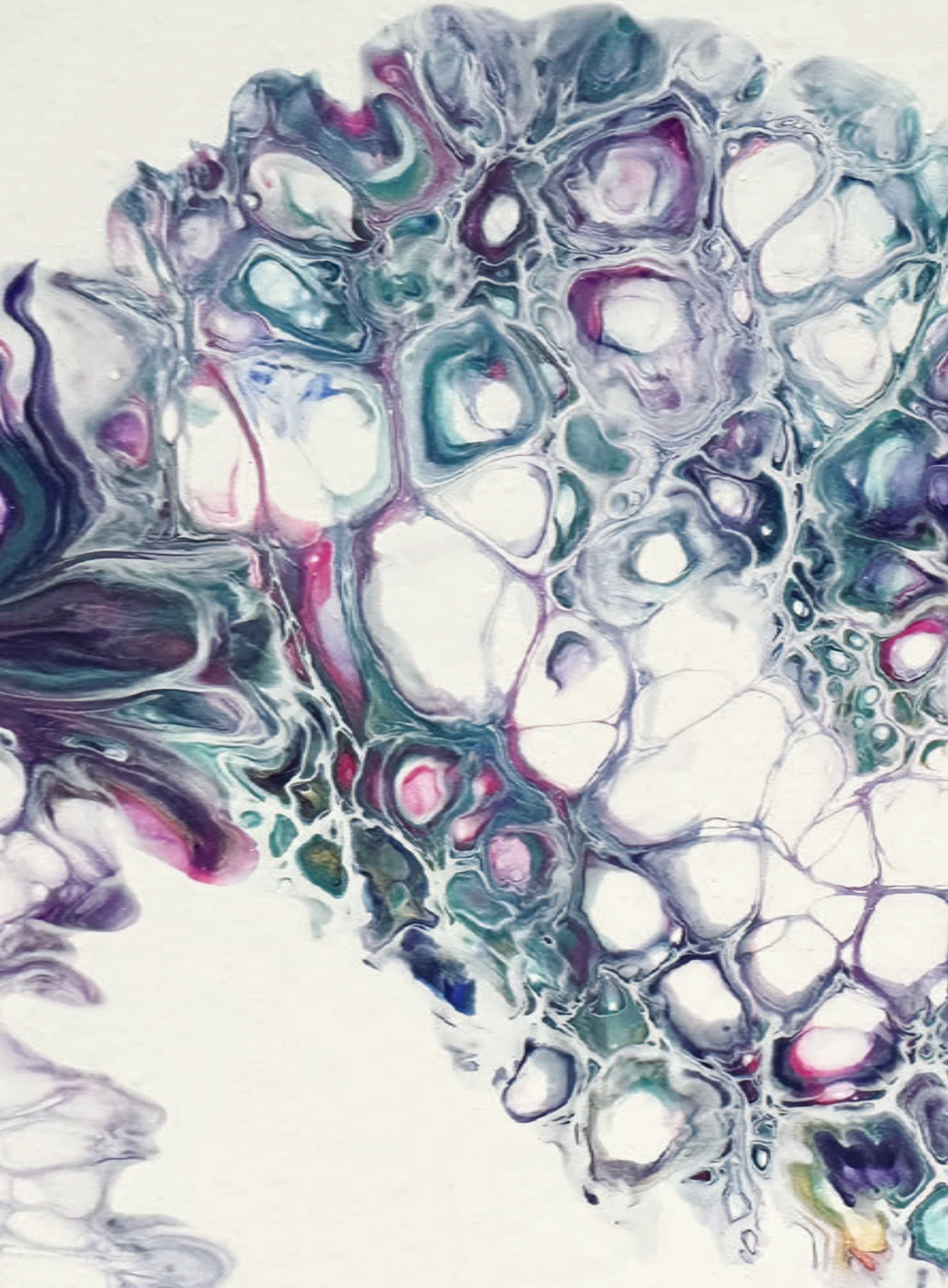
Manon Christel Bouwmeester was born on the 17th of June 1991 in Twello, the Netherlands. She grew up with her parents and one older brother. After completing high school at the Etty Hillesum Lyceum in Deventer, she started at Saxion, University of Applied Sciences. There, she successfully finished her Bachelor in Biology and Medical Laboratory Research in 2014. As part of her Bachelor studies she completed two internships, one at the clinical laboratory of the Department of Immunology (St. James's Hospital, Dublin) under the supervision of dr. Jean Dunne and one research internship at the department of Innovative Testing Strategies at the Dutch Institute of Health and Environment (RIVM) under the supervision of dr. Leo van der Ven. The thesis written during the latter internship was awarded the Best Thesis of the Year-award of Saxion. Moreover, the research described in the thesis resulted in Manon's first scientific publication as first author. Subsequently, she continued her studies at Utrecht University where she obtained her Master of Science in 2016 with a specialization in Toxicology and Environmental Health. As part of her Master studies she performed two research internships at the Institute for Risk Assessment (IRAS, Utrecht University). The first internship was at the department of Toxicology under the supervision of dr. Nynke Kramer and the second internship at the department of Epidemiology under the supervision of dr. Jelle Vlaanderen. After obtaining her Master's degree, Manon returned to the department of Innovative Testing Strategies at the RIVM as a scientific researcher. Her internship with dr. Nynke Kramer had triggered her interest in hepatic *in vitro* systems, and in January 2018 she started as PhD candidate at the department of Clinical Sciences (Utrecht University) under the supervision of prof.dr. Niels Geijsen (later adopted by prof.dr. Juliette Legler), dr. Bart Spee and dr. Nynke Kramer. The results of her four-year PhD-trajectory are published in this thesis. During her PhD, she completed several postgraduate courses of the Postgraduate Education in Toxicology (PET) to obtain her registration as a European Registered Toxicologist (ERT). Since May 2023, Manon returned (again) to the department of Innovative Testing Strategies at RIVM as a scientific researcher.